Technische Universität Braunschweig

High-ordered protein complexes for bacterial respiration and motility

Von der Fakultät für Lebenswissenschaften

der Technischen Universität Carolo-Wilhelmina

zu Braunschweig

zur Erlangung des Grades einer

Doktorin der Naturwissenschaften

(Dr. rer. nat.)

genehmigte

D i s s e r t a t i o n

von Katrin Müller

aus Peine

1. Referent: Professor Dr. Dieter Jahn

2. Referent: Professor Dr. Lothar Jänsch

eingereicht am: 11.01.2021

mündliche Prüfung (Disputation) am: 12.03.2021

Druckjahr 2021

Vorveröffentlichungen der Dissertation

Teilergebnisse aus dieser Arbeit wurden mit Genehmigung der Fakultät für Lebenswissenschaften, vertreten durch den Mentor der Arbeit, in folgenden Beiträgen vorab veröffentlicht:

Publikationen

Vera Haskamp, Simone Karrie, Toni Mingers, Stefan Barthels, Francois Alberge, Axel Magalon, Katrin Müller, Eckhard Bill, Wolfgang Lubitz, Kirstin Kleeberg, Peter Schweyen, Martin Bröring, Martina Jahn and Dieter Jahn. The radical SAM protein HemW is a heme chaperone. *J. Biol. Chem.* (2018) 293(7) 2558-2572. DOI 10.1074/jbc.RA117.000229

Müller, K., Mingers, T., Haskamp, V., Jahn, D. & Jahn, M. Biosynthesis and Insertion of Heme. *Aerobic Utilization of Hydrocarbons, Oils, and Lipids*. (2019) p. 201-228. DOI 10.1007/978-3-319-50418-6_17

Posterbeiträge

Katrin Müller, Simone Karrie, Vera Haskamp, Martina Jahn and Dieter Jahn :
Phenotypical effects in *Danio rerio* by the novel heme chaperone RSAD1. (Poster). 5th Joint Conference of VAAM & DGHM, Würzburg (2017).

Katrin Müller, José Manuel Borrero-de Acuña, Martina Jahn, Dieter Jahn : Protein-protein interactions of the *Pseudomonas aeruginosa* aerobic respiratory chain supracomplex. (Poster). 70th Annual Conference of VAAM, Wolfsburg (2018).

Katrin Müller, José M. Borrero-de Acuña, Gabriella Molinari, Manfred Rohde, Werner Tegge, Martina Jahn, Dieter Jahn : Molecular basis of the FliC-DnaK-NirS complex in the periplasm of *Pseudomonas aeruginosa*. (Poster). 71th Annual Conference of VAAM, Mainz (2019).

Katrin Müller, José Manuel Borrero-de Acuña, Josef Wissing, Martina Jahn, Dieter Jahn : Protein-protein interactions of the *Pseudomonas* aerobic respiratory chain supracomplex. Proteins Gordon Research seminar and Conference, Holderness USA (2019).

Katrin Müller, José Manuel Borrero-de Acuña, Josef Wissing, Martina Jahn, Dieter Jahn : Protein-protein interactions of the energy generation supracomplex of *Pseudomonas aeruginosa*. 6th Joint Conference of VAAM & DGHM, Leipzig (2020).

Directory

LIST OF FIGURES VII

LIST OF TABLES IX

LIST OF APPENDIX X

LIST OF ABBREVIATIONS XII

1. INTRODUCTION 19

1.1 The bacterium *Pseudomonas aeruginosa* 19

1.2 Energy generation and respiration 19

The aerobic respiratory chains 20

NADH dehydrogenase I 24

Formate dehydrogenase 26

Anaerobic respiration *via* Denitrification 29

Periplasmatic nitrate reductase 31

1.3 Flagellum 33

1.4 Vesicles 36

1.5 Protein-protein interaction 39

1.6 Aim of this work 42

2. MATERIALS AND METHODS 43

2.1 Materials 43

2.1.1 Strains of bacteria and plasmids 43

2.1.2 Oligonucleotides 47

2.1.3 Chemicals 53

2.1.4 Media supplements 55

2.1.5 Enzymes and Buffer 56

2.1.6 Consumable material and kits 57

2.1.7 Devices 58

2.1.8 Progams 62

2.2 Methods 62

2.2.1 Microbiological methods 62
Cultivation of *E. coli* and *P. aeruginosa* 62
Storage of bacteria 63
Determination of the cell density 63
2.2.2 Molecular biological methods 63
Polymerase-Chain-Reaction (PCR) 63
DNA separation by gel electrophoresis 64
DNA extraction from agarose gel 65
Purification of DNA 65
Digestion of DNA *via* restriction endonuclease 65
Ligation of DNA 66
Cloning of the StrepII-tagged bait protein expression plasmid with NEBuilder®HiFi DNA Assembly kit 67
Production of $CaCl_2$-competent *E. coli* cells 68
Transformation of *E. coli* 69
Production and transformation of electrocompetent *P. aeruginosa* cells 69
Diparental mating of *P. aeruginosa* 70
Plasmid preparation from *E. coli* and *P. aeruginosa* using Miniprep Kit (Qiagen) 70
BACTH- (Bacterial Adenylate Cyclase-based Two-Hybrid) System 70
Application of the Bacterial Adenylate Cyclase Two Hybrid (BACTH) 73
BACTH: β-Galactosidase-assay 74
2.2.3 Protein analytical methods 76
Characterization of the *P. aeruginosa dnaK* conditional mutant strain 76
Protein production of DnaK and FliC *via* affinity chromatography on glutathione sepharose 77
Protein concentration measurement *via* the Bradford test 78
SDS-PAGE (Sodium Dodecyl Sulphate-PolyAcrylamide Gel Electrophorese) 79
Interactomics approach 80
Bait-prey protein complex formation under different conditions of oxygen tension and their isolation 82
Protein complex purification *via* affinity chromatography 83
Western blot analysis for the bait proteins 84
Preparation of gel-separated protein complex samples for LC-MS^2 analysis 86
LC-MS^2 analyses using the Orbitrap Fusion™ Tribrid™ system 87
SPOT membrane synthesis for the analysis of the interaction of DnaK and FliC 88
SPOT membrane analysis of the interaction domains of DnaK and FliC 89
Isolation of membrane vesicles from *P. aeruginosa* 90
Size analysis of isolated *P. aeruginosa* membrane vesicles *via* NanoSight NS300 91
Vesicle proteomics 92
DnaK binding capacity analysis *via* the Fast Relaxation Imaging technique 93
Field Emission Scanning Electron Microscopy (FESEM) 94
Transmission Electron Microscopy (TEM) 96
Fluorescence microscopy 97

3. RESULTS AND DISCUSSION 99

3.1 Protein-protein interaction (PPI) of the respirasome of *P. aeruginosa* 99
3.1.1 Construction of the bait protein producing strains 99
3.1.2 Recombinant production of the bait proteins NuoJ, FdhE and NapA and purification of formed complexes formed under aerobic and aerobic to anaerobic shift conditions 100
3.1.3 Dynamic interaction of proteins with NuoJ, NapA and FdhE during the shift from aerobic to anaerobic growth conditions 103
Proteins of the amino acid metabolism differentially interacting with NuoJ, NapA and FdhE 106
Proteins of the TCA cycle differentially interacting with NuoJ, NapA and FdhE 108
Proteins of the cell division and cell wall/membrane/envelope differentially interacting with NuoJ, NapA and FdhE 109
Proteins of the chemotaxis, motility, quorum sensing/biofilm formation and stress detoxification differentially interacting with NuoJ, NapA and FdhE 110
Proteins of the cofactor formation, DNA/RNA metabolism, transcription regulation, translation/modification, protein transport and ABC transporter differentially interacting with NuoJ, NapA and FdhE 112
3.1.4 NADH dehydrogenase I NUO (complex I) functions as core complex in the respirasome under shift conditions 113
3.1.5 Quantification of protein-protein interaction in respirasome complexes 117

3.2 Vesicle production and proteome analysis of different *lemA*-like and the PA14 wildtype strains 122
3.2.1 *P. aeruginosa* LemA1 and LemA2 are both involved in intra- and extracellular vesicle formation 123
3.2.2 Proteome analyses of the *lemA* deletion and overproduction strains 127
The formation of certain proteins of the cell wall, cell membrane and cell envelope are affected by LemA proteins 128
The formation of certain proteins of the chemotaxis and motility, proteases and chaperones, protein transport, quorum sensing and biofilm formation are affected by LemA proteins 131
The formation of certain proteins of the amino acid metabolism, cell division, cofactor formation, ATP synthase and cytochrome oxidases are affected by LemA proteins 134
The formation of certain proteins of the TCA cycle, sulfur metabolism, transport of small molecules, stress and detoxification are affected by LemA proteins 134
LemA1 and LemA2 influenced the composition and formation of MVs 135

3.3 Protein-protein interaction of DnaK and FliC 139
3.3.1 DnaK and FliC were found in vesicles 140
3.3.2 Conditional mutant of DnaK showed reduced flagellum assembly 142
3.3.3 Recombinant DnaK and FliC production 144
3.3.4 Function of DnaK in dependence of the pH and the availability of ATP 145
3.3.5 Determination of the interacting domains of the DnaK/FliC complex 146

SUMMARY 153

OUTLOOK 155

P. aeruginosa respirasome interactomics 155

P. aeruginosa LemA-like proteins 155

P. aeruginosa DnaK and FliC interaction 155

REFERENCES 156

APPENDIX 174

ACKNOWLEDGEMENT 209

List of Figures

Figure 1: Branched respiratory chain in *P. aeruginosa.* 20
Figure 2: The canonical respiratory chain of oxygen respiration. 22
Figure 3: Schematic view of complex I of the respiratory chain (NADH dehydrogenase I)..24
Figure 4: Phylogenetic tree of metal-dependent FDHs based on genome-derived amino acid sequences of FdhD 28
Figure 5: The canonical respiratory chains of denitrification. 30
Figure 6: Schematic model of NAP of *P. aeruginosa.* 32
Figure 7: Structure of the bacterial flagellum. 34
Figure 8: Several routes of MV formation lead to different types of membrane vesicle. 37
Figure 9: Several methods for the investigation of protein-protein interactions. 40
Figure 10: Overview of NEBuilder Assembly approach.....67
Figure 11: Principle of the BACTH system.....71
Figure 12: Plasmid maps of the BACTH. 72
Figure 13: Principle of the *dnaK* conditional mutant..77
Figure 14: Calibration of the Bradford test for the determination of protein concentrations using of BSA.....79
Figure 15: Interactomics approach. 81
Figure 16: Setup of a Western blot.. 85
Figure 17: D/A for $SOD1_{bar}$-G41D in PBS at pH 7 as function of time.. 94
Figure 18: Interactomics of the membrane protein NuoJ with multiple interaction partners.101
Figure 19: Interactomics of the protein FdhE with multiple interaction partners. 102
Figure 20: Interactomics of the membrane protein NapA with multiple interaction partners. 103
Figure 21: Cellular localization of the proteins interacting with NuoJ, FdhE and NapA found under aerobic (A) and aerobic to anaerobic shift (B) conditions..104
Figure 22: Number of interaction partners found for the individual baits, for two or all three of them under aerobic (A) and aerobic to anaerobic shift (B) conditions.. 105
Figure 23: Functional classification of interacting prey proteins of the three bait proteins NuoJ, NapA and FdhE identified under aerobic (A) and shift (B) conditions.....106
Figure 24: Identified proteins involved in amino acid metabolism differentially interacting with the three baits (NuoJ, NapA, FdhE) under aerobic and shift conditions.. 107
Figure 25: Identified proteins involved in TCA cycle and pyruvate metabolism differentially interacting with the three baits (NuoJ, NapA, FdhE) under aerobic and shift conditions.....108
Figure 26: Identified proteins involved in cell division and cell wall/membrane/envelope organization differentially interacting with the three baits (NuoJ, NapA, FdhE) under aerobic and shift conditions.....110
Figure 27: Identified proteins involved in chemotaxis, motility, quorum sensing/biofilm formation and stress/detoxification differentially interacting with the three baits (NuoJ, NapA, FdhE) under aerobic and shift conditions.....111
Figure 28: Identified proteins involved in the electron transfer and the nitrogen metabolism differentially interacting with the three baits (NuoJ, NapA, FdhE) under aerobic (A) and shift (B) conditions. 114
Figure 29: Model of a part of the respirasome supra complex formed under aerobic conditions. 115
Figure 30: Model of a part of the respirasome supra complex formed under shift conditions.. 116

Figure 31: Protein-protein interaction of the anaerobic respirasome quantified *via* the bacterial two-hybrid system approach. 118
Figure 32: Protein-protein interaction of the anaerobic respirasome quantified *via* the bacterial two-hybrid system approach. 118
Figure 33: Quantification of the protein-protein interactions of anaerobic respirasome. 119
Figure 34: Network of interacting proteins of the anaerobic respirasome. 120
Figure 35: Revised model of the anaerobic respirasome. 121
Figure 36: Vesicle isolation from various *lemA* gene mutants and overespression strains and the PA14 WT. 124
Figure 37: Comparison of the vesicle size of various *lemA* mutant and overexpressing strains using NanoSight.. 125
Figure 38: FESEM analyses of *lemA* deletion and oberexpressing strains.. 126
Figure 39: Changes of the abundance of proteins of the cell wall, cell membrane and cell envelope in dependence of the deletion or overexpression of *lemA* genes compared to the wildtype strain. 130
Figure 40: Changes in the abundance of proteins involved in chemotaxis, motility, protein turnover and transport, quorum sensing and biofilm formation in the *lemA* deletion and overexpressing strains in comparison to the wildtype. 132
Figure 41: Swarming motility of different *P. aeruginosa* mutant strains (*fliC*, *nirS*, *nosZ*). ...139
Figure 42: TEM analyses of the localization of DnaK and FliC in *P. aeruginosa* cells with focus on the flagella. 140
Figure 43: Immunogold labeling of DnaK and FliC in outer membrane vesicles of PA14 wildtype strain.. 141
Figure 44: Analyses of *dnaK* conditional mutant strains of *P. aeruginosa* PA01 and PA14.. 143
Figure 45: Recombinant production of DnaK and FliC. 144
Figure 46: Determination of ATP-dependent activity of DnaK. 146
Figure 47: SPOT membrane of DnaK. 147
Figure 48: SPOT membrane of FliC. 148
Figure 49: Interaction model of DnaK/FliC complex for transport. 149
Figure 50: Interaction model of DnaK/FliC complex. 150

List of Tables

Table 1: Strains of bacteria and plasmids 43
Table 2: Oligonucleotides 47
Table 3: Chemicals 53
Table 4: Media supplements 55
Table 5: Enzymes and associated buffer 56
Table 6: Consumable materials and kits 57
Table 7: Devices 58
Table 8: Used programs 62
Table 9: Conditions of PCR for genotyping [10 µl approach] 63
Table 10: PCR conditions for DNA amplification with Phusion or Q5 polymerase for a 25 µl preparation 64
Table 11: Program for amplification using Phusion or Q5 polymerase 64
Table 12: Reaction approach for a test gel 65
Table 13: Approach for a restriction digest of an insert 66
Table 14: Approach for a restriction digestion of a plasmid 66
Table 15: Approach of a ligation 66
Table 16: NEBuilder DNA assembly 68
Table 17: Solution of $CaCl_2$ competent cells 69
Table 18: Composition of 12 % polyacrylamide SDS separating gel 80
Table 19: Composition of the 6 % SDS polyacrylamide collecting gel 80
Table 20: Strains for FESEM analyses 95
Table 21: Proteins found in vesicles and affected by LemA1 and/or LemA2 135

List of Appendix

Appendix 1: Verification of the transposon mutants for interactomics approach. 174
Appendix 2: Plasmid map of pUCP26_*fdhE*-StrepII.....174
Appendix 3: Plasmid map of pUCP26_*napA*-StrepII.....175
Appendix 4: Plasmid map of pUCP26_*nuoJ*-StrepII 175
Appendix 5: Identified proteins involved in cofactor formation differentially interacting with the three baits (NuoJ, NapA, FdhE) under aerobic (A) and aerobic to anaerobic shift (B) conditions......176
Appendix 6: Identified proteins involved in DNA/RNA metabolism differentially interacting with the three baits (NuoJ, NapA, FdhE) under aerobic (A) and aerobic to anaerobic shift (B) conditions.....177
Appendix 7: Identified proteins involved in transcription regulation, translation/modification differentially interacting with the three baits (NuoJ, NapA, FdhE) under aerobic (A) and aerobic to anaerobic shift (B) conditions. 178
Appendix 8: Identified proteins involved in protein transport und ABC transporter differentially interacting with the three baits (NuoJ, NapA, FdhE) under aerobic (A) and aerobic to anaerobic shift (B) conditions.....179
Appendix 9: Plasmid map of BACTH System - Cloning of *narH*.....180
Appendix 10: Plasmid map of BACTH System - Cloning of *nirQ*.....180
Appendix 11: Plasmid map of BATCH System - Cloning of *norC*.....181
Appendix 12: Plasmid map of BACTH System - Cloning of *norD*.....182
Appendix 13: Plasmid maps of BATCH System - Cloning of *dnaK* 183
Appendix 14: Plasmid maps of BACTH System - Cloning of *fliC* 184
Appendix 15: Tables with measured Miller Units of the β-galactosidase assay of the respective PPI used in the BACTH assay.....189
Appendix 16: Measurement of the vesicle diameter *via* Nanosight. 190
Appendix 17: Measurement of the vesicle diameter *via* Nanosight. 190
Appendix 18: Cellular localization of proteins detected in vesicles of the different *lemA* deletion and overexpressing strains.....191
Appendix 19: Cellular localization of proteins detected in vesicles of the different *lemA* deletion and overexpressing strains and the PA14 wildtype strain. 191
Appendix 20: Functional classification of detected proteins in vesicles of *lemA* deletion and overexpressing strains and the PA14 wildtype strain. 192
Appendix 21: Changes of the abundance of proteins of amino acid metabolism (A), cell division and cofactor formation (B) and ATP synthase and cytochrome oxidase (C) in dependence of the deletion or overexpression of *lemA* genes compared to the wildtype strain. 192
Appendix 22: Changes of the abundance of proteins of the TCA cycle and pyruvate metabolism (A-B), stress/detoxification and sulfur metabolism and transcription regulators and transport of small molecules (D) in dependence of the deletion or overexpression of *lemA* genes compared to the wildtype strain.....193
Appendix 23: Changes of the abundance of proteins of the DNA/RNA metabolism (A-B), energy metabolism (C) and putative enzymes and phage-related proteins (D) in dependence of the deletion or overexpression of *lemA* genes compared to the wildtype strain. 194
Appendix 24: Changes of the abundance of proteins of the translation and modification in dependence of the deletion or overexpression of *lemA* genes compared to the wildtype strain. 194
Appendix 25: Pre-testing of the optimal protein production conditions of DnaK and FliC. ...195
Appendix 26: Pre-testing of the optimal protein production conditions of DnaK and FliC. ...195

Appendix 27: SPOT membrane application scheme of DnaK. 196
Appendix 28: List of spotted peptides of DnaK SPOT membrane 196
Appendix 29: SPOT membrane application scheme of FliC. 202
Appendix 30: List of spotted peptides of the SPOT membrane of FliC 202
Appendix 31: Model of determined interacting domains of FliC and DnaK. 207
Appendix 32: Production of DnaK testing of different storage solutions. 208

List of Abbreviations

Abbreviation	Name
A	Adenosine
Å	Ångström (1Å = 0.1 nm)
AcGFP1	*Aequorea coerulescens* GFP (monomeric green fluorescent protein)
ACN	Acetonitrile
ADP	Adenosine-di-phosphate
AHL	N-acyl homo-serine lactone
ALA	5-Aminolevulinic acid
Amp	Ampicillin
AP	Alkaline phosphatase
AP-MS	Affinity purification-mass spectrometry
APS	Ammonium persulfate
ATP	Adenosine triphosphate
AUC	Analytical ultracentrifugation
BACTH	Bacterial adenylate cyclase two-hybrid
BCIP	5-Bromo-4-chloro-3-indolyl phosphate p-toluidine salt
BIC	Ammonium hydrogen carbonate
bis-MGD	Bis-molybdenum guanine dinucleotide
bp	Base pair
BRET	Bioluminescence resonance energy transfer
BSA	Bovine serum albumin
°C	Degree centigrade Celsius
C	Cytosine
CBBG	Coomassie Brilliant Blue G-250
CCD	Charge-coupled device
CDS	Color developing solution
CIO	Cyanide-insensitive oxidase
CiP	Alkaline Phosphatase, Calf Intestinal
CMV	Cytoplasmic membrane vesicles
Co-IP	Co-immunoprecipitation
CO_2	Carbon dioxide
C ring	Cytosolic ring of the flagellum
C-terminal	Carboxy-Terminus
Cu_A	Copper center A

Cu_B	Copper center B
Cu_Z	Copper center Z
CV	Column volume
CYO	*bo*$_3$ quinol oxidase
Cys	Cysteine
Cyt *c*	Cytochrome *c*
D/A	Donor over aceptor
ddH_2O	Double deionized water
DMF	N,N-dimethylformamide
DMSO	Dimethyl sulfoxide
DNA	Deoxyribonucleic acid
dNTP	Deoxynucleoside triphosphates
E	Reduction potential
E^0	Standard reduction potential
ΔE^0	Potential difference
e^-	Electron
EDTA	Ethylenediaminetetraacetic acid
ELISA	Enzyme-linked Immunosorbent Assay
EOMV	Explosive outer membrane vesicle
µF	Microfarad
FA	Formaldehyde
FAD	Flavin adenine dinucleotide
FCS	Fetal calf serum
FDH	Formate dehydrogenase
FDH-H	Monomeric formate dehydrogenase
FDH-N	Heteromeric membrane-bound formate dehydrogenase N-class
FDH-O	Heteromeric membrane-bound formate dehydrogenase O-class
[FeS]	Iron sulphur cluster
FESEM	Field Emission Scanning Electron Microscopy
FHL	Formate hydrogenlyase
FMN	Flavin mononucleotide
for	Forward
FP	Fluorescence polarization
FRET	Fluorescence resonance energy transfer
[Fe-S]	Iron sulphur cluster
[2Fe-2S]	Two iron two sulphur cluster

[4Fe-3S]	Four iron three sulphur cluster
[4Fe-4S]	Four iron four Sulphur cluster
g	Gram
G	Guanine
ΔG^0	Released energy
GAL4	Yeast transcriptional activator of galactose-induced genes
GC	Guanine Cytosine content
GST	Glutathione S-Transferase
GV	Gel volume
h	Hour
H+	Proton
HCD/IT	High-energy collision dissociation / iron trap
HCl	Hydrogen chloride
HEPES	4-(2-hydroxyethyl)-1-piperazineethanesulfonic acid
HF	High fidelity
H_2O	Water
HOBt	1-hydroxybenzotriazole
HPLC	High performance liquid chromatography
HPLC-MS	High performance liquid chromatography – mass spectrometry
HQNO	2-n-heptyl-4-hydroxyquinoline N-oxides
Hz	Hertz
IPTG	Isopropyl β-d-1-thiogalactopyranoside
ITC	Isothermal titration calorimetry
Kan	Kanamycin
kb	Kilo base
kDa	Kilo Dalton
kJ/mol	Kilo joule per
KOH	Potassium hydroxide
kV	Kilo volt
L	Liter
µl	Microliter
LB	Lysogeny broth or Luria-Bertani
LBR	Ligand-binding regions
LC	Liquid chromatography
LC-MS	Liquid chromatography – mass spectrometry

L ring	Lipopolysaccharide ring
M	Molar
µm	Micrometer
µM	Micromolar
mA	Milliampere
MALDI-TOF	Matrix-assisted laser desorption ionization time of flight
MBS	Membrane blocking solution
MCS	Multiple cloning site
mCherry	Red monomeric fluorescent protein
min	Minute
mg	Milligram
ml	Milliliter
mm	Millimeter
mM	Millimolar
Mo	Molybdenum
Moco	Molybdenum cofactor
Mo-FDH	Molybdenum formate dehydrogenase
MS	Mass spectrometry
MS ring	Membrane/supermembrane ring of the flagellum
m:s	Minute:second
m/s	Meter per second
MST	Microscale thermosetting
MTT	3-[4,5-dimethylthiazol- 2-yl]-2,5-diphenyltetrazolium bromide
MU	Miller Unit
MV	Membrane vesicle
mV	Mili volt
MW	Molecular weight
N_2	Nitrogen
NAD	Nicotinamide adenine dinucleotide
NADH	Nicotinamide adenine dinucleotide hydrogen
NAP	Periplasmic nitrate reductase
NAR	Respiratory nitrate reductase
NAS	Cytoplasmic nitrate reductase
NBT	p-Nitrotetrzolium blue chloride
NDH-2	NADH dehydrogenase II
ng	Nanogram

NHS	N-hydroxysuccinimide
NiCo21	*E. coli* strain derived from BL21
[NiFe]	Nickel iron hydrogenase
NIR	Nitrite reductase
nl	Nanoliter
nm	Nanometer
NMP	N-methyl-2-pyrrolidone
NMR	Nuclear magnetic resonance
NO	Nitric oxide
N_2O	Nitrous oxide
NO_2	Nitrite
NO_3	Nitrate
NOR	Nitric oxide reductase
NOS	Nitrous oxide reductase
NQR	Na^+-translocating NADH : ubiquinone oxidoreductase
NTA	Nanoparticle Tracking Analysis
N-terminal	Amino terminal
NUO	NADH dehydrogenase I
O_2	Dioxygen
OD	Optical density
OIMV	Outer-inner membrane vesicle
OM	Outer membrane
OMV	Outer membrane vesicle
ON	Overnight
ONPG	Ortho-Nitrophenyl-β-D-Galactopyranoside
opt	Optimized
Δ*p*	Proton and/or sodium electrochemical gradient
PA01	*Pseudomonas aeruginosa* strain 01
PA14	*Pseudomonas aeruginosa* strain 14
PBS	Phosphate buffered saline
PC	Personal computer
PCA	Protein fragment complementation assay
PCR	Polymerase chain reaction
PEG	Polyethylene glycol
pH	Power of hydrogen
Pi	Phosphate
pmf	Proton motive force

PPI	Protein-protein interaction
PQS	*Pseudomonas* quinolone signal
P ring	Peptidoglycan ring of the flagellum
ProtG	Protein G
psi	Pound-force per square inch
PVDF	Polyvinylidene fluoride
Q	Ubiquinone
Q5	Modified bacterial thermostable polymerase
Q-cycle	Quinone cycle
R^2	Coefficient of determination
rev	Reverse
RNA	Ribonucleic acid
rpm	Rotations per minute
RT	Room temperature
s	Second
SBP	Streptavidin-binding peptides
SDS	Sodium dodecyl sulfate
SDS-PAGE	Sodium dodecyl sulfate-polyacrylamide gel electrophoresis
$SOD1_{bar}$	Superoxide dismutase type-1 from human
SOP	Standard Operating Procedure
SOS	Emergency signal “safe our souls”
SPOT	Established name for the method by Ronald Frank
SPR	Surface plasmon resonance
SRP	Signal recognition particle
T	Tyrosine
t_S	Starting time
t_E	Ending time
T4	Tequatovirus 4 (bacteriophage T4)
TAE	TRIS-acetate-EDTA
TAP	Tandem affinity purification
TAT	Twin-arginine Translocation
TBS	Tris-buffered saline
TBS-T	Tris-buffered saline-Tween20
TCEP	Tris(2-carboxyethyl)phosphine
TEAB	Tetraethylammonium borohydride
TEM	Transmission electron microscopy
TEMED	N,N,N′,N′-Tetramethylethylenediamine

TFA	Trifluoroacetic acid
TFB I	Transformation buffer I
TFB II	Transformation buffer II
Tims-TOF	Trapped ion mobility spectrometry - time of flight
TRIS	Tris(hydroxymethyl)aminomethane
TSMS	Tube-shaped membranous structures
UV	Ultraviolet (electromagnetic radiation 10-400 nm)
v	Volume
V	Volt
v/v	Volume / volume
w	Weight
WT	Wildtype
w/v	Weight per volume
x g	Acceleration of gravity
X-Gal	5-Bromo-4-chloro-3-indoxyl-β-D-galactopyranoside
Y2H	Yeast two-hybrid system
Ω	Electrical resistance
+IV	Electrochemical valence (oxidation number)
+V	Electrochemical valence (oxidation number)
+VI	Electrochemical valence (oxidation number)

1. Introduction

1.1 The bacterium *Pseudomonas aeruginosa*

Pseudomonas aeruginosa is a Gram-negative, aerobic rod-shaped γ-Proteobacterium[1]. The bacteria are monotrichous flagellated and produce extracellular hydrolases for the cleavage of gelatine, as well as the pigment pyocyanin from the phenazine class. They are able to use different carbon and energy sources. *P. aeruginosa* can utilize nitrate as a source of nitrogen and belongs to the class of bacteria that is capable to use denitrification for energy generation. Furthermore, they generate *b*-type and *c*-type cytochrome *c* oxidases as terminal oxidase for the electron transfer to accept oxygen[2]. *P. aeruginosa* has a high GC content of 67.2 %, which distinguishes it from the other fluorescent pseudomonads[3]. The genome of *P. aeruginosa* was completely sequenced and has a size of 6.3 million bp. It provides insights into the basics of metabolic versatility and intrinsic antibiotic resistance. It also has a large set of regulatory genes involved in the control of the complex metabolic transport and chemotaxis processes. The distinct gene groups identified (paralogous groups) indicate functional diversity and adaptability[4,5]. *P. aeruginosa* is an opportunistic pathogen that can cause infections in a wide range of organisms, from animals to plants[6]. *P. aeruginosa* is also an opportunistic human pathogenic bacterium most commonly found in nosocomial infections. It is responsible for 8 % of surgical wound infections, 10 % of bloodstream infections, 12 % of urinary tract infections received in hospitals and 16 % of nosocomial pneumonia cases[7]. In this context, three of the most significant human diseases caused by *P. aeruginosa* are: 1) Bacteremia in severe burn victims; 2) chronic lung infection in mucoviscidosis patients; and 3) acute ulcerative keratitis in users of soft contact lenses with long wearing time[8].

1.2 Energy generation and respiration

Bacteria possess an exceptional metabolic versatility and diversity in terms of the different ways in which they generate energy. Pseudomonads are able to use an extraordinary number of different carbon and energy sources[2]. The major goal of energy generation is the formation of ATP and Δ*p* (proton and/or sodium electrochemical gradient). This is possible at the substrate level (fermentation) or *via* a membrane localized electron transport chain[9]. The chemio-osmotic theory describes a proton gradient that serves as an energy source for the endergonic synthesis of ATP from ADP and P_i. Various electron transport chains utilize their redox potential-driven electron transfer for the pumpery of protons/sodium ions across a membrane, resulting in a concentration gradient and electrical potential difference. The free enthalpy is stored in the gradient and is called proton motive force (pmf)[10]. The different sources of carbon that can be used create a variability in the metabolite products that are

produced. The cell changes the ratios by changing the catabolite pathways. *P. aeruginosa* is able to produce energy by aerobic and anaerobic respiration, as well as by the fermentation of arginine and pyruvate[9,11]. *P. aeruginosa* contains a widely branched respiratory chain that ends with various terminal oxidases and denitrification enzymes (Figure 1)[11]. The same core respiration machinery is shared by aerobic respiration and denitrification, consisting of respiratory dehydrogenases, like NADH dehydrogenase I (NUO), the ubiquinone pool, the bc_1 complex and cytochrome *c*[11,12].

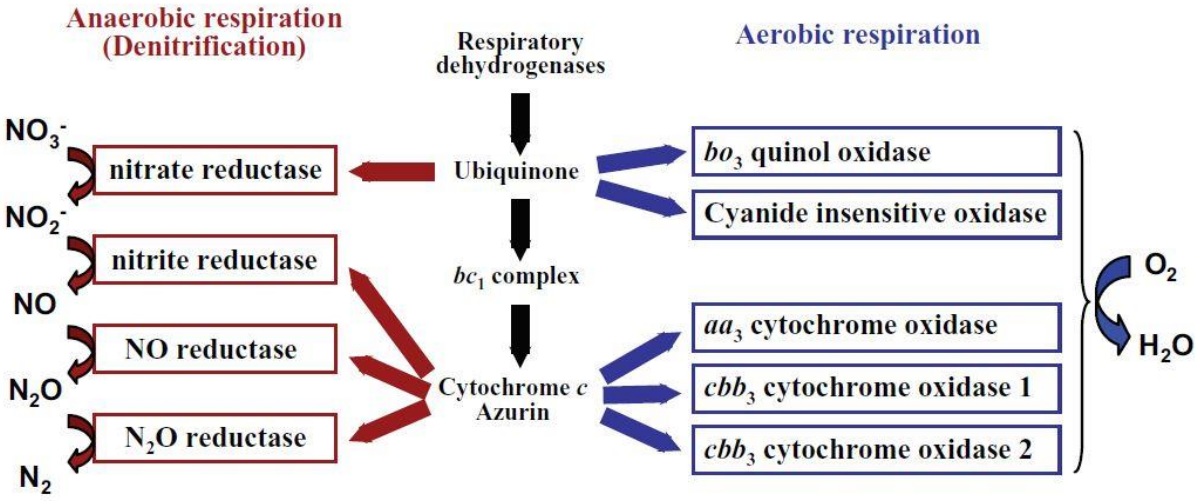

Figure 1: Branched respiratory chain in *P. aeruginosa*. Under aerobic conditions, oxygen is utilized as terminal electron acceptor and reduced to water by five terminal oxidases. Under anaerobic conditions, electrons are transferred to nitrogen oxides *via* denitrification enzymes[11].

So far, five terminal oxidases have been identified: three cytochrome *c* oxidases and two quinol oxidases[11]. The aerobic respiratory chain is branched at the ubiquinone pool. At this point the electrons are transferred to either the bo_3 quinol oxidase (CYO) or the cyanide-insensitive oxidase (CIO)[11,13]. Of the 17 various dehydrogenases, 15 are involved in electron transfer from different reduced substrates to ubiquinone and two transfer the electrons directly to nitrate reductase or cytochrome *c*[9]. Although *Pseudomonas* is able to generate energy using aerobic and anaerobic respiration, energy generation *via* aerobic respiration is preferred[9,11,14,15].

The aerobic respiratory chains

Aerobic respiration is a series of coupled redox reactions that describe the transfer of electrons from an electron donor (e.g. NADH, formate, glycerol-3-phosphate, succinate etc.) to molecular oxygen (Figure 2)[12]. On the one hand, this provides the ability to store energy in the form of ATP, and on the other hand, energy-intensive processes (transport of solutes or motility) can be achieved by the utilization of the pmf. Terminal oxidases bind, activate and reduce more than 250 molecules of molecular oxygen per second, the released energy is

coupled to proton translocation. Four electrons are required to reduce molecular oxygen to water and the standard redox potential E^0 is +815 mV[12,16]. The transport of electrons from a redox system with a negative potential to a redox system with a more positive potential is basis of the respiratory chain. The individual components of such a chain can each be assigned a redox potential *E*, a quantitative measure of electron affinity. The electrons are transferred from a redox partner with a negative potential to one with a more positive potential. The difference between these two is the potential difference ΔE^0, a measure of the change in free energy. The more the potential difference ΔE^0 between two redox partners is and the more electrons are transferred, the more free energy ΔG^0 is released. Aerobic respiration can be described by two partial reactions: 1) $NADH \rightarrow NAD^+ + H^+ + 2e^-$, the electron donor has E^0 = -320 mV; 2) $\frac{1}{2}O_2 + 2e^- + 2H^+ \rightarrow H_2O$, the electron acceptor has E^0 = +818 mV The resulting potential difference is ΔE^0 = +1138 mV and is equivalent to a free energy ΔG^0 of -218 kJ/mol[17]. This amount of free energy is high for a biochemical reaction and is not usable in one step. In the respiratory chain, the released energy is distributed over several redox reactions with less free energy. The terminal reaction with oxygen is irreversible and a constant flow of electrons is generated as long as reduction equivalents and oxygen are present[17]. The NADH dehydrogenase I (NUO), the quinone pool, the bc_1 complex and cytochrome *c* form the backbone of the aerobic respiratory chain (Figure 2). In the NUO protein complex the electrons are transferred from NADH (-320 mV) to , and further transferred *via* eight [Fe-S] clusters to the quinone pool (+133 mV for ubiquinone). By a conformational change during electron transport, four protons per two transported electrons are translocated across the membrane. In addition, the reduction of quinol leads to two further proton translocations across the membrane (Q-cycle, see below). The bc_1 complex transfers the electrons from the quinone pool, inside the membrane to cytochrome *c* (+230 mV) in the periplasm. The bc_1 complex consists of an integral membrane protein with two heme *b* cofactors and two periplasmic subunits: the Rieske iron sulfur protein and cytochrome c_1. The protons produced during the oxidation of quinol are released into the periplasm[12,17]. The bc_1 complex can also function as a Q-cycle, which causes additional protons to be translocated across the membrane[12]. Quinol is oxidized to quinone on the outside of the bc_1 complex and releases two H^+ into the periplasm. The quinone re-enters the quinone pool. The path of the two electrons is different. One electron is transferred to cytochrome *c* *via* the Rieske [Fe-S] center and cytochrome c_1. The other electron is returned to the inside *via* the two heme *b* groups. The electron reduces another quinone to the semichinone radical anion. A second quinol is oxidized to quinone, whereby two H^+ are released into the periplasm and the two electrons are seperated again. One electron is transferred to cytochrome *c* and the other to the previously formed semichinone radical anion. This takes up the electron and two H^+ from the cytoplasm and quinol. In total, one quinol is oxidized to quinone, two cytochrome *c* are reduced and four protons are translocated[17]. This Q-cycle is only possible if the membrane potential is low (<~120 mV with ubiquinone). The

Rieske iron sulfur protein requires the TAT (Twin-Arginine Translocation) system because it is transported into the periplasm in a folded state. The electrons are then transferred from cytochrome *c* (+230 mV) by a terminal oxidase to oxygen (+815 mV). The four protons required for the reduction of molecular oxygen to water are taken from the cytoplasm and contribute to the pmf[12].

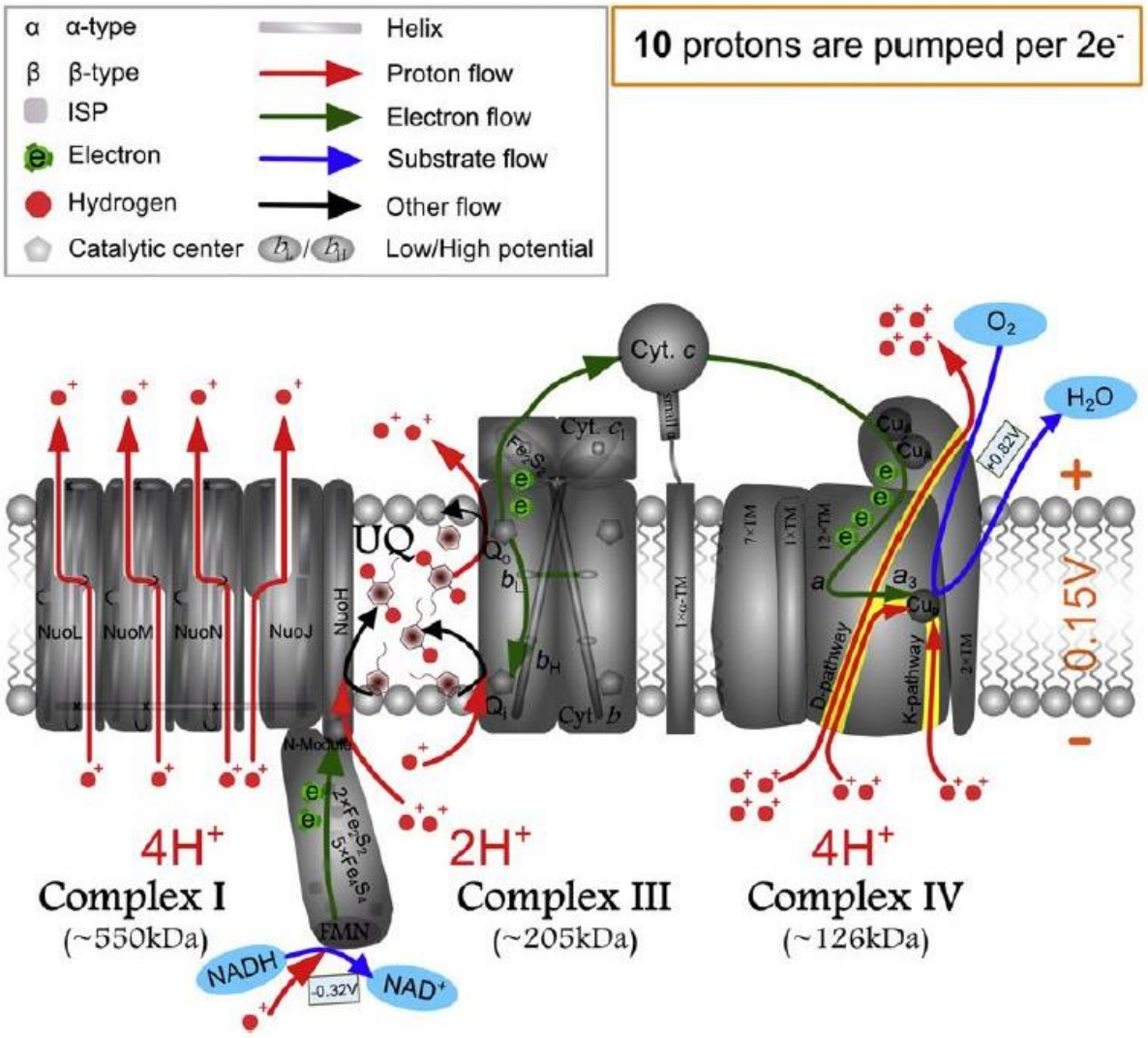

Figure 2: The canonical respiratory chain of oxygen respiration. Electrons are transferred from NADH to complex IV *via* NADH dehydrogenase I (complex I), ubiquinone/ubiquinol, bc_1 complex (complex III) and cytochrome *c*. Protons are pumped across the membrane by complex I, complex III (Q-cycle) and complex IV. Overall, the contribution to the proton motive force is 10 protons per electron pair[12].

The presence of different oxidases is generally explained by their respective properties with respect to their affinity to molecular oxygen, their turnover rate or the stoichiometry of proton translocation[16]. *P. aeruginosa* contains two cbb_3 oxidases and one aa_3 oxidase, which all take electrons from cytochrome *c*. The bo_3 cytochrome *c* oxidase and the cyanide-insensitive *bd*-like cytochrome *c* oxidase obtain the electrons from the ubiquinone pool[11]. The cbb_3 oxidase is a member of the heme-copper oxidase superfamily and only present in bacteria. The oxidase has a high oxygen affinity and a low proton translocation capacity. It is induced

under low oxygen conditions. It is encoded by the tetracistronic operon *ccoNOQP*. The CcoN is the catalytic subunit carrying a binuclear center with high-spin heme b_3 and Cu_B. The subunits CcoO and CcoP are transmembrane monohemic and dihemic cytochrome *c* subunits and the CcoQ is used for stabilization[11,18]. *P. aeruginosa* contains two cbb_3 oxidases. The cbb_3-1 is expressed under high oxygen conditions and is downregulated in the stationary phase[11,19]. The cbb_3-2 is up-regulated at low oxygen conditions or in the stationary phase and exceeds the level of cbb_3-1[20]. The cbb_3-1 plays the major role under aerobic conditions and the cbb_3-2 plays a compensatory, complementary role under oxygen-depleted conditions[11]. Cytochrome aa_3 oxidase is the major member of the heme-copper oxidase superfamily and is characterized by their low oxygen affinity and high proton translocation ability[11,20]. In *P. aeruginosa* it is encoded by the *coxBA*-PA0107 gene cluster[4]. *CoxA* encodes the subunit I which contains the binuclear catalytic centre formed by heme a_3 and Cu_B. Subunit II is encoded by *coxB* and contains Cu_A binding site and forms the electron transfer site with cytochrome *c*. Subunit III (CoxC) is encoded by PA0107 and is a putative cytochrome *c* assembly protein involved in the insertion of copper into subunit I. The aa_3 oxidase plays the major role under high oxygen conditions and possesses the highest efficiency of the five oxidases to generate the proton gradient[11]. The next two oxidases get their electrons directly from the quinone pool and not from cytochrome *c* like the cbb_3 and aa_3 oxidases. The bo_3 quinol oxidase is also a member of the heme-copper oxidase superfamily and is homologous to the aa_3-type oxidases but contains heme *b* and heme *o.* The Cu_A binding site is not present. The bo_3 oxidase has a low oxygen affinity and operates under high oxygen conditions[11]. In *P. aeruginosa* the oxidase is encoded by *cyoABCDE*[4]. In *E. coli* the *cyoABC* encodes the subunits similar to aa_3 I,II,III. The *cyoD* assists in Cu_B binding in subunit I during biosynthesis or assembly of the complex[11,21]. The *cyoE* encodes a protoheme IX farnesyltransferase (heme *o* synthetase), which is required for the synthesis of heme *o* from heme *b*[11,22]. Cyanide-insensitive oxidase (CIO) is a copper-free oxidase and consists of two subunits AB encoded by *cioAB*[4]. These two subunits possess a high homology to the *cydAB* genes encoding the cytochrome *bd*-type quinol oxidase[11,23]. The oxidase has a low oxygen affinity and contains a low-spin heme b_{558}, a high-spin heme b_{595} and heme *d*[11,24]. The *cioAB* genes are upregulated in the stationary phase or at very low oxygen concentrations (0.4 - 0.5 %)[11]. The difference between *bd* oxidase and CIO is the periplasmic loop (Q-loop), which contains the putative quinol binding site, which is significantly shorter in *cioA* compared to the loop in other oxidases[11]. CIO shows high resistance to cyanides[11,24].

NADH dehydrogenase I

In *P. aeruginosa* there are 17 different respiratory dehydrogenases, three of which are different NADH dehydrogenases: complex I (NADH dehydrogenase I), NDH-2 (NADH dehydrogenase) and NQR (Na^+-translocating NADH : ubiquinone oxidoreductase)[9]. All three NADH dehydrogenases transfer electrons from NADH to ubiquinone, but their structure and mechanisms are totally different[25]. Complex I, encoded by *nuoA-N*[4], consists of 14 subunits with a size of 500 kDa and has two [2Fe-2S] clusters (N1a and N1b), six [4Fe-4S] clusters (N2, N3, N4, N5, N6a and N6b) and a non-covalently bound flavin mononucleotide (FMN) as cofactors[13,26](Figure 3). The NUO and NDH-2 are the main dehydrogenases responsible for growth under aerobic conditions[26]. NUO is essential under anaerobic conditions in the presence of nitrate[27]. The NUO is the main entry point for electrons from NADH into the respiratory chain, linking the transfer of two electrons from NADH to ubiquinone with the translocation of four protons across the membrane[25]. The enzyme consists of 14 individual subunits, with the subunits C and D fused together[26].

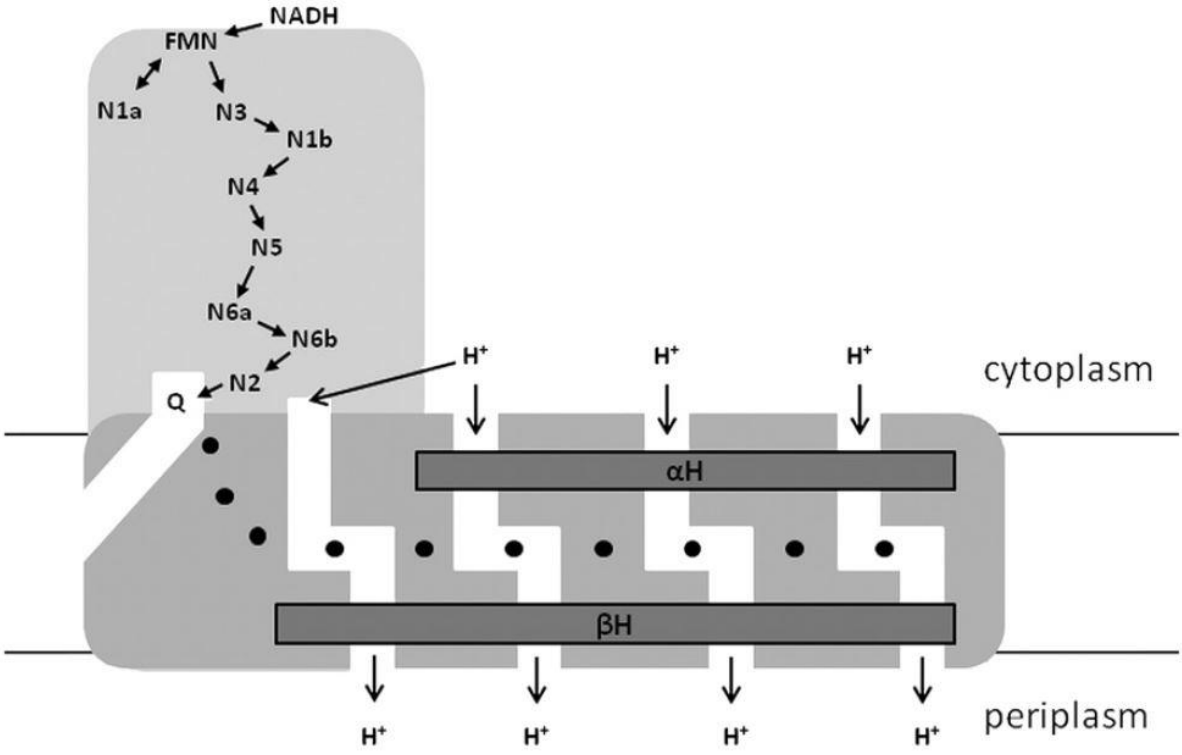

Figure 3: Schematic view of complex I of the respiratory chain (NADH dehydrogenase I). The membrane arm is shown in medium grey and the peripheral arm is shown in light grey. In the membrane arm the horizontal helix (αH) and the β-hairpin helix structures (βH) in dark grey are localized. FMN is the abbreviation for flavin mononucleotide, N*x* stands for the [Fe-S] clusters and Q for ubiquinone. The amino acid residues that form the central hydrophilic axis within the membrane arm are shown as black dots. The adopted proton pathway consists of two half channels each and is illustrated in white like the binding site of ubiquinone[28].

The complex consists of the peripheral arm formed by the globular subunits NuoBCDEFGI and the membrane arm with the polytopic subunits NuoAHJKLMN. The peripheral arm contains

the redox groups: FMN and eight [Fe-S] clusters. In the membrane arm the three subunits NuoLMN show a homology to monovalent cation/proton antiporters involved in proton translocation[28](Figure 3). NADH is oxidized and two electrons are transferred to FMN (first electron acceptor), and further to the ubiquinone binding site *via* the seven [Fe-S] clusters[28]. The reduction site of ubiquinone is unique for membrane proteins. Ubiquinone is reduced by [Fe-S] cluster N2, which is embedded in the peripheral arm above the membrane surface. The hydrophobic ubiquinone is required to move through a tunnel to the reduction site. At the active site, the head group of ubiquinone is bound to ubiquinine binding site *via* a tyrosine and a histidine residue in an electron transfer distance to N2[29]. Two quinone radicals are involved in quinone reduction. It is assumed that the redox reaction of N2 and the reduction of ubiquinone are the key processes of energy conversion[28]. NUO is divided into three major areas: the soluble NADH dehydrogenase module, consisting of NuoEFG with the cofactors FMN and six [Fe-S] clusters; the hydrogenase module, consisting of NuoBCDHIN and the transporter module NuoKLM[28]. The hydrogenase module is amphipathic and part of the multi-subunit membranous hydrogenase [NiFe] family, containing the [Fe-S] clusters N2, N6a and N6b. The transporter module transfers protons across the membrane, thus generating the pmf. Each antiporter subunit (NuoLMN) is a proton pathway consisting of two half channels connected by a hydrophilic axis. The hydrophilic axis consists of charged and polar amino acid residues and is located in the middle of the membrane, traversing the membrane arm along its entire length[28,30]. The fourth proton pathway is formed by the subunits NuoHJK and connects the ubiquinone binding site with the other three proton pathways (NuoLMN). The reduction of N2 and ubiquinone can lead to a conformational change, which is transferred to the membrane arm by electrostatics over a distance of about 180 Å[28,31]. The subunit NuoA codes for a polytopic membrane protein, which could serve as an anchor protein for the further construction of the complex. The ribosome, which translates the *nuo*-mRNA, is directed to the SEC-translocon by the signal recognition particle (SRP) due to the presence of a signal anchor sequence in NuoA. This binds the mRNA to the plasma membrane, which leads to the further translation of NuoB-NuoI (the globular proteins) in the vicinity of the membrane. Together with NuoB, NuoA forms H-bridges, and possibly with NuoCD they provide a platform for further assembly of the dehydrogenase fragment. The further addition of NuoH possibly stabilize the interaction. After strengthening the connection between the peripheral arm and the membrane arm by the addition of NuoJK, the membrane arm is extended by NuoLMN. The subunit NuoL is located at the most distant position in the membrane arm and contains a horizontal helix running parallel to the membrane arm and connecting NuoL with NuoMNJ[28]. It was shown that iron sulfur cluster carrier proteins are involved in the assembly of NUO. In *E. coli* the [Fe-S] cluster carrier protein NfuA has an effect on the activity of NUO, as well as on the succinate dehydrogenase encoded by *sdhABCD*. The protein Mrp, member of the Mrp/NBP35 protein family, has an effect on the activity and stability of NUO. The two proteins NfuA and Mrp are

involved in the transfer of tetranuclear [Fe-S] clusters. Another protein, BolA, is involved in the shaping of cell morphology and in regulatory processes under stress conditions. This seems to be specific for the transfer of the binuclear [Fe-S] cluster N1b in NUO. BolA is not capable of binding an [Fe-S] cluster, therefore it is thought to bind to NuoG and to direct the cluster carrier protein, possibly assisting in [Fe-S] insertion into NuoG. YajL is a multifunctional protein that responds to oxidative stress, has chaperone activity and appears to be involved in tetranuclear [Fe-S] cluster formation. A deletion of the *yajL* gene leads to a doubled formate oxidase activity in the membranes, indicating a metabolic switch to alternative dehydrogenases (e.g. FDH-O). Thus, it could be shown that YajL is also involved in the assembly of NUO[32]. NDH-2, encoded by *ndh*, contains a flavin adenine dinucleotide (FAD) cofactor and is a 46 kDa peripheral protein. The important difference between Complex I (NUO) and NDH-2 is that NDH-2 is not a proton pump[13,25]. NQR, encoded by *nqrA-F*, consists of six subunits and contains a [2Fe-2S] cluster, a riboflavin molecule, a FAD, two covalently bound FMNs and a non-heme Fe center. NQR is an ion pump that specifically transports protons and is resistant to 2-n-heptyl-4-hydroxyquinoline N-oxides (HQNO)[13,27].

Formate dehydrogenase

The oxidation of formate is an important process for energy generation and the reduction of equivalents[33,34]. Formate is a key metabolite for bacteria, being a metabolic product of bacterial fermentation and serves as a growth substrate. Formate is an intermediate in the energy metabolism of various prokaryotes and is used as an electron donor during anaerobic respiration[35]. The reversible conversion of formate to carbon dioxide is catalyzed by formate dehydrogenases (FDHs)[34,36–38]. FDHs are divided into two classes based on whether they require a metal ion for their activity (metal-dependent[37]) or not (metal-independent[39,40]). The metal-independent FDHs are NAD^+-dependent enzymes, which belong to the D-specific dehydrogenases of the 2-oxyacid family and are found in bacteria, plants and fungi[34,36–38]. The metal-dependent FDHs belong to the DMSO family and only occur in bacteria. The metal-dependent FDHs have a tungsten or molybdenum in their active site[38]. The FDHs with molybdenum (Mo-FDHs) vary structurally, but their active site is highly conserved. They are divided into three main classes: 1) the monomeric FDH-H, 2) & 3) the heteromeric (αβγ) membrane-bound respiratory enzymes FDH-N and FDH-O[41]. The molybdenum cofactor (Moco) is present as bis-molybdenum guanine dinucleotide (bis-MGD). All three classes of enzymes generally have a bis-MGD cofactor in their catalytic subunit coordinated by a selenocysteine and a sulfido ligand. An additional cofactor, a [4Fe-4S] cluster, is located in the area of the bis-MGD moiety[42]. FDHs are best characterized from *E. coli*. The FDH-H is associated with hydrogen production and is encoded by the gene *fdhF* and synthesized only under fermentative conditions. FDH-H forms with one of the four [NiFe] hydrogenases (Hyd), Hyd-3, the hydrogen producing formate hydrogenlyase (FHL) enzyme complex. This complex

is synthesized in *E. coli* in the absence of nitrate under anaerobic conditions[43]. FDH-N is induced by the presence of nitrate and is present in high numbers under anaerobic conditions. The enzyme is encoded by the *fdnGHI* operon and is coexpressed with the genes *narGHI*, which encode for the membrane-bound nitrate reductase. The integral FdnI subunit contains a diheme and the FdnH subunit contains four [4Fe-4S] clusters involved in electron transfer during substrate oxidation. The catalytic subunit is the periplasmic FdnG with the bis-MGD cofactor and an additional [4Fe-4S] cluster cofactor in the Moco area. FDH-O is encoded by the *fdoGHI* operon and is expressed under either aerobic or nitrate-respiring conditions. The subunits of FDH-O are arranged similarly to those of FDH-N. The amino acid sequence identity is 75 % between FdnGH and FdoGH and 45 % between FdnI and FdoI. The genes of FDH-O are co-expressed together with the genes *narZYV*[38]. All three FDHs contain the bis-MGD with an oxidized Mo^{IV}, whereby the selenocysteine and the sulfido group coordinate the Mo-ion in a distorted hexacoordinated trigonal prismatic geometry[41]. Formate does not directly bind to the Mo-ion, but instead resides in the 2nd coordination sphere. The proton is transferred to the sulfido group, while the two electrons are transferred to the Mo-ion. The CO_2 product forms a thiocarbonate group with the Cys ligand and cannot be released while the active site is still oxidized with two electrons[41]. The chaperone FdhD is essential for the insertion of the terminal sulfido ligand of Moco in FdhF, FdnG and FdoG. In the sulfuration of bis-MGD, FdhD interacts with the L-cysteine desulfurase IscS. The conserved CXXC motif of FdhD with the cysteines 121 and 124 is supposed to be involved in the sulfur transfer process from IscS to bis-MGD[42]. The inactivation of FdhD leads to the loss of FDH-H and FDH-O activity, but has no effect on protein synthesis[42,43]. By sequence analyses of bacterial and archaeal genomes of five phyla and 33 taxonomic families a phylogenetic tree was obtained (Figure 4). This can be divided into three groups. In group I FdhDs of α-, β- and γ-Proteobacteria are to be found, which include *P. aeruginosa* and *E. coli*. In group II are Actinobacteria, as well as Cyanobacteria, Archaea and γ- and δ-Proteobacteria. Group III contains a larger group of Archaea, additionally Bacilli and Clostridia, as well as γ-, δ- and ε-Proteobacteria. FdhE-like proteins are found in γ-Proteobacteria and some β-Proteobacteria, but never in ε-Proteobacteria. The corresponding gene is always genetically linked to the structural genes for formate dehydrogenase. The deletion of FdhE leads to an inactivation of Fdn and Fdo, but the activity of FdhF is not affected. Normal levels of the FdnI subunit were detected, while the FdnGH was not detected anymore[44]. FdhE is not required for transcription or translation[45].

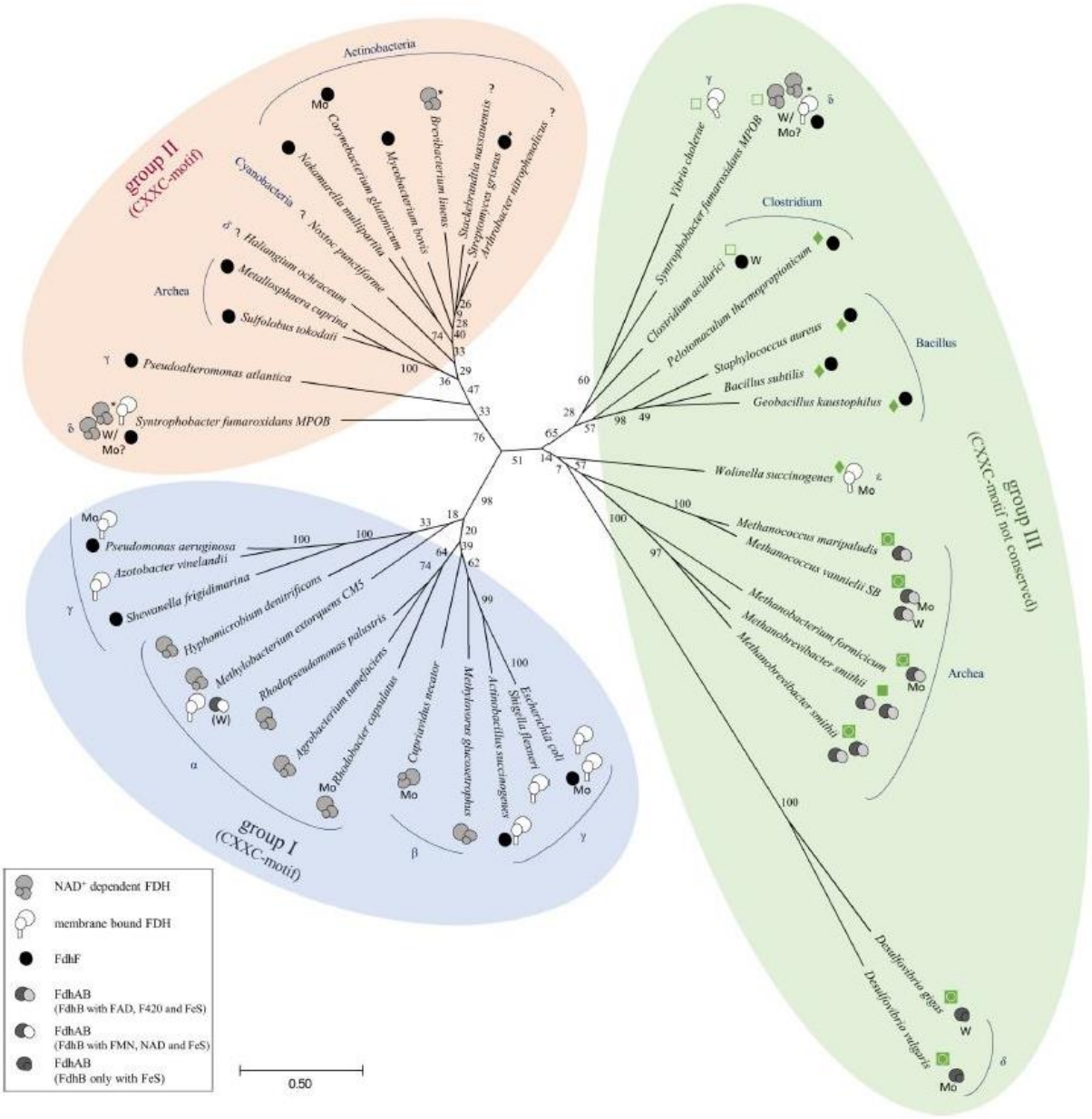

Figure 4: Phylogenetic tree of metal-dependent FDHs based on genome-derived amino acid sequences of FdhD. Domains and classes of prokaryotes are marked in blue: α-Proteobacteria, β-Proteobacteria, γ-Proteobacteria, δ-Proteobacteria, ε-Proteobacteria. There are three main branches. FdhD homologues in group I and II harbor the conserved CXXC-motif, which is not present in group III (♦ - CC-motif, □ - only second cysteine, ■ – CXXXCXC-motif, ◙ - no cysteine)[42].

The FdhE is an iron-binding rubredoxin, present as a monomer or homodimer which interacts with the catalytic subunit G. It is not part of the crystallographically defined complex of the formate dehydrogenase, so there is a possibility that it is needed for reductive activation from the G subunit before it is transported into the periplasm. The homodimer form is stabilized by anaerobiosis. FdhE contains four conserved CXXC motifs at the C-terminus[46], which is essential for physiological activity and is involved in Fe(III) ligation. Each protomer contains two Fe(III), each bound by two CXXC motifs, resulting in the typical rubredoxin-like geometry. The FdhE is most likely involved in electron transfer, like other rubredoxins[46,47]. In

P. aeruginosa the monomeric FDH-H is encoded by PA5181 and the FDH-O encoded by *fdnGHI* are present[42].

Anaerobic respiration *via* Denitrification

Nitrate is used by bacteria for two functions: 1) as nitrogen source for the synthesis of nitrogen-containing molecules (assimilatory nitrate reduction) and 2) as electron acceptor (dissimilatory nitrate reduction)[17]. In the absence of oxygen *P. aeruginosa* is able to grow by dissimilatory nitrate respiration, the nitrogen oxides serve as terminal electron acceptors replacing oxygen[11]. Complete denitrification consists of four steps to reduce nitrate to molecular nitrogen. Each final step of an electron transfer pathway is catalyzed by an individual metal enzyme: nitrate reductase, nitrite reductase, nitric oxide reductase and nitrous oxide reductase (Figure 5)[11,48]. The first step of denitrification is the reduction of nitrate to nitrite, which is catalyzed by the nitrate reductase (NAR) in the following reaction: $NO_3^- + 2H^+ + 2e^- \rightarrow NO_2^- + H_2O$[48]. *P. aeruginosa* contains three types of nitrate reductase: the NAR, the NAP and the NAS, which are located in the cytoplasmic membrane, in the periplasm and in the cytoplasm respectively[4,9,11]. All three nitrate reductases belong to the dimethylsulphoxide (DMSO) reductase family and contain a molybdenum cofactor in the form of a molybdopteringuanine dinucleotide (bis-MGD) as prosthetic group[9,11]. NAR is responsible for anaerobic nitrate respiration[11,49] and is encoded by *narK1K2GHIJ*[4]. The subunits *narK1K2* are nitrate/nitrite antiporters, where NarK2 is necessary for growth under denitrifying conditions[11,50]. Nitrate is transported into the cytoplasm *via* this antiporter, where it gets reduced to nitrite, which in turn is transported into the periplasm *via* the same antiporter[17]. The subunits NarGHI are the structural subunits, with the the cytoplasmic catalytically active NarG (118 - 150 kDa), the cytoplasmic NarH (55 - 64 kDa) and the transmembrane NarI (19 - 21 kDa)[9]. NarI is the cytochrome *b* subunit which oxidizes the quinol on the periplasmic side. Two protons are translocated into the periplasm during nitrate reduction contributing to the proton gradient[51]. The two electrons are transferred *via* heme *b* from NarI across the membrane to the [Fe-S] clusters of NarH. From there they are transferred to the bis-MGD subunit NarG which reduces nitrate to nitrite[9,48]. The protein NarJ and cardiolipids are involved in the formation of the complex with its different cofactors[48]. The *narXL* genes upstream of *narK2* encode a two-component transcriptional regulator[11]. The periplasmic nitrite reductase catalyzes the second step by the following reaction: $NO_2^- + 2H^+ + e^- \rightarrow NO + H_2$[48]. *P. aeruginosa* contains a cytochrome cd_1-type nitrite reductase encoded by the gene cluster *nirSMCFDLGHJEN, nirS* is the structural gene for the enzyme. The nitrite reductase NirS is a homodimer, each dimer consists of a subunit with covalently bound electron-receiving heme *c* and non-covalently bound heme d_1, which is the catalytic active side and reduces nitrite to nitric oxide[9,11,48]. NirM

and NirC encode two monohaem *c*-type cytochromes. NirM is a cytochrome c_{551}, which has the function of an electron donor for nitrite reductase. A functional cytochrome bc_1 complex (complex III) is essential for the reduction of nitrite and is involved in the electron transfer from the quinol pool to NirS *via* NirM[9,11]. The genes *nirFDLGHJE* are involved in the biosynthesis of heme d_1. A further *c*-type cytochrome is encoded by *nirN*, there is a similarity to *nirS*, but the function is not clarified[11].

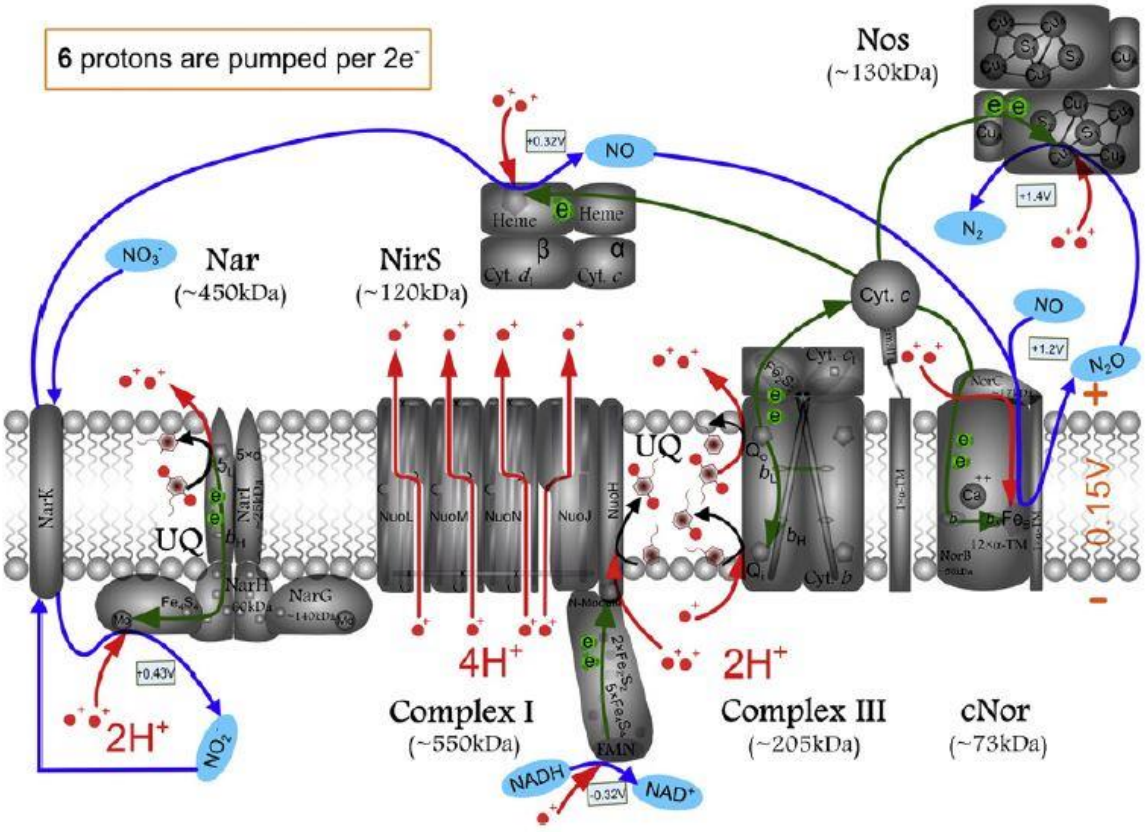

Figure 5: The canonical respiratory chains of denitrification. Electrons are transferred from NADH to NOx reductases (e.g. nitrate, nitrite, nitric oxide and nitrous oxide reductases) *via* complex I, ubiquinone/ubiquinol, complex III and cytochrome *c* respectively. Protons are removed from the cytoplasm by complex I, complex III (Q-cycle) and the cytoplasmic subunit of nitrate reductase. Overall, the contribution to the proton motive force is six protons per electron pair[12].

The third step of denitrification is catalyzed by the nitric oxide reductase by the following reaction: $2NO + 2H^+ + 2e^- \rightarrow N_2O + H_2O$[48]. The nitric oxide reductase (NOR) is encoded by *norCBD* and is a membrane-bound cytochrome *bc* complex that receives electrons from soluble cytochrome *c*. The NOR has no proton pumping activity and obtains electrons from the cytochrome bc_1 complex (complex III) *via* the soluble cytochrome *c*. The membrane-bound subunits NorC (17 kDa) and NorB (53 kDa) are cytochrome *c* and cytochrome *b* subunits[9]. NorC mediates the electron transfer from soluble cytochrome *c* to the catalytic NorB. NorB contains the binuclear catalytic center, which coordinates the two NO substrates[48] consisting of heme b_3 and a non-heme Fe_B and a further heme *b*[9]. Required for the production of the active enzyme is presumably a soluble protein encoded by *norD*[11]. NOR not only serves as a respiratory enzyme, but also as a detoxifying enzyme for exogenous NO[11]. The *nirQOP* operon

is located between *nirS* and *norCB*. It is assumed that NirQ is required for fine-tuning the expression and activation of NIR and NOR. The *nirOP* genes encode transmembrane proteins[4,11]. The last step, where nitrous oxide is reduced to molecular nitrogen, is catalyzed by nitrous oxide reductase (NOS) after the following reaction: $N_2O + 2H^+ + 2e^- \rightarrow N_2 + H_2O$[48]. The NOS is a periplasmic enzyme encoded by *nosRZDFYL*[4,9,11]. The structural gene for the enzyme is *nosZ* and the periplasmic domain of the transmembrane Fe/S flavoprotein NosR is essential for NosZ function[48]. The lipoprotein NosL is a copper-binding protein, localized in the periplasm, anchored to the outer membrane and involved in NosZ maturation[48]. The *nosDFY* genes encode proteins involved in the processing and insertion of copper into the enzyme[11]. NosZ has two types of copper centres, the mixed-valent dinuclear Cu_A on the electron entry side and the tetranuclear Cu_Z centre on the catalytically active side, where nitrous oxide is reduced to molecular nitrogen. NosZ obtains the electrons from the cytochrome bc_1 complex (complex III) *via* the soluble cytochrome *c*[11].

Periplasmatic nitrate reductase

P. aeruginosa contains three types of nitrate reductase: the NAS, the NAR and the NAP, which are located at the cytoplasm, in the cytoplasmic membrane and in the periplasm[4,9,11]. All three nitrate reductases belong to the dimethylsulphoxide (DMSO) reductase family and contain a molybdenum cofactor in the form of molybdopterin guanine dinucleotide (bis-MGD) as prosthetic group[9,11]. NAS is an assimilatory nitrate reductase located in the cytoplasm, it reduces NO_3^- to NH_4^+ which serves as a nitrogen source for the synthesis of nitrogenous molecules[9]. The gene cluster consisting of the three genes PA1781-PA1780-PA1779 are annotated for *nirB*, *nirC* and *nasC*. The genes *nirB* and *nirC* encode for the large and small subunit of an assimilatory nitrite reductase. The putative assimilatory nitrate reductase is encoded by *nasC*. The NAS contains a bis-MGD cofactor and a [4Fe-4S] cluster. NAR is cytoplasmic membrane-bound and encoded by *narK1K2GHIJ*[4]. The subunits NarGHI are the structural subunits, with the the cytoplasmic catalytically active NarG (118 - 150 kDa), the cytoplasmic NarH (55 - 64 kDa) and the transmembrane NarI (19 - 21 kDa)[9]. The NAP is encoded by *napEFDABC* operon, consists of two subunits and is located in the periplasm, with the catalytic bis-MGD cofactor and [4Fe-4S] cluster containing NapA (90 kDa) and the biheme cytochrome *c* NapB (13 - 19 kDa). The membrane-bound tetraheme cytochrome *c*, encoded by *napC*, is required by NapAB for electron transfer (Figure 6)[9]. NapD is essential for NapAB activity and is postulated to function as a chaperone involved in NapAB maturation prior to export to the periplasm. The non-heme iron sulfur protein NapF is possibly playing a role in the post-translational maturation of NapA[52].

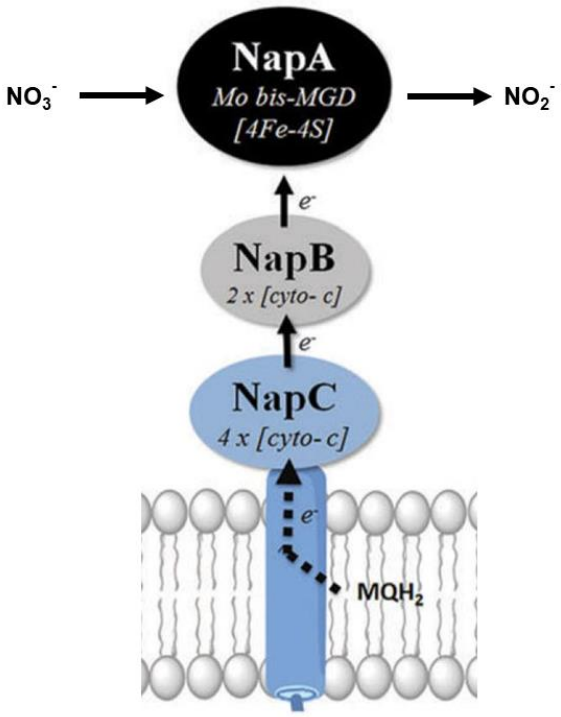

Figure 6: Schematic model of NAP of *P. aeruginosa.* The electrons are derived from the quinone pool and are transferred *via* NapC and NapB to the catalytic subunit NapA[53].

Periplasmic nitrate reductase is a quinol oxidase where the oxidation of quinol and the electron transfer to nitrate for reduction to nitrite does not result in the formation of a redox loop and thus no contribution to the pmf is achieved[9,11]. In nature, nitrate reduction is coupled with formate oxidation, resulting in a proton gradient formation across the membrane[53]. In *Pseudomonas sp*. G-179 NAP is the only nitrate reductase and responsible for anaerobic growth. In *E. coli* NAP is induced under anaerobic conditions, but at very low nitrate concentrations. This suggests that NAP plays a supporting role in anaerobic respiration under nitrate limiting environmental conditions[9]. Denitrification is not a solely anaerobic process, since it has been shown in *P. aeruginosa* to be capable of aerobic denitrification. Aerobic denitrification is a respiratory process that supplements or competes with aerobic respiration[9,54]. In a switch from aerobic to anaerobic conditions with nitrate addition, it has been shown that there is no difference in the expression of NAP in *P. aeruginosa*[9]. Furthermore, it was shown that NarL directly represses the expression of NAP, since there is a maximum induced expression of NAR during anaerobic growth[52]. Kinetic studies of α-, β- and γ-Proteobacteria show that NapA has a relatively high affinity to nitrate. The Moco is located 15 Å inside the protein, where the molybdenum (Mo) is coordinated by four dithiols sulphur and a fifth sulphur ligand derived from a conserved cysteine residue in the active site of NapA[53,55]. Two different proposed catalytic mechanisms for nitrate reduction were identified. In *Desulfovibrio desulfuricans* the Mo is present in the reduced +IV state, being penta-coordinated. The nitrate binds *via* an oxygen atom, thus Mo is sixcoordinated. Nitrate is reduced to nitrite, the bound oxygen of nitrate is transferred to Mo and serves as terminal oxo

group. The Mo is oxidized and in +VI state, the terminal oxygen is protonated to water. The reduction of Mo by releasing water regenerates the penta-coordinated state of Mo in the +IV state. In *E. coli* nitrate binds to the penta-coordinated Mo in the +V state *via* an oxygen atom. Thus, Mo is sixcoordinated reduced by one electron to Mo +IV. Nitrate is reduced to nitrite and released. Mo is oxidized to monooxo-Mo (+VI) and protonated, resulting in a sixcoordinated Mo +VI state with coordinated water. This state is reduced by one electron and water is released, resulting in the regeneration of Mo in the +V state[53].

1.3 Flagellum

The flagellum is a supramolecular complex consisting of three parts: the basal body (reversible motor), the hook (universal joint) and the filament (helical propeller)[56–59]. Bacteria like *E. coli* and *Salmonella enterica* serve as model organisms[58] to investigate the structure, assembly and function. The flagellar assembly begins with the basal body, followed by the hook and ending with the filament (Figure 7)[59]. The basal body consists of the C (cytoplasmic) ring, the MS (membrane/supermembrane) ring, the P (peptidoglycan) ring, the L (lipopolysaccharide) ring and the rod. The C, MS, P and L rings are located in the cytoplasm, cytoplasmic membrane, peptidoglycan and outer membrane respectively[58,59]. The rod is a drive shaft with an average length of 30 nm, consisting of three proximal rod proteins (FlgB, FlgC and FlgF) and one distal rod protein (FlgG), traverses the periplasmic space and connects rotor rings with the hook[58,60]. The flagellar motor consists of two parts: 1. the rotor, with the C, MS, LP rings and 2. over a dozen stator proteins[57]. The C-MS ring complex is a reversible rotor consisting of the C ring with the proteins FliG, FliM and FliN and the MS ring consisting of a single protein, FliF[58,59]. The proteins FlgH and FlgI accumulate around the rod in the peptidoglycan layer and the outer membrane and form the LP ring, which acts as a molecular bushing[58]. The flagellar motor can rotate at a speed of 200 - 300 Hz, this in both directions (clockwise and counter clockwise), starting from the view from the filament to the basal body[60]. The proteins of the C ring are responsible for changing the direction of motor rotation. By binding phosphorylated response regulator CheY, a chemotactic signaling protein, to FliM and FliN, a co-operative confirmation change is induced in the FliG ring, causing the motor to rotate clockwise[56–58].

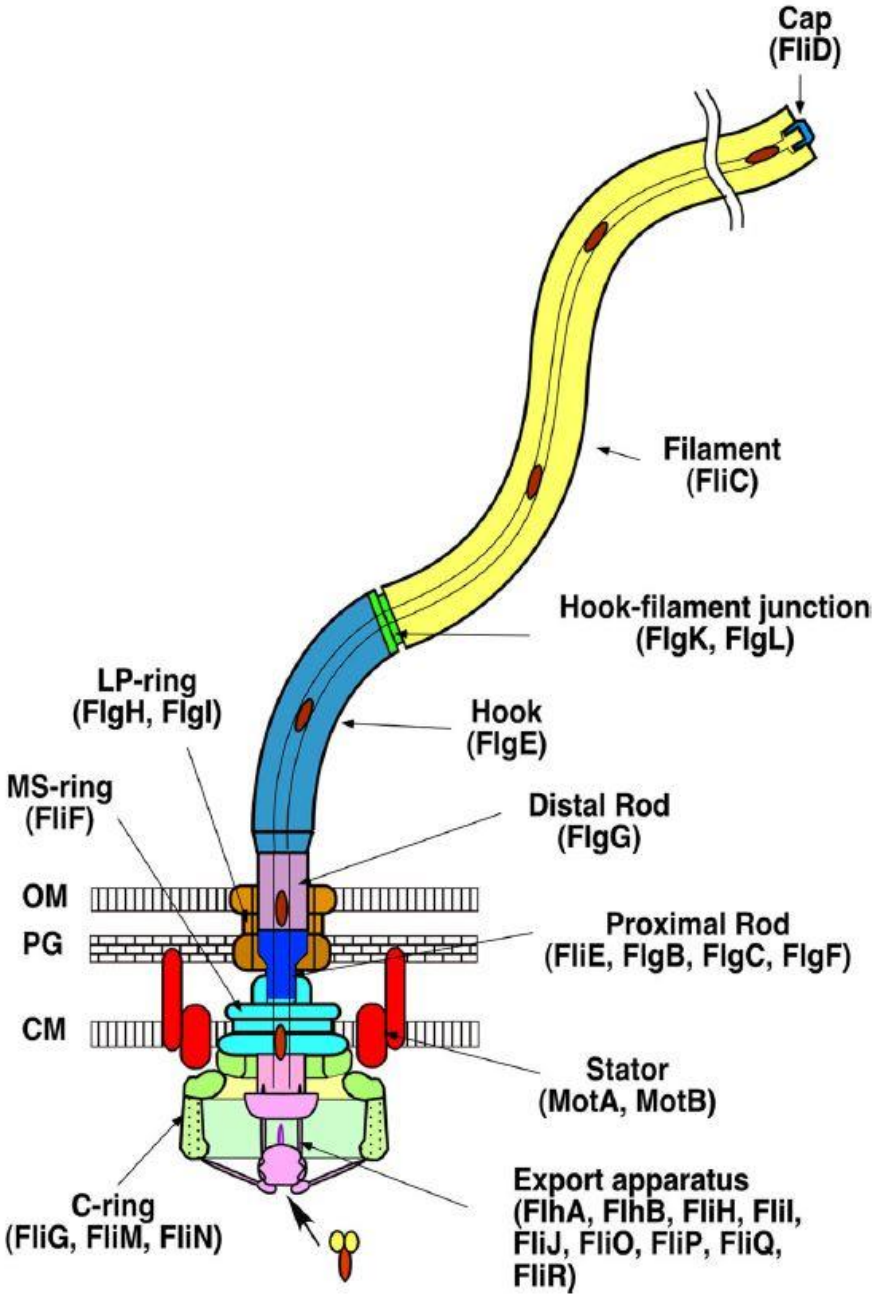

Figure 7: Structure of the bacterial flagellum. Different functional units are represented in different colors. Each functional unit has its specific component proteins. The export apparatus is shown in light purple, consisting of FlhA, FlhB, FliH, FliI, FliJ, FliO, FliP, FliQ and FliR. The C-ring colored in light green consist of FliG, FliM and FliN. The stator is shown in red consisting of MotA and MotB. The MS-ring consists of FliF and is colored in light blue. The proximal rod is colored in blue and consists of FliE, FlgB, FlgC and FlgF. The distal rod consists of FlgG and is colored in purple. The LP-ring covers the proximal and distal rod, colored in brown and consists of FlgH and FlgI. The hook is colored in medium blue and consists of FlgE. The Filament consists of FliC and is colored in yellow. Between the hook and the filament, the hook-filament junction is located, consists of FlgK and FlgL colored in green. The cap is on the top of the filament consists of FliD and colored in blue. CM inner membrane, PG peptidoglycan layer, OM outer membrane[60].

The flagellar motor consists of over a dozen stator proteins distributed around the C-MS ring[56,57]. The stator contains an ion channel that contacts the peptidoglycan layer and converts the ion flow through the channel into mechanical work required for flagellar motor rotation. The stators are not permanently bound around the motor. The stator is formed by four MotA

proteins and two MotB proteins that form the proton channel. The stator is anchored in the peptidoglycan layer *via* a typical OmpA-like structure located in the C-terminal periplasmic domain of MotB[57,58]. The basal body contains a specific protein export apparatus, which is required for the formation of the flagellum[58,59]. The protein export apparatus is a type-3 secretion system and is similar to the injectisome. *Via* the type-3 protein export apparatus, 14 flagellar proteins are transported in a central channel inside the growing structure and assemble at the distal end[59]. The type-3 protein export apparatus consists of a transmembrane export gate complex formed by FlhA, FlhB, FliP, FliQ and FliR and a cytoplasmic ATPase complex consisting of FliH, FliI and FliJ[59]. The proteins FliM and FliN of the C ring are the binding site for the cytoplasmic ATPase complex in conjunction with the export substrate and export chaperone substrate complexes[59]. The proteins FlhA, FlhB, FliP, FliQ and FliR form the transmembrane export gate complex within the MS ring[59,61]. The protein FlhA contains a hydrophobic N-terminal transmembrane domain and a large C-terminal cytoplasmic domain. A cytoplasmic ring structure is formed by nine C-terminal domains of FlhA, creating an ion channel that conducts protons and sodium ions, which plays an important role in the energy-coupled mechanism with the cytoplasmic ATPase[58,59]. The transmembrane domain interacts with FlhB, FliF and FliR[59,61]. The cytoplasmic domain of $FlhA_9$ interacts with FliH, FliI, FliJ, flagellar type-3 export chaperones and export substrates and thus coordinates flagellar protein export with assembly[59]. A conserved dimple is directly involved in the interaction with the FlgS, FliS and FliT chaperones in complex with their substrates. The protein FlhB is involved in a substrate specific switching with a secreted molecular ruler protein, FliK. FliK is secreted *via* the type-3 protein export apparatus during hook formation. FlhB consists of a hydrophobic N-terminal domain and a relatively large C-terminal cytoplasmic domain[59]. The C-terminal domain of FliK binds to the C-terminal domain of FlhB, thereby terminating the export of rod and hook proteins and initiating the export of filament proteins[59,62]. The proteins FliP, FliQ and FliR form the core structure of the transmembrane export gate complex[59,61]. The structure of the core complex assumes a right-handed helical assembly consisting of five FliP, four FliQ and one FliR. FliP and FliR form a $FliP_5FliR_1$ complex and the four FliQ subunits are attached to the outside of this complex, with FliR stabilizing the helical structure. The assembled $FliP_5FliQ_4FliR_1$ core complex has a central pore with a diameter of 1.5 nm and is likely the protein translocation channel[59,63]. The transmembrane protein FliO is required for an efficient assembly of the export gate complex, but it is not essential for flagellar protein export[59,61]. The protein FliO consists of an N-terminal periplasmic tail, a single transmembrane helix and a C-terminal cytoplasmic domain. FliO forms a 5 nm ring structure with three flexible clamp-like structures that bind to FliP to support FliP oligomerization[59,61]. The FliO ring complex protects FliP from proteolytic degradation and promotes stable $FliP_5FliR_1$ complex formation[59]. The FliO ring complex acts as a structural scaffold to support the helical structure of the $FliP_5FliR_1$ complex[59,61]. The cytoplasmic ATPase ring complex consists of 12 FliH, six FliI and

one FliJ[59,64]. Hydrolysis of ATP by the ATPase ring complex activates the transmembrane protein export gate complex through the interaction between FliJ and FlhA. This enables the protein export gate complex to use the pmf across the cytoplasmic membrane to transport flagellar proteins[58,59]. The $FliH_{12}FliI_6FliJ_1$ complex is structurally similar to the F-type ATPases, indicating an evolutionary relationship[59,64]. FliI is a Walker-type ATPase and forms a homo-hexamer for the full exercise of its ATPase activity. ATP binds to the ATP binding site located between the FliI subunits in the ring structure, indicating that ring formation is required for ATP hydrolysis. FliJ binds at the center of the FliI ring structure and promotes the formation of the hexameric structure. The highly conserved amino acid residues on the surface of FliJ are involved in the interaction with FlhA. This interaction coordinates ATP hydrolysis through the $FliI_6$ ring with proton-coupled protein export[58,59]. FliH forms a homodimer and forms a $FliH_2FliI_1$ complex with FliI in the cytoplasm[58,59]. Flagellar export chaperone substrate complexes bind to $FliH_2FliI_1$ through an interaction between the FliI ATPase and the chaperone[59]. The $FliH_2FliI_1$ complex assumingly acts as a dynamic carrier to bring export substrate and chaperone-substrate complexes from the cytoplasm to the transmembrane export gate complex[59]. The C ring is required to efficiently recruiting the $FliH_2FliI_1$ complex to the protein export apparatus for efficient flagellar protein export[59]. The hook, a short segment with an average length of 55 nm and is formed by the protein FlgE which functions as a universal joint that transmits motor torque to the filament. Between the hook and the filament is the hook-filament junction, which consists of FlgK and FlgL[60]. The filament bears a thin structure with a diameter of 20 nm and a length of 15 µm. The filament is formed by over 20,000 flagellar filamentary protein subunits, the flagellin FliC[60]. The flagellin FliC consists of three domains, D0, D1 and D2, where D0 and D1 are conserved domains and D2 is a variable[65]. The D0 domain consists of N-terminal and C-terminal helices that form a coiled-coil structure. The D0 domain stabilizes the filament structure and the subunit interactions are hydrophobic[60]. The D1 domain consists N-terminal of two α-helices and two β-sheets and C-terminal of one α-helix, it is folded into a rod-shaped structure. The variable D2 domain has a cup-like structure containing of two β-sheets with a handle and an α-helix[65]. At the distal end of the filament a star-shaped homo-pentamer, consisting of FliD, is attached as a cap. FliD not only functions as a cap at the open end of the filament, it also assists in the formation of flagellin below the pentameric structure[60].

1.4 Vesicles

Membrane vesicles (MV) occur in all three domains of life[66,67]. There exist several types of membrane vesicles: outer membrane vesicles (OMV), outer-inner membrane vesicles (OIMV), cytoplasmic membrane vesicles (CMV) and tube-shaped membranous structures (TSMS)[68–70]. The size of membrane vesicles is between 20 - 400 nm in diameter. They affect various

biological processes involving virulence, horizontal gene transfer, export of cellular metabolites, phage infection and cell-cell communication[66,70,71]. The structure and composition of the MV is the result of the various forms of formation. A further option for the formation of MV is the phage-endolysin triggered cell lysis (Figure 8)[70].

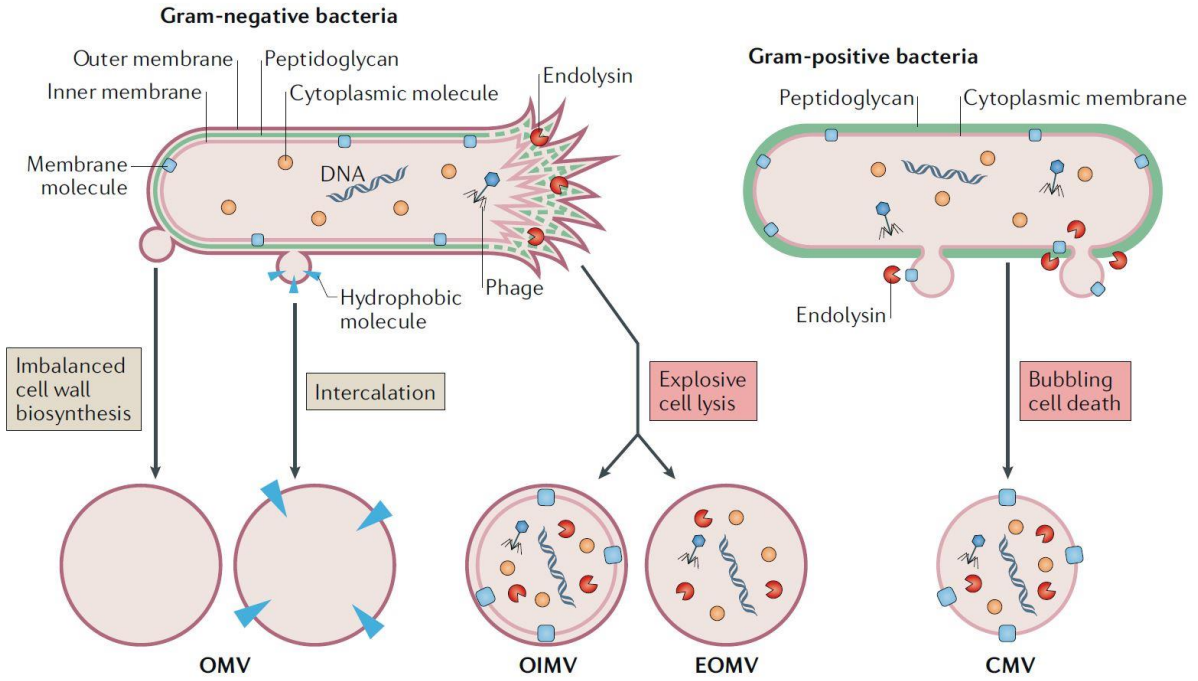

Figure 8: Several routes of MV formation lead to different types of membrane vesicle. In Gram-negative bacteria two routes and in Gram-positive bacteria only one route are proposed to exist. The two main routes in Gram-negative bacteria for vesicle formation are blebbing of the outer membrane and explosive cell lysis. Blebbing leads to the production of outer membrane vesicles (OMV) and appears as a result of cell envelope disturbance, caused by the intercalation of hydrophobic molecules in the outer membrane or an imbalance in the peptidoglycan biosynthesis. Explosive cell lysis is caused by an endolysin which disrupts the peptidoglycan layer. The cell rounds and explodes, the membrane fragments round and self-assemble into outer inner membrane vesicles (OIMV) and explosive outer membrane vesicles (EOMV). In Gram-positive bacteria, cytoplasmic membrane vesicles (CMV) are proposed to be derived from endolysin-triggered bubbling cell death[70].

The MV formed by cell lysis differ from those formed by blebbing of living cells in their composition and content, which has an influence on their function[70]. The MV produced by Gram-positive bacteria by blebbing are CMV, as they lack the outer membrane, but CMV can also be produced by dying cells[69,70]. In the Gram-negative bacterium *Acidiphilium cryptum* JF-5 large intracellular vesicles were found under anaerobic growth conditions[70,72]. TSMS are nanotubes, nanowires or nanopods and are formed by different bacteria, they are located on the cell surface and form bridges between cells. In Gram-positive bacteria, the tube-like structures are protuberances of the cytoplasmic membrane and serve for the exchange of cytoplasmic content such as proteins and plasmid DNA[70,73]. In Gram-negative bacteria, the protrusion consists of the outer membrane and enables the intercellular transfer of periplasmic metabolites, membrane proteins and lipids[70,73]. The simplest version is a structure formed by a chain of OMVs (*Mycococcus xanthus*, *Shewanella oneidensis*)[70,74,75]. OMVs are spherical particles composed of the asymmetric bilayer of the outer membrane, which consists of an

outer leaflet containing lipopolysaccharides and an inner leaflet containing phospholipids[70,76]. The classical OMVs are formed by blebbing of Gram-negative bacteria and exhibit membrane proteins. Furthermore, the specific lipid composition and the content of the vesicles shows a dependence on the present growth conditions[70,77,78]. Vesicles containing periplasmic and cytosolic components as well as RNA and DNA are OIMVs[70,79]. There are two principal ways of vesicle formation in Gram-negative bacteria. 1) blebbing of membrane vesicles in living cells, which results in the classical OMVs and 2) endolysin-triggered cell lysis, which leads to OIMVs and EOMVs formation[70]. “Blebbing results from cell envelope disturbances caused by an unbalanced biosynthesis of cell wall components or the intercalation of hydrophobic molecules into the outer membrane”[70]. OMVs are released during normal cell growth without affecting cell viability. Growth conditions may have an influence on vesiculation[70,80]. Cell-cell communication is mediated by quorum sensing. The N-acyl homo-serine lactone (AHL) is the most widely used signal for quorum sensing in proteobacteria. *P. aeruginosa* has two types of AHLs C4-HSL and 3-oxo-C12-HSL and a quinolone signal, the *Pseudomonas* quinolone signal (PQS). These three signals belong to the global transcription factors, which are recognized by specific receptors and mediate the expression of over 200 genes, including those for pathogenicity[71]. In *P. aeruginosa* the MVs are involved in quorum sensing. PQS induces MV formation by intercalating into the outer leaflet of OM[70,71,81]. In *P. aeruginosa*, DNA-damaging stress induces the expression of endolysin, as part of the pyocin biosynthesis gene cluster, leading to the degradation of peptidoglycan[68,70]. As a consequence, cells are rounding up and finally explode. This phenomenon is called explosive cell lysis. The remaining membrane fragments self-assemble to EOMVs[68,70]. For the formation of OIMVs, a model exists that the peptidoglycan layer is weakened by autolysin, which causes the inner membrane to invert into the periplasm and allows cytoplasmic components to enter the vesicles[70]. Gentamycin destabilizes the OM of *P. aeruginosa* and leads to the formation of membrane blebs, vesicles and the formation of holes in the cell surface[79,82]. The gentamycin-induced MVs belong to the OIMVs because they consist of inner and outer membranes and contain DNA and enzymes that are part of the pathogenicity. There are MVs that contain autolysin, members of the glycosidases, amidases and endopeptidases, which are called predatory MVs. They have an enzyme mix of hydrolytic enzymes that lyse the peptidoglycan sacculus[82]. *P. aeruginosa* produces vesicles by PQS induction during planktonic growth[81,83,84] and by RecA-mediated SOS response in interstitial biofilms[68,81], but PQS also plays a role in vesicle formation by biofilms[81]. The content of the vesicles differs between biofilm and planktonic growth. The MVs of planktonic cells contain virulence factors like LasA, LasB and alkaline protease B. The MVs from the biofilm contain proteins for iron uptake such as FptA[71].

1.5 Protein-protein interaction

Proteins are the active components of living cells. The aim of proteomics analyses is to investigate the identity, amount, localization and dynamics of all these proteins. It has been discovered that the human genome consists of 19,000 genes coding for ~500,000 proteins[85,86]. Over 80 % of all proteins interact with another protein and form stable or transient complexes[86–88]. The protein-protein interactions (PPI) play an important role in all biological processes, such as metabolism, structural organization, transport, transcription, immune response and cell cycle control[86,89,90]. The holistic investigation of PPI at large scale, using methods of the so-called interactomics, provides the basis for the systematic understanding of the dynamics of the protein networks. The molecular basis underlying the organization of the proteome is one of the most important targets of systems biology research, which is concerned with clarifying of the function, location and dynamic aspects of this cellular system. For this purpose, mapping of the PPI network of model organisms and humans is currently being established[86,91]. PPI can be divided into two main categories based on the arising contact interfaces: Domain-domain and domain-motif interactions. The domain-domain interaction describes the bond between two globular domains, resulting in a large contact interface (~2000 Å). This is characterized by a relatively strong affinity in the low nanomolecular or even picomolar range. In domain-motif interaction, a short linear motif (~20 - 30 amino acid residues) of one protein binds to the domain of the interaction partner. The resulting contact interface is small (~300 - 500 Å) and characterized by an affinity in the low to medium nanomolar range[86,92]. For the investigation of PPIs, a variety of experimental methods exist, based on biophysical, biochemical or genetic principles (Figure 9). Each of these methods has its strengths and limitations in terms of sensitivity and specificity[86]. The biophysical methods include: Fluorescence polarization measurement (FP), surface plasmon resonance (SPR)[93] spectroscopy, nuclear magnetic resonance (NMR) spectroscopy, circular dichroism spectroscopy, static and dynamic light scattering, analytical ultracentrifugation (AUC), isothermal titration calorimetry (ITC) and microscale thermosetting (MST).

Figure 9: Several methods for the investigation of protein-protein interactions. The biophysical methods: Fluorescence polarization (FP), surface plasmon resonance (SPR), nuclear magnetic resonance (NMR), circular dichroism, static and dynamic light scattering, analytical ultracentrifugation (AUC), isothermal titration calorimetry (ITC) and microscale thermosetting (MST).The biochemical methods: Fluorescence and bioluminescence resonance energy transfer (FRET/BRET), AlphaScreen and AlphaLISA, protein fragment complementation assay (PCA), pull down, tandem affinity purification (TAP), single affinity purification, enzyme-linked immunoabsorbent assay (ELISA), co-immunoprecipitation (Co-IP) and cross-linking. The genetic methods: phage display, yeast two-hybrid system and other two-hybrid systems and protein microarray[86].

The genetic methods include: phage display, yeast two-hybrid (Y2H)[94,95] system and other two-hybrid systems and protein microarray analyses. In the two-hybrid systems, the bait and the prey protein, whose interaction is to be investigated, are co-expressed. In Y2H one of the two domains of GAL4 is fused to the bait and the other to the prey protein, so that the interaction of bait and prey results in the reconstitution of a functional GAL4 allowing the transcription of GAL4-*lacZ* reporter gene, which in turn allows to measure the resulting β-galactosidase activity. The Y2H system is a powerful technique for the identification and analysis of PPIs *in vivo*[86]. The two-hybrid system in *E. coli* has some advantages compared to Y2H, as cell compartments are lacking and there is a fast growth rate[86]. The bacterial adenylated cyclase two-hybrid (BACTH) system, for example, is based on the reconstitution

of the adenylate cyclase activity analogously to GAL4. The strength of the bait-prey interaction can be deduced from the coupled β-galactosidase activity assay[86,95,96]. The genetic methods Y2H, phage display and protein microarray are used for PPI identification and PPI network mapping[86]. The biochemical methods include: Fluorescence and bioluminescence resonance energy transfer (FRET/BRET), AlphaScreen and AlphaLISA, protein fragment complementation assay (PCA), affinity chromatography and cross-linking[86]. Affinity chromatography is used to separate and purify specific molecules from complex mixtures. This method is based on the specific interaction between two molecules such as enzyme and substrate, antibody and antigen, and receptor and ligand. This type of technology includes pull down[97], tandem affinity purification (TAP), single affinity purification and antibody-based methods such as enzyme-linked immunoabsorbent assay (ELISA) and co-immunoprecipitation (Co-IP)[86,98]. In the TAP method a dual-affinity TAP tag is fused to the bait protein and purified using two different affinity chromatographies[86,99]. These two purifications decrease the unspecific background compared to simple affinity chromatography[86,100]. TAP tags include FLAG, HA, Myc, streptavidin-binding peptides (SBP), StrepII and *Streptococcus* Protein G (ProtG)[86]. For the identification of interaction partners, affinity chromatography is in many cases coupled with mass spectrometry techniques (MS)[86,90]. By combining affinity purification and mass spectrometry (AP-MS), multi-protein complexes can be isolated directly from the cell lysate and complex components can be identified by MS. The AP-MS method can be performed under physiological conditions. An advantage of the method is that it can be used to study dynamic changes in the composition of protein complexes[90,101]. Furthermore, the technology can be combined with other strategies such as chemical cross-linking[90]. Cross-linkers are chemical reagents that connect two or more reactive groups through a spacer or linker region. When used with a cross-linker, two or more proteins in a complex are linked together by covalent binding[102]. The reactive groups are separated by the spacer arm, which is defined by its length (5 - 15 Å)[90]. The application stabilizes transient PPIs in a dynamic process or enables the detection of low-affinity PPIs *in vitro* and *in vivo*. A variety of cross-linkers are available, which differ in chemical reactivity, spacer arm length, water solubility, cell membrane permeability and other properties[86,103]. The most used cross-linker is a homo-bifunctional one carrying two NHS esters, which targets primary amines with high reaction efficiency under physiological conditions[102]. The hetero-bifunctional cross-linkers usually consist of an amino-reactive group and a sulfhydryl group, such as malmeimide and iodoactyl. The photo-reactive cross-linkers can be induced to bind to proteins by irradiation with UV light[86,104]. The membrane permeable cross-linkers, such as formaldehyde, allow the identification of PPIs in their native environment[86]. Formaldehyde can also be used for *in vivo* cross-linking with subsequent MS analysis[90].

1.6 Aim of this work

In this thesis the structure, dynamics and function of various protein complexes from the bacterium *P. aeruginosa* were investigated. Firstly, the dynamic changes of supra complexes (respirasomes) of electron transport-based energy generation were of interest. Changing protein composition of these complexes formed under aerobic and aerobic to anaerobic shift conditions were to investigated with the interactomics approach (cross-linking, affinity purification, LC-MS^2). Secondly, the influence of two proteins, which are members of the LemA superfamily proteins, on the formation and assembly of outer membrane vesicles should be investigated by isolation and analysis of the proteome. Thirdly, the determination of the exact chemical nature of previously found unusual protein-protein interaction between the flagellum protein FliC and the chaperone $DnaK^{105}$ was the final task. Overall, general principles of protein-protein interaction dynamics were deduced.

2. Materials and Methods

2.1 Materials

2.1.1 Strains of bacteria and plasmids

Table 1: Strains of bacteria and plasmids

Strain	Genotype	Reference
E. coli BTH 101	F-, *cya-99*, *araD139, galE15, galK16, rpsL1 (Str r)*, *hsdR2, mcrA1, mcrB1*	EUROMEDEX[96], Souffelweyersheim, Frankreich
E. coli DH10B	F– *mcrA* Δ(*mrr-hsdRMS-mcrBC*) φ80*lacZ*ΔM15 Δ*lacX74 recA1 endA1 araD139* Δ (*ara-leu*)7697 *galU galK* λ– *rpsL*(Str^R) *nupG*	Invitrogen, Carlsbad, USA (Grant *et al*., 1990[106])
E. coli ST18	*pro thi hsdR*$^+$ Tp^r Sm^r; chromo-some::RP4-2 Tc::Mu-Kan::Tn7 λ*pir* Δ*hemA*	Thoma and Schobert, 2009[107]
E. coli BL21(DE3)	F– *omp*T *hsdS*$_B$ (r_B–, m_B–) *gal dcm* (DE3)	ThermoFisher Scientific, Waltham, USA
P. aeruginosa PA01	Wildtype	Holloway, 1969[108]
P. aeruginosa PA14	Wildtype	Rahme *et al*., 1995[109]
P. aeruginosa PA14 Δ*nuoJ*	PA14*MAR2xT7 nuoJ* transposon mutant	Liberati *et al*., 2006[110]
P. aeruginosa PA14 Δ*fdhE*	PA14*MAR2xT7 fdhE* transposon mutant	Liberati *et al*., 2006[110]

P. aeruginosa PA14 Δ*napA*	PA14*MAR2xT7 napA* transposon mutant	Liberati *et al*., 2006[110]
P. aeruginosa PA14 pSEVA634	pSEVA634	Dr. José M. Borrero-de Acuña
P. aeruginosa PA14 Δ56810 pSEVA634	Δ56810 + pSEVA634	Dr. José M. Borrero-de Acuña
P. aeruginosa PA14 Δ06990 pSEVA634	Δ06990 + pSEVA634	Dr. José M. Borrero-de Acuña
P. aeruginosa PA14 Δ56810 / Δ06990 pSEVA634	Δ56810 / Δ06990 + pSEVA634	Dr. José M. Borrero-de Acuña
P. aeruginosa PA14 Δ56810 + pSEVA634-56810	Δ56810 + pSEVA634-56810	Dr. José M. Borrero-de Acuña
P. aeruginosa PA14 Δ06990 + pSEVA634-06990	Δ06990 + pSEVA634-06990	Dr. José M. Borrero-de Acuña
P. aeruginosa PA14 Δ56810 Δ06990 + pSEVA634-56810-06990	Δ56810 Δ06990 + pSEVA634-56810-06990	Dr. José M. Borrero-de Acuña
P. aeruginosa PA01 pSEVA634-antisense *dnaK*	PA01 WT + pSEVA634-antisense *dnaK*	Dr. José M. Borrero-de Acuña
P. aeruginosa PA14 pSEVA634-antisense *dnaK*	PA14 WT + pSEVA634-antisense *dnaK*	Dr. José M. Borrero-de Acuña
pKT25	encodes the T25 fragment (the first 224 AS from CyaA), Kan^R, MCS is located at the 3` end of the T25 fragment, low-copy plasmid	EUROMEDEX[96], Souffelweyersheim, Frankreich

pKNT25	encodes the T25 fragment (the first 224 AS from CyaA), Kan^R, MCS is located at the 5` end of the T25 fragment, low-copy plasmid	EUROMEDEX[96], Souffelweyersheim, Frankreich
pUT18	encodes the T18 fragment (the 224-399 AS from CyaA), Amp^R, MCS is located at the 5` end of the T18 fragment, high-copy plasmid	EUROMEDEX[96], Souffelweyersheim, Frankreich
pUT18C	encodes the T18 fragment (the 224 399 AS from CyaA), Amp^R, MCS is located at the 3` end of the T25 fragment, low-copy plasmid	EUROMEDEX[96], Souffelweyersheim, Frankreich
pKT25-*nirQ*$_{P.a.}$	pKT25 derivative, encoding C-terminal fusion of *nirQ* with T25	this work
pKT25-*narI*$_{P.a.}$	pKT25 derivative, encoding C-terminal fusion of *narI* with T25	Katrin Müller Master thesis 2016[111]
pKT25-*narH*$_{P.a.}$	pKT25 derivative, encoding C-terminal fusion of *narH* with T25	this work
pKT25-*norC*$_{P.a.}$	pKT25 derivative, encoding C-terminal fusion of *norC* with T25	this work
pKT25-*norD*$_{P.a.}$	pKT25 derivative, encoding C-terminal fusion of *norD* with T25	this work
pKT25-*dnaK*$_{P.a.}$	pKT25 derivative, encoding C-terminal fusion of *dnaK* with T25	this work
pKT25-*fliC*$_{P.a.}$	pKT25 derivative, encoding C-terminal fusion of *fliC* with T25	this work
pKNT25-*narI*$_{P.a.}$	pKNT25 derivative, encoding N-terminal fusion of *narI* with T25	Katrin Müller Master thesis 2016[111]
pKNT25-*narH*$_{P.a.}$	pKNT25 derivative, encoding N-terminal fusion of *narH* with T25	this work

pKNT25-*norC*$_{P.a.}$	pKNT25 derivative, encoding N-terminal fusion of *norC* with T25	this work
pKNT25-*norD*$_{P.a.}$	pKNT25 derivative, encoding N-terminal fusion of *norD* with T25	this work
pKNT25-*dnaK*$_{P.a.}$	pKNT25 derivative, encoding N-terminal fusion of *dnaK* with T25	this work
pKNT25-*fliC*$_{P.a.}$	pKNT25 derivative, encoding N-terminal fusion of *fliC* with T25	this work
pUT18-*narI*$_{P.a.}$	pUT18 derivative, encodes N-terminal fusion of *narI* with T18	Katrin Müller Master thesis 2016[111]
pUT18-*narH*$_{P.a.}$	pUT18 derivative, encodes N-terminal fusion of *narH* with T18	this work
pUT18-*norC*$_{P.a.}$	pUT18 derivative, encodes N-terminal fusion of *norC* with T18	Christoph Riemenschneider Bachelor thesis 2019[112]
pUT18-*norD*$_{P.a.}$	pUT18 derivative, encodes N-terminal fusion of *norD* with T18	this work
pUT18-*dnaK*$_{P.a.}$	pUT18 derivative, encodes N-terminal fusion of *dnaK* with T18	this work
pUT18-*fliC*$_{P.a.}$	pUT18 derivative, encodes N-terminal fusion of *fliC* with T18	Christoph Riemenschneider Bachelor thesis 2019[112]
pUT18C-*nirQ*$_{P.a.}$	pUT18C derivative, encoding C-terminal fusion of *nirQ* with T18	this work
pUT18C-*narI*$_{P.a.}$	pUT18C derivative, encoding C-terminal fusion of *narI* with T18	Katrin Müller Master thesis 2016[111]
pUT18C-*narH*$_{P.a.}$	pUT18C derivative, encoding C-terminal fusion of *narH* with T18	this work
pUT18C-*norC*$_{P.a.}$	pUT18C derivative, encoding C-terminal fusion of *norC* with T18	this work
pUT18C-*norD*$_{P.a.}$	pUT18C derivative, encoding C-terminal fusion of *norD* with T18	this work

pUT18C-*dnaK*$_{P.a.}$	pUT18C derivative, encoding C-terminal fusion of *dnaK* with T18	this work
pUT18C-*fliC*$_{P.a.}$	pUT18C derivative, encoding C-terminal fusion of *fliC* with T18	this work
pUCP26t	pRO1600 oriV, pRO1600 Rep, *lacZα*, Tet^R	Olsen,R.H. *et al*.,1982[113]
pUCP26t-P*nuoJ-nuoJ*-StrepII	encoding promoter sequence of *nuo* operon and *nuoJ* with a fused StrepII-tag	this work
pUCP26t-P*fdhE-fdhE*-StrepII	encoding promoter sequence of *fdn* operon and *fdhE* with a fused StrepII-tag	this work
pUCP26t-P*napA-napA*-StrepII	encoding promoter sequence of *nap* operon and *napA* with a fused StrepII-tag	this work
pGEX-6P-1	pBR322, *lacZα*, *tac*, precision cleavage site, Amp^R	GE Healthcare, Chalfont St Giles, UK
pGEX-*dnaK*$_{P.a.}$	encoding C-terminal fusion of *dnaK* with GST-tag	this work
pGEX-*fliC*$_{P.a.}$	encoding C-terminal fusion of *fliC* with GST-tag	this work

2.1.2 Oligonucleotides

Table 2: Oligonucleotides

Name	Sequence	Usage
pKT25 for	GTATTCCACTGACGGCGGATATCGAC	vector primer of pKT25 5’ of MCS
pKT25 rev	TAAGTTGGGTAACGCCAGGGTTTTCC	vector primer of pKT25 3’ of MCS
pKNT25 for	AGGCACCCCAGGCTTTACACTTTATG	vector primer of pKNT25 5’ of MCS

pKNT25 rev	CAGGCGGAACATCAATGTGGCGTTTT	vector primer of pKNT25 3’ of MCS
pUT18 for	TATGCTTCCGGCTCGTATGTTGTGTG	vector primer of pUT18 5’ of MCS
pUT18 rev	ACGCCGATATTCATGTCGCCGTCGTA	vector primer of pUT18 3’ of MCS
pUT18C for	AGTTCTCGCCGGATGTACTGGAAACG	vector primer of pUT18C 5’ of MCS
pUT18C rev	GGCTGGCTTAACTATGCGGCATCAGA	vector primer of pUT18 3’ of MCS
narI for *Xba*I	ACTCTAGAGATGTCGACCAATCTTCTG	amplification with *Xba*I recognition site
narI nS rev *Eco*RI	CATTGAATTCTGGCAGGACGTTT	amplification with *Eco*RI recognition site of pKNT25/pUT18 no stop
narI nS rev *Eco*RI	CATTGAATTCTTCAGGCAGGACGTTT	amplification with *Eco*RI recognition site of pKT25/pUT18C
narH for	ATGAAAATTCGTTCGCAAGTCGGC	gene primer of *narH* forward
narH rev	CTCCTGGATCTGCACGACCT	gene primer of *narH* reverse
narH rev wS	TCACTCCTGGATCTGCACGACC	gene primer of *narH* with stop
narH for *Xba*I	ACACTCTAGAGATGAAAATTCGTTCGCAAG	amplification with *Xba*I recognition site
narH rev *Eco*RI	CATTGAATTCGACTCCTGGATCTGC	amplification with *Eco*RI recognition site
narH rev *Eco*RI pKT25	CATTGAATTCTCACTCCTGGATCTGC	amplification with *Eco*RI recognition site for pKT25

nirQ for	ATGCGGGACGCGACACC	gene primer of *nirQ* forward
nirQ rev	GGCGACATGGAGATCGACG	gene primer of *nirQ* reverse
nirQ rev wS	TCAGGCGACATGGAGATCGACG	gene primer of *nirQ* with stop
nirQ for *Xba*I	ACACTCTAGAGATGCGGGACGC	amplification with *Xba*I recognition site
nirQ rev *Eco*RI	CATTGAATTCGAGGCGACATGGA	amplification with *Eco*RI recognition site
nirQ rev *Eco*RI pKT25	CATTGAATTCTTTCAGGCGACATGG	amplification with *Eco*RI recognition site for pKT25
norC for	ATGTCCGAGACCTTTACCAAAGGCA	gene primer of *norC* forward
norC rev	ACCCTCCTTGTTCGGCGG	gene primer of *norC* reverse
norC rev wS	TCAACCCTCCTTGTTCGGCG	gene primer of *norC* with stop
norC for *Xba*I	ACACTCTAGAGATGTCCGAGACCTTTAC	amplification with *Xba*I recognition site
norC rev *Eco*RI	CATTGAATTCGAACCCTCCTTGTTCG	amplification with *Eco*RI recognition site
norC rev *Eco*RI pKT25	CATTGAATTCTTTCAACCCTCCTTGTTC	amplification with *Eco*RI recognition site for pKT25
norD for	ATGGCCTTCGCCGTCGAG	gene primer of *norD* forward
norD rev	GCGGCGCAGGCGCCGATA	gene primer of *norD* reverse

norD rev wS	TCAGCGGCGCAGGCGC	gene primer of *norD* with stop
norD for *Xba*I	ACACTCTAGAGATGGCCTTCGCC	amplification with *Xba*I recognition site
norD rev *Eco*RI	CATTGAATTCGAGCGGCGCA	amplification with *Eco*RI recognition site
norD rev *Eco*RI pKT25	CATTGAATTCGAGCGGCGCA	amplification with *Eco*RI recognition site for pKT25
norD rev *Eco*RI pKT25 **opt**	CATTGAATTCTTTCAGCGGCGCAGGCGCC	amplification with *Eco*RI recognition site **optimized**
dnaK for	ATGGGCAAAATCATTGGCATCGAC	gene primer of *dnaK* forward
dnaK rev nS	CTTGTTGTCCTTGACCTCTTCGAACT	gene primer of *dnaK* reverse no stop
dnaK for *Xba*I	CATTTCTAGAGATGGGCAAAATCATTGGCA	amplification with *Xba*I recognition site
dnaK rev *Xma*I	CATTCCCGGGGCTTGTTGTCCTTGA	amplification with *Xma*I recognition site
fliC for	ATGGCCCTTACAGTCAACACGAAC	gene primer of *fliC* forward
fliC rev nS	GCGCAGCAGGCTCAGGA	gene primer of *fliC* reverse no stop
fliC for *Xba*I	CATTTCTAGAGATGGCCCTTACAGTCAACAC	amplification with *Xba*I recognition site
fliC rev *Xma*I	CATTCCCGGGGAGCGCAGCAGG	amplification with *Xma*I recognition site
dnaK rev	TTACTTGTTGTCCTTGACCTCTTCGAAC	gene primer of *dnaK* reverse
fliC rev	TTAGCGCAGCAGGCTCAGGA	gene primer of *fliC* reverse

dnaK for *Bam*HI	TATTGGATCCATGGGCAAAATCATTGG	amplification with *Bam*HI recognition site
dnaK rev *Xho*I	TATTCTCGAGTTACTTGTTGTCCTTGAC	amplification with *Xho*I recognition site
fliC for *Bam*HI	TATTGGATCCATGGCCCTTACAGTC	amplification with *Bam*HI recognition site
fliC rev *Xho*I	TATTCTCGAGTTAGCGCAGCAG	amplification with *Xho*I recognition site
pGEX-5FP-GATC	AACGTATTGAAGCTATCCC	vector primer of pGEX-6P-1
pGEX-3RP-GATC	TCAAGAATTATACACTCCG	vector primer of pGEX-6P-1
P*fdh* for	GCTGTTCGGCGAGGCCA	gene primer of promoter *fdh* forward
P*fdh* rev	CGTGCATCTCCTGCATCAGGC	gene primer of promoter *fdh* reverse
fdhE for **opt**	GTGTCACGCACCATTCTTCAGCCGGGG	gene primer of *fdhE* forward **optimized**
fdhE rev **opt**	TTCGCCGCCGGGGGCCAGCAA	gene primer of *fdhE* reverse **optimized**
fdhE Strep rev	TTCCGGGGATCCCAGTTCGCCGCCGGG	gene primer of *fdhE*-StrepII reverse
NEB P*fdh* for	ATTCGAGCTCGGTACGCTGTTCGGCGAG	amplification of overlapping regions + promoter *fdh* forward
NEB P*fdh* rev	AATGGTGCGTGACACCGTGCATCTCCTG	amplification of overlapping regions + promoter *fdh* reverse
NEB *fdhE* for	TGCAGGAGATGCACGGTGTCACGCACC	amplification of overlapping regions + *fdhE* forward

NEB STREPII rev	TCACTTTTCAAACTGAGGATGTGACCA TTCCGGGGATCCC	amplification of StrepII reverse
NEB Strep pUCP rev	GACTCTAGAGGATCCCCGGTCACTTTT CAAACTGAGGATG	amplification of overlapping regions + StrepII reverse
P*nap* for	GAAACCTCTGCTGACTGCCCT	gene primer of promoter *nap* forward
P*nap* rev	GCGGCCTCCCTCAGGGTTT	gene primer of promoter *nap* reverse
napA for	ATGAACCTCACCCGTCGTGAATT	gene primer of *napA* forward
*napA r*ev	GGCCAGGTTGAGCAGTTCGATG	gene primer of *napA* reverse
napA Strep rev	TTCCGGGGATCCCAGGGCCAGGTTGA GCAG	gene primer of *napA*-StrepII reverse
NEB P*nap* for	ATTCGAGCTCGGTACGAAACCTCTGCT GAC	amplification of overlapping regions + promoter *nap* forward
NEB P*nap* rev	ACGGGTGAGGTTCATGCGGCCTCCCT CAG	amplification of overlapping regions + promoter *nap* reverse
NEB *napA* for	CTGAGGGAGGCCGCATGAACCTCACC CGT	amplification of overlapping regions + *napA* forward
NEB Strep pUCP rev **opt**	CTAGAGGATCCCCGGTCACTTTTCAAA CTG	amplification of overlapping regions + StrepII reverse **optimized**
P*nuo* for	CGCACCTCCGGAGCGACT	gene primer of promoter *nuo* forward
P*nuo* rev	GCTGATACTCCTTCTGTACCGG	gene primer of promoter *nuo* reverse

nuoJ for	GTGGAATTCGCTTTCTATTTCGC	gene primer of *nuoJ* forward
nuoJ rev	TTGTTTGGCGTCTTGACGACCC	gene primer of *nuoJ* reverse
nuoJ Strep rev	TTCCGGGGATCCCAGTTGTTTGGCGTCTTG	gene primer of *nuoJ*-StrepII reverse
NEB P*nuo* for	GAATTCGAGCTCGGTACCGCACCTCCGGAG	amplification of overlapping regions + promoter *nuo* forward
NEB P*nuo* rev	GAAAGCGAATTCCACGCTGATACTCCTTCT	amplification of overlapping regions + promoter *nuo* reverse
NEB *nuoJ* for	AGAAGGAGTATCAGCGTGGAATTCGCTTTC	amplification of overlapping regions + *nuoJ* forward
pUCP26 for	GGGGGGCGGAGCCTATGGAAA	vector primer pUCP26 forward
pUCP26 rev	GCCTCTTCGCTATTACGC	vector primer pUCP26 forward

2.1.3 Chemicals

Table 3: Chemicals

Chemical	Manufacturer
4-(2-hydroxyethyl)-1-piperazineethanesulfonic acid (HEPES)	Roth, Karlsruhe, Germany
Acetic acid	Roth
Acetonitrile	Roth
Acrylamide	Roth
Agar-agar	Roth
Agarose	Roth

Ammonium hydrogen carbonate	Roth
Ammonium persulfate (APS)	Roth
Ammonium sulfate	Roth
Bovine serum albumin	Roth
Calcium chloride	Roth
Chloroform	Roth
Citric acid	Roth
Coomassie® Brilliant blue G250	Merck, Darmstadt, Germany
D-Desthiobiotin	Roth
di-Potassium hydrogen phosphate	Roth
di-Sodium hydrogen phosphate	Roth
Ethanol	Roth
Ethylenediaminetetraacetic acid (EDTA)	Roth
Formaldehyde	Roth
Galactoside	Roth
o-nitrophenyl-β-D-galactopyranoside (ONPG)	
Glycerol	Roth
Glycine	Roth
Hydroxy-azophenyl-benzoic acid (HABA)	Roth
InstantBlue®	Merck
Iron sulfate heptahydrate	Roth
Magnesium chloride	Roth
Magnesium sulfate	Roth
Magnesium sulfate heptahydrate	Roth
Maltose	Roth
Manganese chloride	Roth
Methanol	Roth

N,*N*,*N*',*N*'-Tetramethylethylendiamin (TEMED)	Fluka, St. Louis, USA
Potassium acetate	Roth
Potassium chloride	Roth
Potassium di-hydrogen phosphate	Roth
S-Methyl methanethiosulfonate (MMTS)	Merck
Sodium chloride	Serva, Heidelberg, Germany
Sodium di-hydrogen phosphate	Roth
Sodium dodecyl sulfate	Roth
Sodium MOPS	Roth
β-Mercaptoethanol	Roth
Sucrose	Roth
TRIS	Roth
Tris(2-carboxyethyl)phosphin	Merck
Triton™ X-100	Roth
Tryptone	Roth
Tween20	Roth
Yeast extract	Roth

2.1.4 Media supplements

Table 4: Media supplements

Media supplement	**Manufacturer**	**Stock concentration**
Ampicillin sodium salt	Roth	100 mg/ml
Avidin	Roth	2 mg/ml
BCIP (5-Bromo-4-chloro-3-indolyl phosphate p-toluidine salt)	Roth	50 mg/ml
IPTG (Isopropyl-β-D-thiogalactopyranosid)	Roth	1 M

Gentamycin sulfate	Roth	10 mg/ml
Kanamycin sulfate	Roth	50 mg/ml
MTT (3-(4,5-dimethylthiazole-2-yl)-2,5-di-phenyltetrazolium bromide)	ThermoFisher Scientific	50 mg/ml
NBT (p-Nitrotetrzolium blue chloride)	Roth	50 mg/ml
Streptomycin sulfate	Sigma Aldrich, St. Louis, USA	10 mg/ml
Tetracyclin hydrochloride	Roth	10 mg/ml
X-Gal (5-Brom-4-chlor-3-indoxyl-β-D-galactopyranoside)	Roth	40 mg/ml

2.1.5 Enzymes and Buffer

Table 5: Enzymes and associated buffer

Enzyme/Buffer	Manufacturer
Alkine Phosphatase, Calf Intestinal (CiP)	New England Biolabs GmbH, Frankfurt am Main, Germany
*Bam*HI-HF	New England Biolabs GmbH
cOmplete™, Mini Protease Inhibitor Cocktail	Roche, Rotkreuz, Switzerland
cOmplete™, Mini EDTA-free Protease Inhibitor Cocktail	Roche
10x Cutsmart Buffer	New England Biolabs GmbH
*Eco*RI-HF	New England Biolabs GmbH
Gene Ruler DNA Ladder #SM0331	ThermoFisher Scientific
T4 Ligase	New England Biolabs GmbH
10x T4 Ligase Buffer	New England Biolabs GmbH
6x Loading dye	ThermoFisher Scientific
PageRuler™ Plus Prestained Protein Ladder, 10 to 180 kDa #26616	ThermoFisher Scientific

PageRuler™ Plus Prestained Protein Ladder, 10 to 250 kDa #26619	ThermoFisher Scientific
Phusion High-Fidelity DNA Polymerase	New England Biolabs GmbH
Precission protease 500U	AG Jahn, TU Braunschweig, Germany
5x HF Buffer	New England Biolabs GmbH
Q5® High-Fidelity DNA Ploymerase	New England Biolabs GmbH
5x Q5 High GC Enhancer	New England Biolabs GmbH
5x Q5 Reaction Buffer	New England Biolabs GmbH
*Xba*I	New England Biolabs GmbH
*Xma*I	New England Biolabs GmbH
*Xho*I	New England Biolabs GmbH

2.1.6 Consumable material and kits

Table 6: Consumable materials and kits

Material	Manufacturer
Cuvette of polystyrol	Sarstedt, Nürnbrecht, Germany
Filtropur BT50 0.2 µm	Sarstedt
Gene Pulser® cuvettes	Bio-Rad, Hercules, USA
Glutathione sepharose	Sigma Aldrich
Loop soft 10 µl sterile	VWR, Radnor, USA
Mini-Protean™ glass plates	Bio-Rad
Mini-Protean™ spacer plates	Bio-Rad
Microlance™ 3, needle No. 18,	Becton Dickenson GmbH (BD), Heidelberg, Germany
Parafilm PM-996	Bemis Company, Neenah, USA
Petri dish	Sarstedt
Poly-Prep® chromatography columns 10 ml	Bio-Rad
Poly-Prep® chromatography columns 15 ml	Bio-Rad

Protein LoBind tube 1.5 ml	Eppendorf, Hamburg, Germany
QIAprep Spin Miniprep Cat-No. 27106	Qiagen, Venlo, Netherlands
QIAquick Gel Extraction Cat-No. 28704	Qiagen
QIAquick PCR Purification Cat-No. 28104	Qiagen
Reaction tube 1.5 ml and 2 ml	Eppendorf
Strep-Tactin®Superflow®high capacity	IBA Lifesciences, Göttingen, Germany
Syringe 1 ml NORM-JECT	Henke Sass Wolf, Tuttlingen, Germany
Syringe 2, 5 and 10 ml	B|Braun, Melsungen, Germany
Vivaspin Turbo 15 centrifugal concentrators	Sartorius, Göttingen, Germany
Vivaspin Turbo 4 centrifugal concentrators	Sartorius
Whatman GB003	GE Healthcare

2.1.7 Devices

Table 7: Devices

Device	Model	Manufacturer
Agarose electrophoresis systems	Mini-Sub®Cell GT	Bio-Rad
	Wide Mini-Sub®Cell GT	Bio-Rad
Autoclavs	LVSA 50/70 LVSA	Zirbus, Bad Grund, Germany
	FVA/A1	Fedegari, Albuzzano, Italy
Cell disruptors	FastPrep®-24	MP Biomedicals, Eschewege, Germany

	French® pressure cell press	Thermo electron corporation, Waltham, USA
	+ French® Press cell	Thermo electron corporation
Centrifuges	My FUGE mini C1008-B	Benchmark Scientific, Sayreville, USA
	Heraeus™ Megafuge™ 1.0R	ThermoFisher Scientific
	Avanti J-E centrifuge	Beckman Coulter, Brea, USA
	+ JA 14	Beckman Coulter
	+ JLA 9.1000	Beckman Coulter
	Optima™ L-90K	Beckman Coulter
	+ 70.1 Ti	Beckman Coulter
	+ SW 40 Ti	Beckman Coulter
	Heraeus Megafuge 8R	ThermoFisher Scientific
	MiniSpin	Eppendorf
	5425R	Eppendorf
Electroporation system	Gene pulser Xcell	Bio-Rad
	CE Module	Bio-Rad

	PC Module	Bio-Rad
	Shock pod	Bio-Rad
Incubators	OV 2	Biometra, Göttingen, Germany
	Heraeus™B 6120	ThermoFisher scientific
Magnetic stirrers + heaters	RSM-10HS	Phoenix Instrument GmbH, Garbsen, Germany
	MR 3001	Heidolph, Schwabach, Germany
Milli-Q	IQ 7000	Merck
pH meter	CG 842	Schott, Mainz, Germany
Power supply	Power Pac basic	Bio-Rad
Safety workbench	HERAsafe KS	ThermoFisher Scientific
Scales	Entris (Ultra micro lab scale)	Sartorius
	BP 61S	Sartorius
	Scaltec SBA 52	Denver Instrument, Denver, USA
	Entris (Analytical lab scale)	Sartorius

SDS gel and Blot scanner	Bio-5000 plus	Microtek, Hsinchu, Taiwan
SDS gel system	Mini-Protean® Tetra system	Bio-Rad
Shakers	Orbitron	Infors HT, Bottmingen, Austria
	Multitron Pro	Infors HT
	Grant Instruments™Grant-bio™PS-3D	ThermoFisher Scientific
Spectrophotometers	UV-1600PC	VWR
	ND-1000	Peqlab, Erlangen, Germany
Thermal cycler	T100™	Bio-Rad
Thermomixer	Thermomixer compact	Eppendorf
	ThermoStat C	Eppendorf
Ultra Low freezer	MDF-DU700VH	Panasonic, Kadoma, Japan
UV light	UV transilluminator	Wealtec, Sparks, USA
Vortexer	Vortex-2 Genie	Scientific Indutries, New York, USA
	Mini Vortex	Roth

2.1.8 Progams

Table 8: Used programs

Name	Usage	Manufacturer
Proteome Discoverer 2.3	Analysis of proteome data	ThermoFisher Scientific
NanoSight NTA NS300	Analysis of vesicle	Malvern Panalytical, Malvern, UK
PEAKS Studio X	Analysis of proteome data	Bioinformatics Solutions Inc., Waterloo, USA
PyMOL 2.3	Analysis of protein structure	Schrödinger, New York, USA
Phyre2	Prediction of protein structure	Structural Bioinformatics Group, London, UK

2.2 Methods

2.2.1 Microbiological methods

Cultivation of *E. coli* and *P. aeruginosa*

Liquid precultures were inoculated with a glycerol stock or a single colony taken from a plate culture. Cultivation was carried out overnight at 37 °C and 200 rpm. To prepare plate cultures, bacteria were taken from a glycerol stock and spread with a sterile inoculation loop or plated from liquid cultures on LB-agar plates with sterile glass spheres. The incubation was performed at 37 °C. The *E. coli* BTH101 are an exception with regard to the incubation temperature as this is 30 °C.

Lysogeny Broth complex medium

The cultivation of *E. coli* was carried out in complex medium according to Bertani (LB)[114].

LB medium:

Tryptone	10 g/L
Yeast extract	5 g/L
NaCl	10 g/L

Before autoclaving, agar-agar was added to the medium in a quantity of 15 g/L to produce solid media.

Storage of bacteria

The production of glycerin stocks allows for a long-term storage of bacteria. For this purpose, a liquid culture was prepared, consisting of 300 µL 80 % (w/v) sterile glycerol mixed with 700 µl bacterial suspension and stored at -80 °C.

Determination of the cell density

Cell density in liquid cultures was determined as optical density (OD) using a photometer at 578 nm (OD_{578}). An absorbance of one corresponds to a cell density of 1 x 10^9 cells/ml.

2.2.2 Molecular biological methods

Polymerase-Chain-Reaction (PCR)

The Polymerase Chain Reaction (PCR) is a standard method and serves for the amplification of DNA fragments. In this work, PCR was used to check the genotype of strains and the uptake of the plasmid (Table 9) after transformation. On the other hand, the PCR was used for the amplification of the DNA used for the formation of new constructs (

Table 10). In both cases the genomic DNA served as a template. Table 11 shows the cycler program used for Phusion Polymerase and Q5 Polymerase.

Table 9: Conditions of PCR for genotyping [10 µl approach]

Reagent	Volume [µl]
Phusion / Q5 5 x Reaction Buffer	2
dNTP´s (10 mM)	0.2
DMSO / Q5 5 x Enhancer	0.3
FOR-Primer (10 µM)	0.4
REV-Primer (10 µM)	0.4
ddH_2O	5.6
Phusion / Q5	0.1
DNA Template	1

Table 10: PCR conditions for DNA amplification with Phusion or Q5 polymerase for a 25 µl preparation

Reagent	Volume [µl]
5 x Reaction Buffer	5
dNTP`s (10 mM)	0.5
DMSO / Q5 5 x Enhancer	0.75
FOR-Primer (10 µM)	1.25
REV-Primer (10 µM)	1.25
Phusion / Q5	0.25
ddH_2O	15
DNA Template (100 ng gDNA)	1

Table 11: Program for amplification using Phusion or Q5 polymerase

Temperature [°C]	Time [m:s]	
98	∞ (Hot Start)	
98	1:00	
98	0:10	
50-72	0:30	25x
72	20-30 s/kb	
72	4:00	
4	∞	

DNA separation by gel electrophoresis

For the separation of the PCR products a 1 % agarose gel was prepared. For this purpose, 2 g agarose were dissolved in 200 ml 1 x TAE buffer under heat. The gel was poured in to the holder and transferred to the electrophoresis chamber, which was filled with 1 x TAE buffer. Subsequently the samples were placed in the slots (25 µl) and for size comparison 5 µl of the DNA marker of 1 kb #SM0331 (ThermoFisher Scientific, Waltham, USA) were added. The agarose gel electrophoresis was run at 120 V. The gel was incubated for 5 - 10 min in a 0.1 % ethidium bromide bath. Only a small amount (5 µl) was applied for a test gel (Table 12), to

check the band size or linearization of a plasmid after restriction digestion. Detection was carried out under UV light, as ethidium bromide intercalates in DNA. Its absorption spectrum remains in the UV range, but its emission spectrum increases 50 - 100 times.

Table 12: Reaction approach for a test gel

Reagent	Volume [µl]
DNA	2
6 x Loading dye (NEB)	3

DNA extraction from agarose gel

The extraction of DNA from agarose gel is used for purification of the amplificates. The respective DNA fragment was excised of the gel under UV light and purified with the QIAquick Gel Extraction Kit from Qiagen (28704) according to the protocol of the manufacturer. The column was dried for 5 min at 70 °C and the DNA was eluted with 25 µl elution buffer at the same temperature.

Purification of DNA

For the purification of PCR products, cut DNA fragments from agarose gel or plasmid DNA, the QIAquick PCR Purification Kit from Qiagen (28104) was used. The purification was performed according to the manufacturer's protocol. The column was incubated after the washing step to dryness at 70 °C for 5 min and then eluted with 25 µl water at the same temperature.

Digestion of DNA *via* restriction endonucleases

The method of DNA digestion by using restriction endonucleases is employed to liberate DNA fragments from plasmids, to generate DNA fragments with identical interfaces for ligation, or to verify a ligation process. In the two tables below the approaches for a standardized restriction digest of an insert (Table 13) and a plasmid (Table 14) are listed. The incubation of the restriction digest was performed for 2 hours at 37 °C. After the incubation period a heat inactivation of the restriction enzymes was performed for 20 min at 65 °C. When using *Bam*HI, which cannot be heat inactivated, inactivation was performed using a QIAquick PCR Purification Kit (Qiagen).

Table 13: Approach for a restriction digest of an insert

Reagent	Volume [µl]
PCR fragment (insert)	20
10 x CutSmart Buffer (NEB)	2.5
Enzyme 1 (NEB)	1.25
Enzyme 2 (NEB)	1.25
ddH_2O	0

Table 14: Approach for a restriction digestion of a plasmid

Reagent	Volume [µl]
Plasmid	2 (high copy) / 7 (low copy)
10 x CutSmart Buffer (NEB)	1
Enzyme 1 (NEB)	0.5
Enzyme 2 (NEB)	0.5
ddH_2O	5/0
CiP	1 (added 1.5 hours later after incubation started)

Ligation of DNA

The approach for a standard ligation is listed in Table 15. The ligation was either carried out for 2 hours at 25 °C or overnight at 17 °C. The reaction was stopped at 65 °C for 20 min or purified with the QIAquick PCR Purification Kit (Qiagen) by using *Bam*HI.

Table 15: Approach of a ligation

Reagent	Volume [µl]
Insert	7.5
Vector	1
T4-Ligase	0.5
10x T4-Ligase-Buffer	1

Cloning of the StrepII-tagged bait protein expression plasmid with NEBuilder®HiFi DNA Assembly kit

The cloning method of the NEBuilder® HiFi DNA Assembly Kit (Figure 10) was further developed, improved and resulted in the Gibson Assembly Kit from NEB. This method ensures efficient, fast and easy assembly of DNA fragments.

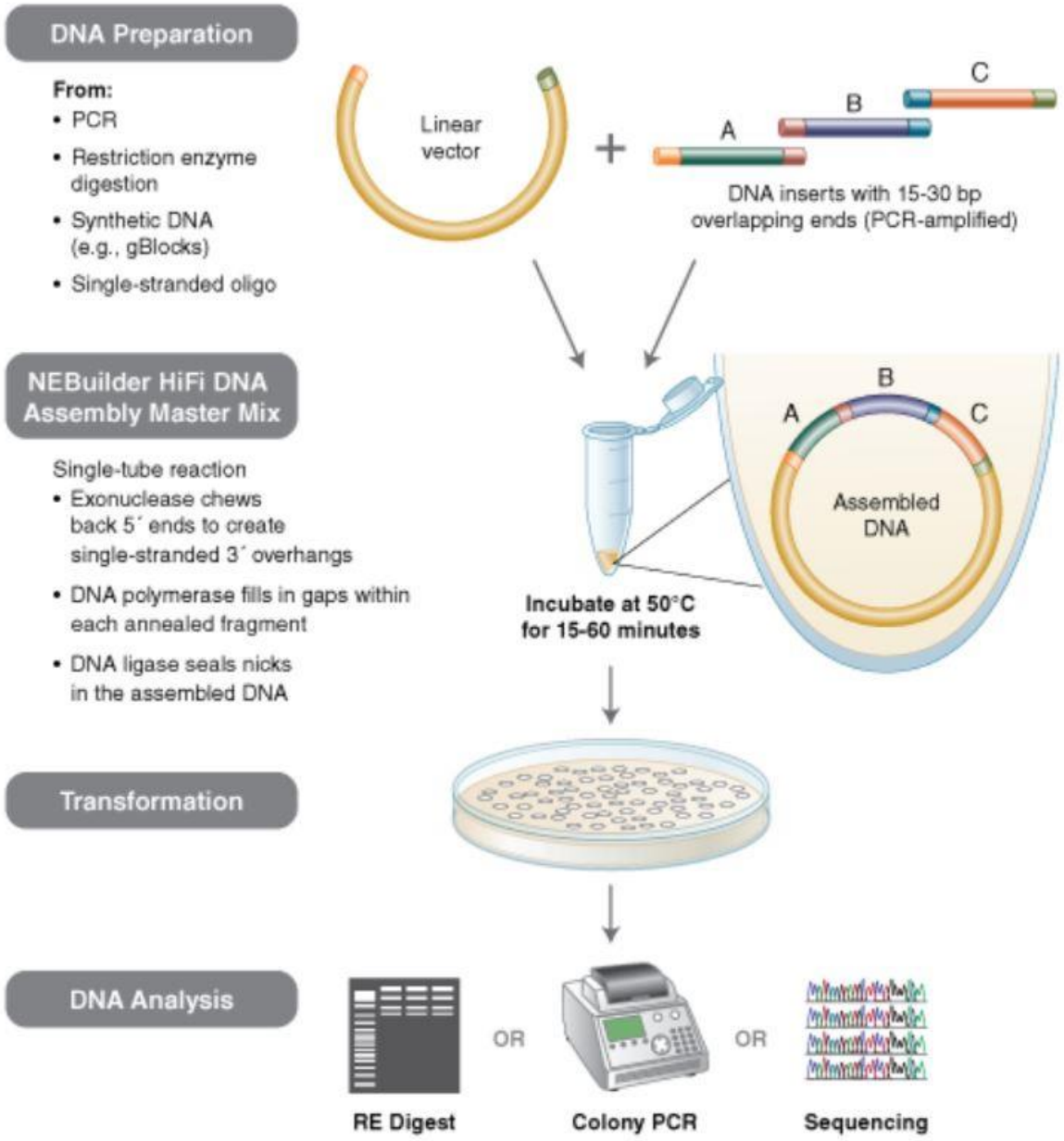

Figure 10: Overview of NEBuilder Assembly approach. The first step is the DNA preparation, the selected DNA fragments are amplified by PCR and a 15 - 30 bp overhang is created, which has an overlapping sequence to the next DNA fragment to be attached. The vector is linearized by digestion with a restriction enzyme. The second step is the assembly of the linearized vector with the DNA fragments in conjunction with the NEBuilder Master Mix, consisting of exonuclease, DNA polymerase and DNA ligase, with an incubation at 50 °C for 15 - 60 min. In the third step the vector is transformed into competent *E. coli* cells and plated on selective media. After successful transformation, the clones are analyzed for correct assembly of the plasmid using restriction digestion or colony PCR with subsequent DNA sequencing[115].

The NEBuilder has the advantage of assembling several fragments of different sizes in one step due to the different enzymes in the Master Mix. First, the pUCP26 plasmid was cleaved with a restriction enzyme so that it is linear. The promoter sequence and the bait gene sequence were amplified by PCR. A 15 bp overhang on both sides of the promoter sequence was amplified by PCR. The StrepII-tag DNA sequence was first fused to the bait gene sequence at the C-terminal end of the encoded gene by PCR and another PCR was used to amplify the overlapping 15 bp ends at both ends. The amount of the fragments and the digested plasmid were optically set *via* gel electrophoresis and the determined volumes were mixed with the Master Mix of this kit (Table 16) and incubated for 20 min at 50 °C. Subsequently, 3 µl were transformed into DH10B cells and spread on LB agar plates with the necessary antibiotic, IPTG and XGal for selection. To check the cloning, first a PCR was performed with the plasmid primers and the plasmid as template. If the plasmid tested positive, it was sent to Seqlab (Göttingen, Germany) for DNA sequencing to check the DNA sequence and to exclude point mutations or frame shifts.

Table 16: NEBuilder DNA assembly

Reagent	**vector:insert=1:2**	**Volume [µl]**
promoter fragment		~3
gene fragment		~5
digested pUCP26		2
Master mix		10

Production of $CaCl_2$-competent *E. coli* cells

For the production of chemically competent *E. coli* cells, a preculture with a volume of 20 ml LB medium was prepared in an Erlenmeyer flask with baffles, inoculated and ON incubated at 37 °C at 200 rpm. The 50 ml main culture was inoculated with 500 µl of the preculture and incubated at 37 °C and 200 rpm to an OD_{600} of 0.4 - 0.6. The bacterial suspension was transferred to a 50 ml reaction tube and centrifuged at 4 °C and 3000 *x* g for 30 min. The supernatant was discarded and the pellet resuspended in 20 ml ice-cold TFBI buffer (Table 17). The suspension was incubated on ice for 5 min and then centrifuged at 4 °C and 3000 *x* g for another 30 min. The supernatant was discarded and the cell pellet resuspended in 2 ml ice-cold TFBII buffer (Table 17). An additional incubation of 10 - 60 min followed, during which time the 1.5 ml reaction tubes were pre-cooled. Aliquots of 50 µl were then prepared and stored at 80 °C.

Table 17: Solution of $CaCl_2$ competent cells

TFB I		**TFB II**	
Potassium acetate	30 mM	Na-MOPS	10 mM
Manganese chloride	50 mM	Calcium chloride	75 mM
Potassium chloride	100 mM	Potassium chloride	10 mM
Calcium chloride	10 mM	Glycerol	15 % v/v
Glycerol	15 % V/V		
adjust to pH 5.8 (HCl) sterile filtration		adjust to pH 6.5 (HCl) sterile filtration	

Transformation of *E. coli*

The competent *E. coli* cells (stored at -80 °C) were slowly thawed for 20 min on ice. Five µl of the ligation mix were added to 25 µl of thawed *E. coli* cells and incubated on ice for 20 min. Then, the transformation was heat-shocked at 42 °C for 45 s, followed by a cooling phase of 2 min on ice. Three hundred µl LB medium were added to the preparation and the cells were incubated at 37 °C for 1 hour on the Thermomix at 300 rpm. After incubation, the cell suspension was plated with 100 µl using glass beads on LB plates with appropriate antibiotic addition. Incubation was performed at 37 °C overnight. The plates were sealed with parafilm and stored at 4 °C.

Production and transformation of electrocompetent *P. aeruginosa* cells

A 6 ml culture, in a 15 ml screw vessel, was inoculated with cells from the glycerol stock and was incubated at 37 °C and 200 rpm overnight, respective antibiotics were added. Then the culture was equally distributed into 4 microcentrifuge tubes. The cells were harvested by centrifugation at room temperature for 1 - 2 min at 13400 rpm (MiniSpin®; Eppendorf). For the preparation 100 ml of a 300 mM sucrose solution were prepared and sterile filtered. Each cell pellet of each tube was washed twice with 1 ml 300 mM sucrose of room temperature. The four cell pellets were then resuspended in a combined total of 100 µl in 300 mM sucrose,

containing on average 10^9 - 10^{10} viable bacteria. For the electroporation of chromosomal DNA 500 ng DNA were mixed with 100 µl of electrocompetent cells. For plasmid transformation 50 - 100 ng of replicative plasmid and 300 - 500 ng of non-replicative plasmid were used. The mixture was transferred to a 2 mm gap-width electroporation cuvette. The settings for the electroporation were 25 µF, 200 Ω, 2.5 kV. Afterwards 1 ml LB medium of room temperature was added and transferred to a reaction tube and incubated at 37 °C and 200 rpm for 1 h. A part of the mixture (100 µl) was plated on an LB agar plate containing the respective antibiotic plate. The plate was incubated at 37 °C until colonies appear (usually within 24 h), control plates included cells pulsed without added DNA.

Diparental mating of *P. aeruginosa*

Pre-cultures of the donor strain *E. coli* ST18 and the recipient strain *P. aeruginosa* PA14 were inoculated and incubated at 37 °C 200 rpm ON. For diparental maturing 1 ml of ST18 culture was mixed with 100 µl *P. aeruginosa* culture and centrifuged for 2 min at 3500 rpm (MiniSpin®; Eppendorf). The supernatant was removed and the cell pellet was added to 100 µl LB medium containing 1 µl ALA (50 mg/ml). The suspension was added as drops to an LB agar plate and dried for 30 min under sterile conditions. The culture was incubated for 6 hours at 37 °C, inducing the transfer of the plasmid DNA from the donor to the recipient strain. The biofilm was removed with an inoculating loop and the cells were gently resuspended in 1 ml LB medium. Dilutions of 1:500 and 1:1000 were prepared and 10 µl and 50 µl of the suspension were plated out to 100 µl LB on LB agar plates with ampicillin (100 µg/ml) and incubated at 37 °C ON.

Plasmid preparation from *E. coli* and *P. aeruginosa* using Miniprep Kit (Qiagen)

The plasmid preparation with the Miniprep kit from Qiagen was performed according to the attached protocol of the manufacturer. One step was added after the centrifugation step, which is used to dry the pellet, by incubation at 70 °C on the Thermomix for 10 min. The pellet was then resuspended in 35 µl of 70 °C tempered ddH_2O and stored at -20 °C.

BACTH- (Bacterial Adenylate Cyclase-based Two-Hybrid) System

The BACTH (Bacterial Adenylate Cyclase-based Two-Hybrid) system is a simple and fast method to detect and characterize *in vivo* protein-protein interaction in bacteria. The BACTH system was developed by the group of Dr. D. Ladant at the Pasteur Institute and is based on the reconstitution of the adenylate cyclase activity of a adenylate cyclase deficient *E. coli*[96]. The fact that the catalytic domain of adenylate cyclase of *Bordetella pertussis* consists of two complementary fragments, T25 and T18 (Figure 11 A), which are inactive after separation

(Figure 11 B), is used in this system[96]. These fragments are fused to potentially interacting polypeptides (X = bait and Y = prey). In the case of the protein-protein interaction of the bait and prey proteins the heterodimerization of T18 and T25 of the hybrid proteins leads to functional complementation of an intact adenylate cyclase (Figure 11 C). This in turn leads to the synthesis of cAMP (cyclic AMP) and allows for cAMP binding to CAP (Catabolic Activator Protein) (Figure 11 D). The resulting cAMP/CAP complex is a pleiotropic regulator for transcription in *E. coli* (Figure 11 D). Among the expressing genes are also the *lac* and *mal* operon genes, which play a role in lactose and maltose catabolism. This gives *E. coli* the ability to use lactose and maltose as the only source of carbon, which can be used as an indicator or for selection.

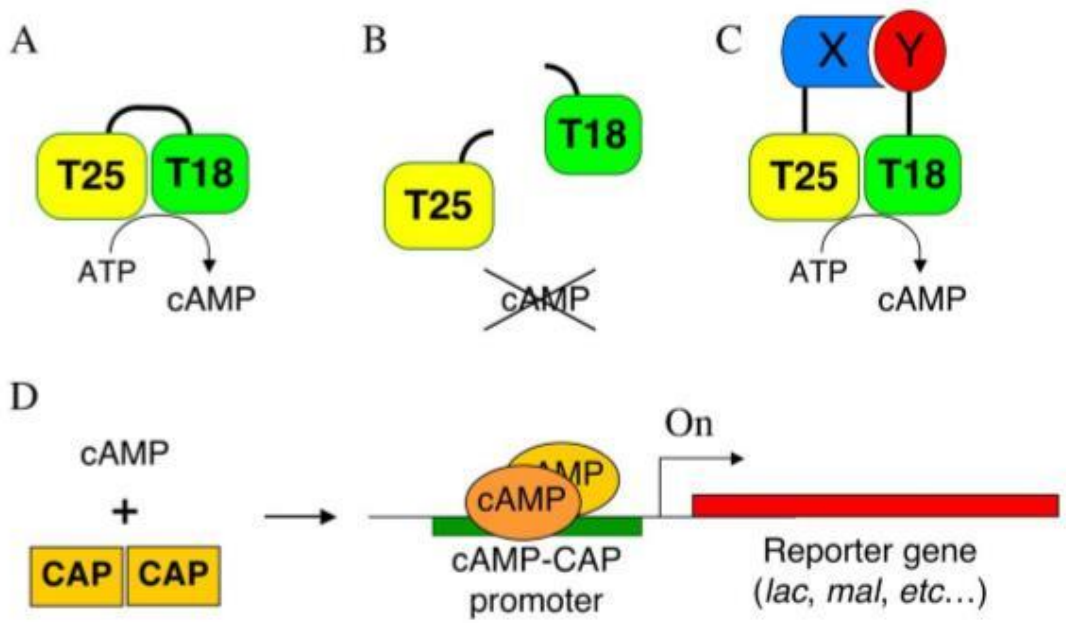

Figure 11: Principle of the BACTH system. A. The active form of the adenylate cyclase fragments T25 and T18 are in contact with each other, consequently ATP is transformed into cAMP **B.** The inactive form of adenylate cyclase is present, when fragments T25 and T18 are separated, cAMP cannot be formed **C.** First, the gene for T25 fragment is fused to the gene of protein X to be investigated and T18 fragment is correspondingly fused to protein Y to be investigated. When X interacts with Y, T25 and T18 recombine to an active adenylate cyclase and cAMP is formed from ATP. **D.** cAMP binds to catabolic activator protein (CAP) and binds to the promoter sequence of various reporter genes (*lac*, *mal*, etc)[96].

For the use of the BACTH system, two different sets of compatible vectors[96] are provided, allowing the generation of hybrid proteins with C- and N-terminal fusion of T25 and T18 fragments (Figure 12).

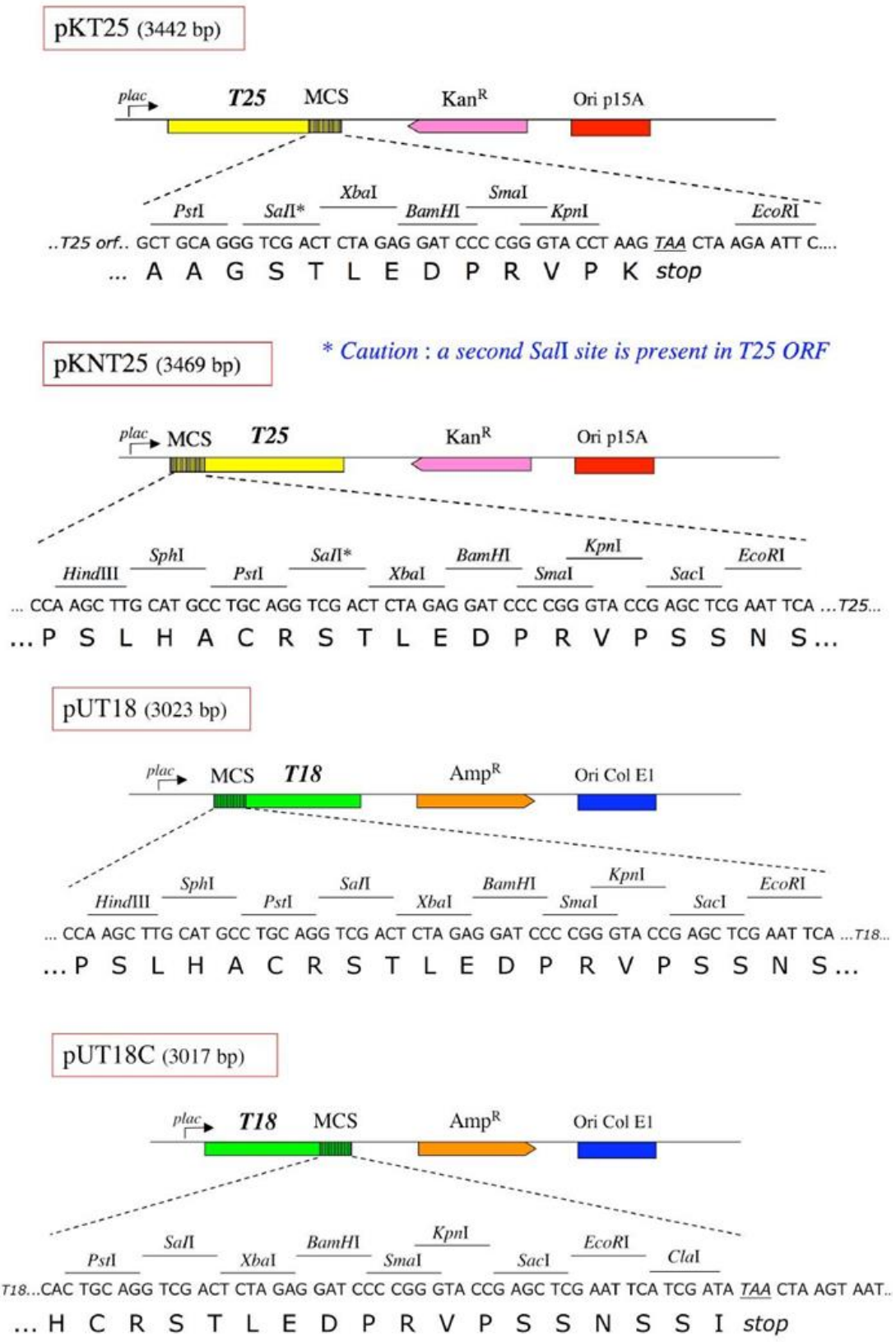

Figure 12: Plasmid maps of the BACTH. Schematic illustration of the linear plasmid map with the multiple cloning side (MCS) within the DNA encoding T25 or T18 fragment. The MCS is located in the gene encoding at the C-terminal part of the T25 fragment in pKT25 and in the DNA at the N-terminal part in pKNT25. The MCS is located in pUT18 in the DNA for the N-terminal part and in pUT18C in the DNA for the C-terminal part of the T18 fragment[96].

The advantages of the BACTH system are based on its implementation in the model organism *E. coli*, which facilitates the fast screening and characterization of protein-protein interactions. *E. coli* has a faster growth rate than *Saccharomyces cerevisae*, is easy to transform with high efficiency and only standard molecular biological methods are required for the utilization of the system. In addition, the system is based on a signaling cascade that uses the secondary messenger molecule cAMP. This enables the analysis of protein-protein interactions that occur in the cytoplasm, at the inner membrane or at the DNA level.

Application of the Bacterial Adenylate Cyclase Two Hybrid (BACTH)

The competent *E. coli* BTH101 cells (stored at -80 °C) were slowly thawed on ice for 20 min. One µl of each of the two co-transforming plasmids were added to 25 µl of thawed *E. coli* cells and incubated on ice for 20 min. The choice of plasmids to interact was based on 8 possible combinations: testing for the interaction of the proteins NarI, NarH, NorB, NorC, NirQ, DnaK and FliC

pKT25 X/pUT18 Y, pKT25 X/pUT18C Y, pKNT25 X/pUT18 Y, pKNT25 X/pUT18C Y, pUT18 X/pKT25 Y, pUT18 X/pKNT25 Y, pUT18C X/pKT25 Y and pUT18C X/pKNT25 Y.

In addition, a negative control consisting of the plasmid combinations pKT25/pUT18C or pKNT25/pUT18 without encoded bait and prey proteins and a positive control using pKT25-zip/pUT18C-zip with the leucine zipper of GCN4 as X and Y were prepared. The transformation of the BTH101 cells was performed using heat shock, 45 s at 42 °C, followed by a cooling phase of 2 min on ice. Three hundred µl LB medium were added to the preparation and the cells were incubated at 37 °C using a Thermomix at 300 rpm for 1 h. The bacterial suspension was then centrifuged at 3500 rpm (MiniSpin®, Eppendorf) for 8 min and the supernatant was discarded. The pellet was resuspended in 1 ml M63 liquid medium; this washing procedure was repeated. The pellet was finally resuspended in 300 µl M63 liquid medium and 200 µl of the interaction samples and 100 µl of the controls were plated onto M63 plates using sterile glass beads and incubated at 30 °C for 5 - 8 days.

M63 5x Salt solution pH 7.00 (KOH)

$(NH_4)_2SO_4$	10 g
KH_2PO_4	68 g
$FeSO_4 \cdot 7H_2O$	0.0025 g
with H_2O to 1 liter	
adjust to pH 7.00 using 3 M KOH	
autoclave	

M63 Medium

Water agar	400 ml
M63 5x Salt solution	100 ml
IPTG (1 M)	250 µl
X-Gal (40 mg/ml)	500 µl
Streptomycin (10 mg/ml)	5 ml
Kanamycin (50 mg/ml)	500 µl
Ampicillin (100 mg/ml)	500 µl
Magnesium sulphate heptahydrate (1 M)	500 µl
Maltose (20 %)	5 ml
Vitamin B1 (0.05 %)	1 ml
fill up to 500 ml with H_2O	

M63 Liquid medium

Water	400 ml
M63 5x Salt solution	100 ml
IPTG (1 M)	250 µl
X-Gal (40 mg/ml)	500 µl
Streptomycin (10 mg/ml)	5 ml
Kanamycin (50 mg/ml)	500 µl
Ampicillin (100 mg/ml)	500 µl
Magnesium sulfate heptahydrate (1 M)	500 µl
Maltose (20 %)	5 ml
Vitamin B1 (0,05 %)	1 ml
fill up to 500 ml with H_2O	

BACTH: β-Galactosidase-assay

The enzyme β-galactosidase catalyzes the hydrolysis of the glycosidic bond of β-galactopyranosides. The disaccharide lactose is the natural substrate of β-galactosidase. In the β-galactosidase assay the natural substrate is replaced by the synthetic galactoside o-nitrophenyl-β-D-galactopyranoside (ONPG). Like lactose, ONPG is hydrolyzed by β-galactosidase and the reaction products galactose and nitrophenol are formed, which causes a yellow colorformation in the test for positive samples.

Hence, 5 ml of LB medium were mixed with appropriate antibiotics (Amp 100 µg/ml; Kan 50 µg/ml), inoculated with a positive colony of the BACTH transformation and were incubated at 30 °C and 200 rpm ON.

Subsequently, growth was stopped by incubation for 20 min on ice. From this preculture 100 µl were taken and centrifuged at 3500 rpm (MiniSpin® Eppendorf) at 4 °C for 5 min. The supernatant was discarded and the pellet resuspended in 900 µl Z-buffer. The OD_{600} was then measured and recorded. The membrane was permeabilized by adding one drop of 0.1 % SDS and one drop of chloroform using a Pasteur pipette and incubating at 30 °C for 5 min. The reaction (t_S) was started by the addition of 200 µl ONPG (4 mg/ml). Incubation was carried out at 30 °C until yellow coloration was obtained. The reaction (t_E) was stopped by the addition of 500 µl 1M Na_2CO_3 solution. Centrifugation was then carried out for 5 min at 13000 rpm (MiniSpin® Eppendorf), which removed the cell debris and chloroform. The photometric measurement of the supernatant was performed at 420 nm and 550 nm.

The Miller Unit (MU) for the measured β-galactosidase activity was calculated by the following formula and is based on the change in A_{420}/min/ml of cells/OD_{600}

$$\mathbf{MU = 1000 \times [(OD_{420} - 1.75 \times OD_{550})] / (t \times V \times OD_{600})}$$

OD_{420} und OD_{550}: direct measurement of the optical density at the wavelengths 420 and 550 nm after the end of the enzyme reaction
OD_{600} is a measurement of the amount of the applied washed cell material at 600 nm
t: Response time (t_E-t_S) in min
V: Volume in ml

Z-Buffer

Na_2HPO_4	60 mM
NaH_2PO_4	40 mM
KCl	10 mM
$MgSO_4$	1 mM
β-Mercaptoethanol	50 mM (175 µl/50 ml)

adjust to pH 7.00

storage at 4°C

100 mM Phosphate buffer

$Na_2HPO_4 \cdot 7 \cdot H_2O$	60 mM
$NaH_2PO_4 \cdot H_2O$	40 mM
adjust to pH 7.00 using 3 M KOH storage at RT	

ONPG

ONPG	4 mg/ml
with 100 mM phosphate buffer always freshly prepared before use	

2.2.3 Protein analytical methods

Characterization of the *P. aeruginosa dnaK* conditional mutant strain

The principle for the construction of the *P. aeruginosa dnaK* conditional mutant is shown in Figure 13. The *dnaK* gene is located in an operon together with *grpE* and *dnaJ,* and is synthesized in the *P. aeruginosa* wildtype as polycistronic mRNA. A *dnaK*-antisense RNA is synthesized from a corresponding DNA sequence localized on a plasmid under the control of an IPTG-inducible promoter (*Dr. José M. Borrero-de Acuña*). The antisense mRNA binds to the mRNA of the polycistronic RNA, a double-stranded RNA hybrid is formed, which stops the translation and should prevent the formation of DnaK in the cell.

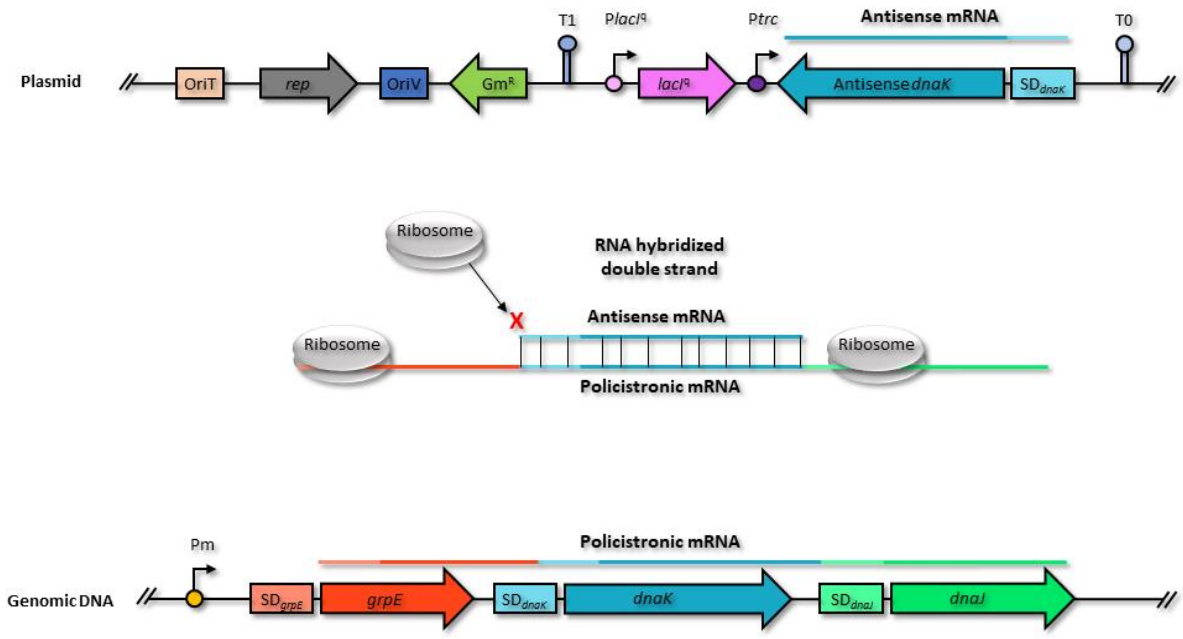

Figure 13: Principle of the *dnaK* conditional mutant. The *dnaK* gene is located in an operon together with *grpE* and *dnaJ* and is synthesized in the wildtype as polycistronic mRNA. An antisense mRNA is synthesized by a plasmid encoded antisense *dnaK* sequence, which is under the control of an IPTG-inducible promoter. The antisense mRNA binds to the mRNA of the polycistronic RNA, a double-stranded RNA hybrid is formed. Thus, translation of the *dnaK* mRNA is prevented.

Precultures of the PA14 *dnaK* conditional mutant and the PA01 *dnaK* conditional mutant were incubated overnight at 37 °C with the addition of 50 mg/ml gentamycin. The main culture consisted of 100 ml LB with addition of 50 mg/ml gentamycin and was inoculated to an OD_{578} of 0.05 with the main culture and 0.5 mM IPTG were added. Sample were collected at time points 0, 1, 2, 4, 6, 8 and adjusted to an OD_{578} of 0.5.The bacterial suspension was centrifuged at 13,000 rpm (MiniSpin®, Eppendorf) for 2 min. The supernatant was discarded and the pellet resuspended in 30 µl SDS loading buffer and heated at 95 °C for 5 min.

Protein production of DnaK and FliC *via* affinity chromatography on glutathione sepharose

A preculture of 6 ml LB medium (Amp 100 µg/ml) was inoculated with *E. coli* BL21 cells carrying the plasmid pGEX-6P-*dnaK* or pGEX-6P-*fliC* and incubated at 37 °C and 200 rpm ON. The main culture from 500 ml LB medium (Amp 100 µg/ml) was inoculated with 5 ml of the preculture and incubated at 37 °C at 200 rpm up to an initial OD_{578} = 0.4 - 0.6, 200 µM of IPTG was added and incubation was continued at 17 °C at 200 rpm ON. Cell harvest was performed at 3,500 rpm (Avanti J-26, Beckham Coulter) at 4 °C for 20 min. The pellet was resuspended in 10 ml 1 x PBS and the cell disruption was performed *via* FrenchPress at 1200 psi. After this step the solution was centrifuged at 100000 *x* g at 4 °C for 1 hour. Five ml glutathione sepharose were equilibrated with 1 x PBS at 17 °C for 2 h. Then the column was washed four times with three column volumes of 1 x PBS, whereby the first and the last

washing step were collected. For the elution of the protein, 500 units of Precission protease were mixed with 7 ml 1 x PBS and added to the column and mixed carefully. The column was incubated at 17 °C ON. The protein was eluted with 7 ml of 1 x PBS and afterwards washed twice with 15 ml 1 x PBS. All four fractions were collected and stored at 4 °C until further usage. For the elution of the bound GST tag, 2.5 mM glutathione were dissolved in 1 x PBS and the column was washed twice and corresponding fractions were collected.

10 x PBS

NaCl	81.8 g/L
KCl	2 g/L
$Na_2HPO_4 \cdot 2H_2O$	17.8 g/L
KH_2PO_4	2.45 g/L

Protein concentration measurement *via* the Bradford test

The Bradford test is a photometric method for the quantitative determination of protein concentrations down to in the range of micrograms per milliliter. The triphenylmethane dye Coomassie Brilliant Blue G-250 (CBBG) forms complexes in acidic solution with cationic and non-polar side chains of proteins. Complex formation with proteins stabilizes the dye in its blue, unprotonated, anionic sulfonate form and shifts the absorption maximum to 595 nm. Since the extinction coefficient of the dye-protein complex is also much higher than that of the free dye, the increase in absorbance at 595 nm due to the formation of the complex can be measured photometrically with high sensitivity and used for the measurement of the protein concentration of the solution. Calibration is necessary to determine the concentration of a particular protein. Standard proteins are used for calibration are chymotrypsin, lysozyme or BSA.

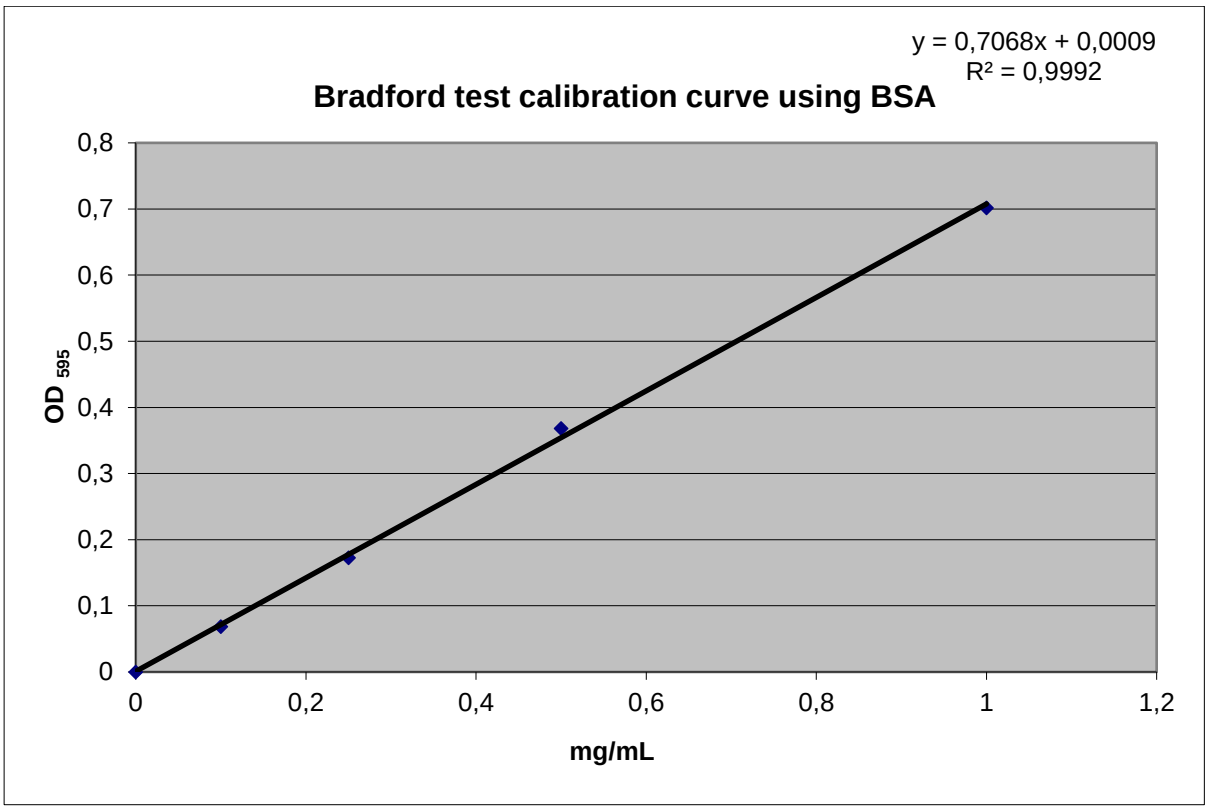

Figure 14: Calibration of the Bradford test for the determination of protein concentrations using of BSA

For the measurement usually 1 ml of Bradford reagent was used with 30 µl of protein solutionto be tested, mixed and incubated for 10 min in the darkness. Within the next 30 min the photometric measurements should be made. For the calibration curve with BSA (Figure 14) different concentrations in the range of 0.25 - 2 mg/ml of BSA were used.

SDS-PAGE (Sodium Dodecyl Sulphate-PolyAcrylamide Gel Electrophorese)

SDS-PAGE is a denaturing polyacrylamide gel containing the detergent SDS in which proteins are separated according to their relative molecular masses. PAGE consists of two types of polyacrylamide gel, the collecting gel (Table 19) and the separating gel (Table 18). In the pH-neutral collecting gel, the denatured, due to the SDS treatment uniformly negatively charged proteins are concentrated, and subsequently separated according to their relative molecular mass in the basic separating gel. The running buffer consists of 1 x SDS buffer. Ten µl were applied per sample and the Pierce™ Unstained Protein MW Marker #26610 (ThermoFisher Scientific, Waltham, USA) were applied. After application of the samples, the chamber was connected to the power supply and the electrophoresis run at 45 mA for 30 min.

Table 18: Composition of 12 % polyacrylamide SDS separating gel

Reagent	Amount – separating gel			
	2	4	6	8
30 % Acrylamide	4 ml	8 ml	12 ml	16 ml
1.5 M TRIS pH 8.8	2.5 ml	5 ml	7.5 ml	10 ml
H_2O	3.5 ml	7 ml	10.5 ml	14 ml
10 % APS	100 µl	200 µl	300 µl	400 µl
TEMED	10 µl	20 µl	30 µl	40 µl

Table 19: Composition of the 6 % SDS polyacrylamide collecting gel

Reagent	Amount – collecting gel			
	2	4	6	8
30 % Acrylamide	1 ml	2 ml	3 ml	4 ml
500 mM TRIS pH 6.8	1.25 ml	2.5 ml	3.64 ml	5 ml
H_2O	2.75 ml	5.5 ml	8.24 ml	11 ml
10 % APS	50 µl	100 µl	150 µl	200 µl
TEMED	5 µl	10 µl	15 µl	20 µl

The Instant*Blue*® stain contains the dye Coomassie Blue R-250 and is a ready-to-use staining solution for the visualization of protein bands. The SDS gel was incubated in a staining dish for 5 - 15 min on a shaker with 10 ml Instant*Blue*® solution. The staining solution was removed and the gel was rinsed with tap water and de-stained overnight with tap water on the shaker.

Interactomics approach

The basic unit of a cellular protein network is the single protein-protein interaction. It can be at the whole cellular level analyzed using the Interactomics approach according to Gingras[90]. The approach is divided into two sections, the DNA processing part and the protein processing part (Figure 15). The first step is to choose a suitable bait protein. The gene or cDNA for this protein is first amplified in the first section of the method, then cloned into the corresponding vector

and finally transformed into the organism to be tested. In the second part of the method the formed protein complex at the bait protein is processed. The bait protein fused to an affinity tag is produced and formaldehyde may be used for *in vivo* cross linking. The cross-linked protein complex is then purified by affinity chromatography emplayed is the attached affinity tag and its composition may be checked by SDS PAGE and Western blot (Figure 15 A). Isolated protein complex composition is subsequently analyzed by MALDI-TOF or LC/MS^2. False positive interactions with the bait may also purified. These are detected by appropriate background control including the analysis of proteins unspecifically binding to the affinity material (Figure 15 B and Figure 15 C).

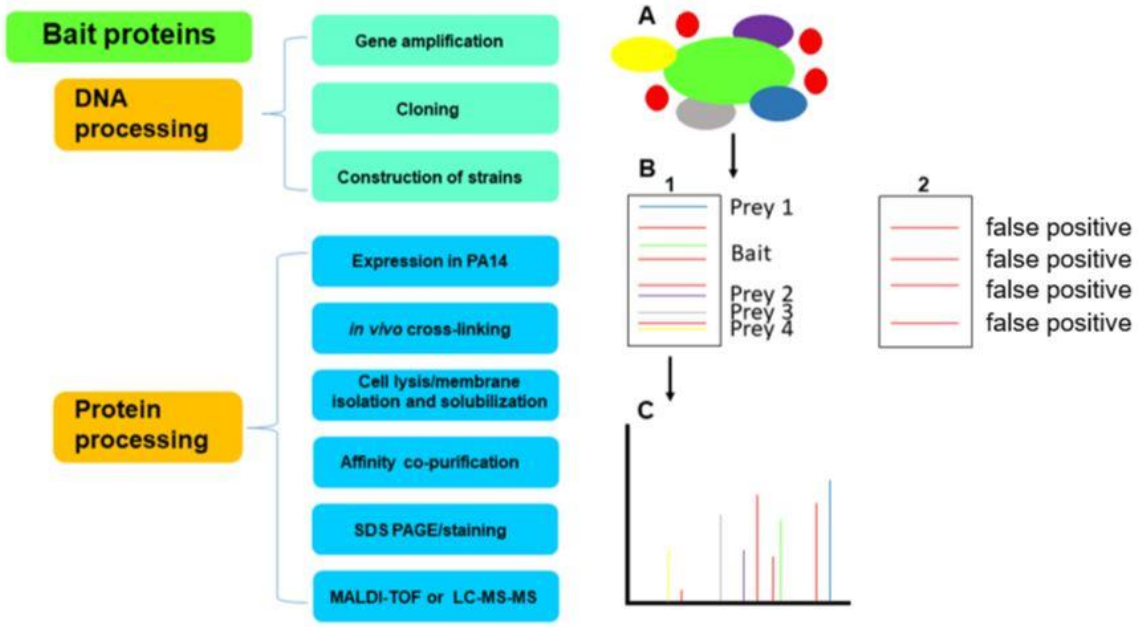

Figure 15: Interactomics approach. The two main steps are the DNA processing and the protein processing. DNA processing consists of amplification, cloning of the bait protein gene/cDNA with the construction of test organism. Protein processing consists of bait protein production, *in vivo* cross-linking, cell lysis/membrane isolation and solubilization, affinity chromatography, SDS PAGE/staining and analysis of the formed at the bait protein by MALDI-TOF or LC-MS^2. **A.** Interaction partners bind to the bait protein. **B.** 1) Bait protein sample: Separation of the interaction partners, the bait protein and false positive. 2) Background sample: Separation of the false positives. **C.** Analysis of the proteins by MALDI-TOF or LC-MS^2

In this thesis several bait proteins (NuoJ, NapA and FdhE) from the pathogenic bacterium *P. aeruginosa* for their interaction partner under various growth conditions were tested. For this purpose, these bait protein genes were expressed in the appropriate genetic background with the chromosomally copy of the bait protein gene knock out. Resulting bait-prey protein complexes were isolated, resolved and analyzed as outlined in detail below. For evaluation the Proteome Discoverer 2.3 program was used and the data, the values of the samples were divided by the respective values of the WT sample to determine an accumulation of proteins in the sample.

Bait-prey protein complex formation under different conditions of oxygen tension and their isolation

The 30 ml preculture (50 µg/ml gentamycin, 30 µg/ml tetracycline) were inoculated with a tip from a glycerol stock and was incubated overnight aerobically at 37 °C and 200 rpm in Erlenmeyer flask with baffles. For each replicate two liter of the main culture (50 µg/ml gentamycin, 30 µg/ml tetracycline) were inoculated with the preculture, divided into 4 x 1 liter Erlenmeyer flasks with baffles, starting with an OD_{578} of 0.05 and incubated at 37 °C and 200 rpm until an OD_{578} = 1.6 - 1.8 was reached (close to the end of the exponential phase). The *in vivo* cross-linking was performed with the addition of 0.25 % of formaldehyde (37 %) to the culture and further incubated for 15 min at 17 °C and 200 rpm. The reaction was stopped with the addition of 200 mM glycine (1M) and an incubation of 10 min at 17 °C and 200 rpm. Afterwards, the harvesting of the cells was performed in one liter harvesting flasks (Beckman Coulter, Brea, USA) at 3,000 rpm (JLA 9.1000, Beckman Coulter) at 4 °C for 20 min. Each cell pellet was resuspended with 6 ml lysis buffer and divided into 15 ml screw vessels (containing 3 g glass beads 70 - 100 µm). The cell disruption was performed *via* FastPrep (MP, Biomedicals, Eschewege, Germany) twice at 6.0 m/s, 35 seconds at 4 °C. After this mechanical disruption, the screw vessels were centrifuged for 25 min at 3500 *x* g at 4 °C and the supernatant was collected. This supernatant was centrifuged for an hour at 4 °C and 100000 *x* g. The resulting supernatant was stored at 4 °C subsequently, 0.3 g of the pellet was weighed in a new 15 ml screw vessel and mixed with membrane dissolution buffer overnight at 4 °C.

For protein production under aerobic to anaerobic shift conditions, an aerobic preculture was inoculated as described above. The 2 liters main culture were inoculated with the preculture the next day, so that it started with an OD_{578} of 0.05, with the same concentration of antibiotics as described above. Incubation was carried out at 37 °C and 200 rpm until an OD_{578} of 1.4 - 1.6 was reached. The bacterial suspension was transferred to 1 liter anaerobic flasks and incubated under anaerobic conditions for further 4 hours at 37 °C and 200 rpm with no significant change in OD_{578}. For cross linking the suspension was first mixed with 0.25 % formaldehyde and incubated for 15 min at 17 °C and 200 rpm. This reaction was stopped with the addition of 200 mM glycine. Afterwards, harvesting and further steps were carried out as described for the experiments carried out under aerobic conditions.

Lysis buffer

TRIS, pH 7.5	20 mM
$MgCl_2$	10 mM
sterile filtration	
add Roche Protease Inhibitor pill before use	

Membrane dissolution buffer

K_2HPO_4	18.8 mM
KH_2PO_4	1.2 mM
adjust to pH 8.0	
Triton™ X-100	2 % (v/v)

Protein complex purification via affinity chromatography

After *in vivo* cross-linking, purification of the resulting protein complexes was performed by the StrepII-tag of the bait protein on a 2 ml Strep-Tactin column. For this purpose, the lysates (cytoplasmic proteins carrying supernatant and diluted membrane fractions prepared as outlined on page 87) were mixed with avidin (0.3 mg per 1 L culture volume) and incubated for 15 min at 4 °C on a roll incubator. The affinity chromatography material was equilibrated (Strep-Tactin®Superflow®high capacity 50 % suspension, IBA, Göttingen, Germany) twice with wash buffer pH 8.0, using five times the column volume (CV). After avidin incubation, the protein suspension was added to the column material and incubated on the roll incubator at 4 °C for 45 min. The column material was washed 8 x with 2.5 SV wash buffer, only the first and the last washing steps were collected. For elution, 4 ml elution buffer was added to the column material and the elution fraction was collected and concentrated at 4 °C. The column material was regenerated with 3 x 2.5 SV of the regeneration buffer (color change from white to red-orange) and afterwards the column material was washed until the column material was decolorized with the wash buffer pH 10.5 and then stored at 4 °C.

Elution buffer

HEPES-NaOH, pH 8.00	50 mM
NaCl	100 mM
D-Desthiobiotin	2.5 mM

Regeneration buffer

TRIS-HCl, pH 8.00	50 mM
EDTA	1 mM
NaCl	100 mM
Hydroxy-azophenyl-benzoic acid (HABA)	1 mM

Wash buffer, pH 10.5

TRIS-HCl, 10.5	100 mM
EDTA	1 mM
NaCl	150 mM

Wash buffer, pH 8.0

TRIS-HCl, pH 8.0	100 mM
EDTA	1 mM
NaCl	150 mM

Western blot analysis for the bait proteins

Western blotting is a technique which allows for the immunological detection of proteins, separated before *via* PAGE. For the transfer of the separated protein from the SDS gel to a membrane to be proved by antibodies a blot is performed as outlined. An electric field directed perpendicular to the polyacrylamide gel is applied (electro transfer), causing the SDS-loaded and negatively charged proteins to migrate towards the anode (positive pole) and, thus, onto the polyvinylidene difluoride (PVDF)-membrane. The charged membrane immobilizes the proteins.

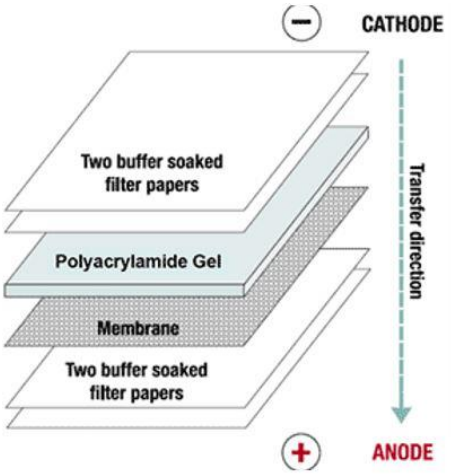

Figure 16: Setup of a Western blot. Two Whatman papers soaked with blotting buffer are the base on which the equilibrated PVDF-membrane is centered, on top of this the SDS gel and on top of this again two soaked Whatman papers are placed. The transfer of the protein from the SDS gel onto the PVDF-membrane takes place by the current flow from the cathode (negative pole) to the anode (positive pole)[116].

The PVDF-membrane and two Whatman papers were cut to the size of the SDS gel (7 x 9 cm). The SDS gel was equilibrated for 10 min in blotting transfer buffer and the PVDF-membrane was activated with methanol for 30 s. After activation the methanol was removed with water and the membrane was transferred to transfer blotting buffer and equilibrated for 10 min. The papers, membrane and gel were stacked without air bubbles as shown in Figure 16 and clamped in the wet module carriage. The trans blot module was placed in the 4 °C room and run at 25 - 30 V overnight.

Blotting transfer buffer

TRIS, pH 8.5	25 mM
Glycine	150 mM
Methanol	20 %

The PVDF membrane was transferred in blocking buffer and incubated at room temperature with gentle shaking for 1 h. Afterwards the membrane was washed 3 x 5 min with 20 ml PBS-Tween buffer. The incubation of the membrane with the antibody anti-Streptavidin AP-conjugated (1:4000) was performed in 10 ml PBS-Tween 20 and at room temperature with gentle shaking for 1 h. The next washing steps were PBS-Tween 20 for 2 x 1 min and 2 x 1 min with PBS buffer. Afterwards, for the chromogenic detection of the blotted antigen on the PVDF-membrane, the membrane was incubated with 20 ml reaction buffer + 10 µl p-Nitrotetrzolium blue chloride (NBT) (75 mg/ml) + 60 µl 5-Bromo-4-chloro-3-indolyl phosphate p-toluidine salt (BCIP) (50 mg/ml) was incubated for 5 min and then washed with ddH_2O (stop of the reaction).

PBS (phosphate buffered saline)

KH_2PO_4, pH 7.0	4 mM
Na_2HPO_4	16 mM
NaCl	115 mM

Blocking buffer

PBS	
BSA	3 %
Tween 20	0.5 % v/v

PBS-Tween 20 buffer

PBS	
Tween 20	0.1 % v/v

Reaction buffer

TRIS, pH 8.8	100 mM
$MgCl_2$	5 mM
NaCl	100 mM

Preparation of gel-separated protein complex samples for LC-MS² analysis

The samples (elution fractions from the affinity chromatography of the bait-prey protein complexes) were applied to a SDS gel and run for 1 cm into the separating gel. Then the gel was colored and this 1 cm was excised with a scalpel and transferred into 2 ml LoBind centrifugation tube (Eppendorf, Hamburg, Germany). From this step on, work was carried out under a fume hood. The slice was washed 3 x 10 GV (gel volumes) with the fixing solution (30 % ethanol, 10 % acetic acid). Then the gel was washed with 10 GV of 50 mM ammonium hydrogen carbonate (BIC) / 30 % acetonitrile (ACN) in H_2O at room temperature with shaking at 800 rpm (discard supernatants) for 30 min. Afterwards the gel piece was shrunk in 100 % acetonitrile and dried (turned white) in a shanking incubator with heating function at 60 °C. After that 10 GV of the 10 % Tris(2-carboxyethyl)phosphine (TCEP) solution was added to the dried gel slice, all incubated at 60 °C and 800 rpm for 2 h. The supernatant was dicarded. In the next step 10 GV of the 5 % S-Methyl methanethiosulfonate (MMTS) solution was added to the gel piece, and all was incubated at RT for 30 min, and then stored at 4 °C overnight. The gel slice was washed with 10 GV of 50 mM BIC, and incubated at 800 rpm for 30 min. Then the slice was washed with 10 GV of 50 mM BIC / 30 % ACN, incubated at 800 rpm for 30 min.

In the next step a second gel slice shrinkage was performed with 100 % acetonitrile treatment and drying in the shaker at 60 °C.

The next steps were performed by Hedwig Schrader at the HZI, the technician of Dr. Josef Wissing.

The gel piece was swelled in digestion buffer consisting of 50 mM Tetraethylammonium borohydride (TEAB) addition of 20 ng trypsin at a protein : protease ratio of 20 : 1. The digestion was performed at 37 °C in a warming cabinet overnight. After the digestion the peptides were in the supernatants. Then the peptides were washed three times with 5 - 10 GV of H_2O, and incubation at 850 rpm in a shaking incubator for 30 min. Then the supernatant was transferred into 1.5 ml LoBind centrifuge tubes (Eppendorf) and the supernatant was dried in the SpeedVac. The peptides were washed another two times with 5 - 10 GV of 0.2 % Trifluoroacetic acid (TFA) and the supernatants were dried down in the SpeedVac. Afterwards the peptides were washed again with 5 - 10 GV of 0.2 % TFA in 30 % CAN, and supernatants were dried in the SpeedVac. Final shrinkage was performed with pure acetonitrile and final drying of the eluted peptide. Then the re-solubilization of the dried peptides was conducted in 0,2 % TFA with 3 % ACN (peptide concentration about 0.5 µg/10 µl). The centrifugation step was performed to separate the polyacrylamide "fines" at 12,000 rpm in the benchtop centrifuge and transferred the supernatant into new LoBind centrifuge tubes (Eppendorf). Then the application of 1 % = 5 µl on EvoTip (Evosep, Odense, Denmark) was conducted.

LC-MS² analyses using the Orbitrap Fusion™ Tribrid™ system

The analyses were performed by Dr. Josef Wissing, HZI Braunschweig.

Liquid chromatography coupled with mass spectrometry (LC/MS, HPLC-MS) is an analytical method for the combined separation and molecular mass determination of molecules by subsequent liquid chromatography (LC) and mass spectrometry (MS). Chromatography is used to separate molecules out of a mixture and subsequent mass spectrometry is used to identify separated molecules. Other analytical devices such as UV/VIS or conductivity detectors are interposed in the LC system. LC-MS^2 analyses of purified and desalted peptides were performed on a Dionex UltiMate 3000 n-RSLC system connected to an Orbitrap FusionTM TribridTM mass spectrometer (ThermoFisher Scientific, Waltham, USA). Peptides of each sample were loaded onto a C_{18} precolumn (3 µm RP18 beads, Acclaim, 0.075 mm × 20 mm), washed at a flow rate of 6 µl/min for 3 min and separated on a C_{18} analytical column (3 mm, Acclaim PepMap RSLC, 0.075 mm × 50 cm, Dionex, Sunnyvale, CA, USA) at a flow rate of 200 nl/min *via* a linear 120 min gradient from 97 % MS buffer A (0.1 % FA) to 25 % MS buffer B (0.1 % FA, 80 % ACN), followed by a 30 min gradient from 25 % MS buffer B to 62 % MS buffer B. The LC system was operated with the Chromeleon software (version 6.8, Dionex) embedded in the Xcalibur software suite (version 3.0.63, ThermoFisher Scientific). The effluent

was electro-sprayed by a stainless-steel emitter (ThermoFisher Scientific). Using the Xcalibur software, the mass spectrometer was controlled and operated in the “top speed” mode, allowing the automatic selection of as many doubly and triply charged peptides in a 3 sec time window as possible, and the subsequent fragmentation of these peptides. Peptide fragmentation was carried out using the higher energy collisional dissociation mode and peptides were measured in the ion trap (HCD/IT).

SPOT membrane synthesis for the analysis of the interaction of DnaK and FliC

The SPOT membrane was generated by Dr. Werner Tegge, HZI Braunschweig.

The synthesis of the peptide arrays (SPOT synthesis) was carried out with an Intavis MultiPep automated SPOT array synthesizer (Intavis Bioanalytical Instruments, Cologne, Germany) on an amino-PEG functionalized SPOT synthesis paper membrane (AIMS Scientific Products, Berlin, Germany) with a size of 9 x 13 cm. The entire protein sequences of DnaK and FliC were divided into 159 and 209 overlapping peptides, respectively, with a length of 15 amino acids with a shift of three amino acids for every consecutive sequence. For each peptide position, first β-alanine was coupled to the paper by using Fmoc-βAla-OPfp (300 mM) and 1-hydroxy-1*H*-benzotriazole (HOBt) (300 mM) in NMP, to which 10 µl/ml diisopropylcarbodiimide was added. The activated amino acid was added at 0.2 µl to each position, reaction time was 45 min. Afterwards, the free amino groups on the membrane were acetylated with 2 % acetic acid anhydride in dimethylformamide (DMF) (capping solution) for one hour. The Fmoc group from the β-alanine was cleaved by an 8 min treatment with 20 % piperidine in DMF. After washing with DMF, the SPOT peptide positions were stained with bromophenol blue (2 % in DMF of an ethanol stock solution of 10 mg/ml), followed by washing of the membrane with ethanol and drying. The corner positions of the arrays were marked with a pencil for a later identification of the peptide positions. The peptide sequences were assembled by utilizing Fmoc amino acid derivatives (200 mM in NMP) with pre-activation using equimolar amounts of diisopropylcarbodiimide and hydroxybenzotriazole for 30 min. The activated amino acids were spotted three times to each position with 0.2 µl each. After the third spotting the reaction was allowed to proceed for a further 30 min, thereafter the membrane was washed with DMF and capping was carried out for 7 min. Fmoc was removed and the SPOTs were stained with bromophenol blue as stated above. After final assembly of the peptide chains and cleavage of the terminal Fmoc group, the free N-terminus was acetylated with the capping solution for 15 min.

The membranes with the completed arrays were washed with DMF, ethanol and dried. Side chain protection groups were cleaved off by two consecutives 2 hours treatments with trifluoroacetic acid containing 5 % dichloromethane, 3 % di-isopropyl silane and 2 % water. Afterwards, the membranes were washed repeatedly with dichloromethane and ethanol and

finally dried. The ready-to-use peptide arrays were sealed in plastic foil and stored at -20 °C until usage.

SPOT membrane analysis of the interaction domains of DnaK and FliC

The SPOT peptide array was generated and used in ligand overlay assays in this thesis. The membrane was placed in a polystyrene box and kept wet with a few drops of alcohol. This is to enhance rehydration of some hydrophobic peptide spots. The peptide locations should not be visible as white spots. If this happen, the membrane is to be treated with alcohol in a sonication bath at room temperature until spots have disappeared. Then the membrane was washed 3 times for 10 min with 10 ml TRIS based saline (TBS). First, incubation was performed with 10 ml membrane blocking solution (MBS) overnight. Afterwards the membrane was washed once with 10 ml TBS-T for 10 min. The membrane was incubated with the protein probe diluted in 10 ml MBS for 4 h. For this purpose, 5 µg of purified protein per milliliter incubation volume was used. The membrane was completely covered with incubation solution and drying out was prevented by using a lid. Afterwards the membrane was washed 3 times 10 min with 10 ml TBS-T. The incubation with the first antibody directed against the protein of interest diluted 1:2500 in 10 ml MBS was performed at RT for 2 h. Then the membrane was washed 3 times with 10 ml TBS-T and further incubated with AP-conjugated secondary antibody 1:10000 diluted in 10 ml MBS for 2 h. Subsequently, the membrane was washed twice for 10 min with 10 ml TBS-T. Furthermore, the membrane was washed twice for 10 min with 10 ml CBS. The detection was performed for 5 to 10 min with fresh prepared 10 ml CDS (color developing solution).

TBS (TRIS based saline)

TRIS	6.1 g
NaCl	8.0 g
KCl	0.2 g
adjust to pH 7.0	
fill up to 1 l using ddH_2O	
autoclave and store at 4 °C	

TBS-T

TBS	
Tween 20	0.05 % (v/v)

MBS

Skim milk powder	2 % (w/v)
Tween 20 in TBS	0.2 % (v/v)

CBS

Citric acid·H_2O	10.51 g
NaCl	8.0 g
KCl	0.2 g
adjust to pH 7.0	
fill up to 1 l using ddH_2O	
autoclave and store at 4 °C	

MTT (3-[4,5-dimethylthiazol- 2-yl]-2,5-diphenyltetrazolium bromide), 50 mg/ ml in 70 % DMF, stored at -20 °C

BCIP (5-bromo-4-chloro-3-indolylphosphate *p*-toluidine salt), 60 mg/ ml in DMF, stored at -20 °C

CDS (10 ml)

CBS	10 ml
1 M $MgCl_2$	50 µl
MTT	60 µl
BCIP	40 µl

Isolation of membrane vesicles from *P. aeruginosa*

The aim of the study was to determine the influence of the *P. aeruginosa* genes *lemA1* (PA14_56810) and *lemA2* (PA14_06990) on the amount and diameter of extracellular vesicles. For this purpose, *lemA1*, *lemA2* and *lemA1-lemA2* deletion mutants as well as LemA1, LemA2 and LemA1 + LemA2 overproducing strains were analyzed. For the sample preparation an LB plate without antibiotics was inoculated from glycerol stock of the *P. aeruginosa* strain to be tested and incubated at 37 °C overnight. The precultures consisted of 100 ml LB in 500 ml baffled flasks and were inoculated with a small single colony from the plate. The respective antibiotics were added and the preculture was incubated at 37 °C and 180 rpm for 6 - 8 h. Afterwards the main culture which consisted of 6 x 300 ml LB in 2-liter baffled flasks supplemented with appropriate antibiotics, was inoculated to a starting OD_{578} of 0.05. If necessary, the target gene (*lemA1, lemA2, lemA1-lemA2*) expression was induced with the addition of 0.1 mM IPTG directly during inoculation of the main culture. The cell harvesting was performed after 16 - 17 h of incubation at 37 °C and 180 rpm. For harvesting, the culture was transferred to 500 ml flasks and centrifuged at 7000 *x* g at 4 °C for 20 min. The supernatant was filtrated through a 0.2 µm filter and centrifugated at 10500 *x* g at 4 °C with a deceleration ´slow´ for 16 - 20 h. Subsequently, the supernatant was discarded and the pellet was gently

resuspended in 3 x 1 ml MV stabilization buffer and stored on ice. For the sucrose gradient a 100 % sucrose solution was prepared in a 100 ml glass cylinder by adding 20 g sucrose and 7 ml 50 mM HEPES buffer, pH 6.8. Then, the solution was gently heated in the microwave until a homogeneous solution was obtained and cooled down to RT. The sample was processed by adding the 100 % sucrose solution to the sample to be analyzed containing the isolated vesicles, resulting in a 60 % sucrose sample. Then the sample was transferred in an ultra-centrifugation tube start with 3 ml sample. Following the sample, 2 ml 50 %, 2 ml 40 %, 3 ml 33 % and 2 ml 25 % sucrose solutions were added. The centrifugation was performed at 96000 *x* g at 4 °C with the setting: acceleration `slow` and deceleration `no break` for 16 - 18 h. After the run, pictures with dark and bright background were taken and the bands were collected with a Pasteur pipette. The opalescent (white) and brown band were separated into different new ultra-centrifugation tubes and filled up 1 : 5 with MV stabilization buffer. For the washing step the samples were centrifugated at 96000 *x* g at 4 °C with a slow deceleration for 2 h. Due to the unstable pellet, the supernatant was removed very carefully and the pellet was resuspended in 300 µl MV stabilization buffer, frozen for storage.

MV stabilization buffer

HEPES, pH 6.8	50 mM
MiniComplete EDTA-free (Roche)	
stored at 4 °C	

Sucrose gradient (per 50 ml)

25 %	12.5 g
33 %	16.5 g
40 %	20 g
50 %	25 g
solved in MV stabilization buffer	

Size analysis of isolated *P. aeruginosa* membrane vesicles *via* NanoSight NS300

The vesicles were characterized concerning their diameter distribution with the NanoSight NS300 (Malvern, Worcestershire, UK). With the NS300, which has a size range for particle diameter determination from 10 nm to 2000 nm, the size distribution and concentration of the vesicles was determined. The NanoSight NS300 utilizes Nanoparticle Tracking Analysis (NTA) technology and uses the two properties of particles during light scattering and Brownian motion to determine the size distribution and particle concentration in suspensions. The laser beam is guided through the sample chamber and hits the particles, which scatter the light and can be detected by a microscope with 20 x zoom with a mounted camera. The camera operates at 30

frames per second and generates a video file of the particles in Brown motion. The software analyses individual particles and calculates the hydrodynamic diameter using the Stokes-Einstein equation. Before switching on the PC, pump, microscope and laser, the laser module must be prepared. The optical disk was first cleaned with filtered water and a lint-free cloth. Then the flow-cell top-plate was placed on the optical plate of the module and fixed with four screws. The two pipes were connected to the flow-cell top-plate. One pipe connects the pump with the module through which the sample is injected into the flow-cell top-plate and the waste pipe which leads from the module directly into a waste collection container. In the next step all devices were switched on and a 1 ml syringe was connected to the flow-cell top-plate *via* the sample injection tube. To clean the sample chamber, 3 ml of filtered water was first injected. The sample was diluted to a concentration of $10^8/10^9$ particles/ml. After flushing the chamber, 100 µl of the sample to be measured were injected first. The module was placed and fixed in the device and the syringe was clamped in the pump. The focus of the camera was set, with camera level 12 and detection limit 5, and the standard operating procedure (SOP) was loaded, recording three times one minute. The pump was started and then the SOP. After the run all video files were processed with a tresholding program, minimizing the background. After each sample, the chamber was flushed with filtered water. At the end of the measurement, the flow-cell top-plate was detached from the module and the remaining water was removed from the chamber with air pressure, the optical plate was cleaned with filtered water and a lint-free cloth.

Vesicle proteomics

Sample preparation was performed by Hedwig Schrader at the HZI, the technician of Dr. Josef Wissing.

Provided lysates were incubated with 5 mM TCEP (in TRIS) at 56°C for 30 min. The solution was brought to 10 mM MMTS (in TRIS) for 15 min, to reduce and protect cysteine residues, respectively. Protein purification, protein digestion, and peptide purification were performed according to a slightly adapted Single-Pot Solid-Phase-enhanced Sample Preparation (SP3) protocol[117,118]. Sequencing grade trypsin (Promega, Fitchburg, USA) was added at a ratio of 1 : 50 weight per weight in 50 mM HEPES, pH 8.00. After overnight incubation at 37 °C, beads containing the digested peptides were not acidified, shaken and incubated at RT overnight after raising the ACN concentration to at least 95 %. Adsorbed peptides were washed once with pure ACN and then air dried. Peptides were eluted in the first step with 20 µl 2 % DMSO for 30 min and in the second step with water for 30 min. Peptides were vacuum dried and dissolved in in 0.2 % trifluoroacetic acid/3 % ACN for subsequent ultracentrifugation (50000 *x* g, 30 min, RT).

The sample analyses was performed by Dr. Josef Wissing.

Dried peptides after digest were re-dissolved in 0.1 % formic acid and an aliquot containing no more than 500 ng in 20 µl was applied onto RP18 EvoTips (Evosep, Odense, Denmark).

For LC-MS^2 peptides were separated on HPLC using an 8 cm ID 100 µm column filled with 3 µm 120 Å ReproSil C_{18} phase (PepSep, Marslev, Denmark) connected to a Bruker timsTOF Pro (powered by PASEF) mass spectrometer.

For LC we used a preformed 60 separations per day method. For MS^2 we used a PASEF protein identification method (Bruker, Billerica, USA). For in depth information see the following publications[119–121].

Resulting raw data files were evaluated using Proteome Discoverer 2.2/2.3 (Thermo Scientific, Waltham, USA) using Beta methylthiolation as a fixed and oxidation of methionine as a variable modification. We allowed 1 missing cleavage and a false positive rate of 1 %. Mass errors were allowed 7 ppm for MS and 0.4 Da for MS^2 data. Databases were actual PAO1 and PA14 fasta files downloaded from Uniprot.org.

DnaK binding capacity analysis *via* the Fast Relaxation Imaging technique

Experiments were performed by Sara da-Silva Ribeiro, working group of Prof. Dr. Simon Ebbinghaus, BRICS Braunschweig

Thermal denaturation was analyzed using Fast Relaxation Imaging technique (FReI)[122]. This technique is based on fast temperature jumps combined with fluorescence microscopy and Foster resonance energy transfer (FRET) mechanism that allows both spatial and temporal resolution of protein folding kinetics both *in vitro* and inside a living cell. $SOD1_{bar}$ mutant G41D was genetically engineered with AcGFP1 at the N-terminal and mCherry at the C-terminal, expressed in NiCo21 bacteria and further purified as described previously[123]. The purified protein was dissolved in buffer Mix (20 mM acetate, 20 mM MES, 20 mM sodium phosphate buffer) with a final pH of 6 or 7 prepared by adjusting the pH stepwise with concentrated solutions of HCl (12 M) and NaOH (10 M) (Mettler Toledo pH meter FiveEasy, Columbus, USA). For the solutions prepared with DnaK 12 and 20 µM or ATP 2 mM, pH value was re-adjusted to the desired value prior to the thermal unfolding experiments.

Samples were individually heated by consecutive ~2°C IR diode laser temperature jumps (7 to 12 for each measurement), with a duration of 25 seconds each. Images were recorded using Zeiss AxioObserver Z1 widefield fluorescence microscope, where emission of the AcGFP1 (Donor) (497-527 nm) and mCherry (Acceptor) (581-679 nm) were detected by two CCD

cameras every two frames per second. AcGFP1 was excited by a 470 nm LED light with a similar exposure time for each measurement. The data was evaluated using ImageJ (National Institutes of Health, Bethesda, USA) and the Matlab software (MathWorks, Natick, USA). Briefly, the ratio of donor over acceptor (D/A) was determined by averaging the pixel intensity of each picture both from ACGFP and mCherry channels and further plotted versus time (Figure 17). The kinetic amplitudes determined from fitting each individual T-jump to a single exponential function were plotted as function of temperature and fitted to the equation described by Girdhar K., *et al*[124]. Using this model both T_m and $\Delta G_f^{37°C}$ were determined. For statistical significance, analyses were performed using GraphPad Prism V. 6.01. An average of five replicates were made for each condition, in at least two independent days.

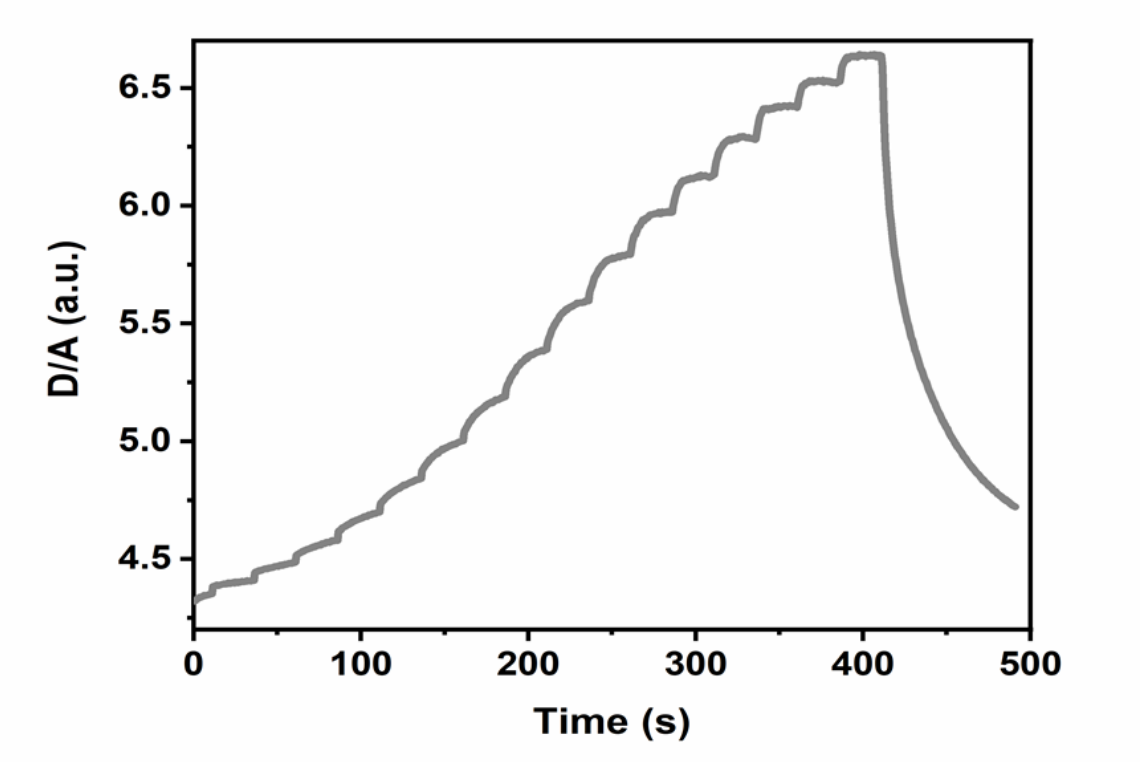

Figure 17: D/A for $SOD1_{bar}$-G41D in PBS at pH 7 as function of time. Protein unfolding traces are detected by the increase of D/A as the solution is heated to higher temperatures. After ~410 seconds, cooling takes place and a decrease of the D/A, closer to the initial value is observed (*performed by Sara da-Silva Ribeiro).*

Field Emission Scanning Electron Microscopy (FESEM)

The electron microscopy studies were performed by Dr. Gabriella Molinari, HZI Braunschweig.

The field electron microscope (also: field emission microscope) belongs to the group of high-resolution microscopes, with which a spatial resolution in the atomic range is possible. This instrument was developed in 1936 by Erwin Wilhelm Müller. It consists of a highly evacuated glass bulb which functions as an anode. Inside is a fine tip (its diameter is a few nm) - for example a tungsten needle - which is the cathode. A potential difference of a few kilovolts

between the cathode and the anode generates an approximately spherically symmetrical electric field. At field strengths of over 109 V/m, electrons are released from the cathode (field emission, promoted by the tunnel effect) and accelerated towards the anode. A luminescent layer in the glass bulb then displays a picture of the cathode tip magnified a million times[125].

For the FESEM analyses of various *P. aeruginosa* strains, cultures were grown in LB without antibiotics. Cultures were originally inoculated with an overnight preculture grown with appropriate antibiotics to an initial OD_{578} of 0.05. Two hours after culture start 0.1 mM IPTG were added to induce *lemA* expression and incubation was continued for three hours. Cultures were incubated in 100 ml Erlenmeyer flasks (not baffled) with 15 ml LB + 50 mg/ml gentamycin, 130 rpm 37 °C overnight. The inoculation of the flasks were from fresh plates (with antibiotic). Cultures were inoculated from the overnight cultures in 1 liter flasks with 200 ml LB 5 g/L NaCl, starting OD_{578} of 0.05 without antibiotic. After two hours of growth IPTG was added for three hours induction with 0.1 mM IPTG (20 µl IPTG 1 M in each flask). Growth further three hours at 37 °C 180 rpm without antibiotic. After the total incubation time of five hours, 10 ml sample was transferred to tubes prepared for the fixation for Field Emission Scanning Electron Microscopy.

Table 20: Strains for FESEM analyses

Strains	**overproduction**
PA14 wildtype + pSEVA634 empty plasmid	Control
PA14 Δ*lemA1* + pSEVA634 empty plasmid	Control
PA14 Δ*lemA2* + pSEVA634 empty plasmid	Control
PA14 Δ*lemA1*Δ*lemA2* + pSEVA634 empty plasmid	Control
PA14 Δ*lemA1* + pSEVA634-*lemA1*	LemA1
PA14 Δ*lemA2* + pSEVA634-*lemA2*	LemA2
PA14 Δ*lemA1*Δ*lemA2* + pSEVA634-*lemA1*-*lemA2*	LemA1 + LemA2

Samples were fixed with 2 % glutaraldehyde in the growth medium, left for 30 min and then formaldehyde was added to a final concentration of 5 %. After one hour on ice fixed bacteria were washed twice for 10 min with TE buffer (20 mM TRIS, 1 mM EDTA, pH 6.9), dehydrated with a graded series of acetone (10, 30, 50, 70, 90 %) for 15 min for each step on ice. Samples in the 100 % acetone step were allowed to reach room temperature before another change into 100 % acetone was done. Samples were then subjected to critical-point drying with liquid CO_2 (CPD 30, Bal-Tec, Liechtenstein). Dried samples were fixed onto aluminum stubs with a conductive adhesive tape and covered with a gold/palladium film by sputter coating (SCD 500 Bal-Tec, Liechtenstein) before examination in a field emission scanning electron microscope

Zeiss Merlin (Zeiss, Oberkochen) using the Everhart Thornley HESE2 detector and the inlens SE detector in a 25:75 ratio with an acceleration voltage of 5 kV using the SEM software 5.5. Contrast and brightness were adjusted with Adobe Photoshop CS5.

Transmission Electron Microscopy (TEM)

TEM analyses were performed by Dr. Gabriella Molinari, HZI Braunschweig.

TEM microscopy was used in this thesis for the analyses of the co-localization of proteins of interest. For this purpose, antibodies against the proteins of interest were generated and differentially coupled to gold particles of different size. Differentially gold particle-labelled antibodies were emplayed to investigate the potential co-localization of two proteins of interest in *P. aeruginosa* using TEM. The gold particles with a diameter of 5, 10 or 20 nm were coupled to the secondary antibody. With the different diameters different antigens can be labeled in parallel[126]. The gold particles have a comparatively high electron density and are therefore less permeable to the cathode ray, which makes the particles appear as dark, high-contrast dots in the TEM image.

Alternatively, a gold-labelled Protein A or Protein G can be used instead of the gold-labelled secondary antibody[127]. Subsequent silver staining lowers the detection limit by a factor of 200[128]. This allows the label to be observed under a light microscope[129]. Immunogold staining is also used for scanning tunneling microscopy[130]. For the TEM analysis, vesicles from *P. aeruginosa* wildtype strain were isolated and subjected to immunogold-based localization of DnaK and FliC.

For vesicle preparation *P. aeruginosa* LB cultures were grown aerobically overnight at 37 °C and 120 rpm, inoculated from fresh LB agar plates. Four 500 ml Erlenmeyer flasks containing 150 ml of LB were used and inoculated with the overnight cultures to start the main culture at an optical density of 0.5 at 600 nm (OD_{600}). Cultures were incubated for 8 h under identical growth conditions. The bacterial cells were pelleted by centrifugation at 4 °C for 15 min at 7000 x *g* in a Sorvall RC 6 Plus centrifuge (Thermo Scientific, Waltham, USA) in 500 ml Nalgene bottles (Thermo Scientific, Waltham, USA) using the SLA 3000 rotor (Thermo Scientific, Waltham, USA). The supernatants were filtered through 0.22 µm pore-size vacuum filtration devices (Sartorius, Göttingen, Germany). Extracellular vesicles were obtained by centrifugation at 10000 rpm at 4 °C for 20 h using the same Sorvall centrifuge and rotor as mentioned above. After centrifugation, the pelleted vesicles were collected in adequate volume of 50 mM HEPES pH 6.8 (Sigma). Vesicles were again pelleted in an Eppendorf 5415R centrifuge at 13000 rpm and 4 °C for one hour and finally resuspended in an adequate volume of 50 mM HEPES, pH 6.8.

Purified vesicles were fixed with 2 % formaldehyde in buffer and kept at 7 °C. After centrifugation the pellets were embedded into 1.75 % water agar. After solidification small cubes were cut and incubated for overnight in 0.5 % aqueous uranyl acetate. Dehydration of samples was performed following the PLT (progressive lowering of temperature) protocol with a graded series of ethanol (10 and 30 % ethanol on ice, 50 % ethanol at -20 °C, 70, 90 and 100 % ethanol at -30 °C. 100 % ethanol was changed twice. Samples were then infiltrated with a Lowicryl K4M resin at -30 °C following the following scheme: one part K4M/1 part 100 % ethanol for overnight, two parts K4M/1 part 100 % ethanol for 8 h, 100 % K4M with several changes over two days. After placing the samples into 0.5 ml gelatine cups and filling with pure resin, samples were polymerized with UV-light (366 nm) for one day at -30 °C, followed by further polymerisation for two days at room temperature.

For localization studies of DnaK and FliC ultrathin sections were cut with a diamond knife and collected onto butvar coated 300 mesh nickel grids and incubated in a 1:10 dilution of the protein sepharose-A affinity purified specific anti-IgG antibodies against *P. aeruginosa* DnaK or FliC for overnight at 7 °C. After intensive washing with PBS, bound antibodies were made visible by incubating with protein A/G-conjugates coupled to gold nanoparticles (PAG) of 15 nm (DnaK) and 10 nm (FliC) in size (1:75 dilution of the stock solution) for 30 min at room temperature. After washing with PBS containing 0.1 % Tween 100 sections were washed with TE buffer and distilled water. Sections were counterstained with 4 % aqueous uranyl acetate for one min and lead citrate for 30 sec. Samples were then examined in a TEM910 transmission electron microscope (Carl Zeiss, Oberkochen, Germany) at an acceleration voltage of 80 kV. Images were recorded digitally at calibrated magnifications with a Slow-Scan CCD-Camera (ProScan, 1024x1024, Scheuring, Germany) with ITEM-Software (Olympus Soft Imaging Solutions, Münster, Germany). Contrast and brightness were adjusted with Adobe Photoshop CS5.

Fluorescence microscopy

The fluorescence microscopy studies were performed by Dr. Gabriella Molinari, HZI Braunschweig.

For indirect immunofluorescence staining of DnaK and FliC in *Pseudomonas* strains, bacteria were grown overnight in LB at 37 °C and 120 rpm. Cultures were diluted 1:10 in fresh medium and further incubated for three hours under the same conditions, then fixed by adding the same volume of a 6 % paraformaldehyde (PFA) solution in PBS and further incubation at room temperature for 20 min. No washing or mixing was performed to avoid possible damage of the flagellar structures. Aliquots von 1.5 ml were centrifuged in an Eppendorf 5415R centrifuge at 3500 rpm for 3 min and pellets were resuspended in 100 µl of PBS. In parallel coverslips

coated with a 0.01 % Poly-L-lysine solution in water were prepared as previously described[105]. Coverslips were first incubated with 50 µL of bacterial suspension and then fixed with a 3 % PFA solution in PBS. The coverslips were transferred to a 24 wells plate, were treated with a 10 mM glycine in PBS quenching solution and then washed with PBS. The immunostaining was performed at room temperature and coverslips were rinsed twice with PBS after each immunostaining step. Samples were permeabilized with 0.1 % Triton™ X-100 in PBS for 5 min, washed twice and incubated with blocking buffer (10 % fetal calf serum (FCS) in PBS) for 1 h before different parallel staining were performed. Immunostainings using only one primary antibody were performed to stain FliC or DnaK in parallel samples. Coverslips were incubated with the anti-FliC or anti-DnaK primary rabbit polyclonal antibodies diluted 1:100 in blocking buffer for 1 h. After washing, samples were incubated 45 min with the fluorescently-labeled secondary antibodies. Goat anti-rabbit Alexa Fluor 488 (ThermoFisher Scientific, Waltham, USA) and goat anti-rabbit Alexa Fluor 564 (ThermoFisher Scientific) were used for staining FliC and DnaK, respectively. After several washing steps, the coverslips were mounted using ProLong Gold antifade reagent containing nuclear staining (DAPI) (ThermoFisher Scientific). This method was used for the double labeling of FliC and DnaK in the same sample, first labeling FliC and after several washing steps, DnaK was labeled. The immunostaining experiments, done in triplicate, have been repeated with at least three biological independent bacterial cultures. Samples were analyzed with an Axio Imager A1 at 100 and 63 x magnification, AxioCam MRm camera (Zeiss, Oberkochen; Germany), and AxioVision Rel. 4.6 software using AxioVision 4 module multichannel fluorescence and filters 49 and 44.

3. Results and Discussion

3.1 Protein-protein interaction (PPI) of the respirasome of *P. aeruginosa*

The structure and biochemistry of different enzyme complex systems involved in the respiratory chain are well understood[131]. In contrast, much less is known about the dynamic interactions of these protein complexes in the respirasome. It has been proposed and proven that supracomplexes exist in humans[132], cattle[133], mice[134], spinach[135], potatoes[136] and yeast species[137,138]. In 2016 the assembly of the supracomplex of the denitrification apparatus formed under anaerobic conditions was published by José Borrero-de Acuña. The results show the nitric oxide reductase subunits NorBC represents a major assembly platform for the denitrification apparatus[48]. For the further analysis of the composition of the super complex of the respirasome under aerobic and aerobic to anaerobic shift conditions Interactomics studies were performed. For this purpose, three proteins playing a role in energy generation were chosen as bait proteins. Proteins were selected, of which there was also a transposon mutant in the corresponding gene in *Pseudomonas aeruginosa* PA14 library (PA14 Tn mutant library Harvard) available. The proteins NuoJ, FdhE and NapA were chosen for the analyses. NuoJ is part of NADH dehydrogenase I (complex I), FdhE is an associated protein of formate dehydrogenase and NapA is the catalytic part of periplasmic nitrate reductase. The approach was performed to study the protein composition of the complex and whether there is a change in the arrangement when the O_2-conditions were changed. Another technique for studying protein-protein interactions is the Bacterial Adenylate Cyclase Two-Hybrid (BACTH) system, which uses a coupled β-galactosidase assay to determine the strength of the interaction of two tested protein candidates. The BACTH system was used to perform a refinement of the PPI. The proteins NorC, NorD, NarH, NarI, NirQ, DnaK and FliC were chosen for this approach.

3.1.1 Construction of the bait protein producing strains

The analysis of the PPI was performed in the gene deletion background of the respective protein chosen as bait. The complementation of the respective deletion mutant was accomplished with the *Pseudomonas* shuttle vector pUCP26 containing the corresponding bait gene with fused C-terminal StrepII tag DNA expressed under the control of the native promoter.

First, the respective transposon mutants were spread out on LB plates with 50 µg/ml gentamycin. Clones were picked from these plates and tested for the presence of the transposon using PCR and the corresponding gene primers (Appendix 1). A positively tested clone was selected and made electrocompetent for later transformation.

The plasmid for bait protein expression was designed with NEBuilder (Appendix 2, Appendix 3, Appendix 4). First, the promoter and gene sequences of the respective proteins were amplified from the genome using appropriate primers, extracted from the agarose gel and purified. Then another PCR was performed to generate the overlapping ends. These PCR products were also extracted from the gel and purified. The promoter sequences were ready for ligation after this PCR. The StrepII tag DNA and its overlapping end at the C-terminus of the gene sequences were generated by two further PCRs with the primers NEB_StrepII and NEB_StrepII_pUCP. The plasmid pUCP26 was cleaved with the restriction enzyme *Xma*I and assembled together with the promoter sequence, the associated gene sequence and the NEBuilder master mix (Cloning of the StrepII-tagged bait protein expression plasmid with NEBuilder®HiFi DNA Assembly). After the ligation step the transformation was performed by electroporation and the transformed cells were plated onto LB plates with 50 µg/ml gentamycin and 50 µg/ml tetracyline. The multiple cloning site of this plasmid is located in the *lac*Z gene, allowing the selection of positive clones by IPTG/XGal addition in the LB plates with blue and white colony selection. Successful sequencing of the plasmids was done by Seqlab with pUCP vector primers.

3.1.2 Recombinant production of the bait proteins NuoJ, FdhE and NapA and purification of formed complexes formed under aerobic and aerobic to anaerobic shift conditions

The deletion mutants, PA14Δ*nuoJ*, PA14Δ*fdhE* and PA14Δ*napA*, were supplemented with the plasmids pUCP26-*nuoJ*, pUCP26-*fdhE* and pUCP26-*napA*, respectively, and they all contained the respective native promoter and the corresponding gene with DNA for a fused StrepII tag at the C-terminus. The native promoter allowed the bait protein to be produced in native amounts and to be purified *via* the fused StrepII tag. By using formaldehyde as crosslinker, the interacting protein partners of the respective proteins were covalently bound to the bait protein.

The complemented strains: PA14Δ*nuoJ* + pUCP26-*nuoJ*, PA14Δ*fdhE* + pUCP26-*fdhE* and PA14Δ*napA* + pUCP26-*napA* were cultivated under aerobic and shift conditions as described in the Material and Method section *Interactomics* harvested and purified by streptavidin affinity chromatography. After purification, the elution fraction was further concentrated using Viva Spin columns. The SDS sample buffer was then added to the flow-through, the wash fractions 1 and 8 and the concentrated elution fraction, heat denaturated and applied to a denaturing SDS gel (Figure 18 A and B, Figure 19 A and B, Figure 20 A and B). To confirm that the bait protein was produced and purified, a Western blot was performed with the elution

fractions of the triplicates. Figure 18 shows the SDS PAGE and Western blot analyses for the purification of NuoJ as bait. The membrane and supernatant fractions were compared under aerobic and shift conditions. The Western blot showed that NuoJ with a size of 17,6 kDa was only present in the membrane fraction. The presence of NuoJ only in the membrane fraction indicated insolubility and location within the cytoplasmic membrane by its integral transmembrane domains[139]. Furthermore, the presence of NuoJ under aerobic and shift conditions indicated a permanent aerobic and anaerobic presence of NuoJ within the respiratory system[26,27].

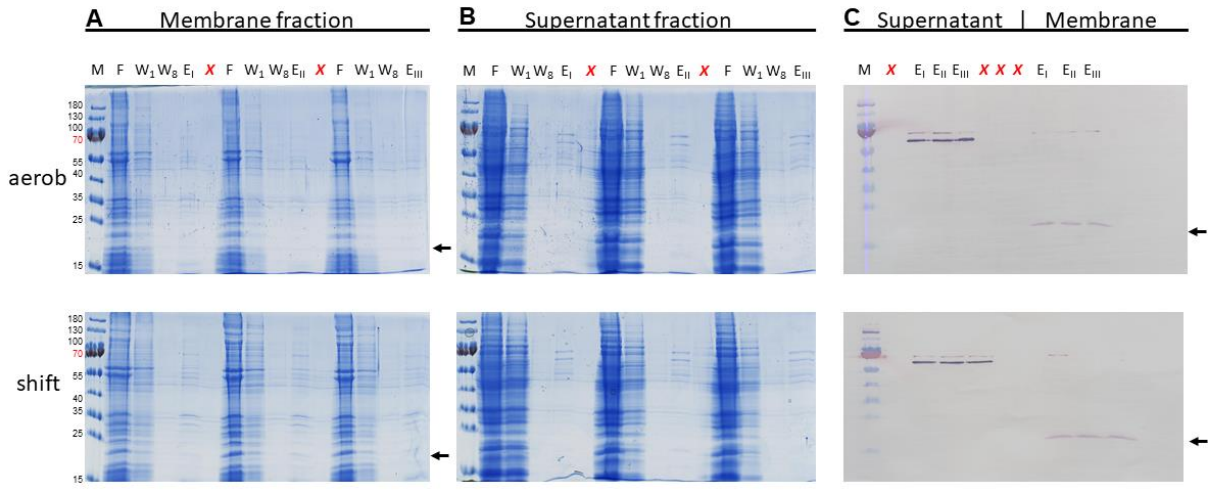

Figure 18: Interactomics of the membrane protein NuoJ with multiple interaction partners. The tagged bait protein were produced as StrepII tag fusion protein in *P. aeruginosa*, chemically cross-linked to interaction partners, and affinity purified. The fractions were resolved on an 12 % SDS-PAGE gel and contained proteins visualized by Instant*Blue*® staining. **A.** SDS-PAGE analyses of the membrane fraction of experiments performed in triplicates with NuoJ as bait protein **B.** SDS-PAGE of the soluble supernatant fraction of experiments performed in triplicates with NuoJ as bait protein **C.** Confirmation of the presence of the bait protein *via* Western blot. M: PageRuler 180 kDa; F: flow-through; W_1: wash fraction 1; W_8: wash fraction 8; E_I: concentrated elution fraction I; E_{II}: concentrated elution fraction II; E_{III}: concentrated elution fraction III; *X*: empty lane.

The protein bands, which were visible between 50 and 70 kDa on the Western blot (Figure 18 C), is background. This background can be caused by a similar sequence related to the eight amino acid sequence (WSHPQFEK) of the StrepII tag in another protein and was also detected in the Western blot as the antibody (Strep-Tactin®AP, IBA) used is directed against the StrepII tag[140,141]. When FdhE was used as bait protein, a clear difference was detected between aerobic cultivation and the shift condition (Figure 19).

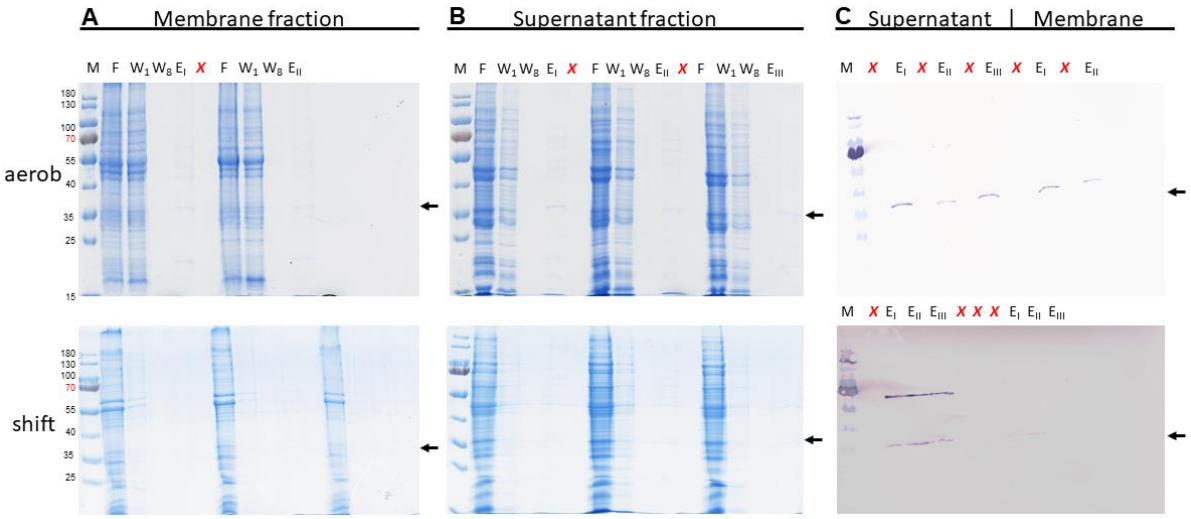

Figure 19: Interactomics of the protein FdhE with multiple interaction partners. The tagged bait protein were produced as StrepII tag fusion protein in *P. aeruginosa*, chemically cross-linked to interaction partners, and affinity purified. The fractions were resolved on an 12 % SDS-PAGE gel and contained proteins visualized by Instant*Blue*® staining. **A.** SDS-PAGE analyses of the membrane fraction of experiments performed in triplicates of purification with FdhE as bait protein **B.** SDS-PAGE analyses of the soluble supernatant fraction of experiments performed in triplicates of purification with FdhE as bait protein **C.** Confirmation of the presence of the bait protein *via* Western blot. M: PageRuler 180 kDa; F: flow-through; W_1: wash fraction 1; W_8: wash fraction 8; E_I: concentrated elution fraction I; E_{II}: concentrated elution fraction II; E_{III}: concentrated elution fraction III; *X*: empty lane.

When comparing the membrane fraction and the supernatant under aerobic conditions (Figure 19 A and B), the protein band of FdhE, which has a M_r = 35,000, was detected and confirmed in both fractions *via* Western blotting (Figure 19 C). The soluble protein FdhE is an accessory protein that controls the biosynthesis of formate dehydrogenase and interacts with the catalytic subunit FdnG, which is located in the periplasm. FdhE can be present in two forms, monomeric and homodimeric, whereby the homodimer is stabilized by anaerobic conditions[46]. Therefore, FdhE was detected in the soluble fraction as well as in the membrane fraction under both conditions. Figure 20 shows the protein patterns of preys bound when using NapA as bait protein. NapA is a soluble protein present in the periplasm which interacts *via* NapB with the subunit NapC, which is a membrane protein[53].

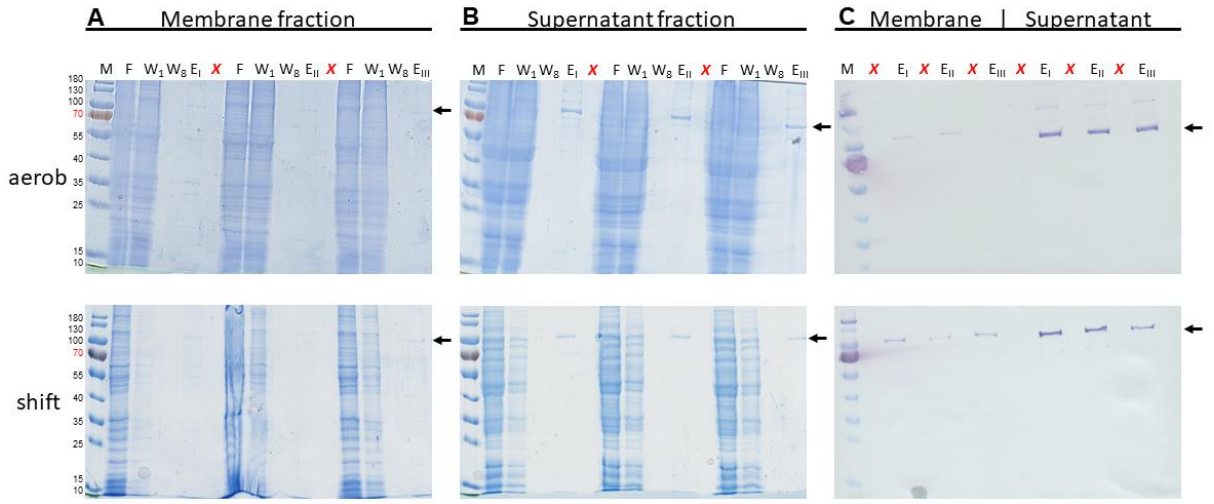

Figure 20: Interactomics of the membrane protein NapA with multiple interaction partners. The tagged bait proteins were produced as StrepII tag fusion protein in *P. aeruginosa*, chemically cross-linked to interaction partners, and affinity purified. The fractions were resolved on an 12 % SDS-PAGE gel and visualized by Instant*Blue*® staining. **A.** SDS-PAGE analyses of the membrane fraction of experiments performed in triplicates of purification with NapA as bait protein **B.** SDS-PAGE analyses of the soluble supernatant fraction of experiments performed in triplicates of purification with NapA as bait protein **C.** Confirmation of the presence of the bait protein *via* Western blot. M: PageRuler 180 kDa; F: flow-through; W_1: wash fraction 1; W_8: wash fraction 8; E_I: concentrated elution fraction I; E_{II}: concentrated elution fraction II; E_{III}: concentrated elution fraction III; *X*: empty lane (*performed by Dominik B. Schuntermann*[142]).

The Western blot confirmed the presence of NapA with a M_r = 93500 in both fractions under both conditions. These results indicated that NapA is permanently under aerobic and anaerobic conditions present in the respirasome.

3.1.3 Dynamic interaction of proteins with NuoJ, NapA and FdhE during the shift from aerobic to anaerobic growth conditions

In order to identify the interaction partners of NuoJ, NapA and FdhE in the respirasome an Interactomic approach was performed. The data were used to determine dynamics in PPI between aerobic and shift conditions.

First, the interacting proteins of the three baits (NapA, FdhE, NuoJ) were classified according their cellular localization. Figure 21 shows the distribution of the interacting proteins based on their localization in percentage ratio under aerobic and shift conditions. For all three bait proteins the proportion of cytoplasmatic localized proteins was above 50 % under both conditions. The bait protein NuoJ revealed almost 20 % periplasmic interacting proteins under aerobic conditions. It was remarkable that with NapA as bait under aerobic conditions also 10 % extracellular proteins were found, the comparison under shift conditions only 2 % were found. Under shift conditions, in general the amount of proteins localized in the cytoplasmic

membrane and the periplasm, with the exception of NuoJ, was found increased for all three bait proteins.

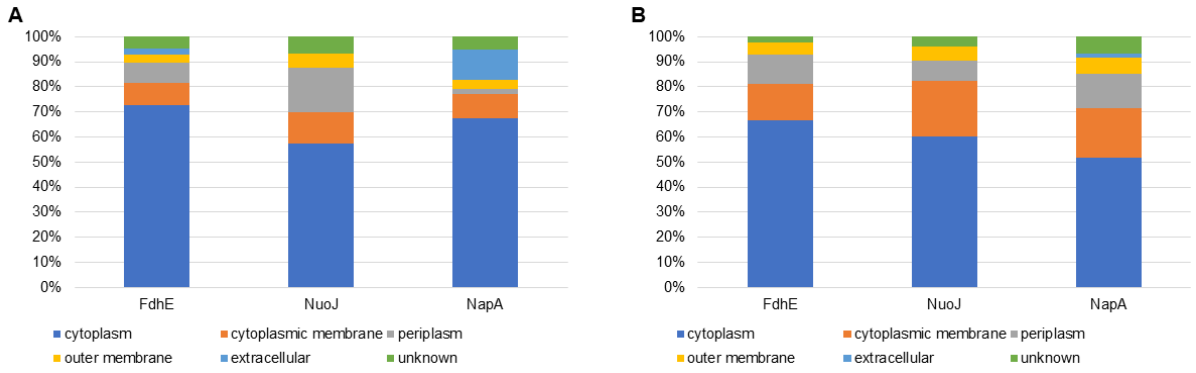

Figure 21: Cellular localization of the proteins interacting with NuoJ, FdhE and NapA found under aerobic (A) and aerobic to anaerobic shift (B) conditions. The bar charts show the distribution of the cellular protein localization **A.** Distribution of protein localization found under aerobic conditions of the bait proteins FdhE, NuoJ and NapA with a localization of cytoplasmic (blue), cytoplasmic membrane (orange), periplasm (grey), outer membrane (yellow), extracellular (light blue) and unknown (green). **B.** Distribution of interacting protein localization under shift conditions of the bait proteins FdhE, NuoJ and NapA with a localization of cytoplasmic (blue), cytoplasmic membrane (orange), periplasm (grey), outer membrane (yellow), extracellular (light blue) and unknown (green).

Next, the numbers of interactions of the individual bait proteins were examined. Figure 22 shows the percentage of interaction partners that they found for only an individual bait protein, for two or all three of them.

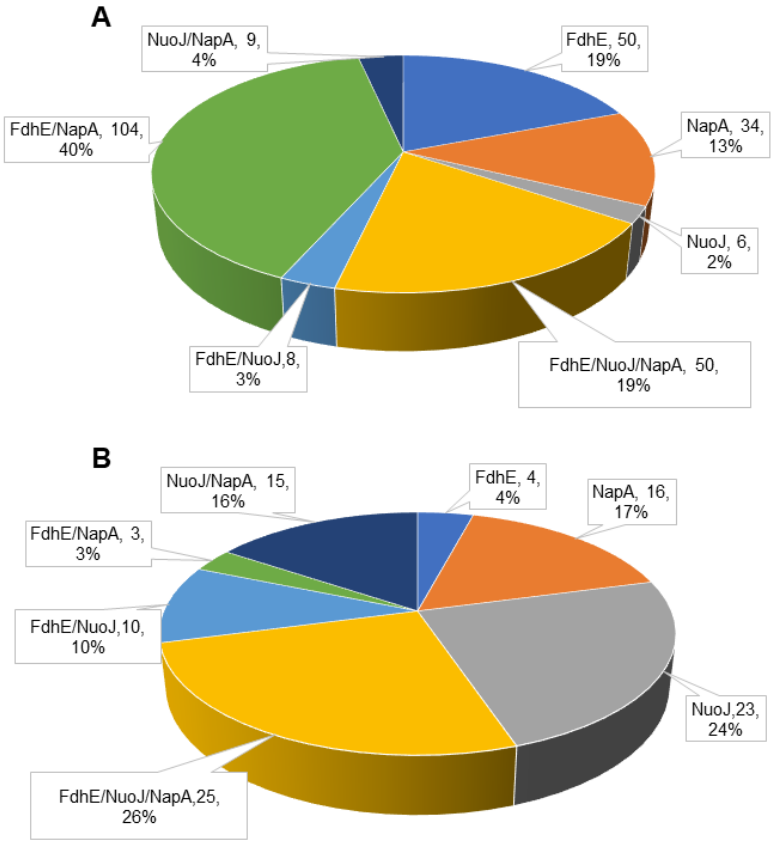

Figure 22: Number of interaction partners found for the individual baits, for two or all three of them under aerobic (A) and aerobic to anaerobic shift (B) conditions. The pie chart illustrates the number of proteins present under aerobic (**A**) and aerobic to anaerobic shift (**B**) conditions interacting which only in one bait sample: FdhE (blue), NuoJ (grey) and NapA (orange); or with two: FdhE/NuoJ (light blue), FdhE/NapA (green) and NuoJ/NapA (dark blue) or all bait protein samples: FdhE/NuoJ/NapA (yellow).

Interestingly, under aerobic conditions FdhE and NapA shared 40 % of their interaction partners (Figure 22 A), while under shift conditions it was only 3 % (Figure 22 B). Furthermore, FdhE revealed under aerobic conditions with a ratio of 19 % solely FdhE binding proteins, while under shift conditions it was only 4 %. A decrease of exclusive interaction partners for FdhE under shift conditions was shown. NapA interacted with 13 % the total interacting protein, exclusively under aerobic conditions alone and with 17 % under shift conditions. When looking at the interactions of NuoJ, exclusive protein interaction partners increased from 2 % under aerobic conditions to 24 % under shift conditions. Also, an increase of the joint interaction partners of NuoJ with NapA and of all three bait proteins together under shift conditions was observed.

In order to obtain a functional distribution of interacting prey protein a gene ontology-based distribution for the three bait proteins tested under aerobic and shift conditions was performed (Figure 23).

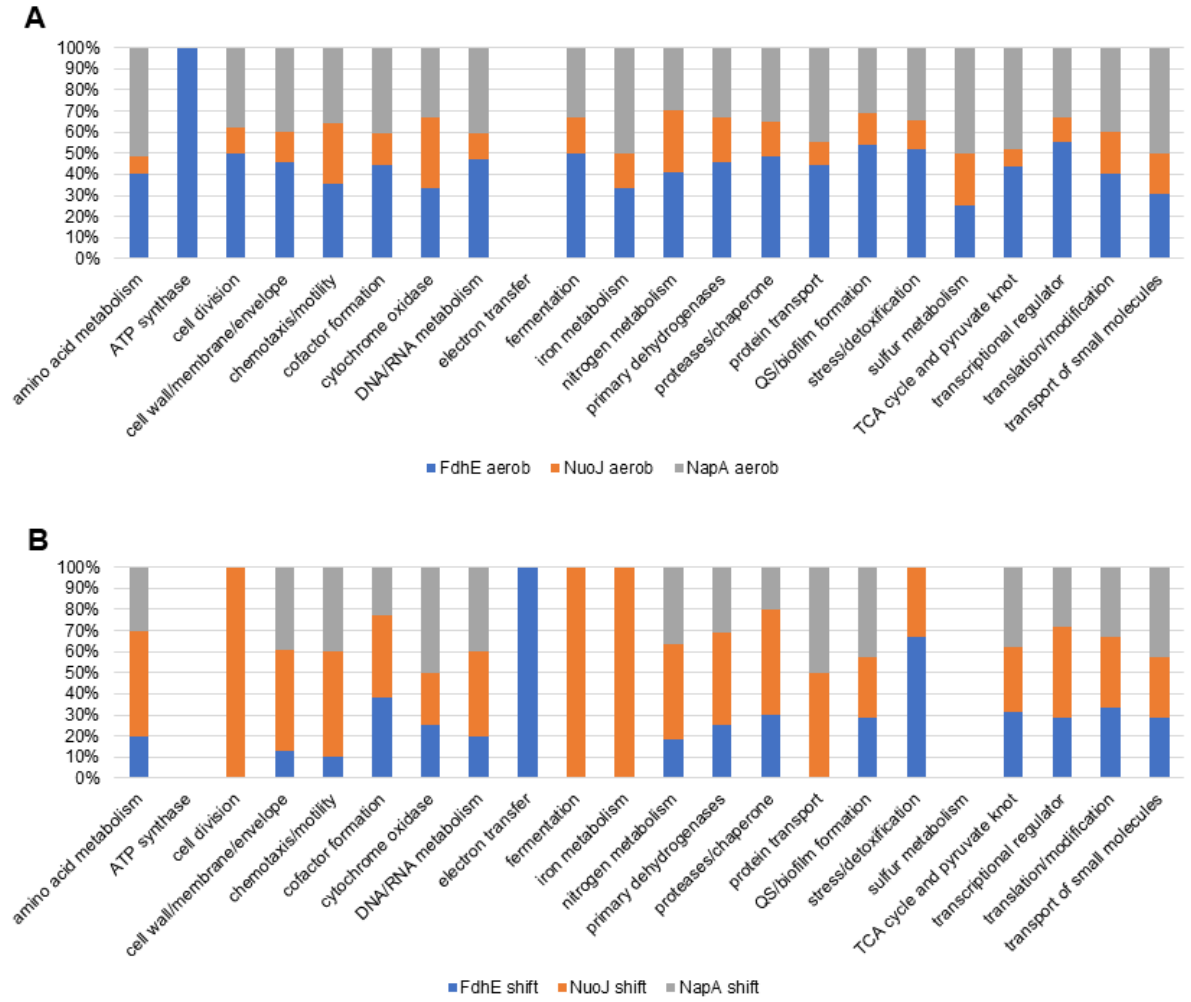

Figure 23: Functional classification of interacting prey proteins of the three bait proteins NuoJ, NapA and FdhE identified under aerobic (A) and shift (B) conditions. A. The classification of proteins interacting under aerobic conditions with the bait proteins FdhE (blue), NuoJ (orange) and NapA (grey) is shown. **B.** Functional classification of interacting prey proteins identified under shift conditions for the bait proteins FdhE (blue), NuoJ (orange) and NapA (grey).

The number of proteins interacting with FdhE decreased under shift conditions. The same was observed for the proteins interacting with NapA, here again the percentage of proteins interacting with NapA decreased under shift conditions. In contrast, the number of interacting proteins identified for NuoJ increased under shift conditions.

Proteins of the amino acid metabolism differentially interacting with NuoJ, NapA and FdhE

For a detailed view and comparison of the identified proteins interacting with the bait proteins under the two conditions, they were grouped into different gene ontology classes. First the data for the proteins involved in the amino acid metabolism were compared. Figure 24 shows that under aerobic conditions (A) most proteins of these pathways interacted with NapA and FdhE. These proteins were isolated from the supernatant fraction of both bait proteins. Interestingly, the three proteins BkdA1 (2-oxoisovalerate dehydrogenase subunit alpha), PepA (leucyl aminopeptidase) and PheS (phenylalanyl-tRNA synthetase subunit alpha) did not

interact with any of the three bait proteins under aerobic conditions. However, under shift conditions BkdA1 interacted with NuoJ and FdhE. It was also found in the membrane fraction. PepA and PheS, however, interacted only with NuoJ. The protein PhhB (pterin-4-alpha-carbinolamine dehydratase) was found under aerobic conditions in both fractions soluble, insoluble-solubilized interacting with FdhE and NuoJ. Under shift conditions it no longer interacted with any of the bait protein. This was true for almost all proteins, under shift conditions (B), only seven proteins were detected that are involved in the amino acid metabolism.

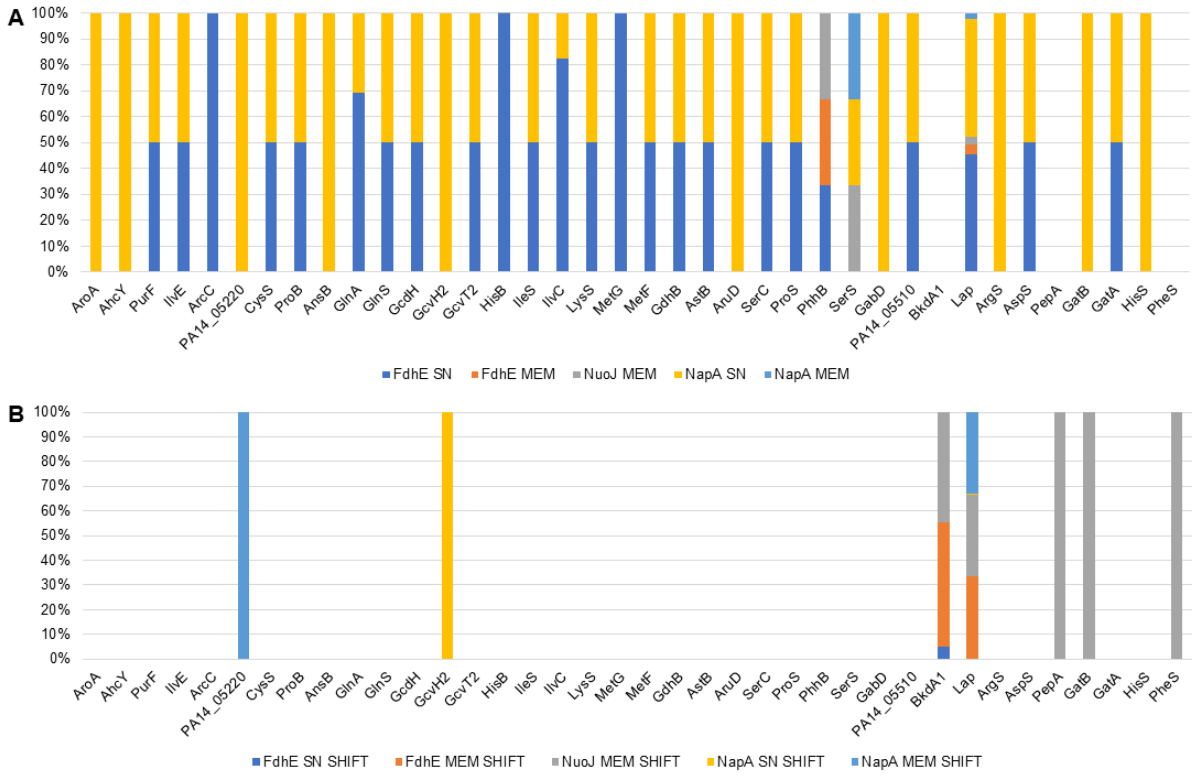

Figure 24: Identified proteins involved in amino acid metabolism differentially interacting with the three baits (NuoJ, NapA, FdhE) under aerobic and shift conditions. A. Identified proteins of the amino acid metabolism interacting under aerobic conditions with FdhE found in supernatant (soluble) fraction (blue), corresponding interaction partners of FdhE detected in the membrane fraction (orange), interacting partners of NuoJ found in the membrane fraction (grey) under aerobic condition, interacting partners of NapA present in the soluble supernatant fraction (yellow) and interacting partners of NapA detected in the membrane fraction (light blue). **B.** Identified proteins of the amino acid metabolism interacting under shift conditions with FdhE present in the soluble supernatant fraction (blue), interacting partners of FdhE found in the membrane fraction (orange), interacting partners of NuoJ detected in the membrane fraction (grey), interacting partners of NapA present in the soluble supernatant fraction (yellow) and interacting partners of NapA found in the membrane fraction (light blue).

A change in the interaction partners became clearly visible. But also, a change of interaction partners was observed. For example, the protein PA14_05220 (cystathionine beta-synthase) was found under aerobic conditions interacting with NapA, while under shift conditions it was found interacting with FdhE. At last, GatB (Glu-tRNA(Gln) amidotransferase subunit B) was identified as binding to NapA under aerobic conditions and changed the interaction partner under shift conditions to NuoJ. Also interesting was the observation of a change of solubility of

certain interacting proteins between aerobic and shift conditions. The protein Lap (low-molecular-weight alkaline phosphatase) was found interacting under aerobic conditions with FdhE and NapA in the soluble supernatant fraction, while under shift conditions it was identified only in the membrane fraction interacting with all bait proteins.

Proteins of the TCA cycle differentially interacting with NuoJ, NapA and FdhE

When comparing the identified proteins involved in the TCA cycle and the pyruvate metabolism, a similar observation was made as for the amino acid metabolism. Most of the interacting proteins were detected under aerobic conditions in the supernatant (soluble) fractions of FdhE and NapA (Figure 25).

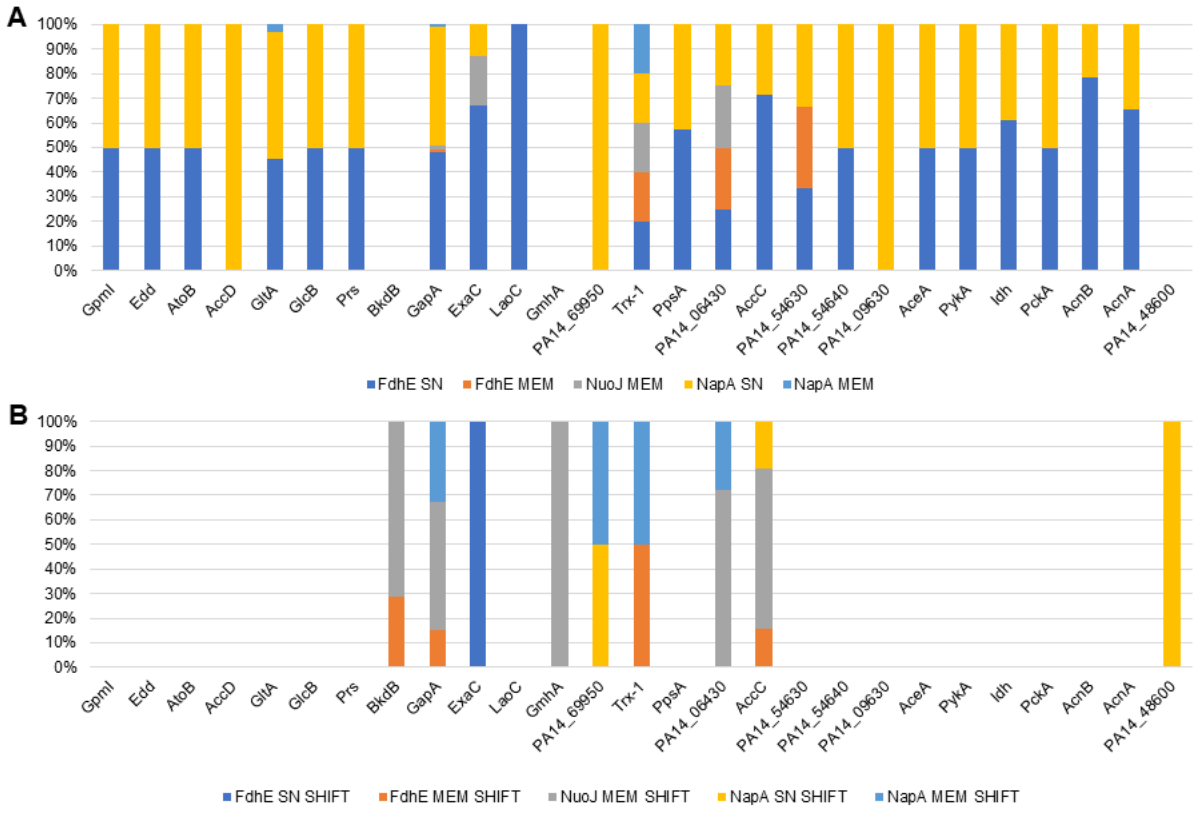

Figure 25: Identified proteins involved in TCA cycle and pyruvate metabolism differentially interacting with the three baits (NuoJ, NapA, FdhE) under aerobic and shift conditions. A. Identified proteins of the amino acid metabolism interacting under aerobic conditions with FdhE found in supernatant (soluble) fraction (blue), corresponding interaction partners of FdhE detected in the membrane fraction (orange), interacting partners of NuoJ found in the membrane fraction (grey) under aerobic condition, interacting partners of NapA present in the soluble supernatant fraction (yellow) and interacting partners of NapA detected in the membrane fraction (light blue). **B.** Identified proteins of the amino acid metabolism interacting under shift conditions with FdhE present in the soluble supernatant fraction (blue), interacting partners of FdhE found in the membrane fraction (orange), interacting partners of NuoJ detected in the membrane fraction (grey), interacting partners of NapA present in the soluble supernatant fraction (yellow) and interacting partners of NapA found in the membrane fraction (light blue).

The proteins ExaC (NAD^+ dependent aldehyde dehydrogenase), Trx-1 (thioredoxin) and PA14_06430 (hypothetical protein, acetyl-CoA carboxylase activity) were also found interacting with NuoJ under aerobic conditions. Furthermore, BkdB (branched-chain alpha-

keto acid dehydrogenase subunit E2), GmhA (phosphoheptose isomerase) and PA14_48600 (AMP-binding protein) were not found interacting with any of the three bait proteins under aerobic conditions. Under shift conditions only 9 of 27 proteins were present. For the amino acid metabolism, a change in the interacting bait protein for some proteins was observed, as well as a change in the fraction. Under shift conditions the majority of the interacting proteins were found in the membrane fractions of the bait proteins.

Proteins of the cell division and cell wall/membrane/envelope differentially interacting with NuoJ, NapA and FdhE

The comparison of the abundance of interacting proteins found that are involved in cell division and the structure of the cell wall/membrane/envelope revealed variability (Figure 26). Unlike the proteins involved in the amino acid metabolism and the TCA cycle, the majority of proteins interacting with FdhE and NapA were found in the soluble fraction. The same picture appeared for the interacting proteins with the bait proteins under shift conditions, a large number of the interacting proteins found previously are no longer present and a change of the interacting bait proteins as observed for amino acid metabolism (Figure 24) and the TCA cycle (Figure 25). The protein OsmE (DNA-binding transcriptional activator) was detected under aerobic conditions in the membrane fractions with FdhE and NapA. Under shift conditions it was only present in the soluble fraction of NapA. Furthermore, the proteins PA14_66160 (glycosyl transferase family protein), PA14_05860 (hypothetical protein, thioesterase domain), HflX (GTP-binding protein) and AlgP (alginate regulatory protein) were detected only under shift conditions.

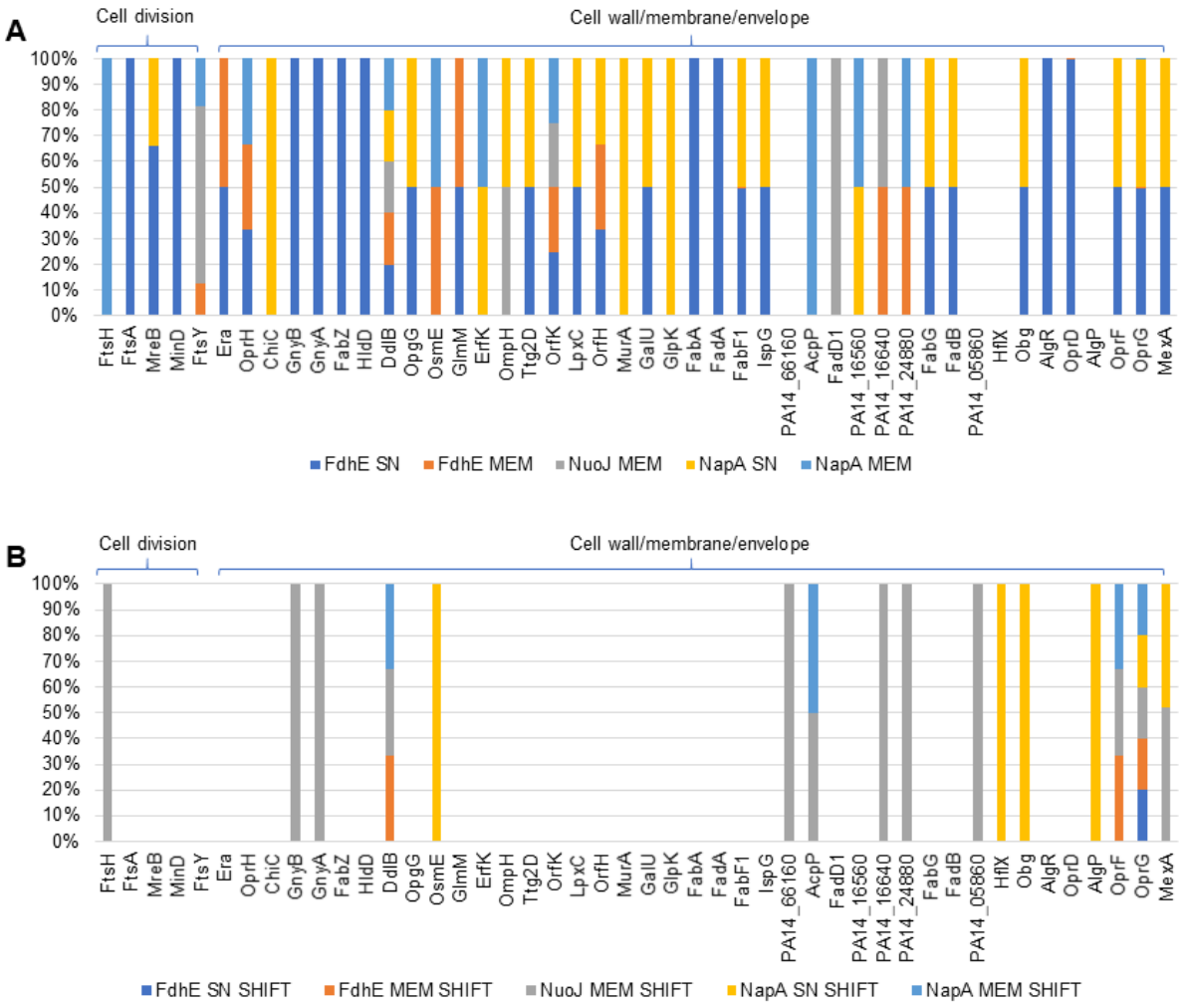

Figure 26: Identified proteins involved in cell division and cell wall/membrane/envelope organization differentially interacting with the three baits (NuoJ, NapA, FdhE) under aerobic and shift conditions. A. Identified proteins of the amino acid metabolism interacting under aerobic conditions with FdhE found in supernatant (soluble) fraction (blue), corresponding interaction partners of FdhE detected in the membrane fraction (orange), interacting partners of NuoJ found in the membrane fraction (grey) under aerobic condition, interacting partners of NapA present in the soluble supernatant fraction (yellow) and interacting partners of NapA detected in the membrane fraction (light blue). **B.** Identified proteins of the amino acid metabolism interacting under shift conditions with FdhE present in the soluble supernatant fraction (blue), interacting partners of FdhE found in the membrane fraction (orange), interacting partners of NuoJ detected in the membrane fraction (grey), interacting partners of NapA present in the soluble supernatant fraction (yellow) and interacting partners of NapA found in the membrane fraction (light blue).

Proteins of the chemotaxis, motility, quorum sensing/biofilm formation and stress detoxification differentially interacting with NuoJ, NapA and FdhE

Figure 27 shows a comparison of the abundance of interacting proteins detected, which are involved in chemotaxis, motility, quorum sensing/biofilm formation and stress/detoxification. Under aerobic conditions, most of the proteins interacted with FdhE and NapA in soluble fractions. Only out of the proteins of chemotaxis and motility, only two of the proteins, CheB and FliC, were not present under shift conditions. Out of the proteins of quorum sensing/biofilm formation only three of seven proteins were present under shift conditions. The proteins PhzF1, PqsD and RhlR interacted with the bait proteins under shift conditions. Previously, PhzF1

interacted with FdhE and NapA, found in their soluble fractions, under aerobic conditions. Under shift conditions PhzF1 was present in membrane fractions of FdhE, NuoJ and NapA. When comparing the prey proteins of stress/detoxification found in aerobic and shift conditions, only two out of 15 proteins were found under shift conditions. The proteins LsfA and ElbB were still present under shift conditions. Under aerobic conditions, LsfA was detected in the soluble fraction of FdhE, under shift conditions it was still present in the membrane fraction of FdhE. As observed before, also a change in the interacting bait protein for the majority of the prey proteins was found, as well as a change in the fraction of the bait proteins.

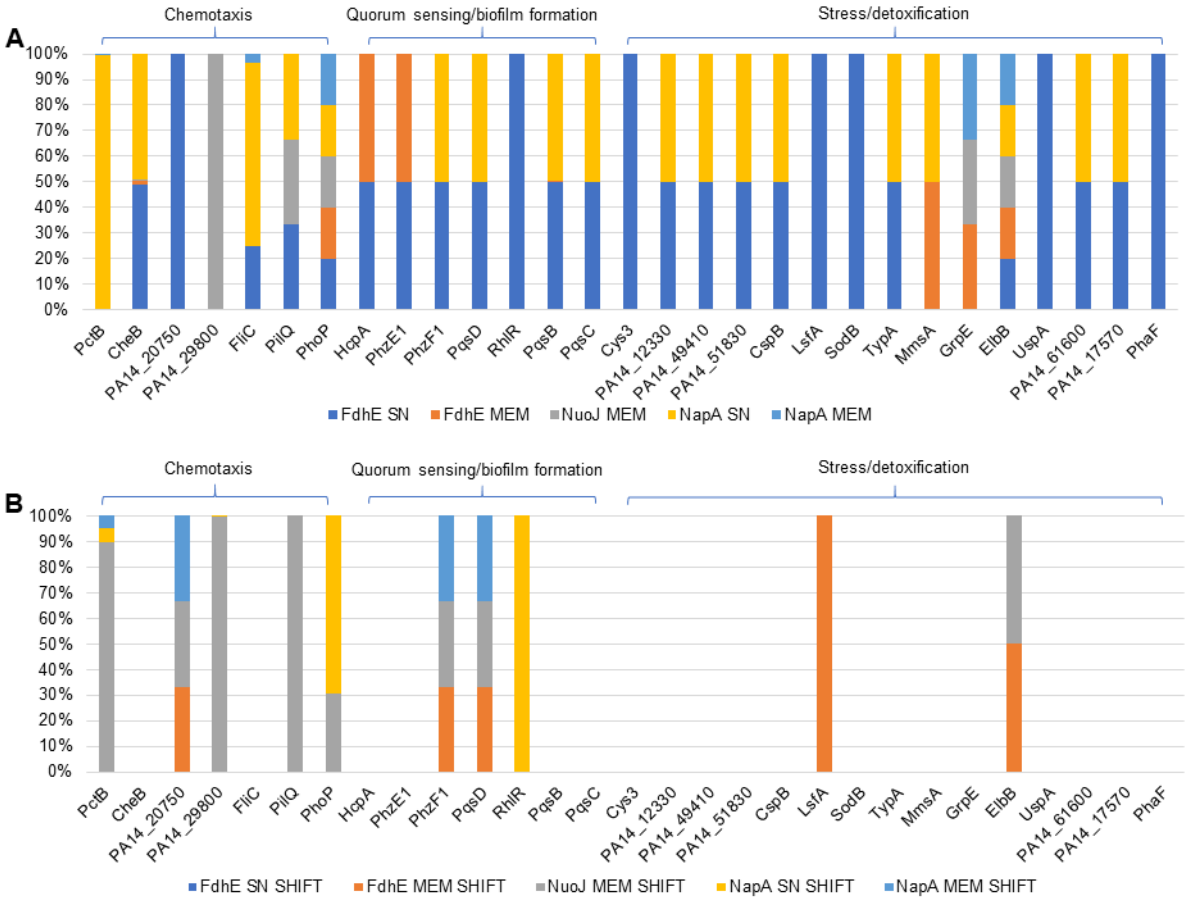

Figure 27: Identified proteins involved in chemotaxis, motility, quorum sensing/biofilm formation and stress/detoxification differentially interacting with the three baits (NuoJ, NapA, FdhE) under aerobic and shift conditions. A. Identified proteins of the amino acid metabolism interacting under aerobic conditions with FdhE found in supernatant (soluble) fraction (blue), corresponding interaction partners of FdhE detected in the membrane fraction (orange), interacting partners of NuoJ found in the membrane fraction (grey) under aerobic condition, interacting partners of NapA present in the soluble supernatant fraction (yellow) and interacting partners of NapA detected in the membrane fraction (light blue). **B.** Identified proteins of the amino acid metabolism interacting under shift conditions with FdhE present in the soluble supernatant fraction (blue), interacting partners of FdhE found in the membrane fraction (orange), interacting partners of NuoJ detected in the membrane fraction (grey), interacting partners of NapA present in the soluble supernatant fraction (yellow) and interacting partners of NapA found in the membrane fraction (light blue).

Proteins of the cofactor formation, DNA/RNA metabolism, transcription regulation, translation/modification, protein transport and ABC transporter differentially interacting with NuoJ, NapA and FdhE

Further comparison of the identified interacting proteins involved in cofactor formation (Appendix 5), DNA/RNA metabolism (Appendix 6), transcription regulation, translation/modification (Appendix 7), protein transport and ABC transporters (Appendix 8) showed that under shift conditions a large number of proteins (HemN, HemL, MoaB1, GuaB, Rho, RapA, SecB and SecD), were no longer present which were detected as interaction partners of NuoJ, NapA and FdhE under aerobic conditions. Under shift conditions identified proteins of NuoJ, NapA and FdhE were found to change their baits and were detected in a different cellular fraction (soluble *versus* insoluble). For example, UbiG (3-demethylubiquinone-9 3-methyltransferase) was found as interaction partner of FdhE (soluble fraction) under aerobic conditions, under shift conditions this protein was present in the insoluble fraction of FdhE and NuoJ. The protein Ppa (inorganic pyrophosphatase), which plays a role in the DNA/RNA metabolism, was detected in the soluble fraction of FdhE and NapA under aerobic conditions. Under shift conditions Ppa was additionally present in the insoluble fraction of FdhE and NuoJ. The protein YajC (preprotein translocase subunit) was found as interaction partner of NapA (soluble fraction) under aerobic conditions and interacted with NuoJ and NapA (insoluble fraction) under shift conditions. Interestingly, all figures show that under shift conditions the most prey proteins were interacted with NuoJ.

Proteins of the TCA cycle, pyruvate metabolism, amino acid metabolism, cell division, cell wall/membrane/cover, chemotaxis, quorum sensing and stress/detoxification form a complex with the supracomplex of the respirasome under anaerobic conditions[48]. With the bait proteins selected here, the same interacting proteins under aerobic conditions were found in part, under shift conditions. There were significantly more interacting proteins from these metabolic pathways present under aerobic conditions. The interactomics studies using NapA, NuoJ and FdhE revealed a complex protein-network around these proteins involving proteins of all central cellular functions. This is in agreement with respirasome interactomics studies under anaerobic denitrification conditions[48]. However, the aerobic and anaerobic networks might differ in their overall arrangement. The majority of proteins interact with each other to initiate a specific biological process [143,144]. Therefore, a shift from aerobic to anaerobic conditions lead to major changes of protein-protein interactions. Consequently, prey proteins moved from one bait to another, even changing from the soluble to the unsoluble fraction and *vice versa*. The protein-protein interaction network performs changes during different stages of the cell cycle resulting in the cellular system being highly dynamic and responsive to environmental factors[144–146]. The dynamic and complex regulatory network allows *P. aeruginosa* to adapt to environmental factors, whereby the large genome (~ 6 Mb) and its plasticity help to adapt to

changing conditions[147]. The periplasmic nitrate reductase is expressed under aerobic and anaerobic conditions[9,52], but under anaerobic conditions nitrate reductase NAR is also expressed[53], can be a reason for resulting in a decrease in protein interactions with NAP.

3.1.4 NADH dehydrogenase I NUO (complex I) functions as core complex in the respirasome under shift conditions

In the previous section, the interacting proteins found were divided into metabolic processes. In most cases NuoJ interacted with proteins identified under shift conditions.

Figure 28 shows the comparison of prey proteins involved in respiration interacting with NuoJ, NapA and FdhE found in the soluble and insoluble fractions between aerobic and shift conditions. Shown are proteins involved in electron transfer, like cytochrome oxidases and primary dehydrogenases, and proteins of the nitrogen metabolism. Like in the other tested cases, less proteins were found under shift conditions than under aerobic conditions. The cytochrome oxidases Snr1 (cytochrome *c*) was detected only under shift conditions. The protein FixG (probable ferredoxin), which is responsible for the electron transfer, was only found under shift conditions. Furthermore, only one protein out of four of fermentation was detected under shift conditions and five out of seven for the nitrogen metabolism were identified under shift conditions. Only half of the primary dehydrogenases were found with the bait proteins under shift conditions.

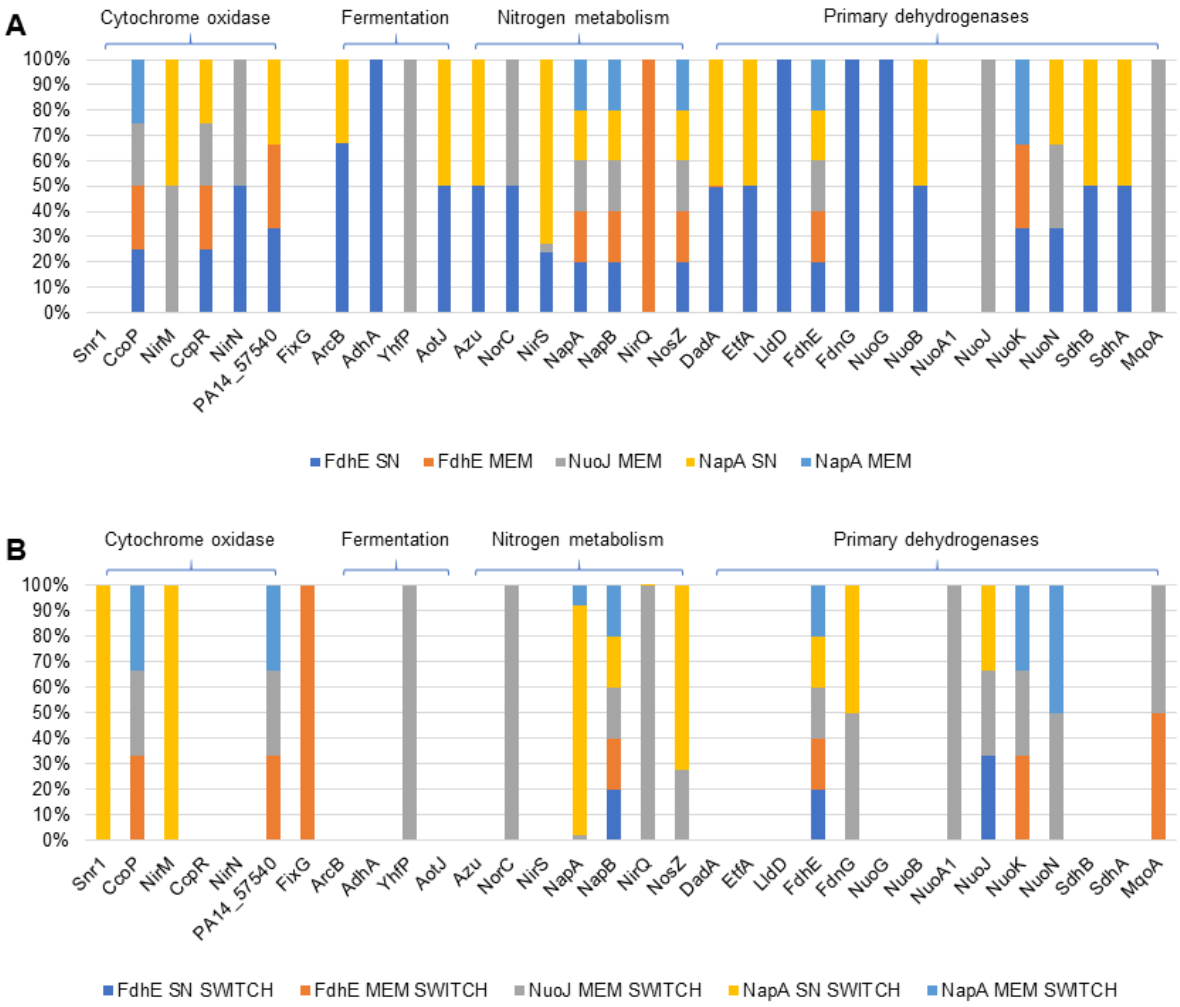

Figure 28: Identified proteins involved in the electron transfer and the nitrogen metabolism differentially interacting with the three baits (NuoJ, NapA, FdhE) under aerobic (A) and shift (B) conditions. A. Identified proteins of the electron transfer and nitrogen metabolism interacting under aerobic conditions with FdhE found in supernatant (soluble) fraction (blue), corresponding interaction partners of FdhE detected in the membrane fraction (orange), interacting partners of NuoJ found in the membrane fraction (grey) under aerobic condition, interacting partners of NapA present in the soluble supernatant fraction (yellow) and interacting partners of NapA detected in the membrane fraction (light blue). **B.** Identified proteins of the amino acid metabolism interacting under shift conditions with FdhE present in the soluble supernatant fraction (blue), interacting partners of FdhE found in the membrane fraction (orange), interacting partners of NuoJ detected in the membrane fraction (grey), interacting partners of NapA present in the soluble supernatant fraction (yellow) and interacting partners of NapA found in the membrane fraction (light blue).

Under aerobic conditions a direct interaction with NirM, the monohaem cytochrome c_{551}, which is an electron donor for nitrite reductase[9,11], existed to NuoJ and NapA. All three bait proteins interacted with the cytochrome cd_1 NirS, which is the catalytic subunit of of the respiratory nitrite reductase[9,11,48]. An interaction was detected between FdhE and NuoJ with NirN, another *c*-type cytochrome involved in NirS function[148]. Furthermore, FdhE interacted with NirQ, an ATP-binding protein required for the activation of NOR, which activates the "green-like" ribulose-1,5-bisposphate carboxylase/oxygenases (RubisCO)[149]. An interaction with the nitric oxide reductase subunit NorC, the cytochrome *c* subunit that mediates electron transfer to the catalytic subunit NorB was found for FdhE and NuoJ[48]. In contrast, all three bait proteins interacted with the catalytic subunit of nitrous oxide reductase, NosZ, which reduces nitrous

oxide to molecular nitrogen[11]. In addition, NuoJ and NapA interacted with FdhE, but only FdhE itself interacted with the catalytic subunit of formate dehydrogenase, FdnG[38]. Furthermore, NuoJ and FdhE interacted with the catalytic subunit of the periplasmic nitrate reductase NapA, and all three bait proteins interacted with the biheme cytochrome *c* subunit NapB[11]. NapA and FdhE interacted with both subunits SdhA and SdhB of the succinate dehydrogenase, which is part of the TCA cycle and oxidizes succinate to fumarate. The resulting electrons are transferred to the quinone pool and play an important role in the energy generation pathway[150]. Succinate dehydrogenase consists of the catalytic subunit SdhA, which binds to the cytoplasmic membrane *via* the [Fe-S] protein SdhB, which directly forms contact with the two integral membrane subunits, SdhC and SdhD[151].

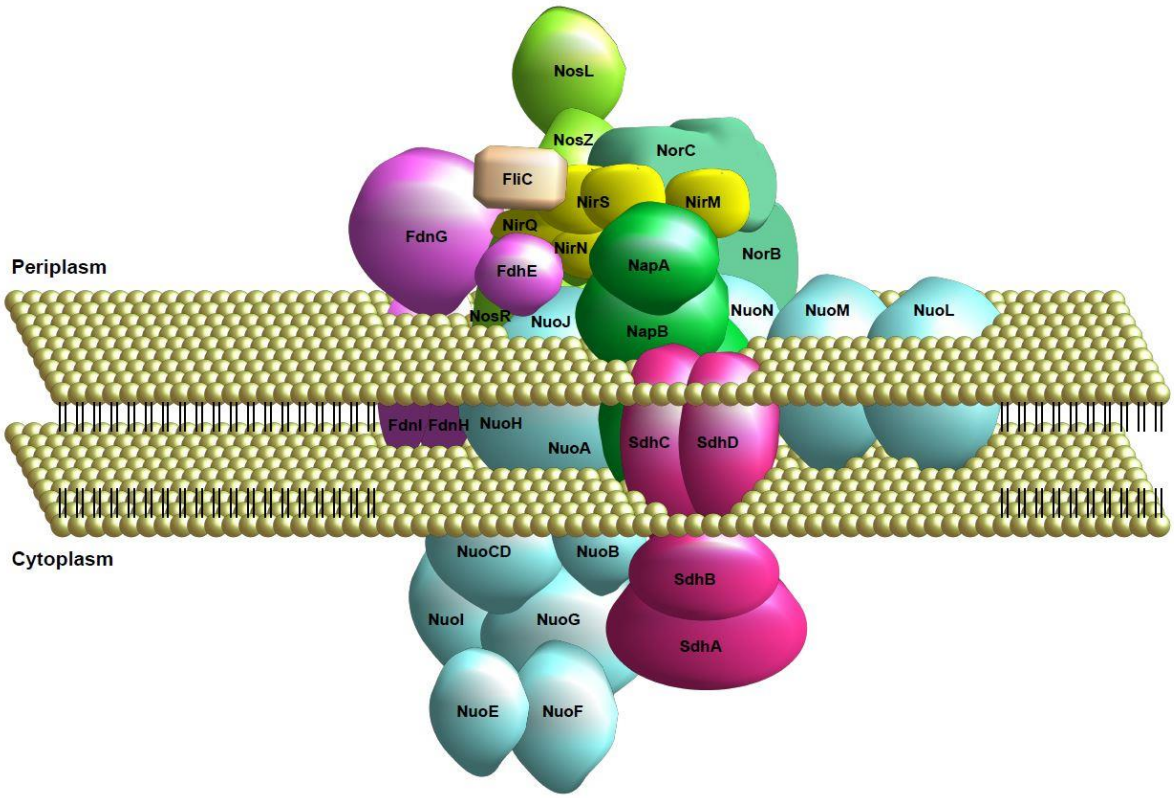

Figure 29: Model of a part of the respirasome supra complex formed under aerobic conditions. Identified protein complexes found interacting with the bait proteins FdhE, NuoJ and NapA under aerobic conditions are shown. NUO (light blue) located in the middle of the supra complex is surrounded by NAP (green), NOS (light green), NIR (yellow), NOR (mint) and FDH-O (purple). Also, the primary dehydrogenase SdhABCD (pink) interacts with NAP.

Based on these data (Figure 28), an interaction model was developed that shows the assembly and interaction of the complexes within the respirasome supracomplex under aerobic conditions (Figure 29). The complex I, NADH dehydrogenase NUO (blue), is located in the middle of the respirasome. The NUO has direct contact to the periplasmic nitrate reductase NAP (green) and to the nitric oxide reductase NOR (mint). It also has contact to the nitrite reductase NIR (yellow) and the nitrous oxide reductase NOS (light green). The formate dehydrogenase (FDH-O) with the associated protein FdhE (purple) interacts with the NUO,

NAP and NIR, and with the filament protein of the flagellum FliC. The periplasmic nitrate reductase interacts with NUO and the succinate dehydrogenase (SdhABCD) complex II of the respiratory chain (pink). The presence of NAP,NIR, NOR and NOS in the supra complex of the respirasome under aerobic conditions points towards the occurrence of aerobic denitrification. Aerobic denitrification is a mechanism of energy generation that acts as a complementary and auxiliary pathway to aerobic respiration[12,54]. A study of biofilms has shown that NAP, NIR and NOR, not NAR, were responsible for the nitrate-dependent repression of colony wrinkling under aerobic conditions[152]. Moreover, it was shown that denitrification is activated under aerobic conditions, in which NorBC plays an important role[153]. In addition, the expression level of NAP is unchanged under aerobic and anaerobic conditions[9]. Under shift conditions, the data showed a movement of the individual complexes (Figure 30).

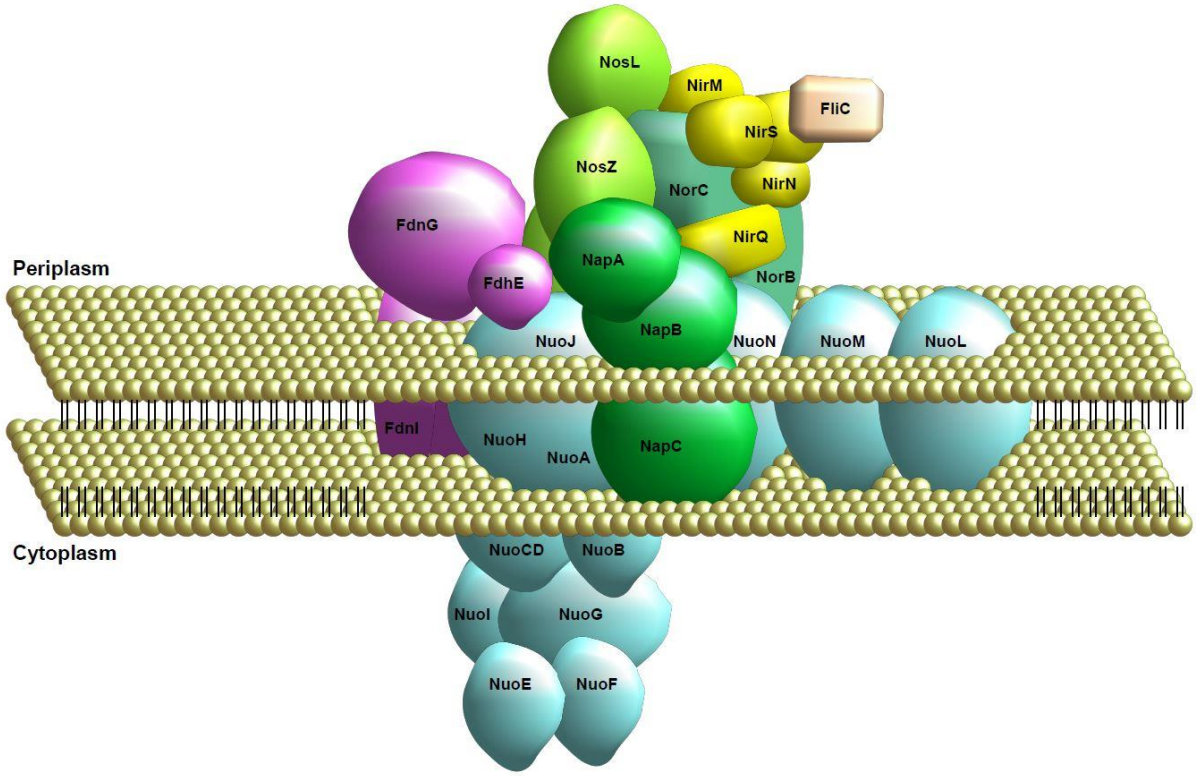

Figure 30: Model of a part of the respirasome supra complex formed under shift conditions. Identified protein complexes found interacting with the bait proteins FdhE, NuoJ and NapA under shift conditions are shown. NUO (light blue) is located in the middle of the supra complex surrounded by NAP (green), NOS (light green), and FDH-O (purple).

Under shift conditions, only NapA interacts with NirM and only NuoJ with NirQ. Furthermore, there is no interaction by the three bait proteins to NirN and NirS. Additionally, an interaction of NorC solely with NuoJ was detected. Another change in the transition complex was found for FdnG, a subunit of formate dehydrogenase which interacted with NuoJ and NapA.

The interaction of NapA and FdhE with the two subunits of the succinate dehydrogenase SdhAB identified under aerobic conditions was no longer present under shift conditions. The results indicate a significant rearrangement within the supra complex of the respirasome. In addition, the interaction by NuoJ increases, which was already observed in the previous diagrams. The observed changes of protein interactions by NuoJ indicate its function as a core protein. NADH dehydrogenase NUO is responsible for growth under aerobic conditions[26] and essential under anaerobic conditions in the presence of nitrate[27]. As NUO is the main entry point for electrons derived from NADH causing four protons to be translocated across the membrane, which generates the proton motive force[25], it is the perfect basis for respirasome complex assembly.

3.1.5 Quantification of protein-protein interaction in respirasome complexes

The Bacterial Adenylate Cyclase Two-Hybrid assay was used to investigate the strength of protein-protein interactions that were discovered in previous studies[48,105]. The studies were focused on protein-protein interactions observed in the anaerobic respirasome[48].

The genes for proteins NarI, NarH, NorC, NorD, NirQ, DnaK and FliC were cloned into the plasmids pKT25, pKNT25, pUT18 and pUT18C of the BACTH system (Appendix 9-15). The interaction between two proteins was performed with each protein in any combination with the other proteins according to the protocol of the manufactures (Application of the Bacterial Adenylate Cyclase Two Hybrid (BACTH). A positive control and a negative control were prepared for comparison. Figure 31 and Figure 32 show the positive control (A) and negative control (B) and the plates (C-P) show colonies comparable to those of the positive control.

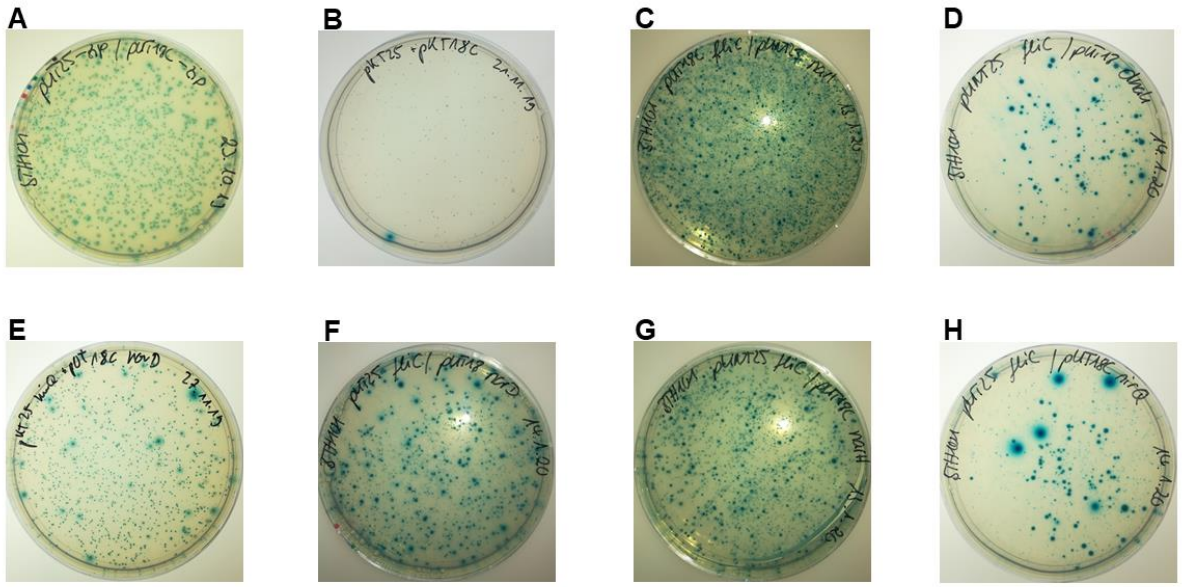

Figure 31: Protein-protein interaction of the anaerobic respirasome quantified *via* the bacterial two-hybrid system approach. Bacterial Adenylate Cyclases Two-Hybrid assays in BTH101 *E. coli* cells on M63 agar with IPTG/Xgal were performed to quantify protein interactions. The following combinations were tested **A.** Positive control pKT25-*zip*/pUT18C-*zip*, **B.** Negative control pKT25/pUT18C, **C.** pUT18C-*fliC*/pKNT25-*narI*, **D.** pKNT25-*fliC*/pUT18-*dnaK*, **E.** pKT25-*nirQ*/pUT18C-*norD*, **F.** pKT25-*fliC*/pUT18-*norD*, **G.** pKNT25-*fliC*/pUT18C-*narH* and **H.** pKT25-*fliC*/pUT18C-*nirQ*

Figure 31 indicated positive interactions between FliC/NarI (C), FliC/DnaK (D), NirQ/NorD (E), FliC/ NorD (F), FliC/NarH (G) and FliC/NirQ (H). Interestingly, the amounts of colonies on plates D and H was less, however, with the same intensive blue coloring than the other plates.

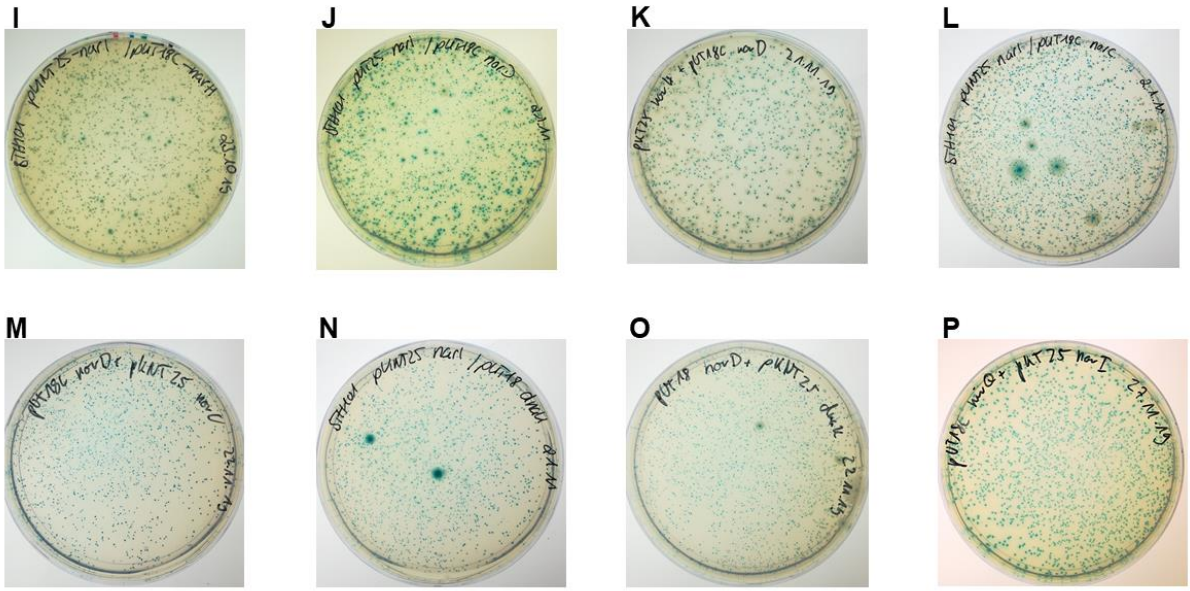

Figure 32: Protein-protein interaction of the anaerobic respirasome quantified *via* the bacterial two-hybrid system approach. Bacterial Adenylate Cyclases Two-Hybrid assays in BTH101 *E. coli* cells on M63 agar with IPTG/Xgal were performed to quantify protein interactions. The following combinations were tested **I.** pKNT25-*narI*/pUT18C-*narH*, **J.** pKT25-*narI*/pUT18C-*norD*, **K.** pKT25-*narH*/pUT18C-*norD*, **L.** pKNT25-*narI*/pUT18C-*norC*, **M.** pUT18C-*norD*/pKNT25-*norC*, **N.** pKNT25-*narI*/pUT18-*dnaK*, **O.** pUT18-*norD*/pKNT25-*dnaK* and **P.** pUT18C-*nirQ*/pKT25-*narI*

Figure 32 revealed positive interactions between NarI/NarH (I), NarI/NorD (J), NarH/NorD (K), NarI/NorC (L), NorD/NorC (M), NarI/DnaK (N), NorD/DnaK (O) and NirQ/NarI (P). These results show that NarI and FliC interacted with most of the other proteins. To determine the strength of these interactions, a β-galactosidase assay was performed (BACTH: β-Galactosidase-assay; page 74). For this assay six clones per plate were selected and analyzed. The calculation of the Miller Unit, MU (see page 74) gave a value for the interaction strength. According to the manufacturer, the positive control is 6000 MU and the negative control between 500 – 700 MU. These values were confirmed with the β-galactosidase assay.

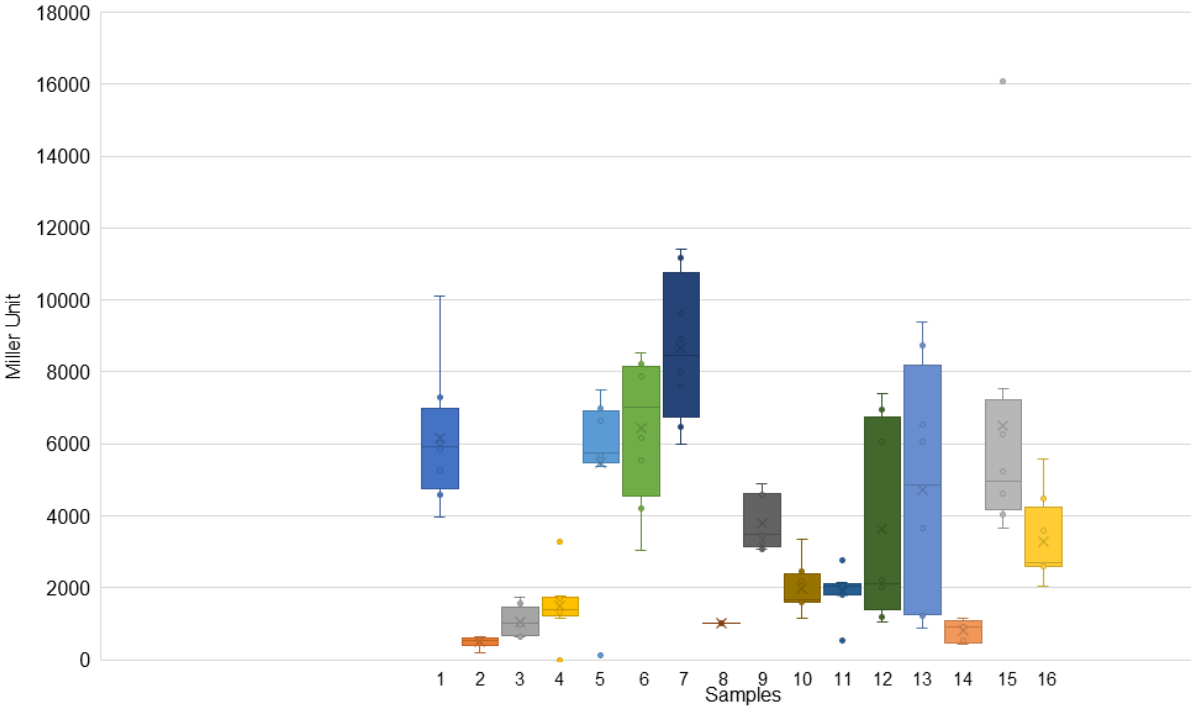

Figure 33: Quantification of the protein-protein interactions of anaerobic respirasome. The strength of interactions between various combinations of two proteins were determined by β-galactosidase assays and expressed in Miller Units. Corresponding box plots of six biological repeats are shown. The following combinations were tested **1.** Positive control, **2.** Negative control, **3.** pKNT25-*fliC*/pUT18C-*narH*, **4.** pKNT25-*narI*/pUT18C-*norC*, **5.** pUT18C-*fliC*/pKNT25-*narI*, **6.** pKT25-*fliC*/pUT18-*norD*, **7.** pKT25-*narI*/pUT18C-*norD*, **8.** pKT25-*narH*/pUT18C-*norD*, **9.** pUT18C-*nirQ*/pKT25-*narI*, **10.** pKNT25-*narI*/pUT18C-*narH*, **11.** pKNT25-*narI*/pUT18-*dnaK*, **12.** pKNT25-*fliC*/pUT18-*dnaK*, **13.** pKT25-*nirQ*/pUT18C-*norD*, **14.** pKT25-*fliC*/pUT18C-*nirQ*, **15.** pUT18C-*norD*/pKNT25-*norC*, **16.** pUT18-*norD*/pKNT25-*dnaK*

The boxplot (Figure 33) shows the Miller Unit values that were decuced from six independent assays. The positive control was in the range of 6000 MU and the negative control in a range of 500 MU. The interaction of the investigated proteins ranged between 800 MU and 10000 MU, whereby an interaction exists. The values of FliC/NarI, FliC/NorD and NarI/NorD were above the values of the positive control. The values for FliC/NarH, NarI/NorC, NarH/NorD and FliC/NirQ were above the values of the negative control and below 2000 MU.

A network diagram was generated to visualize the connections of the individual proteins among each other and the corresponding interaction strength (Figure 34). The result of the BACTH assays were used to devided observed protein-protein interaction into four classes in

dependence of measured Miller Unit. The range 800 – 2000 MU was considered as low strength interaction, between 2000 – 4000 MU as medium strength, from 4000 – 6000 MU as strong strength and from 6000 – 8000 MU as very strong interaction. The four classes were distinguished from each other by color and also by their line thickness.

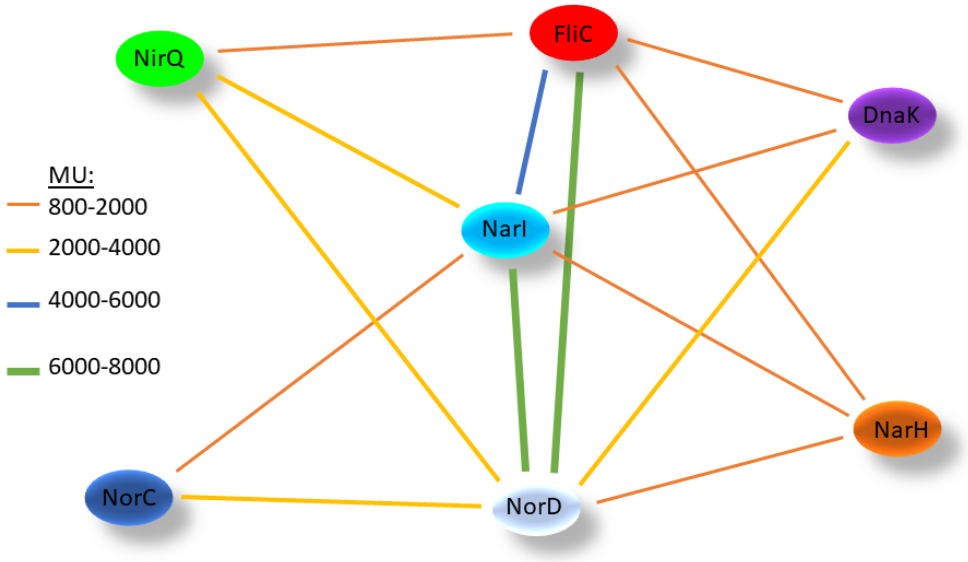

Figure 34: Network of interacting proteins of the anaerobic respirasome. The strength of the interactions between the investigated proteins NarI (light blue), NorC (white), NorD (dark blue), NarH (orange), NirQ (green), FliC (red) and DnaK (purple) was measured *via* the β-galactosidase assay. Resulting MU were used to generate this network diagram. The green line indicates a very strong interaction reflecting 6000 – 8000 MU, the blue line a strong interaction of 4000 – 6000 MU, the yellow line a medium strength interaction and the orange line a weak interaction.

The integral membrane protein of nitrate reductase, NarI, serves as an anchor for the subunits NarGH. NarG is partly located in the cytoplasm and can be purified as a complex without NarI[55]. NarG is connected to NarI *via* NarH, a weak interaction was detected by the assay. The protein NorD is required for the production of the active enzyme NorBC[11] and interacted with the subunit NorC with medium strength, strongly with NarI. The complex formation in the periplasm of DnaK-FliC was shown before[105] and was confirmed here with this assay revealing a weak interaction. A very strong interaction was found between FliC and NorD, a weak FliC interaction was found to NirQ and NarH and a strong interaction to NarI. These interactions indicate spatial proximity and multiple cellular functions for FliC in different cellular compartments due to the existence of different N-glycosylated forms of the protein[105,154,155]. The mean strength of interaction detected between NirQ and NarI and also to NorD were related to spatial proximity as well as to the function of NirQ as fine-tuning and activation of NIR and NOR proteins[4,11]. NirQ is a regulatory protein required for the formation of the denitrification apparatus[156,157]. The previous model of the denitrification apparatus assembly published by Borrero-de Acuña in 2017[157] were revised with the new data from the here obtained new results.

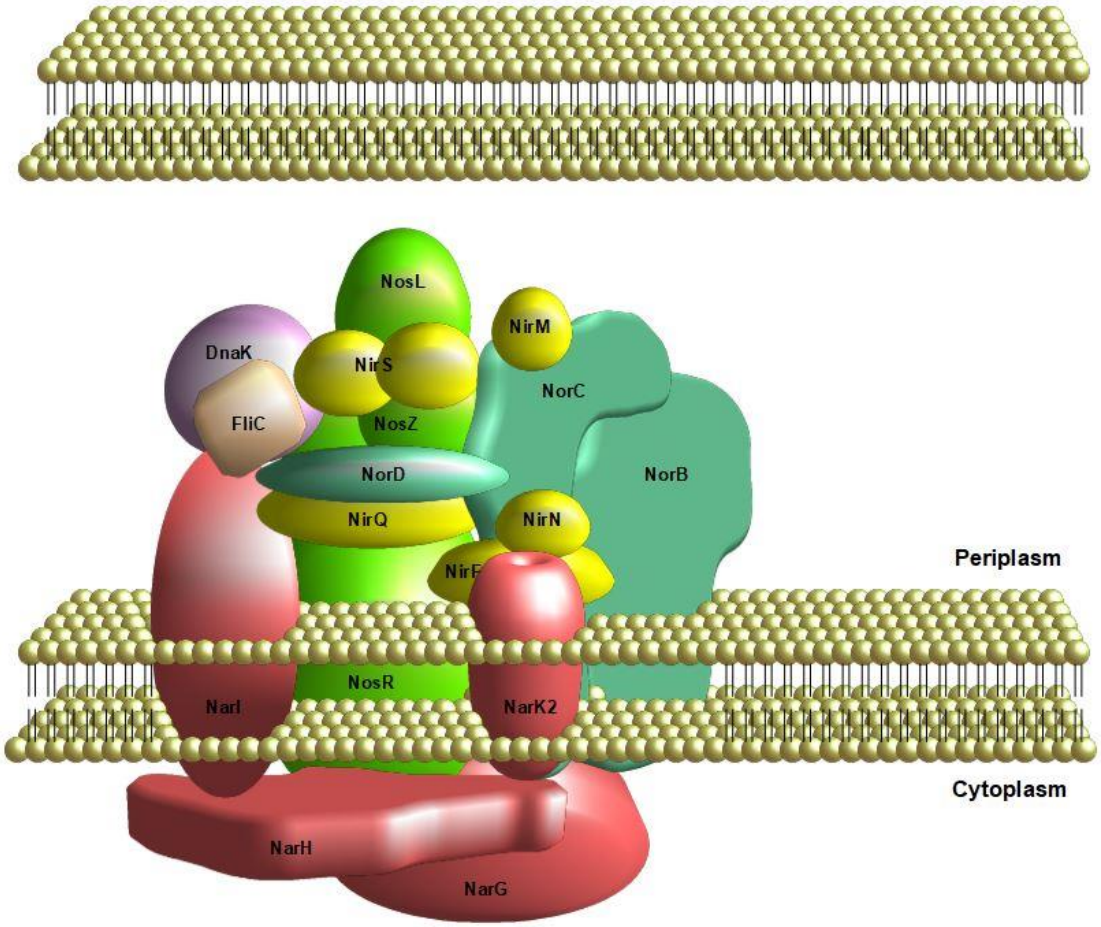

Figure 35: Revised model of the anaerobic respirasome. The denitrification apparatus with its protein complexes NAR (red), NIR (yellow), NOR (green) and NOS (light green) complexed to DnaK (purple) and FliC (light brown) both located in the periplasm of *P. aeruginosa* are shown.

In this model (Figure 35) the nitrate reductase NAR, consisting of the three subunits NarGHI, shown in red, interacts with the nitrite reductase NIR, shown in yellow. The nitric oxide reductase NOR, consisting of NorBCD, shown in green, interacts with NIR in yellow as well as with the nitrous oxide reductase NOS, shown in light green. The complex DnaK-FliC further interacts with NirS as well as with NarI, NirQ and NorD.

3.2 Vesicle production and proteome analysis of different *lemA*-like and the PA14 wildtype strains

In a second project vesicle formation in *P. aeruginosa* was studied. First indications for the involvement of certain proteins of the LemA family were derived from studies on the formation of magnetosomes. Magnetotactic bacteria (MTB) are Gram-negative bacteria that have the ability to orient themselves by the geomagnetic field. This ability is mediated by special suborganelles, the magnetosomes, which consist of magnetite or gregite crystals surrounded by a lipid layer[158]. MTB were discovered in 1975 by Richard Blakemore in marine sediments which initiated the worldwide investigation of these organisms[159]. The formation of magnetosomes is divided into different steps: vesicle invagination from the cell membrane, protein sorting, combined steps of iron transport, biomineralization, and the alignment of the magnetosomes in a chain. The general theory is that magnetosome membranes invaginate from the cytoplasmic membrane to form vesicles. The formation of a functional magnetosome is a highly controlled process, with most of the responsible genes being located in the magnetosome island (MAI), which is conserved among different species. The MAI consists of several operons, the most conserved operon being the *mamAB*. The first step is magnetosome invagination where the genes *mamB*, *I*, *L* and *Q* are involved in magnetosome vesicle formation. MamQ is a magnetosome-integrated membrane protein and homologous to the LemA protein family with unknown function[158]. The LemA protein family is widespread in Gram-negative and Gram-positive bacteria. It was first characterized by Lenz in 1996 as an H2-M3-restricted Listeria epitope[160]. The deletion of *mamQ* showed an effect on the organelle size without completely abolishing it[161]. The production of MamQ in *E. coli* lead to a variety of phenotypes, with the intracellular production of often complex structures, which appeared to be membranous[162]. It was conduced, that the two LemA proteins of *P. aeruginosa* are also involved in the process of vesicle formation. They are encoded by PA14_56810 (*lemA1*) and PA14_06690 (*lemA2*). To study the effect of the LemA-like proteins on vesicle formation, knockout strains of both genes were generated (Δ56810 and Δ06990). Furthermore, the deleted strains were complemented with a plasmid, carrying the respective gene under an IPTG-inducible promoter. In addition, a double knockout mutant was generated and also complemented with a plasmid containing the two genes under the control of an inducible promoter.

3.2.1 *P. aeruginosa* LemA1 and LemA2 are both involved in intra- and extracellular vesicle formation

For the investigation of the effect of the two LemA protein superfamily members LemA1 and LemA2 on vesicle production in *P. aeruginosa*, the respective single knockout strains, double knockout strains of corresponding genes and the complemented strains were generated. For the comparison of vesicle size, quantity and protein composition the vesicles were isolated from WT as reference standard. The production and isolation of the vesicles was performed as described in the methods section. Figure 36 shows the respective vesicle pellets after centrifugation and the vesicle containing bands after sucrose density centrifugation of all strains to be investigated. Figure 36 A shows the isolation of Δ*lemA1* strain and Δ*lemA1* + pSEVA634-*lemA1* strain. In the upper area the vesicle pellet is shown, which was increased only minimally in the complemented strain. The lower part displays the results after sucrose density centrifugation, where only one vesicle band was observed for the Δ*lemA1* strain and two bands were observed for the complemented strain. In Figure 36 B the vesicle pellet is shown in the upper part of the figure of Δ*lemA2* strain and Δ*lemA2* + pSEVA634-*lemA2* strain. There was no obvious difference between the two pellets. In the lower area the separation by sucrose density centrifugation is shown. Again, only one band was visible for the Δ*lemA2* strain and two bands for Δ*lemA2* + pSEVA634-*lemA2* strain.

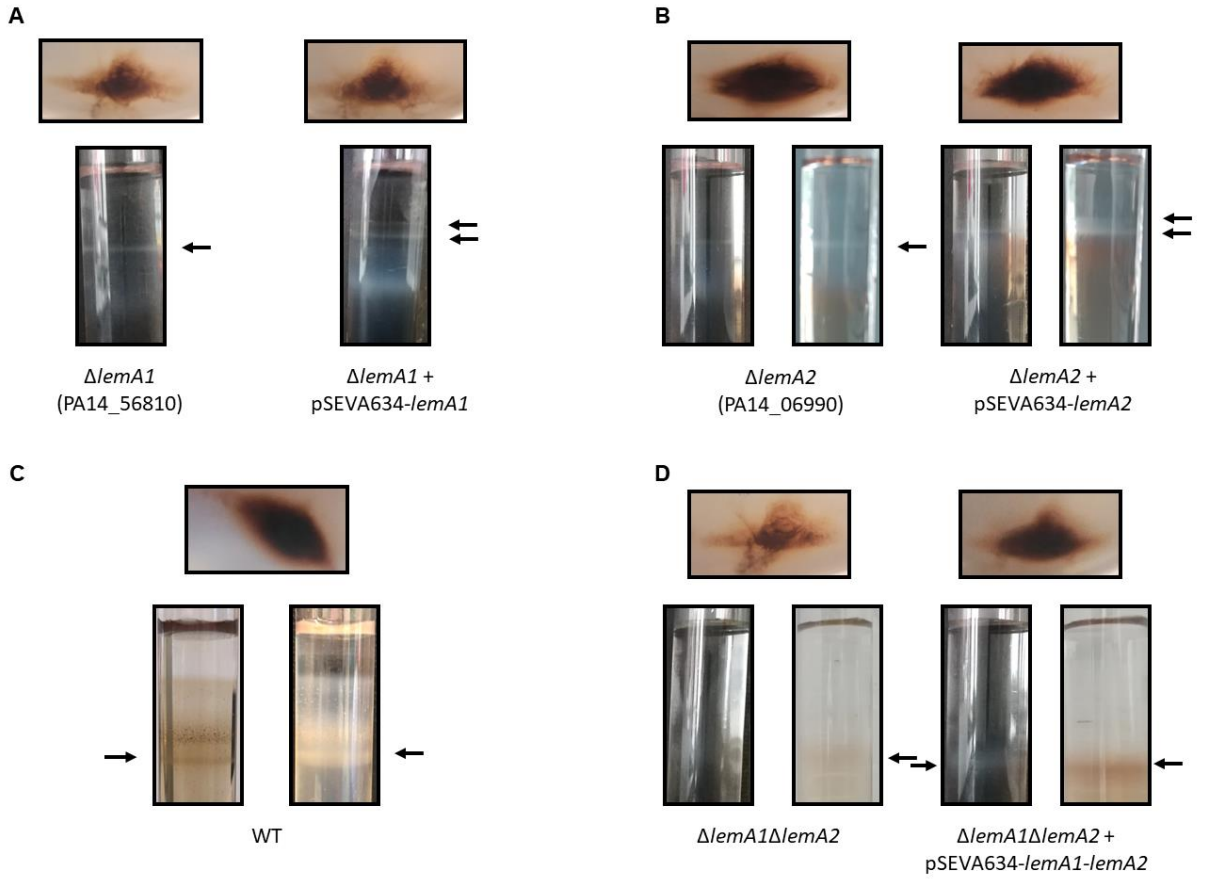

Figure 36: Vesicle isolation from various *lemA* gene mutants and overespression strains and the PA14 WT. A. Vesicle pellets after centrifugation and isolated vesicles after sucrose density centrifugation of Δ*lemA1* and Δ*lemA1* + pSEVA634-*lemA1*, **B.** of Δ*lemA2* and Δ*lemA2* + pSEVA634-*lemA2*, **C.** wildtype strain, **D.** of Δ*lemA1*Δ*lemA2* and Δ*lemA1*Δ*lemA2* + pSEVA634-*lemA1-lemA2* are shown.

The vesicle pellet and corresponding sucrose density centrifugation for WT are shown in Figure 36 C. A closely superimposed double band of vesicles was observed. The lower of the two bands was brownish and above it was a white thin band. Figure 36 D shows the comparison between Δ*lemA1*Δ*lemA2* and Δ*lemA1*Δ*lemA2* + pSEVA634-*lemA1-lemA2*, the vesicle pellet of Δ*lemA1*Δ*lemA2* was significantly smaller than that of the completed strain. When looking at the bands formed by sucrose density centrifugation, a very weak band of Δ*lemA1*Δ*lemA2* and a strong band of Δ*lemA1*Δ*lemA2* + pSEVA634-*lemA1-lemA2* are shown. The vesicle band of the complemented strain was similar to the WT band, with a brownish and a very thin white band closely together. From these results it was concluded that LemA1 has an influence on vesicle production efficency and that complementation of the knockout strain does not completely restore it to the level of WT. LemA2 did not influence vesicle formation efficiency. However, the double mutant Δ*lemA1*Δ*lemA2* significantly reduced vesicle formation. To determine the vesicle size, an analysis using NanoSight was performed as described in the methods section (Size analysis of isolated *P. aeruginosa* membrane vesicles *via* NanoSight NS300). The diameter of the vesicles was determined using a technique that uses the two properties of light scattering and Brown's motion to determine the size distribution

and particle concentration in a suspension. Figure 37 is a diagram showing the size distribution and concentration per strain.

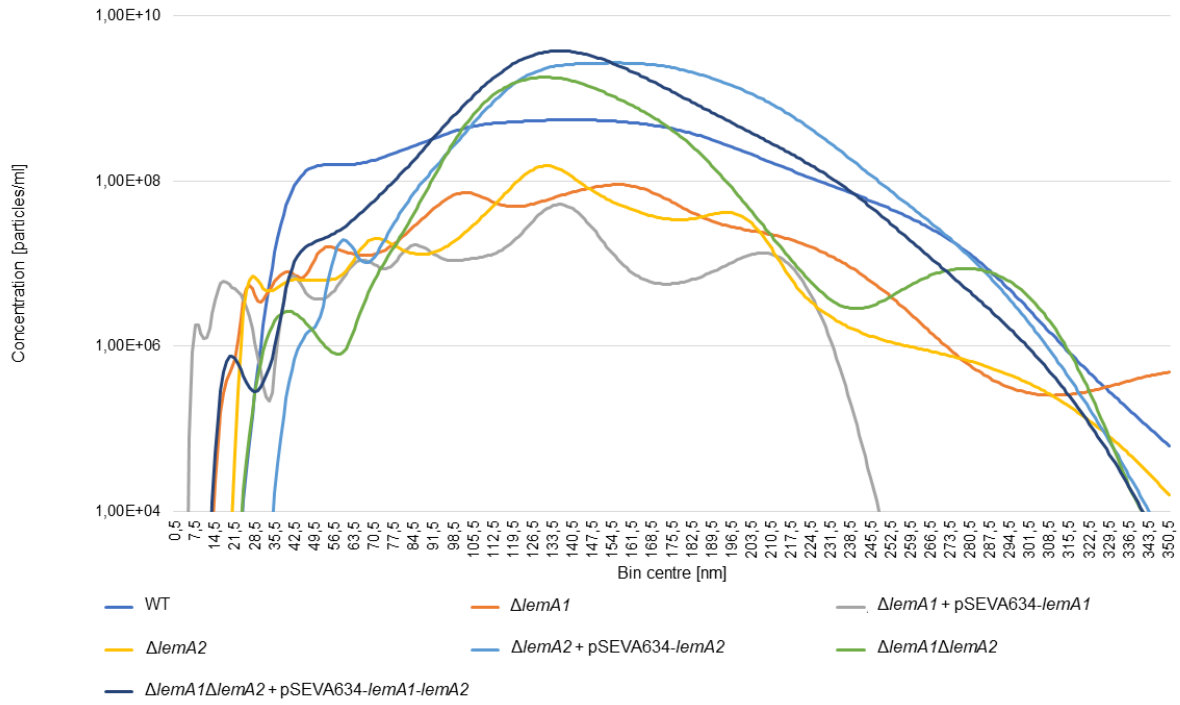

Figure 37: Comparison of the vesicle size of various *lemA* mutant and overexpressing strains using NanoSight. Analyses of the vesicle sizes of wildtype, Δ*lemA1*, Δ*lemA1* + pSEVA634-*lemA1,* Δ*lemA2*, Δ*lemA2* + pSEVA634-*lemA2,* Δ*lemA1*Δ*lemA2* and Δ*lemA1*Δ*lemA2* + pSEVA634-*lemA1-lemA2* strain *via* NanoSight NS300 is shown. Designate data of the x-axis is the bin centre (diameter of the vesicle) in nm and of the y-axis the concentration in particles/ml.

The x-axis shows the diameter of the vesicles, expressed in nm, the y-axis shows the particle concentration in particles/ml and is plotted logarithmically. For the measurement, each vesicle suspension was adjusted to a concentration within the range $1.0E^{08}$-$10.0E^{09}$. The diagrams of each of the individual NanoSight measurements are displayed in Appendix 16 and Appendix 17. Figure 37 shows that the maximum vesicle size was in the range 130 - 145 nm. The vesicles of PA14 were analyzed and differences in size between vesicles of planktonically growing cells and those of biofilm forming cells were detected. The average size of a vesicle from planktonically growing cells is 151.0 ± 5.7 nm[81].

To support the previous data, images were obtained by FESEM. Figure 38 shows two images each of the seven *P. aeruginosa* strains. The FESEM images were taken by Dr. Gabriella Molinari (HZI Braunschweig).

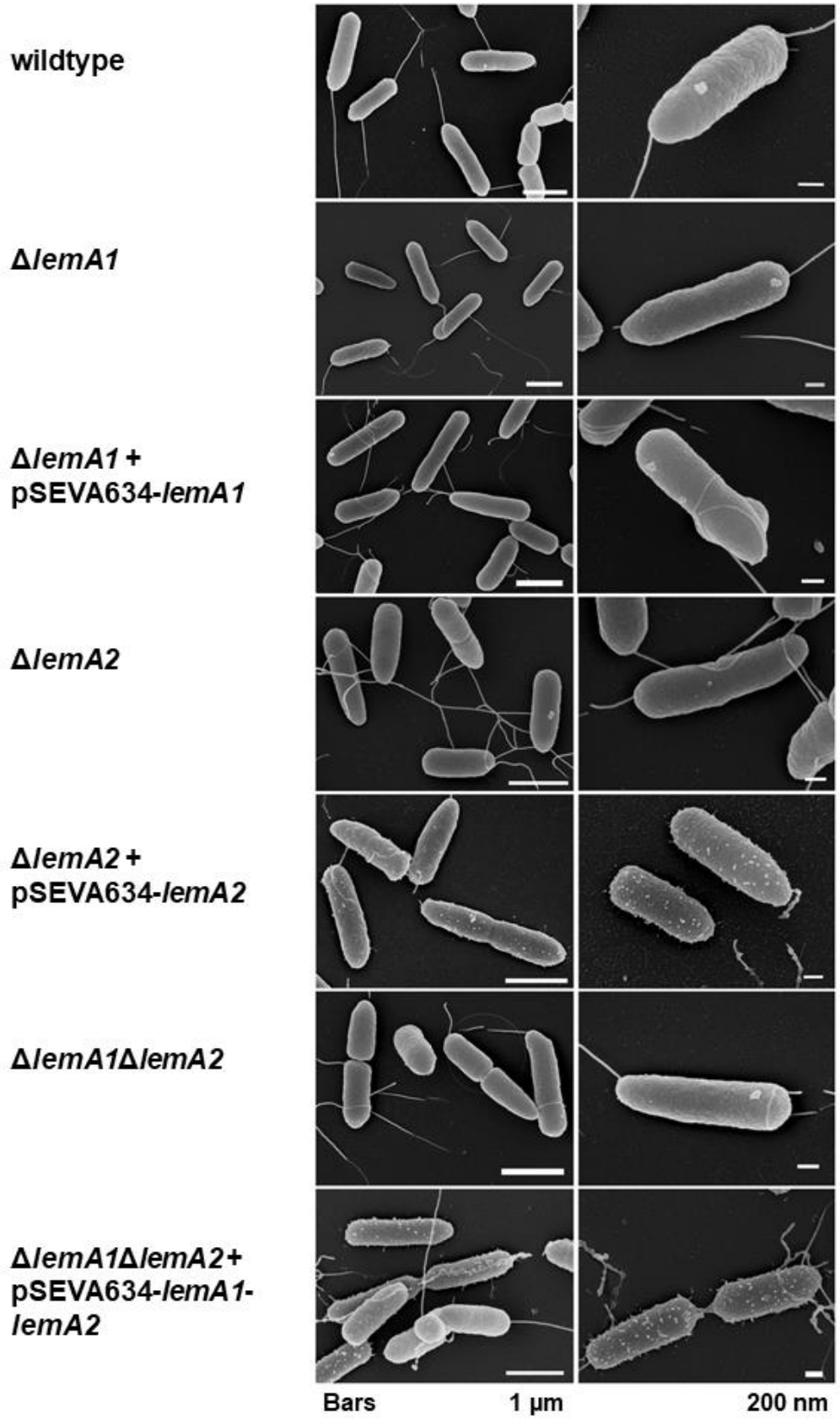

Figure 38: FESEM analyses of *lemA* deletion and oberexpressing strains. FESEM images of the wildtype, Δ*lemA1*, Δ*lemA1* + pSEVA634-*lemA1,* Δ*lemA2*, Δ*lemA2* + pSEVA634-*lemA2,* Δ*lemA1*Δ*lemA2* and Δ*lemA1*Δ*lemA2* + pSEVA634-*lemA1-lemA2* strains are shown and are labeled accordingly. Left panel of images shows an overview of the culture with a bar of 1 µm and the right panel of images show one to two cells of the culture with a bar of 200 nm. (*Images were taken by Dr. Gabriella Molinari, HZI, Braunschweig*).

The left panel of the images shows an overview of the bacterial culture and the right panel of the images shows a close-up of one or two cells. The images show that each strain produced vesicles, which was also shown by vesicle isolation and subsequent analysis using NanoSight. It was striking that the complemented *lemA2* mutant as well as the complemented double mutant showed an increased production of vesicles on the surface.

3.2.2 Proteome analyses of the *lemA* deletion and overproduction strains

In the previous section it was shown that LemA1 has an effect, in terms of quantity on vesicle production. Furthermore, it was shown that overproduced LemA2 causes an increase in the amount of vesicle production on the surface. For further analysis, the proteome of the individual strains was examined to investigate an effect of LemA1 and LemA2 on the protein composition of the vesicles. For a first overview, the distribution of the proteins were considered according to their localization, using the wildtype strain as reference. For the mutant strains Δ*lemA1* (Appendix 18 A), Δ*lemA2* (Appendix 18 B) and Δ*lemA1*Δ*lemA2* (Appendix 19 E) the following protein distribution was found: 46 - 50 % cytoplasmic, 11 - 13 % cytoplasmic membrane, 7 % extracellular, 12 - 14 % outer membrane, 3 - 4 % periplasmic and 15 - 19 % unknown proteins. Within the complemented strains Δ*lemA1* + *lemA1* (Appendix 18 C), Δ*lemA2* + *lemA2* (Appendix 18 D), Δ*lemA1*Δ*lemA2* + *lemA1-lemA2* (Appendix 19 F) the values were enclosed: 47 - 55 % cytoplasmic, 10 - 11 % cytoplasmic membrane, 5 - 7 % extracellular, 10 - 15 % outer membrane, 2 - 3 % periplasmic and 17 - 18 % unknown proteins. When compared with the data for the distribution in the wildtype strain: 56 % cytoplasmic, 12 % cytoplasmic membrane, 5 % extracellular, 10 % outer membrane, 2 % periplasmic and 15 % unknown proteins, no significant changes were found (Appendix 19 G). The distribution of the proteins based on their classification provided a further overview (Appendix 20). It was remarkable that not all strains were represented in fermentation, iron metabolism and sulfur metabolism, as was the case in all other classifications. In fermentation, only the wildtype strain and the complemented double knockout were found. This may indicate that a higher concentration or ratio of *lemA1* and *lemA2* is required to package fermentation proteins into vesicles. In the classification of iron metabolism, only the complemented single knockout strains, the wildtype strain and, interestingly, the double knockout strain were found. In this case it can also be due to the ratio where it had to be analyzed whether the same proteins were involved. In the class of sulfur metabolism only the wildtype, the complemented *lemA1* strain, the single knockout *lemA2* and the double knockout strain were found. This can be due to an effect promoted only by LemA1. For a more detailed analysis, the proteome data of the individual classifications were considered.

The formation of certain proteins of the cell wall, cell membrane and cell envelope are affected by LemA proteins

Figure 39 shows the proteome data of the proteins involved in cell wall, cell membrane and cell envelope metabolism. The values were given as a percentage in order to allow for the easy comparision of the amount of the respective proteins present in the different strains. Remarkably, the proteins PA14_08470 (protoporphorinogen oxidase, HemJ-like protein), LpxK (tetraacyldisaccaride 4`kinase), LpxD (UDP-3-O-[3-hydroxymystoyl]glucosamine N-acetyltransferase), OrfH (UDP-N-acetyl-D-mannosaminuronate dehydrogenase), MexE (RND multidrug efflux membrane fusion protein) and CtpA (carboxyl-terminal processing protease) were found only in the wildtype strain. The intracellular enzymes MurA-MurF are involved in the first steps of peptidoglycan synthesis. They catalyze the synthesis of the precursor UDP-*N*-acetylmuramyl pentapeptide. These enzymes are essential for bacterial survival. Inhibition of one of these enzymes leads to a lethal phenotype. MurE belongs to the four ATP-dependent amide ligases that perform the stepwise addition of amino acids (L-Ala, D-Glu, a di-amino acid and D-Ala-D-Ala) to form the cell wall peptide moiety[163]. In *P. aeruginosa* and other Gram-negative bacteria, UDP-N-acetylglucosamine (UDP-GlcNAc) is also one of the precursors for the synthesis of peptidoglycan and of membrane lipopolysaccharide (LPS). The metabolic steps involved in the formation of UDP-GlcNAc represent a rate-limited step of the overall flow of metabolites, which are produced by the peptidoglycan and LPS pathways. Phosphoglucosamine mutase (GlmM) catalyzes the second of four successive steps that lead to the synthesis of UDP-GlcNAc from fructose-6-phosphate. This enzyme catalyzes the interconversion of glucosamine-6-phosphate (GlcN-6-P) to glucosamine-1-phosphate (GlcN-1-P). Significantly, one *glmM* mutation affects not only peptidoglycan, but also LPS synthesis in *E. coli*. Besides its phosphoglucosamine mutase activity, the *P. aeruginosa* GlmM was shown to display side activities of phosphomannomutase and phosphoglucomutase, which is about 20 % and 2 % of their GlmM activity[164,165]. It was remarkable that these proteins MurE (UDP-N-acetylmuramoylalanyl-D-glutamate-2,6-diaminopimelate ligase) and GlmM (phosphoglucoseamine mutase) occured only in the complemented double knockout strain Δ*lemA1lemA2* + *lemA1lemA2*, thereby showing an influence of both LemA proteins on cell wall biosynthesis and thus on the formation of MVs. Additionally, the proteins FadE (acyl-CoA dehydrogenase), YhiI (conserved hypothetical protein), FabH2 (3-oxoacyl-[acyl-carrier-protein] synthase III), OrfM (NAD ependent epimerase/dehydratase), PA14_61290 (lipoprotein) and PA14_23420 (ZbdP) were found in high numbers in the complemented *lemA1lemA2* strain. The EngA protein is a conserved and essential bacterial GTPase with tandem GTP-binding domains and a C-terminal KH (K homology) domain of broadly enigmatic function. Most studies of EngA have suggested a role in ribosome assembly, the protein has also been involved in various elements of physiology, including chromosome

separation, cell control of division and cell cycle[166]. Bacteria regulate their membrane fatty acid composition to maintain optimum fluidity to support growth under different environmental conditions. This critical role of fatty acid structure is mirrored by the multiple mechanisms that have evolved in bacteria to control the composition of fatty acids incorporated into membrane phospholipids. In *P. aeruginosa*, unsaturated fatty acid (UFA) synthesis is performed exclusively *via* the anaerobic type II biosynthetic pathway and requires the activities of the *fabA* and *fabB* genes. FabA is a β-hydroxydecanoyl acyl carrier protein (ACP) dehydratase isomerase that forms cis-3-decenoyl-ACP, which is then extended by the FabB condensing enzyme. *P. aeruginosa* uses FabA and FabB for the anaerobic formation of UFA *via* the type II pathway, which are expressed coordinatively as a *fabAB* operon. *P. aeruginosa* contains additionally two aerobic pathways for UFA synthesis[167]. The two proteins EngA (GTP-binding protein) and FabB (3-oxoacyl-ACP synthase) were only found in the complemented *lemA2* mutant strain indicating that a high LemA2 level has an influence of lipid formation. In further analyses, only those proteins that do not occur in the knockout strains but in the complemented strains were considered, which allows to speculate about a possible influence of LemA1 or LemA2 on the formation of the respective proteins. DacC, as a low molecular weight (LMW) penicillin binding protein (PBP), has a strong carboxypeptidase activity that enables the cleavage of terminal D-alanine from the pentapeptide side chains of murein components. Peptidoglycan is a critical component in maintaining cell structure stability and cell shape. DacC plays a role in the stabilization of peptidoglycan during the stationary phase[168]. *Pseudomonas sp*. and other closely related soil organisms are unique in that they almost exclusively use specific porins for the general process of uptake *via* the outer membrane. Eleven of the 19 channels in *P. aeruginosa* have clear orthologues in *Pseudomonas putida* and probably share the same function in both organisms. Six proteins in *P. aeruginosa* (OpdJ, OpdI, OpdR, OpdO, OpdD and OpdQ) have no orthologues in *P. putida* and could therefore be derived from post speciation duplication events and might provide functions unique to *P. aeruginosa*[169]. The protein DacC was only found in the strain overexpressing *lemA1* and in the *lemA2* knockout strain. OpdO was found in the completed *lemA1* strain, *lemA2* knockout and *lemA1lemA2* double knockout strain, indicating an influence of LemA1 alone. The Mla system is involved in the maintenance of OM lipid imbalance and consists of seven proteins distributed over the cell envelope. It has been shown that VacJ (also known as MlaA) and other components of the Mla pathway play a role in antibiotic resistance in *P. aeruginosa* and may contribute to the formation of outer membrane vesicles[170]. VacJ (MlaA lipoprotein) was found in the overexpressed *lemA1* strain, not in the *lemA1* deletion strain, and suggests an influence by LemA1 on its formation. Furthermore, the proteins FptA (Fe(III)-pyochelin outer membrane precursor), OprE (anaerobically-induced outer membrane porin OprE precursor) and PA14_56810 (LemA1) were found in increased concentrations in the complemented *lemA1* strain, which also indicates an influence by an increased LemA1 level on its formation.

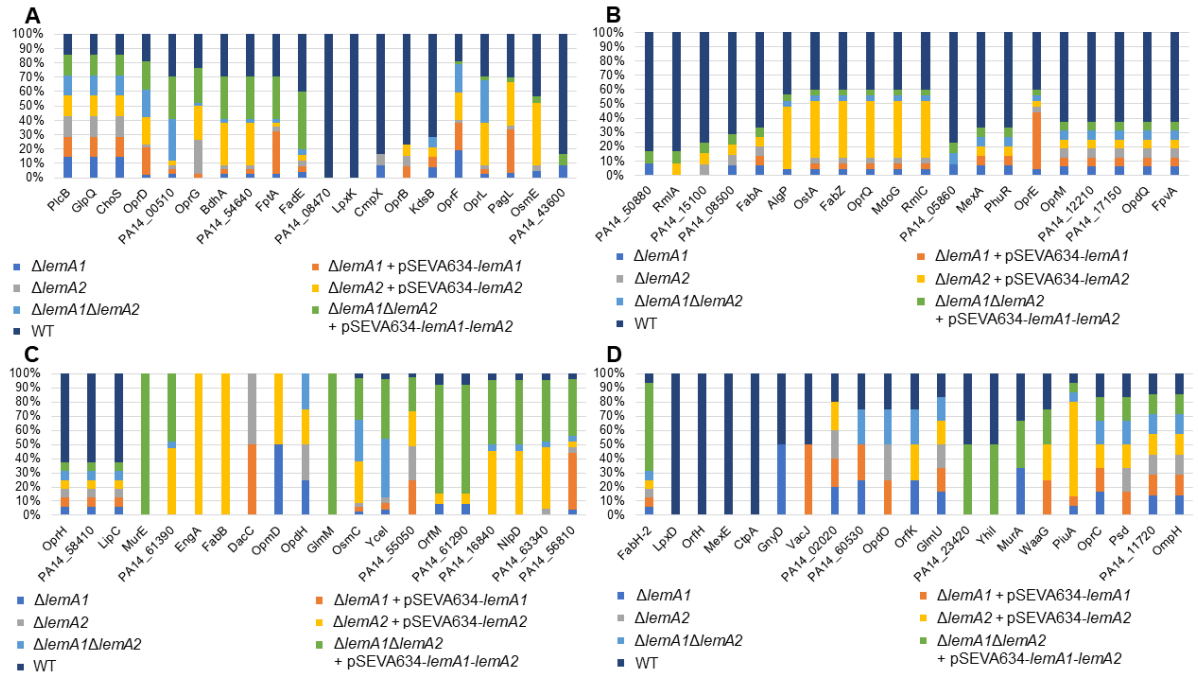

Figure 39: Changes of the abundance of proteins of the cell wall, cell membrane and cell envelope in dependence of the deletion or overexpression of *lemA* genes compared to the wildtype strain. A-D. Abundance of identified proteins of cell membrane and cell envelope in the wildtype (dark blue) and Δ*lemA1* (blue), Δ*lemA1* + pSEVA634-*lemA1* (orange), Δ*lemA2* (grey), Δ*lemA2* + pSEVA634-*lemA2* (yellow), Δ*lemA1*Δ*lemA2* (light blue) and Δ*lemA1*Δ*lemA2* + pSEVA634-*lemA1*-*lemA2* (green) strains.

In Gram-negative bacteria, two enzymes, FabA and FabB, are responsible for the production of unsaturated fatty acids. Unsaturated fatty acids are essential for the cells because the ratio of saturated/unsaturated fatty acids, that is controls the physical properties of the membrane. FabA is a bifunctional enzyme that catalyzes dehydration of the hydroxyacyl acyl carrier protein (ACP) to trans-2-enoyl-ACP. The homologous enzyme FabZ (3R-hydroxymyristoyl-ACP dehydratase) also catalyzes this step[171] and was found in high concentrations in the overexpressed *lemA2* strain, suggesting an effect by LemA2 on its formation. Since FabB was already found only in the complemented *lemA2* strain, it indicates that LemA2 has an influence on the formation of unsaturated fatty acids. The membrane-derived oligosaccharides (MDO) are members of a family of glucans located in the periplasmic space of Gram-negative bacteria[172]. The glucan biosynthesis protein G (*mdoG*) is located in the *mdoGH* operon and is involved in cell wall biosynthesis[173]. It was shown in *E. coli* that an absence of MDO could lead to an abnormal assembly of different envelope components. Furthermore, MDO were used for the regulation of the biosynthesis of various envelope components, especially those involved in osmoregulation such as flagella apparatus and colanic acid synthesis[174]. MdoG was found in a high concentration in the complemented *lemA2* strain indicating an influence of LemA2 on its formation. The TonB-dependent receptors (TBDRs) are able to transport siderophores or vitamin B_{12} in Gram-negative bacteria, as well as carbohydrates, cations and thiamine. Due to their high binding affinity sites, substrates are transported even at low concentrations. They can perform concentrative uptake for entercholine and vitamin B_{12} and uptake large substrate

molecules such as cobalamins, heme or peptide siderophores such as pyoverdin. Uptake *via* the outer membrane of TBDRs requires energy provided by the proton motive force[175]. *P. aeruginosa* possesses 35 of these TonB-dependent receptors, including PiuA. However, the substrate of PiuA is still unknown[176]. A high concentration of PiuA was found in the overexpressed *lemA2* strain, in contrast to the wildtype, indicating an influence by LemA2 on its synthesis. In contrast, the receptor for pyochelin, FptA[176], was found in high concentrations in the complemented *lemA1* strain and complemented *lemA1lemA2* strain, indicating an influence of LemA1 on its build up. WaaG, which encodes UDP-glucose (heptosyl) LPS-1,3-glucosyltransferase, is responsible for lipid A biosynthesis and has been identified as an essential gene. The gene *waaG* required for peptidoglycan synthesis is essential for the growth and survival of *P. aeruginosa*[177]. This protein was found in all overexpressed *lemA* strains and not in the knockout strains, indicating an influence of both LemA proteins on its appearance. Furthermore, other high concentrated proteins were found in the overexpressed *lemA2* strain, namely OpmD, OprQ, OpdH, OsmE, AlgP, OstA and RmlC. Proteins unique to the complemented *lemA2* strain and the complemented double-knockout strain were BdhA, NlpD, PA14_54640, PA14_61390, PA14_16840 and PA14_63340, this also indicates an influence of LemA2.

The formation of certain proteins of the chemotaxis and motility, proteases and chaperones, protein transport, quorum sensing and biofilm formation are affected by LemA proteins

In further analysis, the proteins involved in chemotaxis and motility, proteases and chaperones, protein transport as well as quorum sensing and biofilm formation were compared between wildtype, the complemented strains and the respective knockout strains (Figure 40). First, for the identified proteins of chemotaxis and motility the protein PctB (chemotactic transducer) was solely found in the complemented *lemA1* strain and suggest an influence of LemA1. Bacterial signal transduction is primarily achieved by the action of one-component systems, two-component systems and chemoreceptor-based signals. The chemoreceptor-based signaling cascade mediates flagellum-mediated chemotaxis and type IV pili-mediated motility. The receptor PctB belongs to class II of the ligand-binding regions (LBR) and mediates chemotaxis against L-amino acids, intermediates of amino acid metabolism as well as chemorepulsion on various toxic chlorine-containing compounds such as trichloroethylene and chloroform[178]. One of the main motility systems in *P. aeruginosa* is the type IV pilus system, which is used for twitching motility on solid and semi-solid surfaces. The majority of a pilus fiber is made up of hundreds to thousands of subunits of the major pilin protein PilA[179]. The pilus filament has an important role in tissue adhesion and invasion, 90 % of the adherence to host cells is caused by pili, as well as in biofilm formation and twitching motion. The pilus filament of *P. aeruginosa* plays an important role in the preliminary adhesion to host cells and

the initiation of infection[180]. The production of vesicles also serves to infect host cells[66,181]. The protein PilA (type IV pilin structure subunit) was found in high concentrations in the overexpressed *lemA2* strain as well as in the complemented *lemA1lemA2* strain and not in the *lemA2* knockout strain indicating that LemA2 has an influence on PilA. Moreover, the flagellum proteins FliD, FlgG, FlgK and FlgH could be linked to LemA2 activity. The flagellum proteins are transported *via* the T3SS, but there seems to be an alternative route to form the flagellum *via* vesicle function. Next, the proteins of the protease and chaperone class were considered. The heat-shock response is an important homeostatic mechanism that enables cells to survive a variety of environmental stresses. One set of heat-shock proteins are the chaperonins that are induced when cells are exposed to high temperatures. The chaperonins are a subgroup of the molecular chaperones, to which the GroE subclass belongs. It consists of two proteins, chaperonin 60 (GroEL) and chaperonin 10 (GroES), which are required for survival[182]. The protein GroES (co-chaperonin) was identified in the complemented *lemA1* strain but not in the *lemA1* knockout strain, thereby indicating an influence on GroES. In the complemented strain of the *lemA2* mutant the proteins ClpX (ATP-dependent protease ATP-binding subunit), HflK (protease subunit) and HtpX (heat-shock protein) were identified.

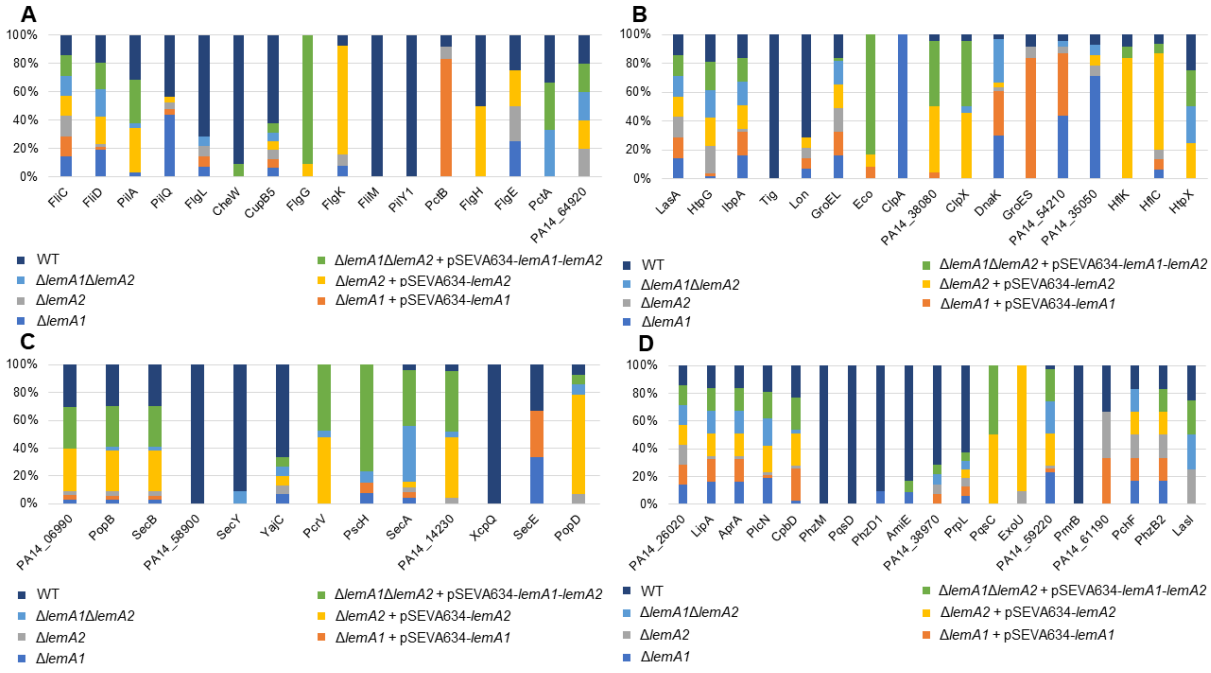

Figure 40: Changes in the abundance of proteins involved in chemotaxis, motility, protein turnover and transport, quorum sensing and biofilm formationin the *lemA* deletion and overexpressing strains in comparison to the wildtype. A. Identified proteins of chemotaxis and motility; **B.** Proteases and chaperones; **C.** Protein transport; **D.** Quorum sensing and biofilm formation of the wildtype (dark blue) and the Δ*lemA1* (blue), Δ*lemA1* + pSEVA634-*lemA1* (orange), Δ*lemA2* (grey), Δ*lemA2* + pSEVA634-*lemA2* (yellow), Δ*lemA1*Δ*lemA2* (light blue) and Δ*lemA1*Δ*lemA2* + pSEVA634-*lemA1-lemA2* (green) strains.

It was remarkable that the proteins Eco and PA14_38080 were found in all three complemented strains, which can be due to a joint influence of LemA1 and LemA2. Looking at the identified proteins involved in protein transport, it became obvious that there was no

correlation of data for the knockout and complemented *lemA1* strain. One of the main pathways through which toxins enter host cells is the T3SS. This supramolecular structure, also called the injectosome, is composed of three structural parts: a basal body, a needle and a translocon. In *P. aeruginosa*, four proteins are necessary for the formation of the translocon: the hydrophobic translocators PopB and PopD, the hydrophilic translocator PcrV and the hydrophobic translocator chaperone PcrH[183]. The three proteins PopB, PopD and PcrV are absolutely required for pore formation and cytotoxicity. It was reported that PcrV is responsible for the anchoring of PopD in red blood cell membranes, as well as necessary for the functional assembly of the membrane-inserted PopB/PopD complex[184]. It was published that vesicles serve for the infection of host cells[66,181]. The protein PcrV was present in high concentration in the overexpressing *lemA2* strain as well as in the overexpressing *lemA1lemA2* strain. The protein PopD found with high concentration in the *lemA2* overexpressing strain, and PopB with high concentration in the complemented *lemA2* as well as *lemA1lemA2* strain. This suggests an influence by LemA2 activity for PcrV, PopD and PopB formation. For the proteins involved in quorum sensing and biofilm formation, the protein PA14_61190 (hypothetical protein) was found to be LemA1 controlled. The regulation of virulence factor expression and biofilm formation is based on quorum sensing (QS), a cell density-dependent intercellular communication system that uses small molecules. The *pqs* QS system is restricted to certain *Pseudomonas* species and uses the *Pseudomonas* quinolone signal (PQS) and its precursor 2-heptyl-4-hydroxyquinoline (HHQ) for cell-cell communication[185]. HHQ and PQS are involved in the expression of many different genes that code for virulence factors such as pyocyanine, elastase B, lectin A, rhamnolipids and hydrogen cyanide and modulate the host immune response[185–187]. Additionally, PQS is able to promote biofilm formation, although the exact mechanism is still unclear[186]. The key metabolite is anthranilic acid which is activated by PqsA to anthraniloyl-CoA, which is then transacylated by the active side cysteine residue of PqsD to 2´-aminobenzoylacetyl-CoA (2-ABA-CoA). The thioesterase PqsE hydrolyzes it into 2´-aminobenzoylacetate (2-ABA) and the heterodimer PqsBC transforms the reactive intermediate into HHQ[185]. The decarboxylation and reaction with octanoate of 2-ABA is mostly performed by PqsC, the carrier of the octanoyl group[188]. In the *lemA2* strain, as well as in the double knockout strain, the protein PqsC was found, indicating a participation of LemA2 in the QS synthesis pathway. In addition, the protein ExoU was found at high concentration in the *lemA2* overexpressing strain, which also indicated an influence of LemA2 on this process. *P. aeruginosa* uses the T3SS for the direct introduction of virulence factors including the four secreted exotoxins ExoU, ExoS, ExoY and ExoT into the host cell[189,190]. The *exoU* gene encodes a cytotoxic protein that rapidly destroys the cell membrane of host cells due to its phospholipase activity[189]. ExoU is activated by interaction with ubiquitin or ubiqitinylated proteins in the host cell cytosol before it is localized on the cell membrane for catalyzing fatty

acids[190]. ExoU phospholipase activity and membrane association were found increased in vesicles[191].

The formation of certain proteins of the amino acid metabolism, cell division, cofactor formation, ATP synthase and cytochrome oxidases are affected by LemA proteins

Furthermore, the proteins involved in amino acid metabolism, cell division, cofactor formation, ATP synthase and cytochrome oxidases (Appendix 21) were considered. The following proteins were identified during the analyses for a possible influence of LemA1 and/or LemA2. In the amino acid metabolism, the proteins GdhB (NAD-dependent glutamate dehydrogenase), AruF (arginine/ornithine succinyltransferase AI subunit) and LysA (diaminopimelate decarboxylase) were found in the complemented *lemA1* strain. In the case of LemA2 the proteins ProS (prolyl-tRNA synthetase), ValS (valyl-tRNA synthetase), PutA (bifunctional proline dehydrogenase/pyrroline-5-carboxylate dehydrogenase), CysD (sulfate adenylyltransferase subunit 2) and TrpS (tryptophanyl-tRNA synthetase) were found in the complemented *lemA2* strain and in the complemented double-knockout strain. In the classification of cell division, the protein FtsE (cell division ATP-binding protein) was identified, which was found in the complemented *lemA2* as well as in the double *lemA* strain. In the case of cofactor formation, the protein PabB (para-aminobenzoate synthase component I) and the protein IlvH (acetolactate synthase 3 regulatory subunit) were found in the complemented single knockout strains (PabB for *lemA1*, IlvH for *lemA2*) and in the complemented double knockout strain, but not in the corresponding knockout strains. No influence of LemA1 or LemA2 on proteins of the ATP synthase were identified. The cytochrome oxidases PA14_57540 (cytochrome c_1) and Cc4 (cytochrome c_4) were only found in the *lemA1* knockout and *lemA1lemA2* knockout strains.

The formation of certain proteins of the TCA cycle, sulfur metabolism, transport of small molecules, stress and detoxification are affected by LemA proteins

The next classifications considered were TCA cycle, stress and detoxification, sulfur metabolism, transcription regulators and small molecule transport (Appendix 22). In the case of the TCA cycle the protein SucC (succinyl-CoA synthetase subunit beta) was found under a possible control of LemA2, and GlpD (glycerol-3-phosphate dehydrogenase) under the possible influence of LemA1 and LemA2, while AcsL ([PrpL] lysyl endopeptidase), was only present when no LemA2 was present. The protein CysI (sulfite reductase), involved in sulfur metabolism, was found in the complemented *lemA1*, and *lemA2* and *lemA1lemA2* knockout strains, suggesting an influence solely by LemA1. The protein, PA14_30430 (thiosulfate sulfurtransferase) was found in the complemented *lemA2* and *lemA1lemA2* strains, indicating an influence of LemA2 only. Furthermore, proteins of the DNA/RNA metabolism, energy metabolism and phage related proteins (Appendix 23) were considered. In the classification of phage related proteins PA14_08120 (tail length determination protein) and PA14_15350

(integrase) were found in the complemented *lemA2* and *lemA1lemA2* strain, indicating a possible influence of LemA2. Appendix 24 shows the proteins involved in translation and modification. The proteins RpsG (30S ribosomal protein S7), RplD (50S ribosomal protein L4), RpmB (50S ribosomal protein L28), RpsP (30S ribosomal protein S16) and RplY (probable ribosomal protein L25), which were found in the complemented *lemA2* strain as well as in the complemented *lemA1lemA2* strain, indicate a possible influence of LemA2. Furthermore, the protein RplP (50S ribosomal protein L16) was found in the complemented *lemA1* strain and *lemA2* knockout strain, indicating an influence by a high concentration of LemA1.

LemA1 and LemA2 influenced the composition and formation of MVs

MVs consist of proteins, phospholipids and polysaccharides. They contain proteins, DNA, RNA and QS signals[192]. There are different types of MVs due to their origin. MVs caused by cell lysis, due to endolysin activity, which is produced in only 1 % of the total cell population, contain cytoplasmic proteins as well as DNA and RNA. This content is not found in MVs caused by blebbing, which are OMVs[71]. The vesicles studied in this proteome analysis were a mixture of CMVs and OMVs, which also contain cytoplasmic proteins such as those responsible for amino acid metabolism and DNA/RNA metabolism. MVs play an important role in the disperal of QS signalling and are important carriers of virulence. It was shown that over 86 % of PQS is present in OMVs[66]. In a previous study it was shown that MVs of planktonic cells carry virulence factors[71], this was also shown here by the high concentration of ExoU. Pathogenic organisms like *P. aeruginosa* use MVs as delivery vehicles for these virulence factors and toxins to host cells[66]. The different packaging of cargo in MVs depends on the bacterial growth phase, environment within the host and status of the microbial community. Proteins involved in metabolic pathways, metabolism in diverse environments and amino acid transport were found in later-stage MVs[66].

Table 21: Proteins found in vesicles and affected by LemA1 and/or LemA2.

Classification	Protein name	Protein	LemA1	LemA2
Cell wall/membrane/envelope	MurE	UDP-N-acetylmuramoyl-alanyl-D-glutamate-2,6-diaminopimelate ligase	+	+
	GlmM	phosphoglucose-amine mutase	+	+
	EngA	GTP-binding protein		+

	FabB	3-oxoacyl-ACP synthase		+
	DacC	D-ala-D-ala-carboxypeptidase	+	
	OpdO	pyroglutamate porin	+	
	VacJ	MlaA lipoprotein	+	
	FptA	Fe(III)-pyochelin outer membrane precursor	+	
	OprE	anaerobically-induced outer membrane porin OprE precursor	+	
	PA14_56810	LemA1	+	
	FabZ	3R-hydroxymyristoyl-ACP dehydratase		+
	MdoG	glucan biosynthesis protein G		+
	PiuA	TonB-dependent receptors,		+
	WaaG	UDP-glucose:(heptosyl) LPS alpha 1,3-glucosyl-transferase	+	+
Chemotaxis and motility	PctB	chemotactic trans-ducer	+	
	PilA	type IV pilin structure subunit		+
	FliD	flagellar capping protein		+
	FlgG	flagellar basal body rod protein		+
	FlgK	flagellar hook-associated protein		+
	FlgH	flagellar basal body L-ring protein		+

Chaperones	GroES	chaperonin 10	+	
	ClpX	ATP-dependent protease ATP-binding subunit		+
	HflX	protease subunit		+
	HtpX	heat-shock protein		+
	Eco	ecotin	+	+
	PA14_38080	hypothetical protein	+	+
Protein transport	PopB	translocator protein		+
	PopD	translocator outer membrane protein PopD precursor		+
	PcrV	type III secretion protein		+
Quorum sensing	PA14_61190	hypothetical protein	+	
	PqsC	PqsC		+
	ExoU	ExoU		+
Amino acid metabolism	GdhB	NAD-dependent glutamate dehydrogenase	+	
	LysA	diaminopimelate decarboxylase	+	
	ProS	prolyl-tRNA synthetase		+
	ValS	valyl-tRNA synthetase		+
	PutA	bifunctional proline dehydrogenase/ pyrroline-5-carboxylate dehydrogenase		+
	CysD	sulfate adenylyltransferase subunit 2		+
	TrpS	tryptophanyl-tRNA synthetase		+

Cell division	FtsE	cell division ATP-binding protein			+
Cofactor formation	PabB	para-aminobenzoate synthase component I	+		
	IlvH	acetolactate synthase 3 regulatory subunit			+
Cytochrome oxidases	PA14_57540	cytochrome c_1		+	
	Cc4	cytochrome c_4	+		
TCA and pyruvate metabolism	SucC	succinyl-CoA synthetase subunit beta			+
	GlpD	glycerol-3-phosphate dehydrogenase	+		+
	AcsL	[PrpL] lysyl endopeptidase	+		
Sulfur metabolism	CysI	sulfite reductase	+		
ABC transporter	PA14_30430	thiosulfate sulfurtransferase			+
Phage related	PA14_08120	tail length determination protein			+
	PA14_15350	integrase			+
DNA/RNA metabolism	RplD	50S ribosomal protein L4			+
	RpsG	30S ribosomal protein S7			+
	RpmB	50S ribosomal protein L28			+
	RpsP	30S ribosomal protein S16			+
	RplY	probable ribosomal protein L25			+

	RplP	50S ribosomal protein L16	+

Taken together, the results of proteome analysis show that LemA1 and LemA2 have an influence on membrane composition as well as proteins responsible for chemotaxis and motility, protein transport and QS and some proteins involved in other metabolic pathways.

3.3 Protein-protein interaction of DnaK and FliC

In 2015, it was shown that a protein-protein interaction exists between the catalytic subunit of periplasmic nitrite reductase, NirS, the chaperone DnaK and the flagella subunit FliC in periplasm under anaerobic conditions[105]. NirS interacts with its cytochrome *c* domain directly with FliC. However, FliC is not required for the interaction between NirS and DnaK, and NirS is not required for the interaction of FliC with DnaK. Furthermore, it has been shown that the *nirS* mutant is deficient in swarming motility. This swarming defect of the *nirS* mutant was previously demonstrated under aerobic conditions[105,193]. The results showed that the *nirS* mutant is impaired in the development of the flagella. Figure 41 shows the swarming motility of the *fliC*, *nirS* and *nosZ* mutant compared to the wild type strain of *P. aeruginosa*.

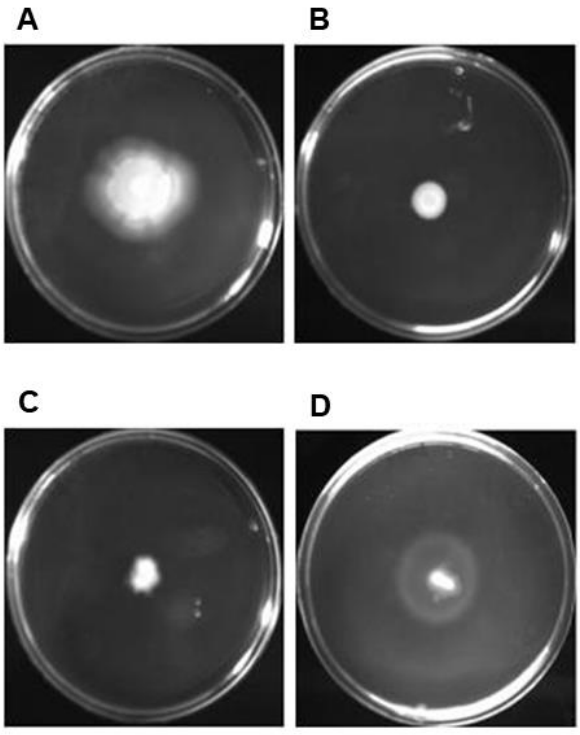

Figure 41: Swarming motility of different *P. aeruginosa* mutant strains (*fliC*, *nirS*, *nosZ*). **A.** Swarming motility of the PA14 wildtype strain. **B.** Swarming motility of the *fliC* mutant strain. **C.** Swarming motility of the *nirS* mutant strain. **D.** Swarming motility of the *nosZ* mutant strain (*modified after Borrero-de Acuña et al.*[105]).

The swarming motility of the *fliC* and *nirS* mutant are heavily impaired compared to the wildtype, whereas the *nosZ* mutant is able to move *via* swarming motility[105]. The protein-protein interaction of DnaK and FliC was further investigated by immunofluorescence labelling and immunogold staining with electron microscopy-based visualization. Figure 42 shows the presence of DnaK at the flagella of *P. aeruginosa* by immunofluorescence labelling (Figure 42 A) and immunogold labelling using Transmission Electron Microscopy (TEM) (Figure 42 B).

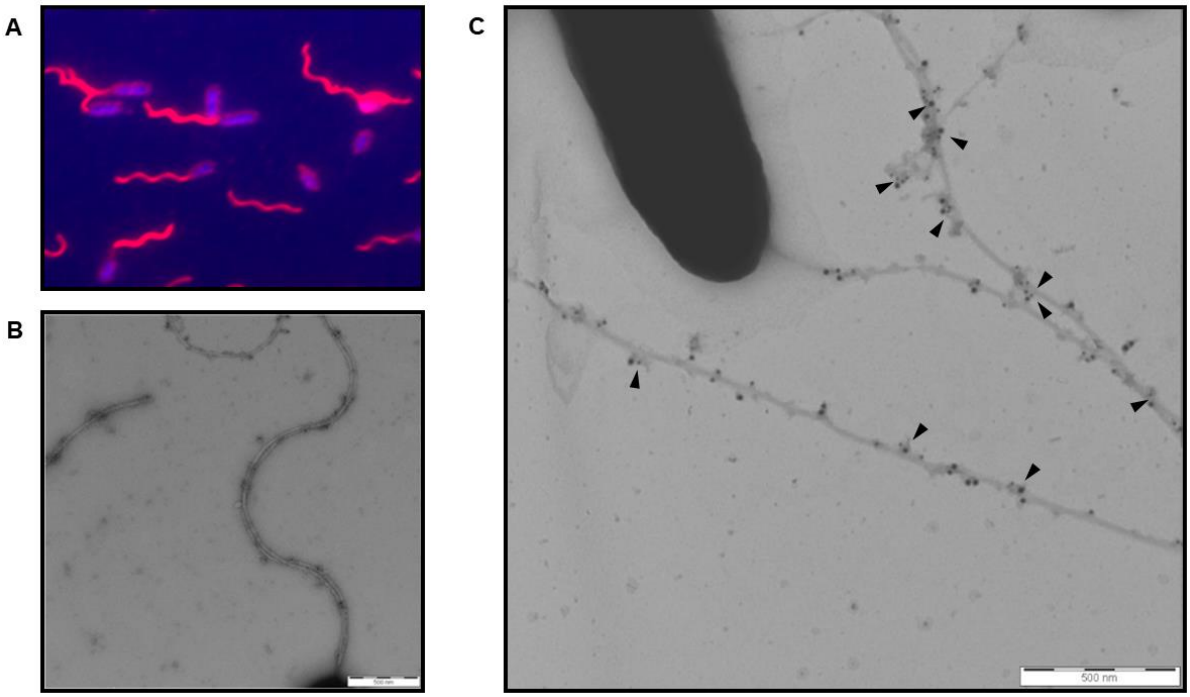

Figure 42: TEM analyses of the localization of DnaK and FliC in *P. aeruginosa* cells with focus on the flagella. A. Immunofluorescence labeling of DnaK with anti-DnaK (red) and the DNA with DAPI (blue) shows the presence of DnaK of the flagella and of the envelope of the cell. **B.** Immunogold labeling *via* Transmission Electron Microscopy (TEM) with anti-DnaK shows the presence of DnaK at the flagellum. **C.** Double immunogold labeling shows the protein-protein interaction between DnaK (dot of 15 nm) and FliC (dot of 10 nm) with a distance of 15 nm indicating a direct interaction at the flagellum (rows) (*unpublished data by Dr. Gabriella Molinari, HZI Braunschweig*).

By double immunogold labelling with anti-FliC and anti-DnaK the direct interaction of both proteins at the flagella was shown (Figure 42 C), where FliC was visualized as the small dot with 10 nm and DnaK with the larger dot with 15 nm. The distance between the two proteins is less than 15 nm, which indicates a direct interaction (*unpublished data by Dr. Gabriella Molinari, HZI Braunschweig*).

3.3.1 DnaK and FliC were found in vesicles

In the previous chapter a proteome analysis of the outer membrane vesicles using LC-MS analysis technique was performed to determine whether the two LemA-like proteins PA14_56810 and PA14_06990 have an influence on vesicle formation. It was found that FliC

was detectable in the proteome of the vesicles in each of the strains investigated. DnaK was also detected in small amounts in the wildtype, *lemA2* mutant, complemented *lemA2* strain and in larger amounts in the *lemA1* mutant and *lemA1lemA2* mutant as well as in the complemented *lemA1* strain. Subsequently, single immunogold staining was performed *via* TEM with anti-DnaK and anti-FliC of the outer membrane vesicles (Figure 43).

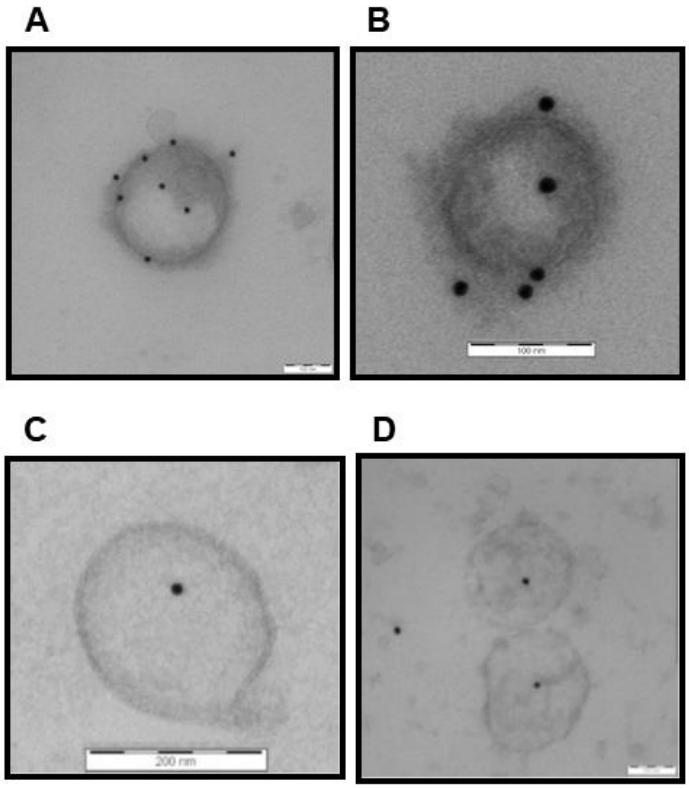

Figure 43: Immunogold labeling of DnaK and FliC in outer membrane vesicles of PA14 wildtype strain. A-B. Immunogold labeling of DnaK in outer membrane vesicles with anti-DnaK (A: bar 200 nm; B: bar 100 nm). **C-D.** Immunogold labeling of FliC in outer membrane vesicles with anti-FliC (bar 200 nm) (*Images were performed by Dr. G. Molinari, HZI Braunschweig*).

The Figure 43 shows the immunogold staining in the PA14 wildtype strain, indicating that more DnaK was detected in the vesicle (Figure 43 A and B) and less FliC (Figure 43 C and D), with a very low background in both cases.

DnaK and FliC form a complex in the periplasm of *P. aeruginosa*[105] and at the flagella (*unpublished data by Dr. G. Molinari, HZI Braunschweig*). DnaK's involvement in the export of periplasmic and outer membrane proteins in a defective SEC system suggests an alternative protein export pathway in which DnaK is involved[105,194]. OMVs consist of phospholipids, lipopolysaccharides, outer membrane proteins and periplasmic components. Among other virulence factors, FliC was also detected in MVs[195]. FliC subunits form the filament of the flagellum, but in addition it also plays a role as a virulence factor[105,154]. The transport *via* vesicles seems to be another transport pathway for FliC to the flagellum besides the T3SS of the flagellum itself[59].

3.3.2 Conditional mutant of DnaK showed reduced flagellum assembly

For further analysis of the function and the requirement of DnaK for flagella assembly a *dnaK* conditional mutant was generated (*performed by Dr. José M. Borrero-de Acuña, TU Braunschweig*). The principle of the conditional mutant is based on the transformation of a plasmid with an IPTG-inducible promoter driving the formation of an antisense RNA to the *dnaK* mRNA translational start site. After addition of IPTG, the antisense RNA was synthesized, which attached to the wildtype *dnaK* mRNA, resulting in a double mRNA that was degraded and not translated (Figure 13). The aim was to reduce the DnaK level to zero in order to investigate the function of DnaK in flagella assembly in relation to FliC. Figure 44 A shows the immunostain results of the PA01 *dnaK* conditional mutant compared to the PA01 wildtype and the PA14 conditional mutant compared to the PA14 wildtype. It was noticeable that in the PA01 conditional *dnaK* mutant the level of DnaK was lower after one to two hours after antisense expression. In comparison with the PA01 wildtype strain, a slight constant increase in DnaK was observed. When comparing the PA14 *dnaK* conditional mutant with the corresponding wildtype strain, it became obvious that there was no decrease in DnaK concentration in the conditional mutant, instead an almost constant level was observed, similar observations were made for PA14 wildtype strain. The comparison between the two *dnaK* conditional mutant strains showed that the level of DnaK in PA01 was about one third of the level in PA14. In the comparison between the two wildtype strains, it was observed that the PA14 wildtype has about twice as much DnaK as PA01.

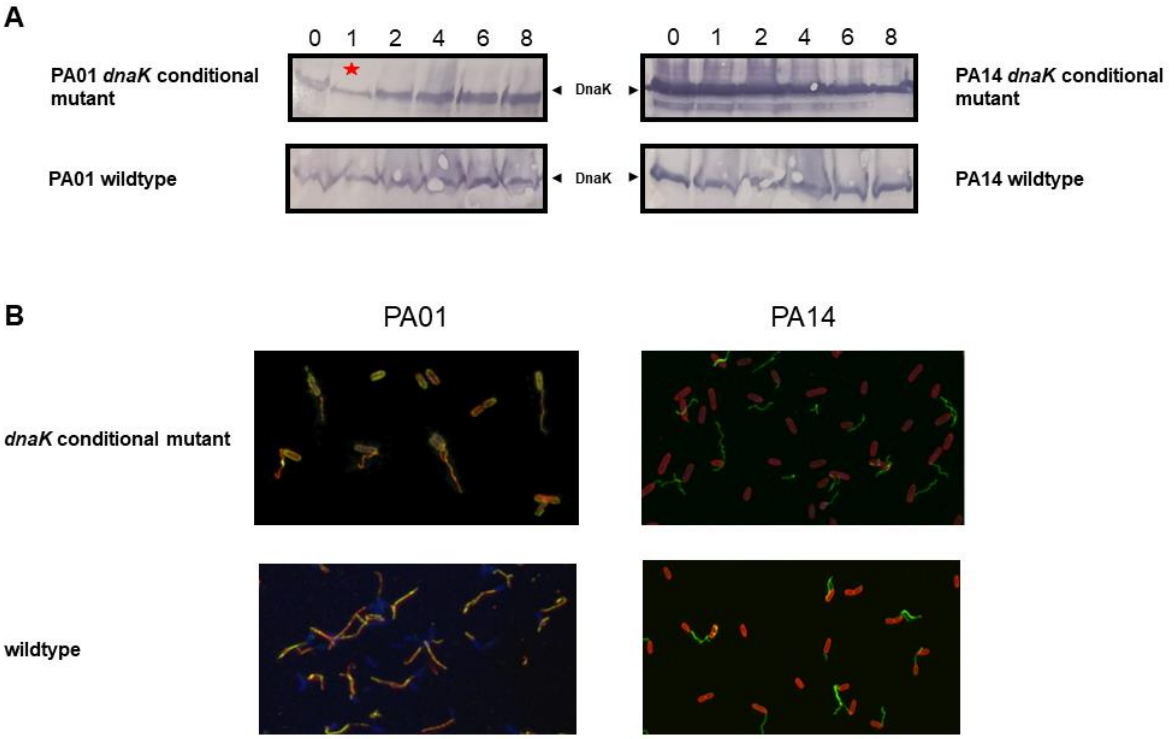

Figure 44: Analyses of *dnaK* conditional mutant strains of *P. aeruginosa* PA01 and PA14. A. Western blot analyses of the PA01 *dnaK* conditional mutant, the PA01 wildtype, the PA14 *dnaK* conditional mutant and the PA14 wildtype 0, 1, 2, 4, 6 and 8 hours after IPTG induction of antisense RNA production. **B.** Electron microscopy analyses of immune fluorescent labeled the PA01 *dnaK* conditional mutant, the PA01 wildtype, the PA14 *dnaK* conditional mutant and the PA14 wildtype 2.5 hours after IPTG induction of *dnaK*-antisense RNA production with DAPI (blue), anti-FliC (green) and anti-DnaK (red).

For further analysis, electron microscopy analysis of the DNA (DAPI stained), DnaK with immune fluorescent labeled anti-DnaK antibody and FliC with corresponding anti-FliC antibody was performed for the respective *dnaK* conditional mutants and in the corresponding wildtype strains after 2.5 hours of IPTG induction of antisense RNA formation (Figure 44 B). The comparison between the two strains shows that the PA14 strains, conditional mutant as well as wildtype, had accumulated more DnaK in the cell than the two PA01 strains. In PA14, no DnaK was detected at the flagella, in contrast to the PA01 strains, where the superimposition of anti-FliC and anti-DnaK labelling was visible at the flagella. In the PA01 *dnaK* conditional mutant FliC was also attached in the periplasm/cell envelope. By introducing the plasmid with the antisense-*dnaK* sequence under an IPTG-inducible promoter into the PA01 and PA14 wildtype, a temporal conditional mutant was generated. Upon induction, the antisense mRNA of *dnaK* was transcribed and attached to the wildtype transcribed mRNA of *dnaK*. This resulted in a double stranded mRNA, which leads to RNA silencing by mRNA degradation[196–198]. The RNA silencing effect was only detected in Western blot of PA01, where less DnaK was present than in the wildtype after one hour. In addition, the immunostain showed an enrichment of DnaK in complex with FliC in the periplasm of PA01 compared to the wildtype. RNA silencing retarded *dnaK* production, resulting in an accumulation and less flagella formation, due to the

fact that conditional mutant and wildtype images were taken at the same time. DnaK is an abundant molecular chaperone that plays an essential role in protein folding[194]. In *E. coli*, DnaK has been shown to be involved not only in protein folding but also in lambda phage replication and heat shock response, cell division, murein synthesis, flagellar assembly and osmoregulation[199].

3.3.3 Recombinant DnaK and FliC production

For a more detailed analysis of the protein-protein interaction of DnaK and FliC, a SPOT membrane of both proteins was generated (*generation of the SPOT arrays was performed by Dr. Tegge, HZI Braunschweig*) and incubated with the respective interaction partner. For the production of the required pure protein, both proteins were N-terminal fused with a GST tag under the control of an IPTG-inducible promoter, produced in *E. coli* BL21 cells and purified *via* the GST tag by affinity chromatography. After successful cloning into the pGEX-6P-1 vector, the optimal production conditions for both proteins were first established. The protein production of DnaK and FliC were analyzed with two different IPTG concentrations at four different temperatures (17, 25, 30 and 37 °C) (Appendix 25 and Appendix 26). Samples of the total protein production were analyzed after one, two four and 24 hours. The figures show that optimal protein production was achieved at 17 °C.

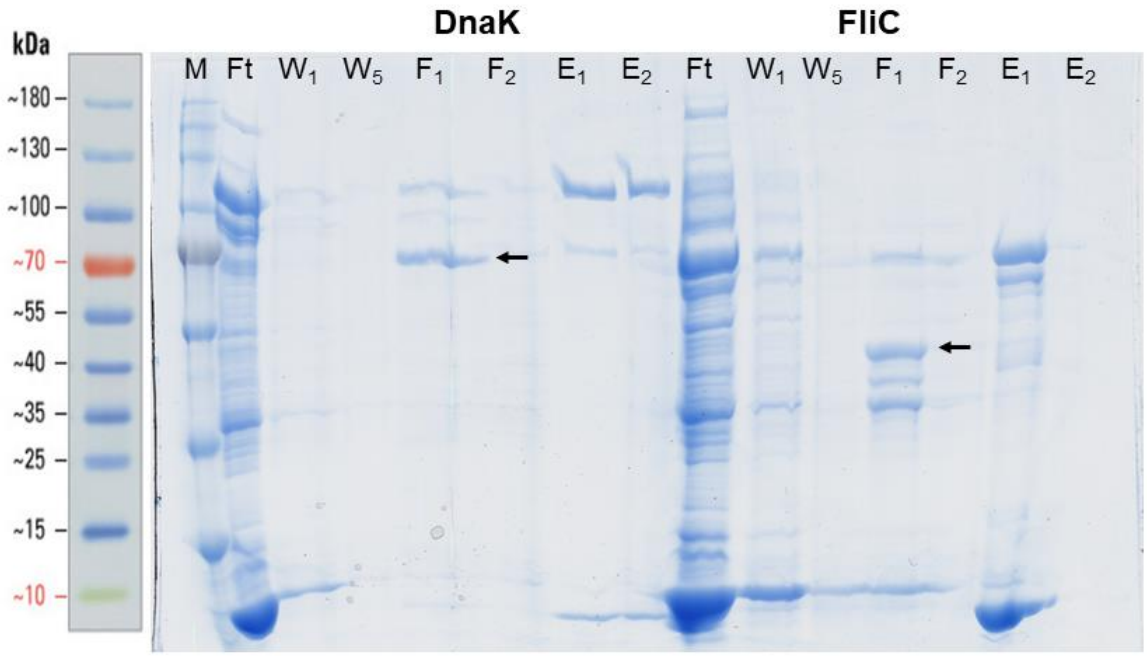

Figure 45: Recombinant production of DnaK and FliC. DnaK was produced under determined optimal conditions with a relative molecular mass of 70,000 and FliC was produced with a relative molecular mass of 50,000. M: Marker, Ft: Flowthrough, W_1: Washing fraction 1, W_8: Washing fraction 8, F_1: Elution fraction 1 of the protein, F_2: Elution fraction 2 of the protein, E_1: Elution fraction 1 of the GST tag, E_2: Elution fraction 2 of the GST tag.

The proteins were produced according to the adapted protocol (Protein production of DnaK and FliC *via* affinity chromatography on glutathione sepharose) and purified using glutathione-sepharose. Figure 45 shows the production of DnaK and FliC with the flow through, wash fraction 1 and wash fraction 5 as well as the elution fractions containing the protein (F1 and F2) and the elution fractions showing the truncated GST tag as well as still fused protein (E1 and E2). DnaK and FliC were purified with relative molecular masses matching their molecular weight of 68.4 kDa (DnaK) and 49.2 kDa (FliC).

3.3.4 Function of DnaK in dependence of the pH and the availability of ATP

Thermal denaturation was performed to investigate the property of DnaK as a chaperone. To evaluate DnaK holdase and unfoldase activities, the *in vitro* thermodynamic stability of G41D mutant of superoxide dismutase 1 barrel ($SOD1_{Bar}$) was determined, a previously established FRET-based folding sensor[123]. This specific mutant has a Tm that is close to 39 °C, so that the heating process can be limited up to 45 - 47 °C. This reduces the probability of thermal unfolding of DnaK, which was reported to occur in a three-step process with two transition melting points, 41 and 71 °C[200]. The probability of unspecific interactions between DnaK and $SOD1_{bar}$-G41D was therefore significantly reduced. Next, $SOD1_{bar}$-G41D was thermally unfolded *via* exposure to a thermic gradient ranging from 23 to 47 °C in the absence or presence of DnaK (12 or 20 µM), with and without ATP (2 mM). The thermodynamic stability was determined by calculating the standard free energy of folding at 37 °C ($\Delta G_f^{37\,°C}$) using the approach "thermodynamics from kinetics"[124]. A significant increase in $\Delta G_f^{37\,°C}$ was observed at both pH 6 and pH 7, when ATP and DnaK (each 20 µM) were present, indicating protein stabilization (Figure 46). A significant increase was also observed for DnaK (12 µM) and ATP, although this case is not statistically different from ATP (2 mM) alone and therefore the effect of ATP or DnaK was not evident. In the highest concentration analyzed, DnaK alone destabilized $SOD1_{bar}$-G41D both at neutral and at more acidic pH values.

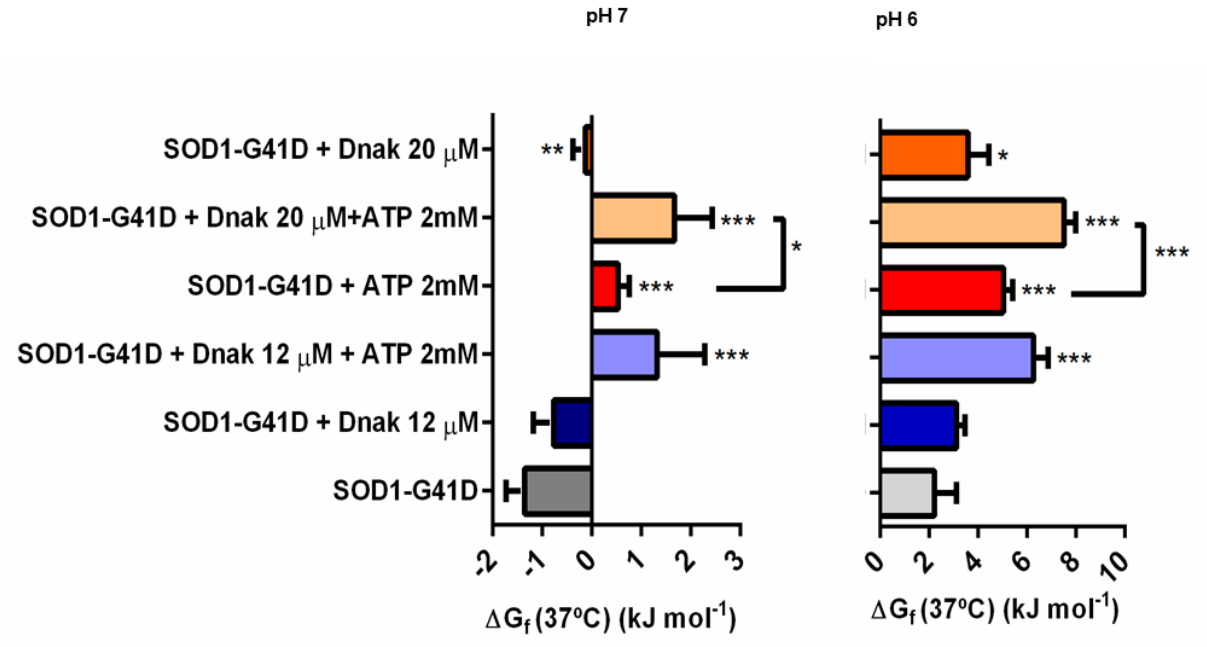

Figure 46: Determination of ATP-dependent activity of DnaK. Standard free energy of folding at 37 °C ($\Delta G_f^{37°C}$) of $SOD1_{bar}$-G41D in buffer mix or when supplemented with DnaK (12 or 20 µM), with and without ATP (2 mM). If not indicated otherwise by arrows, statistical analyses marked for each condition were performed with SOD1-G41D as reference. Statistical significance was achieved using ANOVA analysis followed by post-hoc Tukey test (*p≤0.05, **p≤0.01, ***p≤ 0.001.) (*performed by Sara da-Silva Ribeiro, BRICS Braunschweig*).

The behavior of the ATP-independent holdase reflects the ability of the DnaK to bind misfolded or unfolded proteins in a form that prevents their aggregation. The function of unfoldase refers to the ATP-dependent action of DnaK, where several cycles of substrate release and binding, coupled with ATP hydrolysis, unfold misfolded proteins into competent folding intermediates that can spontaneously fold to their native state[201]. When DnaK acts as holdase or unfoldase, it binds to unfolded conformations and causes a shift of equilibrium towards the unfolded state, which then leads to protein stabilization[202]. Taken together, the results show that DnaK acts both as a holdase and unfoldase under rather neutral or more acidic conditions.

3.3.5 Determination of the interacting domains of the DnaK/FliC complex

The interaction between DnaK and FliC was studied in molecular detail using a SPOT membrane assay, with which the interacting domains of the respective proteins were determined. For this purpose, SPOT membranes of DnaK and FliC were generated according to a standard protocol (SPOT membrane analysis of the interaction domains of DnaK and FliC) and incubated with the respective purified protein to be investigated. The one SPOT membrane onto which DnaK peptides were spotted was incubated with purified FliC and the interacting FliC was detected by corresponding antibody (Figure 47 A). The second SPOT membrane with spotted DnaK serves as a negative control and was incubated with the

antibodies and chromophores only (Figure 47 B). The two membranes were compared to each other to detect false-positive peptide interactions.

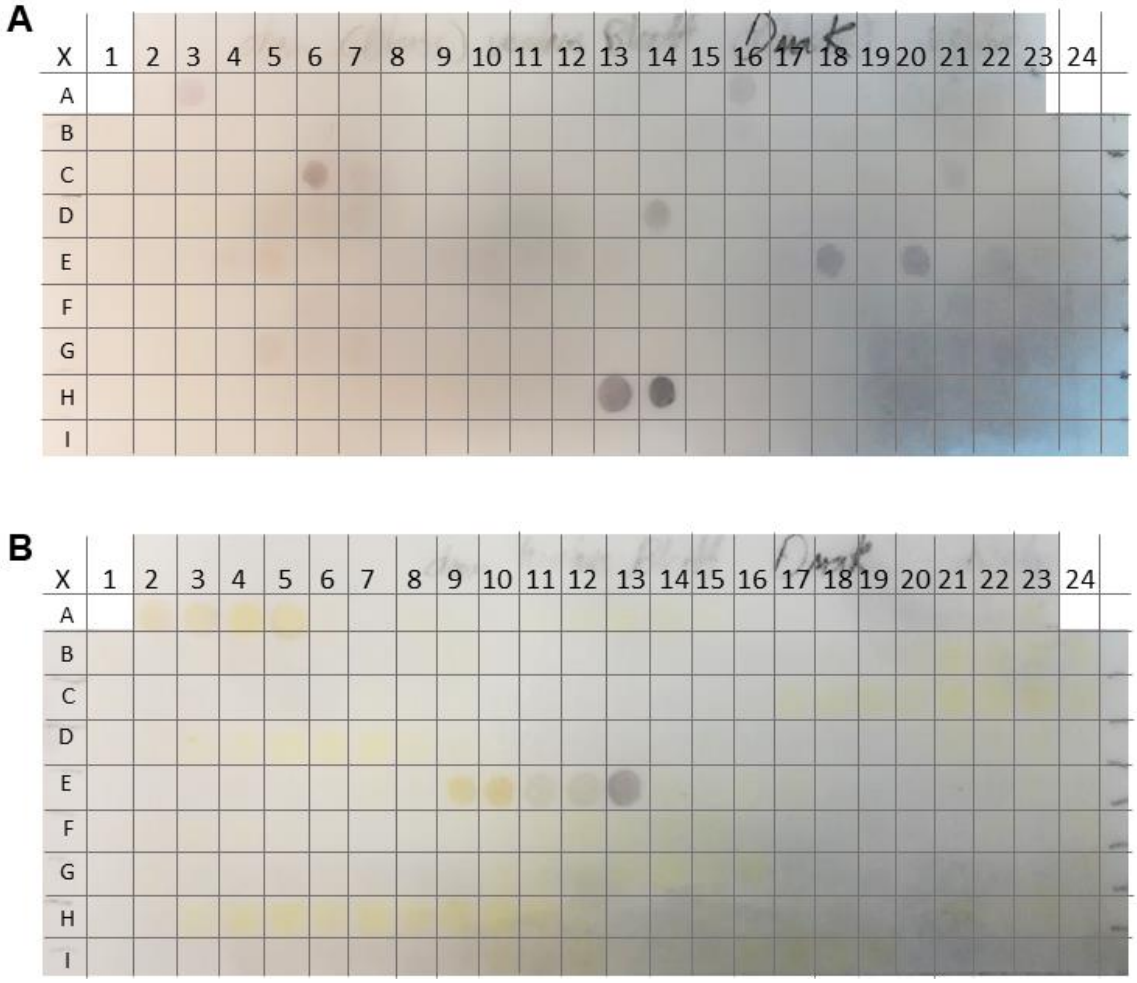

Figure 47: SPOT membrane of DnaK. A. SPOT membrane of DnaK incubated with FliC. Interacting FliC was visualized with antibodies coupled with alkaline phosphatase and the corresponding chromogenic reaction. **B.** SPOT membrane of DnaK incubated with the antibodies alone as negative control.

Using the SPOTs shown in Appendix 27 and the peptide list (Appendix 28), the peptides that interacted with FliC were identified: TNDGETLVGQPAKRQZ, TKDAGRIAGLDVKRIZ, INLKGDPLAMQRLKEZ, IHEVILVGGQTRMPLZ, VGGQTRMPLVQKTVAZ, ARNQGDALVHATRKMZ, QGDALVHATRKMITEZ. The same analysis was performed with the SPOT membrane on which the peptides of FliC were spotted. Figure 48 A shows the SPOT membrane with the spotted FliC peptides incubated with purified DnaK and the interacting DnaK was identified by analogously to FliC before.

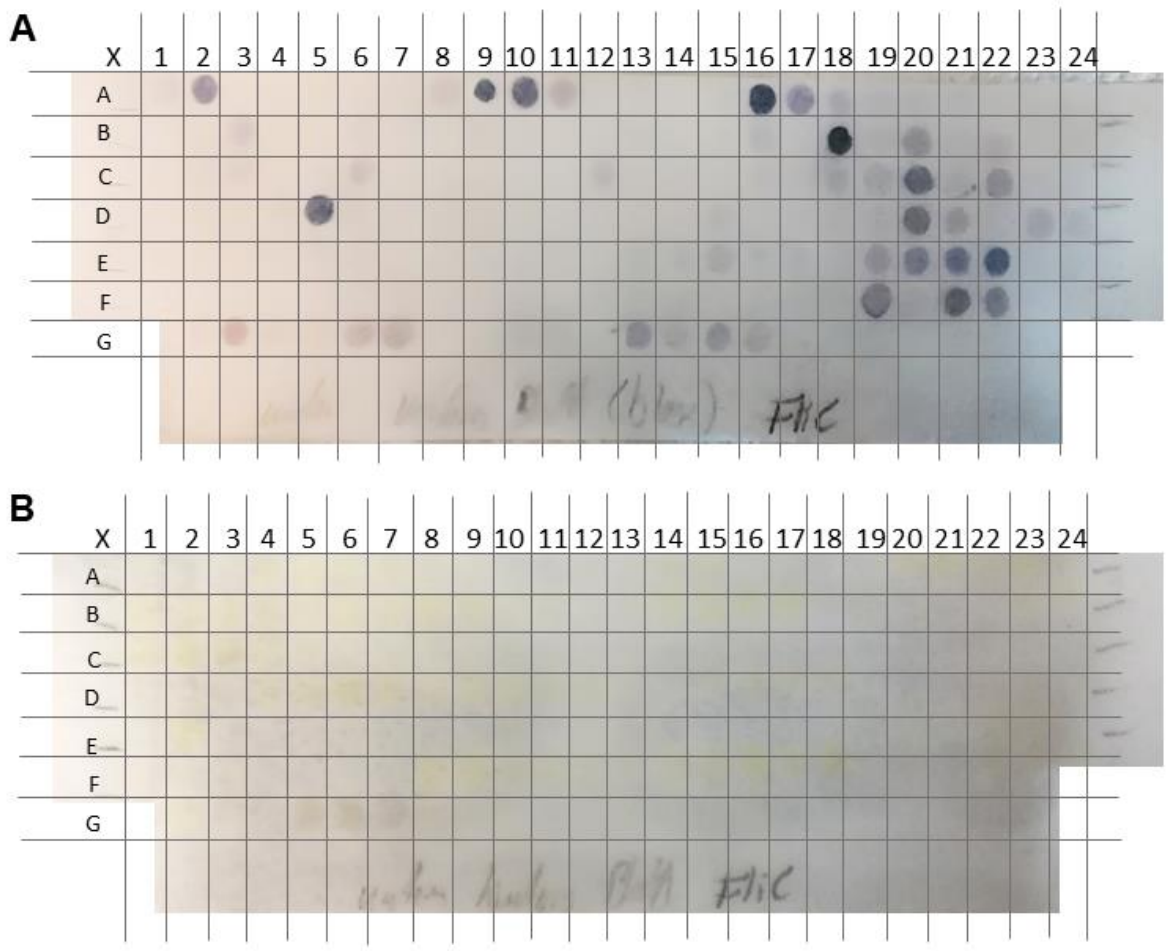

Figure 48: SPOT membrane of FliC. A. SPOT membrane of FliC incubated with DnaK. Interacting DnaK was visualized with antibodies coupled with alkaline phosphatase and the corresponding chromogenic reaction. **B.** SPOT membrane of FliC incubated with both antibodies as negative control.

For analysis of false positive interactions, a second SPOT membrane was incubated with the antibodies and chromophores only. Appendix 29 shows the application of the spots and Appendix 30 shows the corresponding peptides: TVNTNIASLNTQRNLZ, LNTSLQRLTTGYRINZ, SLQRLTTGYRINSAKZ, AGLQISNRLSNQISGZ, QISNRLSNQISGLNVZ, NRLSNQISGLNVATRZ, TRISDTTTFGGRKLLZ, TTFGGRKLLDGSFGTZ, KLLDGSFGTTSFQVGZ, SLQNASASAIGSYQVZ, GAGTVASVAGTATASZ, SGTVNLVGGGQVKNIZ, VNLVGGGQVKNIAIAZ, VGGGQVKNIAAGDZ, GQVKNIAAGDSAKZ, KNIAIAIAAGDSAKAIAZ, LADQLNSNSSKLGITZ, QLNSNSSKLGITASIZ, SKLGITASINDKGVVLZ, GITASINDKGVLTITZ, KFEAAAKNVVAAGTAZ, GTAATTTVVTGYVQLZ, ATTTVVTGYVQLNSPZ, TVVVTGYVQLNSPTAYZ, TGYVQLNSPTAYSVSZ, QRADLGAVQNRFKNTZ, AVQNRFKNTIDNLTNZ, NRFKNTIDNLTNISEZ, ISENATNARSRIKDTZ, QQAGTAILAQANQLPZ, GTAILAQANQLPQAVZ, ILAQANQLPQAVLSLZ, AQANQLPQAVLSLLRZ. For the visualization of the interaction between DnaK and FliC, the amino acid sequence was analyzed using Phyre2, creating a predicted tertiary structure of the proteins. This tertiary structure was processed using PyMol

and the domains of the interacting proteins were color-coded. The interacting domains of FliC were shown in blue (Appendix 31 A-B) and the interacting domains of DnaK were shown in red (Appendix 31 C-D). Furthermore, this figure shows the spatial surface structure of the proteins from two different viewpoints. For further analysis of the interaction, the two proteins were positioned together by using Pymol, so that there is a connection between the interacting domains. Figure 49 shows a possible interaction of DnaK and FliC, where the two proteins were very close to each other.

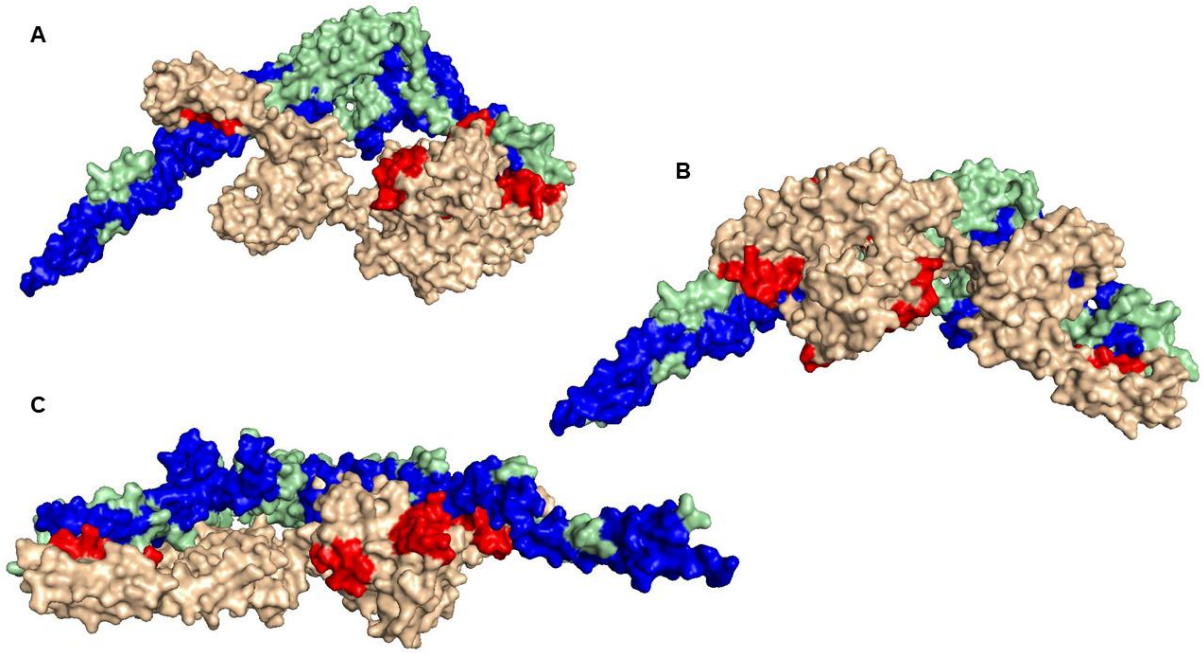

Figure 49: Interaction model of DnaK/FliC complex for transport. A-C. Interaction of the DnaK/FliC complex in a close cooperation; DnaK is colored in light brown with its determined interacting domains colored in red and FliC is colored in light green with its interacting domains colored in blue.

Figure 50 shows another possible interaction between DnaK and FliC from three different perspectives (Figure 50 A-C), where DnaK binded to the D1 domain of FliC.

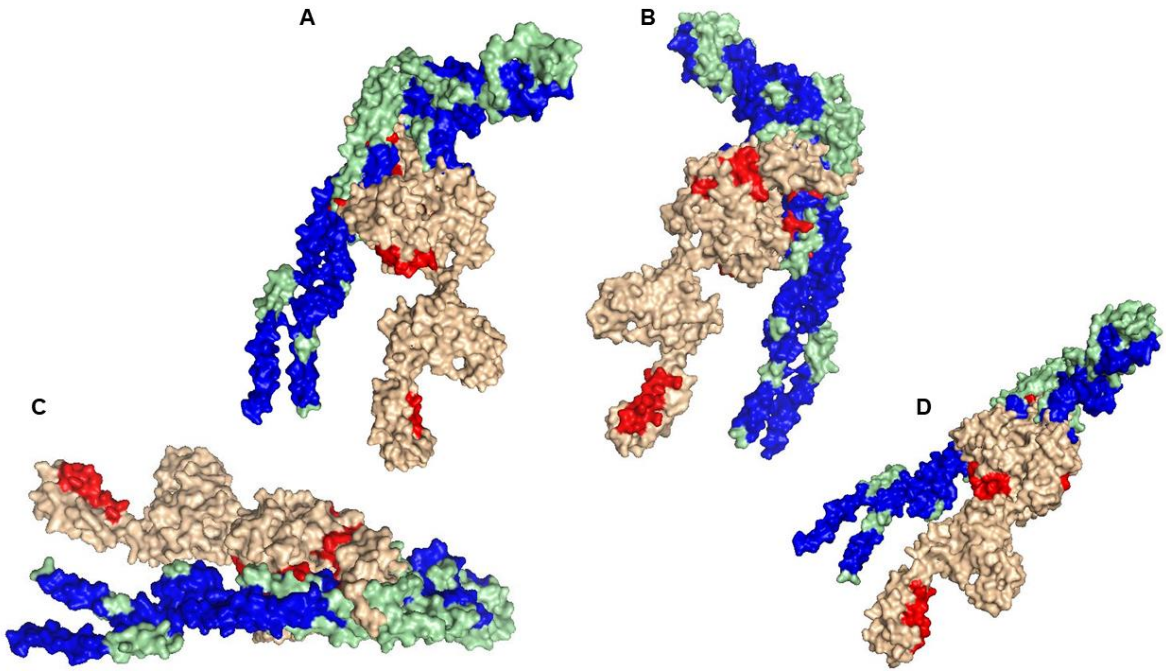

Figure 50: Interaction model of DnaK/FliC complex. A-D. Interaction of DnaK with the D1 domain of FliC; DnaK is colored in light brown with its determined interacting domains colored in red and FliC is colored in light green with its interacting domains colored in blue.

DnaK is a molecular chaperone and belongs to the highly conserved family of 70 kDa heat shock proteins (Hsp70), which is ubiquitous in most cell compartments in all three kingdoms of life. The Hsp70 proteins are involved in various cellular functions such as folding of newly synthesized proteins, prevention of protein aggregation and targeting of proteins for degradation or translocation across membranes. DnaK has two functional domains: a 44 kDa regulatory Nucleotide Binding Domain (NBD) responsible for binding and hydrolysis of ATP, and a 26 kDa Substrate Binding Domain (SBD) responsible for binding and folding of polypeptide chains. The activities of the two domains are allosterically coupled by a short flexible linker that causes structural changes in the SBD[203,204]. The peptide binding site of the protein is located between the two β-sheets of the SBD, forming a large hydrophobic cavity with a surface area of 1713 Å^2. Attached to this cavity is a five helices structure called “lid”. In the general model it is assumed when ATP is bound to NBD, the lid sub-domain is in an "open" configuration from the β sub-domain, allowing easy access for the peptide to the binding site. After ATP hydrolysis, the lid sub-domain shifts to a “closed” form, preventing the binding of a new peptide or its release[204]. The flagellin protein FliC of *P. aeruginosa* consists of three domains: the two conserved D0 and D1 domains and the variable D2 domain. The D0 and D1 domains consist of α-helices and are folded into a rod-shaped structure. The D2 domain is a unique structure of two β-blades and one α-helix. In the flagellar filament, the D0 and D1 domains are inward directed and the D2 domain is located above them on the outward side[65]. In the previous chapter it was shown that DnaK acts as ATP-dependent unfoldase and as ATP-independent holdase. The models generated from the SPOT membrane show no interaction in the SBD of DnaK, rather interactions of the NBD and lid with FliC. This indicates

that DnaK binds FliC in the folded state for which the hydrophobic cavity of the SBD is not required. DnaK is also capable of binding natively folded proteins during stability control[205]. The first model (Figure 49) shows a close binding between DnaK and FliC mimicing complex formation in periplasmic space and vesicles where DnaK protects FliC from degradation. In the second figure (Figure 50) the interaction of DnaK with the D1 domain of FliC is shown, which bind directly in the assembled filament of the flagellum. It was shown that the D1 domain and not the variable D2 domain interacts with TLR5[65]. The interaction at certain intervals of DnaK with FliC in the flagellum filament was shown (*unpublished data by Dr. G. Molinari, HZI Braunschweig*) and indicates a stabilization of the filament.

Summary

Stable and transient protein-protein interactions are essential for cellular functions. They provide *via* the multifunctionality of dynamic protein complexes the molecular basis for efficient energy generation, the safe transport of sensible compounds, cellular mobility, and complex regulatory process. In the framework of this dissertation, first the dynamics of the protein networks involved in the aerobic and anaerobic respiratory energy generation of the opportunistic pathogen *Pseudomonas aeruginosa* were investigated using affinity chromatography and mass spectrometry-based interactomics. In this context the protein interaction networks of subunits of NADH dehydrogenase I (NuoJ), periplasmic nitrate reductase (NapA) and formate dehydrogenase (FdhE) were compared for aerobic and aerobic to anaerobic shift conditions. Moreover, protein interactions of the corresponding, previously elucidated anaerobic protein network for energy generation were quantified using a bacterial two-hybrid system. Overall, a complex rearrangement of protein-protein interactions during the shift from aerobic to anaerobic growth was observed. Surprisingly, major components (NirS, NorBC, NirQ) of anaerobic energy generation *via* denitrification were still present under aerobic conditions and served as molecular platform for protein complex assembly. In a second project the protein composition and size of extracellular membrane vesicles from *P. aeruginosa* derived from wildtype, gene mutants and overexproduction strains of the membrane-structuring proteins LemA1 and LemA2 were determined. Observed clear out differences in the morphology, the protein patterns, and diameters between isolated vesicles pointed towards the importance of proteins involved in all envelope restructuring, motility, protein transport and stability, cell division, and in the metabolism for vesicle formation and function. Thirdly, an exact protein-protein interaction map at the amino acid level for the complex of the chaperone DnaK and the flagellin protein FliC was determined using a SPOT membrane approach. The DnaK-FliC complex was found in the periplasm and outside the cell attached to the flagellum using electron microscopy. An ATP-independent DnaK function was observed.

Overall, important dynamic protein networks involved in the energy metabolism, vesicle formation and flagellum formation of the pathogenic bacterium *P. aeruginosa* were solved and fostered the understanding of its infectious life style.

Outlook

P. aeruginosa respirasome interactomics

For further investigation of the dynamics in the respirasome, the interactomics approach using the three bait proteins NuoJ, FdhE and NapA can be performed under strictly anaerobic conditions, as well as with an anaerobic to aerobic shift. Furthermore, the interactomics approach using the three bait proteins NorB, NorC and NosZ under aerobic conditions can be conducted to determine their interaction partners. By this investigation, the complete dynamics model within the respirasome is obtained. For the localization and study of the interaction of NuoJ, FdhE, and NapA, an electron microscopy-based co-localization study can be performed using double immunogold labelling under aerobic, anaerobic, and both shift conditions.

P. aeruginosa LemA-like proteins

For the study of the influence of LemA1 and LemA2 on vesicle formation and its content, another proteome analysis of the wildtype, Δ*lemA1*, Δ*lemA1* + pSEVA634-*lemA1*, Δ*lemA2*, Δ*lemA2* + pSEVA634-*lemA2*, Δ*lemA1*Δ*lemA2* and Δ*lemA1*Δ*lemA2* + pSEVA634-*lemA1-lemA2* strains under anaerobic conditions and biofilm-forming conditions can be performed. Furthermore, the implementation of an interactomic approach with LemA1 and LemA2 as bait proteins is used to identify ineraction partners and verifies the proteomic data of the vesicle analysis. Additional analysis of the transcriptome of the *lemA1* and *lemA2* deletion strains provides further insight on the influence of the two proteins on transcription.

P. aeruginosa DnaK and FliC interaction

For the interaction study and determination of interacting domains within the DnaK/FliC complex, co-crystallization with DnaK and FliC can be performed. Furthermore, further analysis using SPOT membranes can be conducted. For this study, monclonal antibodies would first need to be produced for the five DnaK peptide domains already identified. Then by incubating the FliC SPOT membrane with DnaK and testing with the new antibodies individually to identify the FliC domains that interacts with the specific DnaK peptide domain. Furthermore, a *dnaK* knockout mutant can be generated to investigate the effect of DnaK on flagellum assembly. Furthermore, an interactomics approach can be used to investigate further periplasmic and extracellular interaction partners of DnaK.

References

1. Bergey, D. H., Krieg, N. R. and Holt, J. G. Bergey's manual of systematic bacteriology. Williams & Wilkins, (1984).
2. Stanier, R. Y., Palleroni, N. J. and Doudoroff, M. The Aerobic Pseudomonads a Taxonomic Study. *J. Gen. Microbiol.* **43**, 159–271 (1966).
3. Mandel, M. Deoxyribonucleic Acid Base Composition in the Genus *Pseudomonas. J. Gen. Microbiol.* **43**, 273–292 (1966).
4. Stover, C. K. *et al.* PAO1, an opportunistic pathogen. *Nature* **406**, 6 (2000).
5. Juhas, M., Eberl, L. and Tummler, B. Quorum sensing: the power of cooperation in the world of *Pseudomonas*. *Environ. Microbiol.* **7**, 459–471 (2005).
6. Walker, T. S. *et al. Pseudomonas aeruginosa* -Plant Root Interactions. Pathogenicity, Biofilm Formation, and Root Exudation. *Plant Physiol.* **134**, 320–331 (2004).
7. Delden, C. V. and Iglewski, B. H. Cell-to-Cell Signaling and *Pseudomonas aeruginosa* Infections. *Emerg. Infect. Dis.* **4**, 10 (1998).
8. Lyczak, J. B., Cannon, C. L. and Pier, G. B. Establishment of *Pseudomonas aeruginosa* infection: lessons from a versatile opportunist. *Microbes Infect.* 10 (2000).
9. Williams, H. D., Zlosnik, J. E. A. and Ryall, B. Oxygen, Cyanide and Energy Generation in the Cystic Fibrosis Pathogen *Pseudomonas aeruginosa. Advances in Microbial Physiology* **52**, 1–71 (2006).
10. Mitchell, P. Coupling of Phosphorylation to Electron and Hydrogen Transfer by a Chemi-Osmotic type of Mechanism. *Nature* **191**, 144–148 (1961).
11. Arai, H. Regulation and Function of Versatile Aerobic and Anaerobic Respiratory Metabolism in *Pseudomonas aeruginosa*. *Front. Microbiol.* **2**, (2011).
12. Chen, J. and Strous, M. Denitrification and aerobic respiration, hybrid electron transport chains and co-evolution. *Biochim. Biophys. Acta BBA - Bioenerg.* **1827**, 136–144 (2013).

13. Liang, P. *et al.* The aerobic respiratory chain of *Pseudomonas aeruginosa* cultured in artificial urine media: Role of NQR and terminal oxidases. *PLOS ONE* **15**, e0231965 (2020).
14. Zannoni, D. The respiratory chains of pathogenic pseudomonads. *Biochim. Biophys. Acta BBA - Bioenerg.* **975**, 299–316 (1989).
15. Eschbach, M. *et al.* Long-Term Anaerobic Survival of the Opportunistic Pathogen *Pseudomonas aeruginosa via* Pyruvate Fermentation. *J. Bacteriol.* **186**, 4596–4604 (2004).
16. Poole, R. K. and Cook, G. M. Redundancy of aerobic respiratory chains in bacteria? Routes, reasons and regulation. *Advances in Microbial Physiology* **43** 165–224 (2000).
17. Eitinger, T. Allgemeine Mikrobiologie. Georg Thieme Verlag, (2017).
18. Peters, A., Kulajta, C., Pawlik, G., Daldal, F. and Koch, H.-G. Stability of the cbb_3-Type Cytochrome Oxidase Requires Specific CcoQ-CcoP Interactions. *J. Bacteriol.* **190**, 5576–5586 (2008).
19. Kawakami, T., Kuroki, M., Ishii, M., Igarashi, Y. and Arai, H. Differential expression of multiple terminal oxidases for aerobic respiration in *Pseudomonas aeruginosa*. *Environ. Microbiol.* (2009)
20. Arai, H., Roh, J. H. and Kaplan, S. Transcriptome Dynamics during the Transition from Anaerobic Photosynthesis to Aerobic Respiration in *Rhodobacter sphaeroides* 2.4.1. *J. Bacteriol.* **190**, 286–299 (2008).
21. Saiki, K., Nakamura, H., Mogi, T. and Anraku, Y. Probing a Role of Subunit IV of the *Escherichia coli bo*-type Ubiquinol Oxidase by Deletion and Cross-linking Analyses. *J. Biol. Chem.* **271**, 15336–15340 (1996).
22. Mogi, T., Saiki, K. and Anraku, Y. Biosynthesis and functional role of haem O and haem A. *Mol. Microbiol.* **14**, 391–398 (1994).
23. Jackson, R. J. *et al.* Oxygen Reactivity of Both Respiratory Oxidases in *Campylobacter jejuni*: the *cydAB* Genes Encode a Cyanide-Resistant, Low-Affinity Oxidase That Is Not of the Cytochrome *bd* Type. *J. Bacteriol.* **189**, 1604–1615 (2007).

24. Mogi, T. *et al.* Biochemical and Spectroscopic Properties of Cyanide-Insensitive Quinol Oxidase from *Gluconobacter oxydans*. *J. Biochem. (Tokyo)* **146**, 263–271 (2009).
25. Kerscher, S., Dröse, S., Zickermann, V. and Brandt, U. The Three Families of Respiratory NADH Dehydrogenases. *Bioenergetics* **45** 185–222 (2008).
26. Torres, A. *et al.* NADH Dehydrogenases in *Pseudomonas aeruginosa* Growth and Virulence. *Front. Microbiol.* **10**, 75 (2019).
27. Raba, D. A. *et al.* Characterization of the *Pseudomonas aeruginosa* NQR complex, a bacterial proton pump with roles in autopoisoning resistance. *J. Biol. Chem.* **293**, 15664–15677 (2018).
28. Friedrich, T., Dekovic, D. K. and Burschel, S. Assembly of the *Escherichia coli* NADH:ubiquinone oxidoreductase (respiratory complex I). *Biochim. Biophys. Acta BBA - Bioenerg.* **1857**, 214–223 (2016).
29. Parey, K., Wirth, C., Vonck, J. and Zickermann, V. Respiratory complex I — structure, mechanism and evolution. *Curr. Opin. Struct. Biol.* **63**, 1–9 (2020).
30. Baradaran, R., Berrisford, J. M., Minhas, G. S. and Sazanov, L. A. Crystal structure of the entire respiratory complex I. *Nature* **494**, 443–448 (2013).
31. Berrisford, J. M., Baradaran, R. and Sazanov, L. A. Structure of bacterial respiratory complex I. *Biochim. Biophys. Acta BBA - Bioenerg.* **1857**, 892–901 (2016).
32. Burschel, S. *et al.* Iron-sulfur cluster carrier proteins involved in the assembly of *Escherichia coli* NADH:ubiquinone oxidoreductase (complex I): Assembly of *E. coli* respiratory complex I. *Mol. Microbiol.* **111**, 31–45 (2019).
33. C. Anthony. The biochemistry of methylotrophic micro-organisms. *Sci. Prog.* **62**, 167–206 (1975).
34. Jormakka, M., Byrne, B. and Iwata, S. Formate dehydrogenase – a versatile enzyme in changing environments. *Curr. Opin. Struct. Biol.* **13**, 418–423 (2003).
35. Leonhartsberger, S., Korsa, I. and Böck, A. The molecular biology of formate metabolism in enterobacteria. *J. Mol. Microbiol. Biotechnol.* **4**, 269–276 (2002).
36. Appel, A. M. *et al.* Frontiers, Opportunities, and Challenges in Biochemical and Chemical Catalysis of CO_2 Fixation. *Chem. Rev.* **113**, 6621–6658 (2013).

37. Hille, R., Hall, J. and Basu, P. The Mononuclear Molybdenum Enzymes. *Chem. Rev.* **114**, 3963–4038 (2014).

38. Hartmann, T., Schwanhold, N. and Leimkühler, S. Assembly and catalysis of molybdenum or tungsten-containing formate dehydrogenases from bacteria. *Biochim. Biophys. Acta BBA - Proteins Proteomics* **1854**, 1090–1100 (2015).

39. Popov V. O. and Lamzin V. S. NAD^+-dependent formate dehydrogenase. *Biochem. J.* **301**, 625-643 (1994).

40. Alekseeva, A. A. *et al.* Stabilization of plant formate dehydrogenase by rational design. *Biochem. Mosc.* **77**, 1199–1209 (2012).

41. Dong, G. and Ryde, U. Reaction mechanism of formate dehydrogenase studied by computational methods. *JBIC J. Biol. Inorg. Chem.* **23**, 1243–1254 (2018).

42. Schwanhold, N., Iobbi-Nivol, C., Lehmann, A. and Leimkühler, S. Same but different: Comparison of two system-specific molecular chaperones for the maturation of formate dehydrogenases. *PLOS ONE* **13**, e0201935 (2018).

43. Iwadate, Y., Funabasama, N. and Kato, J. Involvement of formate dehydrogenases in stationary phase oxidative stress tolerance in *Escherichia coli*. *FEMS Microbiol. Lett.* **364**, (2017).

44. Mandrand-Berthelot, M.-Andr., Couchoux-Luthaud, Gis., Santin, C.-L. and Giordan, G. Mutants of *Escherichia coli* Soecifically Deficient in Respiratory Formate Dehydrogenase Activity. *J. of General Microbiology*. **134**, 11 (1988).

45. Stewart, V., Lin, J. T. and Berg, B. L. Genetic evidence that genes *fdhD* and *fdhE* do not control synthesis of formate dehydrogenase-N in *Escherichia coli* K-12. *J. Bacteriol.* **173**, 4417–4423 (1991).

46. Lüke, I. *et al.* Biosynthesis of the respiratory formate dehydrogenases from *Escherichia coli*: characterization of the FdhE protein. *Arch. Microbiol.* **190**, 685–696 (2008).

47. Hagelueken, G. *et al.* Crystal structure of the electron transfer complex rubredoxin rubredoxin reductase of *Pseudomonas aeruginosa*. *Proc. Natl. Acad. Sci.* **104**, 12276–12281 (2007).

48. Borrero-de Acuña, J. M. *et al.* Protein Network of the *Pseudomonas aeruginosa* Denitrification Apparatus. *J. Bacteriol.* **198**, 1401–1413 (2016).

49. Palmer, K. L., Brown, S. A. and Whiteley, M. Membrane-Bound Nitrate Reductase Is Required for Anaerobic Growth in Cystic Fibrosis Sputum. *J. Bacteriol.* **189**, 4449–4455 (2007).

50. Sharma, V., Noriega, C. E. and Rowe, J. J. Involvement of NarK1 and NarK2 Proteins in Transport of Nitrate and Nitrite in the Denitrifying Bacterium *Pseudomonas aeruginosa* PAO1. *Appl. Environ. Microbiol.* **72**, 3802–3802 (2006).

51. Zumft, W. G. Cell biology and molecular basis of denitrification. *Microbiol. Mol. Biol. Rev. MMBR* **61**, 533–616 (1997).

52. Van Alst, N. E., Sherrill, L. A., Iglewski, B. H. and Haidaris, C. G. Compensatory periplasmic nitrate reductase activity supports anaerobic growth of *Pseudomonas aeruginosa* PAO1 in the absence of membrane nitrate reductase. *Can. J. Microbiol.* **55**, 1133–1144 (2009).

53. Sparacino-Watkins, C., Stolz, J. F. and Basu, P. Nitrate and periplasmic nitrate reductases. *Chem. Soc. Rev.* **43**, 676–706 (2014).

54. Chen, F., Xia, Q. and Ju, L.-K. Aerobic Denitrification of *Pseudomonas aeruginosa* Monitored by Online NAD(P)H Fluorescence. *Appl. Environ. Microbiol.* **69**, 6715–6722 (2003).

55. Coelho, C. and Romão, M. J. Structural and mechanistic insights on nitrate reductases: Insights on Nitrate Reductases. *Protein Sci.* **24**, 1901–1911 (2015).

56. Li, H. and Sourjik, V. Assembly and stability of flagellar motor in *Escherichia coli*: Flagellar motor assembly. *Mol. Microbiol.* **80**, 886–899 (2011).

57. Morimoto, Y. and Minamino, T. Structure and Function of the Bi-Directional Bacterial Flagellar Motor. *Biomolecules* **4**, 217–234 (2014).

58. Minamino, T. and Imada, K. The bacterial flagellar motor and its structural diversity. *Trends Microbiol.* **23**, 267–274 (2015).

59. Minamino, T., Kawamoto, A., Kinoshita, M. and Namba, K. Molecular Organization and Assembly of the Export Apparatus of Flagellar Type III Secretion Systems. *Springer Berlin Heidelberg*, (2019).

60. Imada, K. Bacterial flagellar axial structure and its construction. *Biophys. Rev.* **10**, 559–570 (2018).

61. Fukumura, T. *et al.* Assembly and stoichiometry of the core structure of the bacterial flagellar type III export gate complex. *PLOS Biol.* **15**, e2002281 (2017).

62. Kinoshita, M., Aizawa, S., Inoue, Y., Namba, K. and Minamino, T. The role of intrinsically disordered C-terminal region of FliK in substrate specificity switching of the bacterial flagellar type III export apparatus. *Mol. Microbiol.* **105**, 572–588 (2017).

63. Kuhlen, L. *et al.* Structure of the core of the type III secretion system export apparatus. *Nat. Struct. Mol. Biol.* **25**, 583–590 (2018).

64. Imada, K., Minamino, T., Uchida, Y., Kinoshita, M. and Namba, K. Insight into the flagella type III export revealed by the complex structure of the type III ATPase and its regulator. *Proc. Natl. Acad. Sci.* **113**, 3633–3638 (2016).

65. Song, W. S. and Yoon, S. Crystal structure of FliC flagellin from *Pseudomonas aeruginosa* and its implication in TLR5 binding and formation of the flagellar filament. *Biochem. Biophys. Res. Commun.* **444**, 109–115 (2014).

66. Caruana, J. C. and Walper, S. A. Bacterial Membrane Vesicles as Mediators of Microbe – Microbe and Microbe – Host Community Interactions. *Front. Microbiol.* **11**, 432 (2020).

67. Guerrero-Mandujano, A., Hernández-Cortez, C., Ibarra, J. A. and Castro-Escarpulli, G. The outer membrane vesicles: Secretion system type zero. *Traffic* **18**, 425–432 (2017).

68. Turnbull, L. *et al.* Explosive cell lysis as a mechanism for the biogenesis of bacterial membrane vesicles and biofilms. *Nat. Commun.* **7**, 11220 (2016).

69. Toyofuku, M. *et al.* Prophage-triggered membrane vesicle formation through peptidoglycan damage in *Bacillus subtilis*. *Nat. Commun.* **8**, 481 (2017).

70. Toyofuku, M., Nomura, N. and Eberl, L. Types and origins of bacterial membrane vesicles. *Nat. Rev. Microbiol.* **17**, 13–24 (2019).

71. Toyofuku, M. Bacterial communication through membrane vesicles. *Biosci. Biotechnol. Biochem.* **83**, 1599–1605 (2019).

72. Küsel, K., Dorsch, T., Acker, G. and Stackebrandt, E. Microbial Reduction of Fe(III) in Acidic Sediments: Isolation of *Acidiphilium cryptum* JF-5 Capable of Coupling the Reduction of Fe(III) to the Oxidation of Glucose. *Appl. Environ. Microbiol.* **65**, 3633–3640 (1999).

73. Dubey, G. P. *et al.* Architecture and Characteristics of Bacterial Nanotubes. *Dev. Cell* **36**, 453–461 (2016).

74. Remis, J. P. *et al.* Bacterial social networks: structure and composition of *Myxococcus xanthus* outer membrane vesicle chains: Membrane vesicle chains and membrane network of *M. xanthus*. *Environ. Microbiol.* **16**, 598–610 (2014).

75. Pirbadian, S. *et al. Shewanella oneidensis* MR-1 nanowires are outer membrane and periplasmic extensions of the extracellular electron transport components. *Proc. Natl. Acad. Sci.* **111**, 12883–12888 (2014).

76. Li, A., Schertzer, J. W. and Yong, X. Molecular dynamics modeling of *Pseudomonas aeruginosa* outer membranes. *Phys. Chem. Chem. Phys.* **20**, 23635–23648 (2018).

77. Orench-Rivera, N. and Kuehn, M. J. Environmentally controlled bacterial vesicle-mediated export. *Cell. Microbiol.* **18**, 1525–1536 (2016).

78. Roier, S., Zingl, F., Cakar, F. and Schild, S. Bacterial outer membrane vesicle biogenesis: a new mechanism and its implications. *Microb. Cell* **3**, 257–259 (2016).

79. Kadurugamuwa, J. L. and Beveridge, T. J. Virulence factors are released from *Pseudomonas aeruginosa* in association with membrane vesicles during normal growth and exposure to gentamicin: a novel mechanism of enzyme secretion. *J. Bacteriol.* **177**, 3998–4008 (1995).

80. Sutterlin, H. A. *et al.* Disruption of lipid homeostasis in the Gram-negative cell envelope activates a novel cell death pathway. *Proc. Natl. Acad. Sci.* **113**, 1565-1574 (2016).

81. Cooke, A. C., Nello, A. V., Ernst, R. K. and Schertzer, J. W. Analysis of *Pseudomonas aeruginosa* biofilm membrane vesicles supports multiple mechanisms of biogenesis. *PLOS ONE* **14**, e0212275 (2019).

82. Clarke, A. J. The “hole” story of predatory outer-membrane vesicles. *Can. J. Microbiol.* **64**, 589–599 (2018).
83. Mashburn, L. M. and Whiteley, M. Membrane vesicles traffic signals and facilitate group activities in a prokaryote. *Nature* **437**, 422–425 (2005).
84. Schertzer, J. W. and Whiteley, M. A Bilayer-Couple Model of Bacterial Outer Membrane Vesicle Biogenesis. *mBio* **3**, e00297-11 (2012).
85. Ezkurdia, I. *et al.* Multiple evidence strands suggest that there may be as few as 19000 human protein-coding genes. *Hum. Mol. Genet.* **23**, 5866–5878 (2014).
86. Zhou, M., Li, Q. and Wang, R. Current Experimental Methods for Characterizing Protein-Protein Interactions. *ChemMedChem* **11**, 738–756 (2016).
87. Berggård, T., Linse, S. and James, P. Methods for the detection and analysis of protein–protein interactions. *PROTEOMICS* **7**, 2833–2842 (2007).
88. Miura, K. An Overview of Current Methods to Confirm Protein- Protein Interactions. *Protein Pept. Lett.* **25**, 728–733 (2018).
89. Braun, P. and Gingras, A.-C. History of protein-protein interactions: From egg-white to complex networks. *PROTEOMICS* **12**, 1478–1498 (2012).
90. Gingras, A.-C., Gstaiger, M., Raught, B. and Aebersold, R. Analysis of protein complexes using mass spectrometry. *Nat. Rev. Mol. Cell Biol.* **8**, 645–654 (2007).
91. Vidal, M., Cusick, M. E. and Barabási, A.-L. Interactome Networks and Human Disease. *Cell* **144**, 986–998 (2011).
92. Neduva, V. and Russell, R. B. Linear motifs: Evolutionary interaction switches. *FEBS Lett.* **579**, 3342–3345 (2005).
93. Douzi, B. Protein–Protein Interactions: Surface Plasmon Resonance. *Bacterial Protein Secretion Systems*. **1615**, 257–275 (2017).
94. Lin, J.-S. and Lai, E.-M. Protein–Protein Interactions: Yeast Two-Hybrid System. *Bacterial Protein Secretion Systems*. **1615**, 177–187 (2017).
95. Choi, S. G., Richardson, A., Lambourne, L., Hill, D. E. and Vidal, M. Protein Interactomics by Two-Hybrid Methods. *Two-Hybrid Systems*. **1794**, 1–14 (2018).
96. EUROMEDEX. Bacterial adenylate cyclase two-hybrid system kit. (2005).

97. Louche, A., Salcedo, S. P. and Bigot, S. Protein–Protein Interactions: Pull-Down Assays. *Bacterial Protein Secretion Systems*. **1615**, 247–255 (2017).

98. Lin, J.-S. and Lai, E.-M. Protein–Protein Interactions: Co-Immunoprecipitation. *Bacterial Protein Secretion Systems*. **1615**, 211–219 (2017).

99. Rigaut, G. *et al.* A generic protein purification method for protein complex characterization and proteome exploration. *Nat. Biotechnol.* **17**, 1030–1032 (1999).

100. Butland, G. *et al.* Interaction network containing conserved and essential protein complexes in *Escherichia coli*. *Nature* **433**, 531–537 (2005).

101. Kratchmarova, I. Mechanism of Divergent Growth Factor Effects in Mesenchymal Stem Cell Differentiation. *Science* **308**, 1472–1477 (2005).

102. Lipton, M. S., Pasa-Tolic, L. and Walker, J. M. Mass Spectrometry of Proteins and Peptides: Methods and Protocols. *Humana Press* **492**, (2009).

103. Miernyk, J. A. and Thelen, J. J. Biochemical approaches for discovering protein-protein interactions. *Plant J.* **53**, 597–609 (2008).

104. Weber, P. J. A. and Beck-Sickinger, A. G. Comparison of the photochemical behavior of four different photoactivatable probes. *J. Pept. Res.* **49**, 375–383 (2009).

105. Borrero-de Acuña, J. M. *et al.* A Periplasmic Complex of the Nitrite Reductase NirS, the Chaperone DnaK, and the Flagellum Protein FliC Is Essential for Flagellum Assembly and Motility in *Pseudomonas aeruginosa*. *J. Bacteriol.* **197**, 3066–3075 (2015).

106. Grant, S. G., Jessee, J., Bloom, F. R. and Hanahan, D. Differential plasmid rescue from transgenic mouse DNAs into *Escherichia coli* methylation-restriction mutants. *Proc. Natl. Acad. Sci.* **87**, 4645–4649 (1990).

107. Thoma, S. and Schobert, M. An improved *Escherichia coli* donor strain for diparental mating. *FEMS Microbiol Lett* **294**, 127-132 (2009).

108. B. W. Holloway. Genetics of *Pseudomonas*. *Am. Soc. Microbiol.* **33**, 419–443 (1969).

109. Rahme, L. *et al.* Common virulence factors for bacterial pathogenicity in plants and animals. *Science* **268**, 1899–1902 (1995).

110. Liberati, N. T. *et al.* An ordered, nonredundant library of *Pseudomonas aeruginosa* strain PA14 transposon insertion mutants. *Proc. Natl. Acad. Sci.* **103**, 2833–2838 (2006).

111. Katrin Müller. Charakterisierung eines neuen Häm-Chaperons *in vivo* in *Pseudomonas aeruginosa* und *Danio rerio*. (2016).

112. Christoph Riemenschneider. Charakterisierung der Protein-Protein-Interaktionen des respiratorischen Systems in *Pseudomonas aeruginosa*. (2019).

113. Olsen, R. H., DeBusscher, G. and McCombie, W. R. Development of broad-host-range vectors and gene banks: self-cloning of the *Pseudomonas aeruginosa* PAO chromosome. *J. Bacteriol.* **150**, 60–69 (1982).

114. Bertani, G. STUDIES ON LYSOGENESIS I. The Mode of Phage Liberation by Lysogenic *Escherichia Coli*. **62**, (1951).

115. New England BioLabs. NEBuilder HiFi DNA Assembly Master Mix. https://international.neb.com/products/e2621-nebuilder-hifi-dna-assembly-master-mix#Product%20Information.

116. Bio-Resource. Technical Resources in Biotechnology. http://technologyinscience.blogspot.com/2011_12_01_archive.html#.X_ctBjSg-Uk.

117. Hughes, C. S. *et al.* Ultrasensitive proteome analysis using paramagnetic bead technology. *Mol. Syst. Biol.* **10**, 757 (2014).

118. Sielaff, M. *et al.* Evaluation of FASP, SP3, and iST Protocols for Proteomic Sample Preparation in the Low Microgram Range. *J. Proteome Res.* **16**, 4060–4072 (2017).

119. Meier, F. *et al.* Online Parallel Accumulation–Serial Fragmentation (PASEF) with a Novel Trapped Ion Mobility Mass Spectrometer. *Mol. Cell. Proteomics* **17**, 2534–2545 (2018).

120. Krieger, J. R. *et al.* Evosep One Enables Robust Deep Proteome Coverage Using Tandem Mass Tags while Significantly Reducing Instrument Time. *J. Proteome Res.* **18**, 2346–2353 (2019).

121. Bekker-Jensen, D. B. *et al.* A Compact Quadrupole-Orbitrap Mass Spectrometer with FAIMS Interface Improves Proteome Coverage in Short LC Gradients. *Mol. Cell. Proteomics* **19**, 716–729 (2020).

122. Ebbinghaus, S., Dhar, A., McDonald, J. D. and Gruebele, M. Protein folding stability and dynamics imaged in a living cell. *Nat. Methods* **7**, 319–323 (2010).

123. Gnutt, D. *et al.* Stability Effect of Quinary Interactions Reversed by Single Point Mutations. *J. Am. Chem. Soc.* (2019).

124. Girdhar, K., Scott, G., Chemla, Y. R. and Gruebele, M. Better biomolecule thermodynamics from kinetics. *J. Chem. Phys.* **135**, 015102 (2011).

125. Feynman, R. P., Leighton, R. B., Sands, M. L. and Feynman, R. P. Elektromagnetismus und Struktur der Materie. Oldenbourg, (2001).

126. Roth, J. and Binder, M. Coloidal gold, ferritin and peroxidase as markers for electron microscopic double labeling lectin techniques. *J. Histochem. Cytochem.* **26**, 163–169 (1978).

127. Roth, J., Bendayan, M. and Orci, L. Ultrastructural localization of intracellular antigens by the use of protein A-gold complex. *J. Histochem. Cytochem.* **26**, 1074–1081 (1978).

128. Hayat, M. A. Immunogold-silver staining: principles, methods, and applications. CRC Press, (1995).

129. Oliver, C. Use of Immunogold with Silver Enhancement. *Immunocytochemical Methods and Protocols*. **115**, 241–246 (1999).

130. Hermann, R., Walther, P. and Müller, M. Immunogold labeling in scanning electron microscopy. *Histochem. Cell Biol.* **106**, 31–39 (1996).

131. Martina Jahn and Dieter Jahn. Electron transfer reactions and oxidative phosphorylation. *Biochemical pathways: an atlas of biochemistry and molecular biology* (2012).

132. Moreno-Lastres, D. *et al.* Mitochondrial Complex I Plays an Essential Role in Human Respirasome Assembly. *Cell Metab.* **15**, 324–335 (2012).

133. Dudkina, N. V., Kudryashev, M., Stahlberg, H. and Boekema, E. J. Interaction of complexes I, III, and IV within the bovine respirasome by single particle cryoelectron tomography. *Proc. Natl. Acad. Sci.* **108**, 15196–15200 (2011).

134. Lapuente-Brun, E. *et al.* Supercomplex Assembly Determines Electron Flux in the Mitochondrial Electron Transport Chain. *Science* **340**, 1567–1570 (2013).

135. Krause, F. *et al.* “Respirasome”-like Supercomplexes in Green Leaf Mitochondria of Spinach. *J. Biol. Chem.* **279**, 48369–48375 (2004).

136. Bultema, J. B., Braun, H.-P., Boekema, E. J. and Kouřil, R. Megacomplex organization of the oxidative phosphorylation system by structural analysis of respiratory supercomplexes from potato. *Biochim. Biophys. Acta BBA - Bioenerg.* **1787**, 60–67 (2009).

137. Marques, I., Dencher, N. A., Videira, A. and Krause, F. Supramolecular Organization of the Respiratory Chain in *Neurospora crassa* Mitochondria. *Eukaryot. Cell* **6**, 2391–2405 (2007).

138. Schagger, H. Supercomplexes in the respiratory chains of yeast and mammalian mitochondria. *EMBO J.* **19**, 1777–1783 (2000).

139. Efremov, R. G. and Sazanov, L. A. Structure of the membrane domain of respiratory complex I. *Nature* **476**, 414–420 (2011).

140. iba Lifesciences. Strep-tag: The leading affinity tag in recombinant protein technology. *iba-lifescience* https://www.iba-lifesciences.com/strep-tactin-system-technology.html.

141. Korndorfer, I. P. Improved affinity of engineered streptavidin for the Strep-tag II peptide is due to a fixed open conformation of the lid-like loop at the binding site. *Protein Sci.* **11**, 883–893 (2002).

142. Dominik B. Schuntermann. Charakterisierung der Protein-Protein-Interaktionen der periplasmatischen Nitratreduktase NapA in *Pseudomonas aeruginosa*. (2019).

143. Gavin, A.-C. *et al.* Functional organization of the yeast proteome by systematic analysis of protein complexes. *Nature* **415**, 141–147 (2002).

144. Zhang, J., Zhong, C., Lin, H. X. and Wang, M. Identifying Protein Complexes from Dynamic Temporal Interval Protein-Protein Interaction Networks. *BioMed Res. Int.* **2019**, 1–17 (2019).

145. Przytycka, T. M., Singh, M. and Slonim, D. K. Toward the dynamic interactome: it's about time. *Brief. Bioinform.* **11**, 15–29 (2010).

146. Xiao, Q., Wang, J., Peng, X. and Wu, F.-X. Detecting protein complexes from active protein interaction networks constructed with dynamic gene expression profiles. *Proteome Sci.* **11**, S20 (2013).

147. Guła, G., Dorotkiewicz-Jach, A., Korzekwa, K., Valvano, M. A. and Drulis-Kawa, Z. Complex Signaling Networks Controlling Dynamic Molecular Changes in *Pseudomonas aeruginosa* Biofilm. *Curr. Med. Chem.* **26**, 1979–1993 (2019).

148. Klünemann, T. *et al.* Crystal Structure of Dihydro-Heme d_1 Dehydrogenase NirN from *Pseudomonas aeruginosa* Reveals Amino Acid Residues Essential for Catalysis. *J. Mol. Biol.* **431**, 3246–3260 (2019).

149. Arai, H., Kodama, T. and Igarashi, Y. Effect of nitrogen oxides on expression of the *nir* and *nor* genes for denitrification in *Pseudomonas aeruginosa*. *FEMS Microbiol. Lett.* **170**, 19–24 (1999).

150. Anderson, R. F. *et al.* Electron-Transfer Pathways in the Heme and Quinone-Binding Domain of Complex II (Succinate Dehydrogenase). *Biochemistry* **53**, 1637–1646 (2014).

151. Maher, M. J., Herath, A. S., Udagedara, S. R., Dougan, D. A. and Truscott, K. N. Crystal structure of bacterial succinate:quinone oxidoreductase flavoprotein SdhA in complex with its assembly factor SdhE. *Proc. Natl. Acad. Sci.* **115**, 2982–2987 (2018).

152. Lin, Y.-C. *et al.* Phenazines Regulate Nap-Dependent Denitrification in *Pseudomonas aeruginosa* Biofilms. *J. Bacteriol.* **200**, e00031-18 (2018).

153. Zhou, G. *et al.* Functional roles of *norCB* in *Pseudomonas aeruginosa* ATCC 9027 under aerobic conditions. *J. Basic Microbiol.* **59**, 1154–1162 (2019).

154. Haiko, J. and Westerlund-Wikström, B. The Role of the Bacterial Flagellum in Adhesion and Virulence. *Biology* **2**, 1242–1267 (2013).

155. Cohen, T. S. and Prince, A. S. Activation of inflammasome signaling mediates pathology of acute *P. aeruginosa* pneumonia. *J. Clin. Invest.* **123**, 1630–1637 (2013).

156. Hayashi, N. R., Arai, H., Kodama, T. and Igarashi, Y. The *nirQ* gene, which is required for denitrification of *Pseudomonas aeruginosa*, can activate the RubisCO from *Pseudomonas hydrogenothermophila*. *Biochim. Biophys. Acta*. **1381**, 347-50 (1998).

157. Borrero-de Acuña, J. M., Timmis, K. N., Jahn, M. and Jahn, D. Protein complex formation during denitrification by *Pseudomonas aeruginosa*. *Microb. Biotechnol.* **10**, 1523–1534 (2017).

158. Barber-Zucker, S., Keren-Khadmy, N. and Zarivach, R. From invagination to navigation: The story of magnetosome-associated proteins in magnetotactic bacteria: Magnetosome Proteins in Magnetotactic Bacteria. *Protein Sci.* **25**, 338–351 (2016).

159. Blakemore, R. Magnetotactic bacteria. *Science* **190**, 377–379 (1975).

160. Lenz, L. L., Dere, B. and Bevan, M. J. Identification of an H2-M3-Restricted Listeria Epitope: Implications for Antigen Presentation by M3. *Immunity* **5**, 63–72 (1996).

161. Raschdorf, O. *et al.* Genetic and Ultrastructural Analysis Reveals the Key Players and Initial Steps of Bacterial Magnetosome Membrane Biogenesis. *PLOS Genet.* **12**, e1006101 (2016).

162. Juodeikis, R. Engineering Membranes in *Escherichia coli*: The Magnetosome, LemA Protein Family and Outer Membrane Vesicles. (2016).

163. Paradis-Bleau, C. *et al. Pseudomonas aeruginosa* MurE amide ligase: enzyme kinetics and peptide inhibitor. *Biochem. J.* **421**, 263–272 (2009).

164. Tavares, I. M. *et al.* Identification of the *Pseudomonas aeruginosa glmM* Gene, Encoding Phosphoglucosamine Mutase. *J. Bacteriol.* **182**, 4453–4457 (2000).

165. Tavares, I. M., Leitão, J. H. and Sá-Correia, I. Chromosomal organization and transcription analysis of genes in the vicinity of *Pseudomonas aeruginosa glmM* gene encoding phosphoglucosamine mutase. *Biochem. Biophys. Res. Commun.* **302**, 363–371 (2003).

166. Bharat, A. and Brown, E. D. Phenotypic investigations of the depletion of EngA in *Escherichia coli* are consistent with a role in ribosome biogenesis. *FEMS Microbiol. Lett.* **353**, 26–32 (2014).

167. Subramanian, C., Rock, C. O. and Zhang, Y.-M. DesT Coordinates the Expression of Anaerobic and Aerobic Pathways for Unsaturated Fatty Acid Biosynthesis in *Pseudomonas aeruginosa*. *J. Bacteriol.* **192**, 280–285 (2010).

168. Hu, J. *et al.* Enhancing extracellular protein production in *Escherichia coli* by deleting the D -alanyl- D -alanine carboxypeptidase gene *dacC*. *Eng. Life Sci.* **19**, 270–278 (2019).

169. Tamber, S., Ochs, M. M. and Hancock, R. E. W. Role of the Novel OprD Family of Porins in Nutrient Uptake in *Pseudomonas aeruginosa*. *J. Bacteriol.* **188**, 45–54 (2006).

170. Munguia, J. *et al.* The Mla pathway is critical for *Pseudomonas aeruginosa* resistance to outer membrane permeabilization and host innate immune clearance. *J. Mol. Med.* **95**, 1127–1136 (2017).

171. Moynié, L. *et al.* Structural Insights into the Mechanism and Inhibition of the β-Hydroxydecanoyl-Acyl Carrier Protein Dehydratase from *Pseudomonas aeruginosa*. *J. Mol. Biol.* **425**, 365–377 (2013).

172. Loubens, I., Debarbieux, L., Bohin, A., Lacroix, J.-M. and Bohin, J.-P. Homology between a genetic locus (*mdoA*) involved in the osmoregulated biosynthesis of periplasmic glucans in *Escherichia coli* and a genetic locus (*hrpM*) controlling pathogenicity of *Pseudomonas syringae*. *Mol. Microbiol.* **10**, 329–340 (1993).

173. Heng, S. S. J., Chan, O. Y. W., Keng, B. M. H. and Ling, M. H. T. Glucan Biosynthesis Protein G Is a Suitable Reference Gene in *Escherichia coli* K-12. *ISRN Microbiol.* **2011**, 1–6 (2011).

174. Page, F. *et al.* Osmoregulated Periplasmic Glucan Synthesis Is Required for *Erwinia chrysanthemi* Pathogenicity. *J. Bacteriol.* **183**, 3134–3141 (2001).

175. Moynié, L. *et al.* Structure and Function of the PiuA and PirA Siderophore-Drug Receptors from *Pseudomonas aeruginosa* and *Acinetobacter baumannii*. *Antimicrob. Agents Chemother.* **61**, e02531-16, (2017).

176. Luscher, A. *et al.* TonB-Dependent Receptor Repertoire of *Pseudomonas aeruginosa* for Uptake of Siderophore-Drug Conjugates. *Antimicrob. Agents Chemother.* **62**, e00097-18, (2018).

177. Perumal, D. *et al.* Cloning and Targeted Disruption of Two Lipopolysaccharide Biosynthesis Genes, *kdsA* and *waaG*, of *Pseudomonas aeruginosa* PAO1 by Site-Directed Mutagenesis. *J. Mol. Microbiol. Biotechnol.* **19**, 169–179 (2010).

178. Rico-Jiménez, M., Muñoz-Martínez, F., Krell, T., Gavira, J. A. and Pineda-Molina, E. Purification, crystallization and preliminary crystallographic analysis of the ligand-binding regions of the PctA and PctB chemoreceptors from *Pseudomonas aeruginosa* in complex with amino acids. *Acta Crystallograph. Sect. F Struct. Biol. Cryst. Commun.* **69**, 1431–1435 (2013).

179. Kilmury, S. L. N. and Burrows, L. L. The *Pseudomonas aeruginosa* PilSR Two-Component System Regulates Both Twitching and Swimming Motilities. *mBio* **9**, e01310-18, (2018).

180. Mousavi, M. *et al.* Passive immunization against *Pseudomonas aeruginosa* recombinant PilA in a murine burn wound model. *Microb. Pathog.* **101**, 83–88 (2016).

181. Satarian, F., Nejadsattari, T., Vaziri, F. and Siadat, S. D. Comparative study of immune responses elicited by outer membrane vesicles of different *Pseudomonas aeruginosa* strains. *Comp. Immunol. Microbiol. Infect. Dis.* **66**, 101328 (2019).

182. Clarke, L. Development of a diagnostic PCR assay that targets a heat-shock protein gene (*groES*) for detection of *Pseudomonas spp*. in cystic fibrosis patients. *J. Med. Microbiol.* **52**, 759–763 (2003).

183. Wager, B., Faudry, E., Wills, T., Attree, I. and Delcour, A. H. Current Fluctuation Analysis of the PopB and PopD Translocon Components of the *Pseudomonas aeruginosa* Type III Secretion System. *Biophys. J.* **104**, 1445–1455 (2013).

184. Goure, J. *et al.* The V Antigen of *Pseudomonas aeruginosa* Is Required for Assembly of the Functional PopB/PopD Translocation Pore in Host Cell Membranes. *Infect. Immun.* **72**, 4741–4750 (2004).

185. Allegretta, G. *et al.* In-depth Profiling of MvfR-Regulated Small Molecules in *Pseudomonas aeruginosa* after Quorum Sensing Inhibitor Treatment. *Front. Microbiol.* **8**, 924 (2017).

186. Storz, M. P. *et al.* Validation of PqsD as an Anti-biofilm Target in *Pseudomonas aeruginosa* by Development of Small-Molecule Inhibitors. *J. Am. Chem. Soc.* **134**, 16143–16146 (2012).

187. Prothiwa, M., Englmaier, F. and Böttcher, T. Competitive Live-Cell Profiling Strategy for Discovering Inhibitors of the Quinolone Biosynthesis of *Pseudomonas aeruginosa*. *J. Am. Chem. Soc.* **140**, 14019–14023 (2018).

188. Dulcey, C. E. *et al.* The End of an Old Hypothesis: The *Pseudomonas* Signaling Molecules 4-Hydroxy-2-Alkylquinolines Derive from Fatty Acids, Not 3-Ketofatty Acids. *Chem. Biol.* **20**, 1481–1491 (2013).

189. Subedi, D., Vijay, A. K., Kohli, G. S., Rice, S. A. and Willcox, M. Association between possession of ExoU and antibiotic resistance in *Pseudomonas aeruginosa*. *PLOS ONE* **13**, e0204936 (2018).

190. Foulkes, D. M. *et al. Pseudomonas aeruginosa* Toxin ExoU as a Therapeutic Target in the Treatment of Bacterial Infections. *Microorganisms* **7**, 707 (2019).

191. Springer, T. I., Reid, T.-E., Gies, S. L. and Feix, J. B. Interactions of the effector ExoU from *Pseudomonas aeruginosa* with short-chain phosphatidylinositides provide insights into ExoU targeting to host membranes. *J. Biol. Chem.* **294**, 19012–19021 (2019).

192. Tashiro, Y. *et al.* Interaction of Bacterial Membrane Vesicles with Specific Species and Their Potential for Delivery to Target Cells. *Front. Microbiol.* **8**, (2017).

193. de la Fuente-Núñez, C., Reffuveille, F., Fairfull-Smith, K. E. and Hancock, R. E. W. Effect of Nitroxides on Swarming Motility and Biofilm Formation, Multicellular Behaviors in *Pseudomonas aeruginosa*. *Antimicrob. Agents Chemother.* **57**, 4877–4881 (2013).

194. Qi, H.-Y., Hyndman, J. B. and Bernstein, H. D. DnaK Promotes the Selective Export of Outer Membrane Protein Precursors in SecA-deficient *Escherichia coli*. *J. Biol. Chem.* **277**, 51077–51083 (2002).

195. Tashiro, Y., Uchiyama, H. and Nomura, N. Multifunctional membrane vesicles in *Pseudomonas aeruginosa*: Membrane vesicles of *Pseudomonas aeruginosa*. *Environ. Microbiol.* **14**, 1349–1362 (2012).

196. Han, H. RNA Interference to Knock Down Gene Expression. *Disease Gene Identification*. **1706**, 293–302 (2018).

197. Ryazansky, S., Kulbachinskiy, A. and Aravin, A. A. The Expanded Universe of Prokaryotic Argonaute Proteins. *mBio* **9**, 20 (2018).

198. Lisitskaya, L., Aravin, A. A. and Kulbachinskiy, A. DNA interference and beyond: structure and functions of prokaryotic Argonaute proteins. *Nat. Commun.* **9**, 5165 (2018).

199. de Crouy-Chanel, A., Kohiyama, M. and Richarme, G. Interaction of DnaK with native proteins and membrane proteins correlates with their accessible hydrophobicity. *Gene* **230**, 163–170 (1999).

200. Palleros, D. R., Reid, K. L., McCarty, J. S., Walker, G. C. and Fink, A. L. DnaK, *hsp73*, and their molten globules. Two different ways heat shock proteins respond to heat. *J. Biol. Chem.* **267**, 5279–5285 (1992).

201. Sharma, S., Christen, P. and Goloubinoff, P. Disaggregating Chaperones: An Unfolding Story. *Curr. Protein Pept. Sci.* **10**, 432–446 (2009).

202. Wood, R. J. *et al.* A biosensor-based framework to measure latent proteostasis capacity. *Nat. Commun.* **9**, 287 (2018).

203. Kityk, R., Kopp, J., Sinning, I. and Mayer, M. P. Structure and Dynamics of the ATP-Bound Open Conformation of Hsp70 Chaperones. *Mol. Cell* **48**, 863–874 (2012).

204. Azoulay, I. *et al.* Tracking the Interplay between Bound Peptide and the Lid Domain of DnaK, Using Molecular Dynamics. *Int. J. Mol. Sci.* **14**, 12675–12695 (2013).

205. Mayer, M. P. and Gierasch, L. M. Recent advances in the structural and mechanistic aspects of Hsp70 molecular chaperones. *J. Biol. Chem.* **294**, 2085–2097 (2019).

Appendix

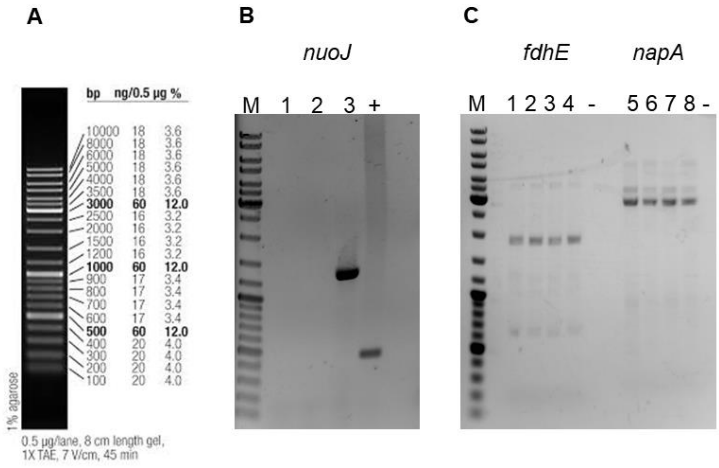

Appendix 1: Verification of the transposon mutants for interactomics approach. Verification of the transposon mutants by respective amplification of the genes *via* agarose gel electrophoresis and ethidium bromide staining. The transposon used in the PA14 transposon library has a size of 1000 bp **A.** Marker standard **B.** Amplification of the *nuoJ* gene: lane 1-3 of the transposon mutants with 1500 bp and lane **+** is the wildtype gene of *nuoJ* as positive control with 500 bp. **C.** Amplification of the *fdhE* and *napA* genes: lanes 1-4 present the transposon mutants of *fdhE* with 1930 bp and lanes 5-8 shows the transposon mutants of *napA* with 3500 bp, **-** shows the negative control.

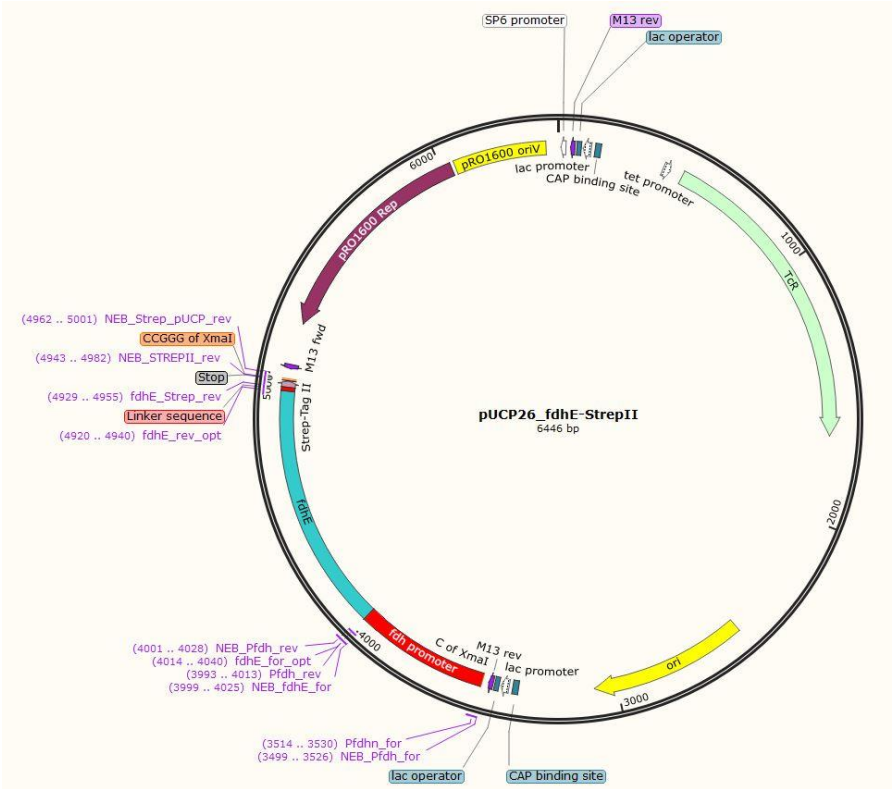

Appendix 2: Plasmid map of pUCP26_*fdhE*-StrepII

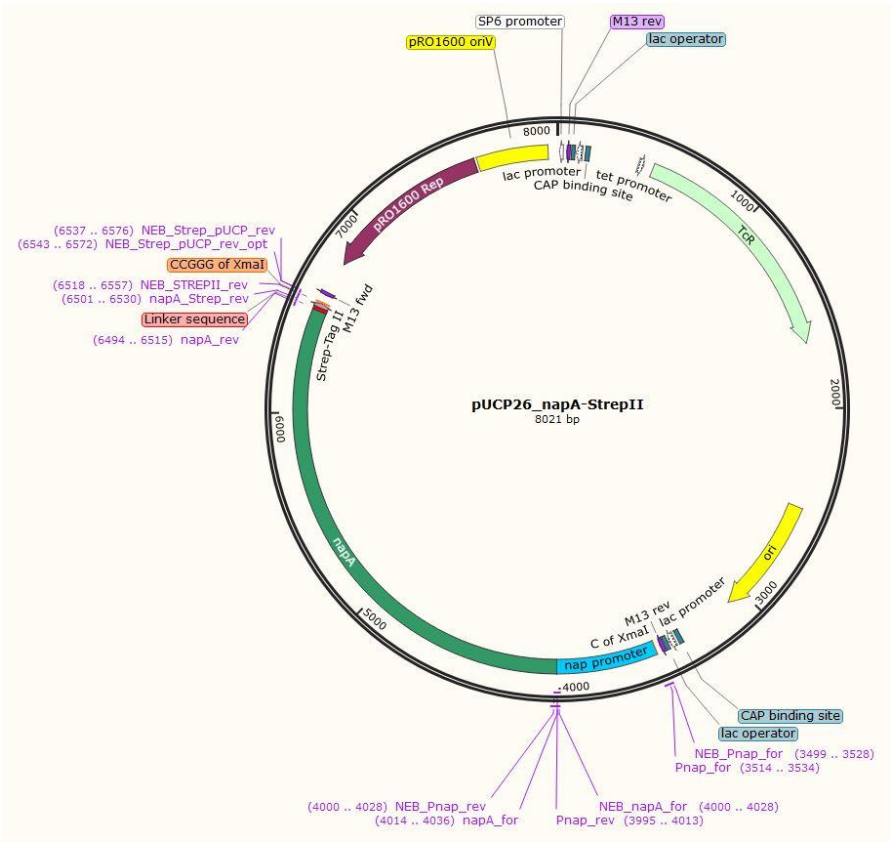

Appendix 3: Plasmid map of pUCP26_*napA*-StrepII

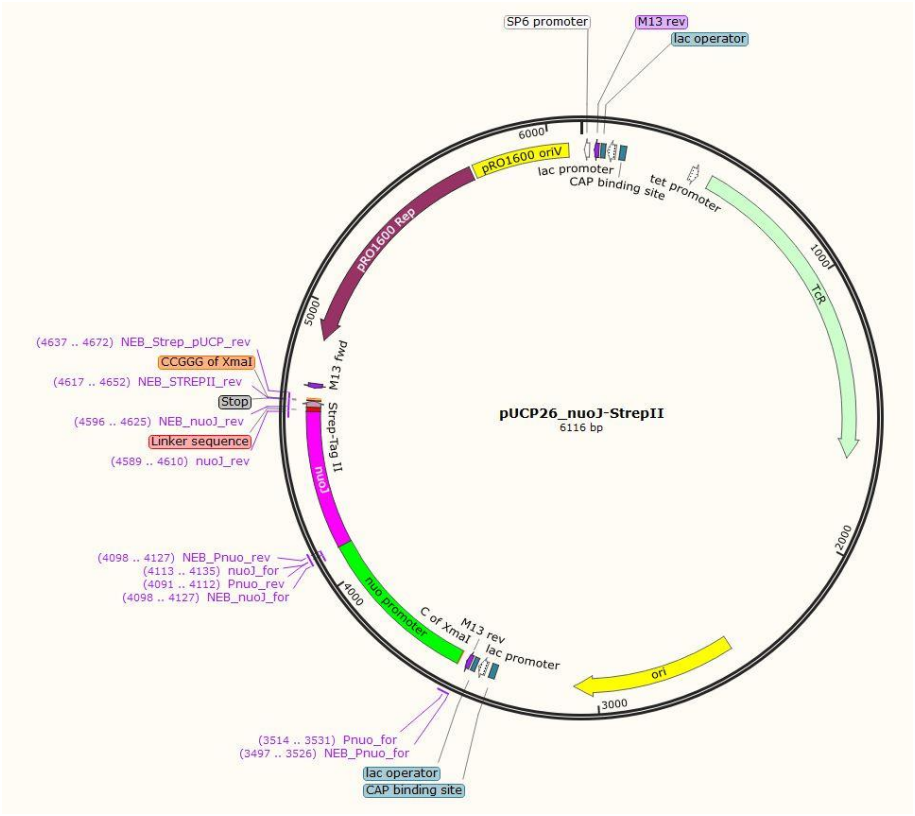

Appendix 4: Plasmid map of pUCP26_*nuoJ*-StrepII

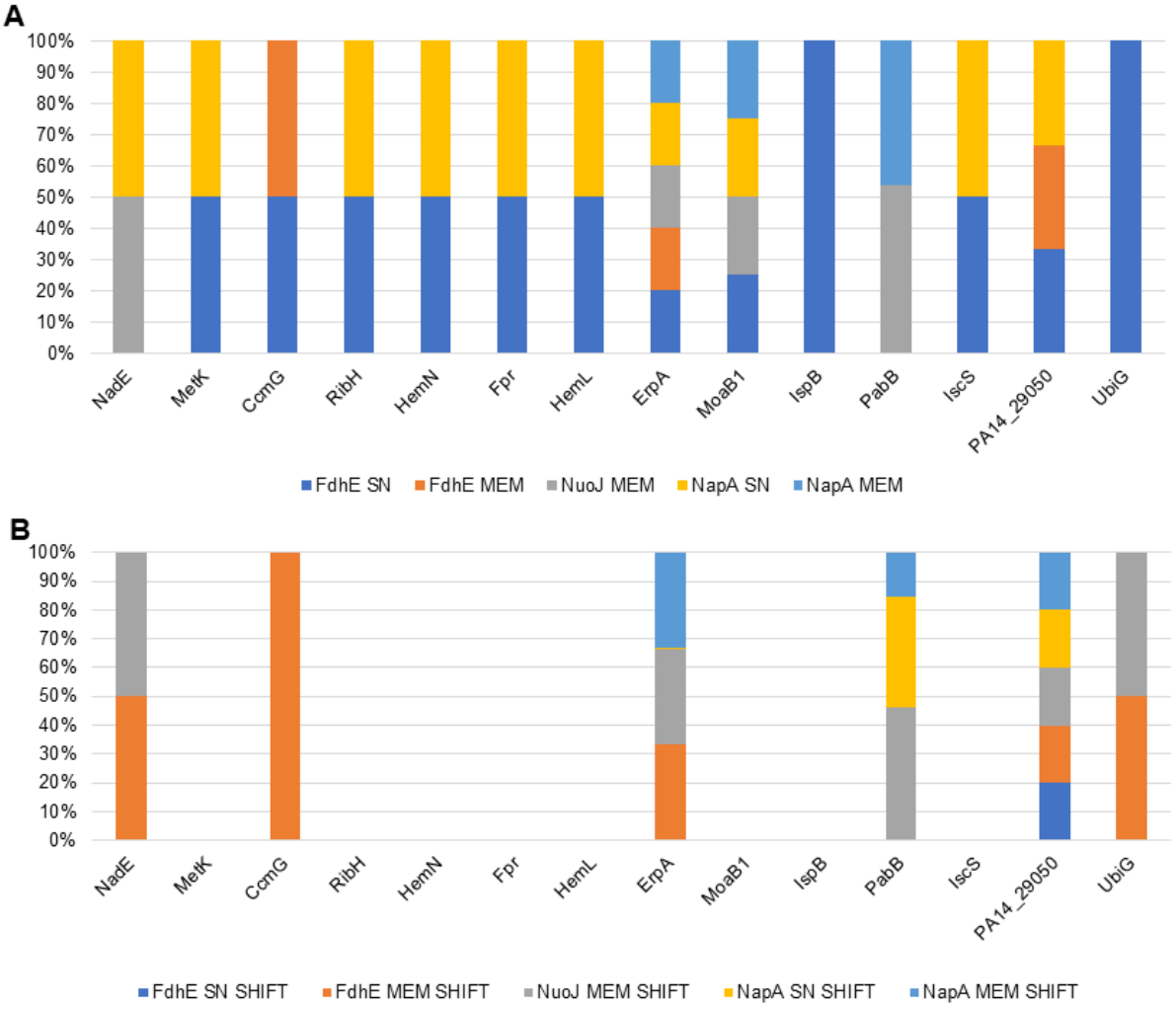

Appendix 5: Identified proteins involved in cofactor formation differentially interacting with the three baits (NuoJ, NapA, FdhE) under aerobic (A) and aerobic to anaerobic shift (B) conditions. A. Identified proteins of cofactor formation interacting under aerobic conditions with FdhE found in the supernatant (soluble) fraction (blue), corresponding interaction partners of FdhE present in the membrane fraction (orange), interacting partners of NuoJ detected in the membrane fraction (grey) under aerobic conditions, interacting partners of NapA found in the soluble supernatant fraction (yellow) and interacting partners of NapA detected in the membrane fraction (light blue). **B.** Identified proteins of cofactor formation interacting under shift conditions with FdhE present in the soluble supernatant fraction (blue), interacting partners of FdhE found in the membrane fraction (orange), interacting partners of NuoJ detected in the membrane fraction (grey) under shift conditions, interacting partners of NapA found in the supernatant (soluble) fraction (yellow) and interacting partners of NapA present in the membrane fraction (light blue).

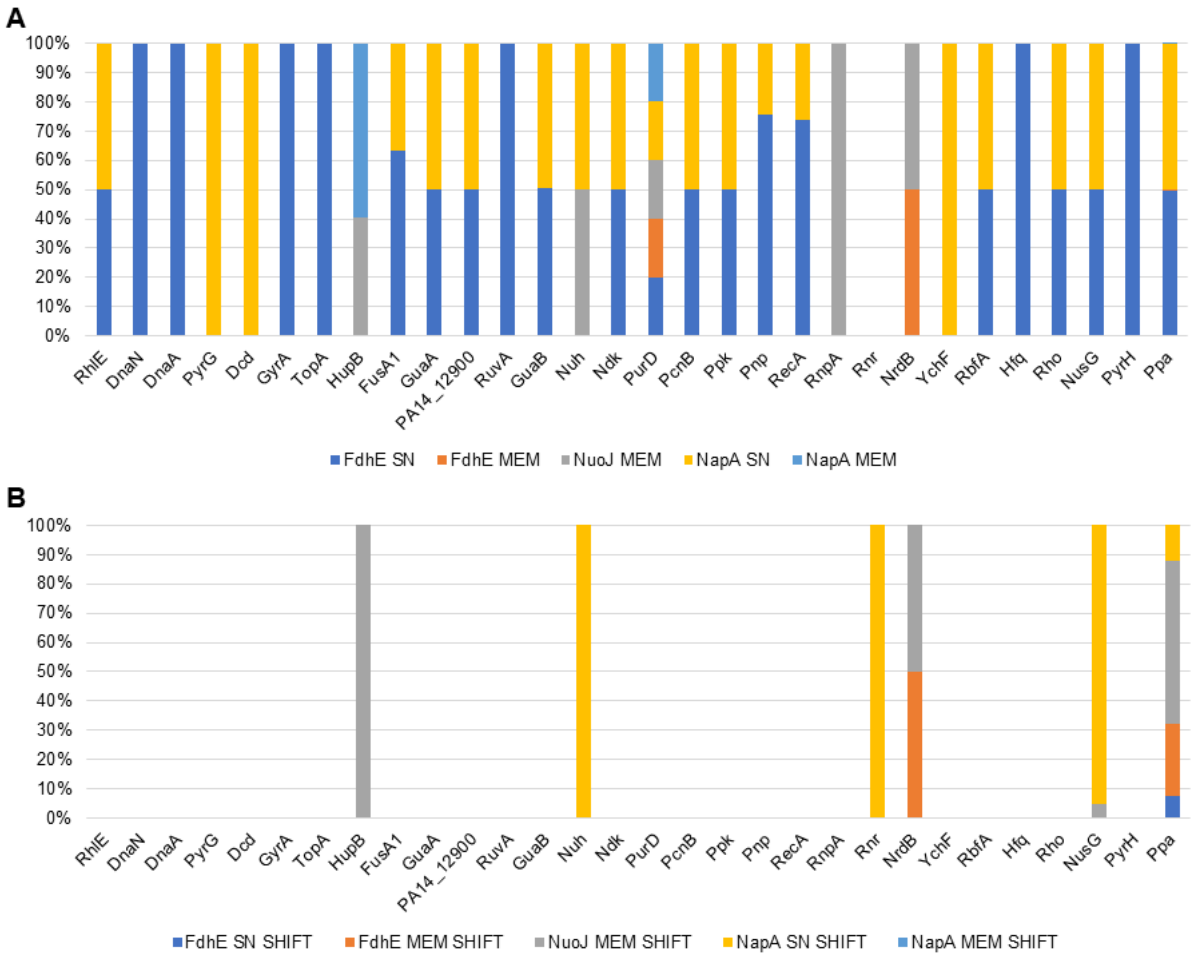

Appendix 6: Identified proteins involved in DNA/RNA metabolism differentially interacting with the three baits (NuoJ, NapA, FdhE) under aerobic (A) and aerobic to anaerobic shift (B) conditions. A. Identified proteins of DNA/RNA metabolism interacting under aerobic conditions with FdhE found in the soluble supernatant fraction (blue), interacting partners of FdhE detected in the membrane fraction (orange), interacting partners of NuoJ present in the membrane fraction (grey) under aerobic conditions, interacting partners of NapA found in the supernatant (soluble) fraction (yellow) and interacting partners of NapA present in the membrane fraction (light blue). **B.** Identified proteins of DNA/RNA metabolism interacting under shift conditions with FdhE detected in the supernatant (soluble) fraction (blue), interacting partners of FdhE present in the membrane fraction (orange), interacting partners of NuoJ found in the membrane membrane fraction (grey) under shift conditions, interacting partners of NapA present in the soluble supernatant fraction (yellow) and interacting partners of NapA detected in the membrane fraction (light blue).

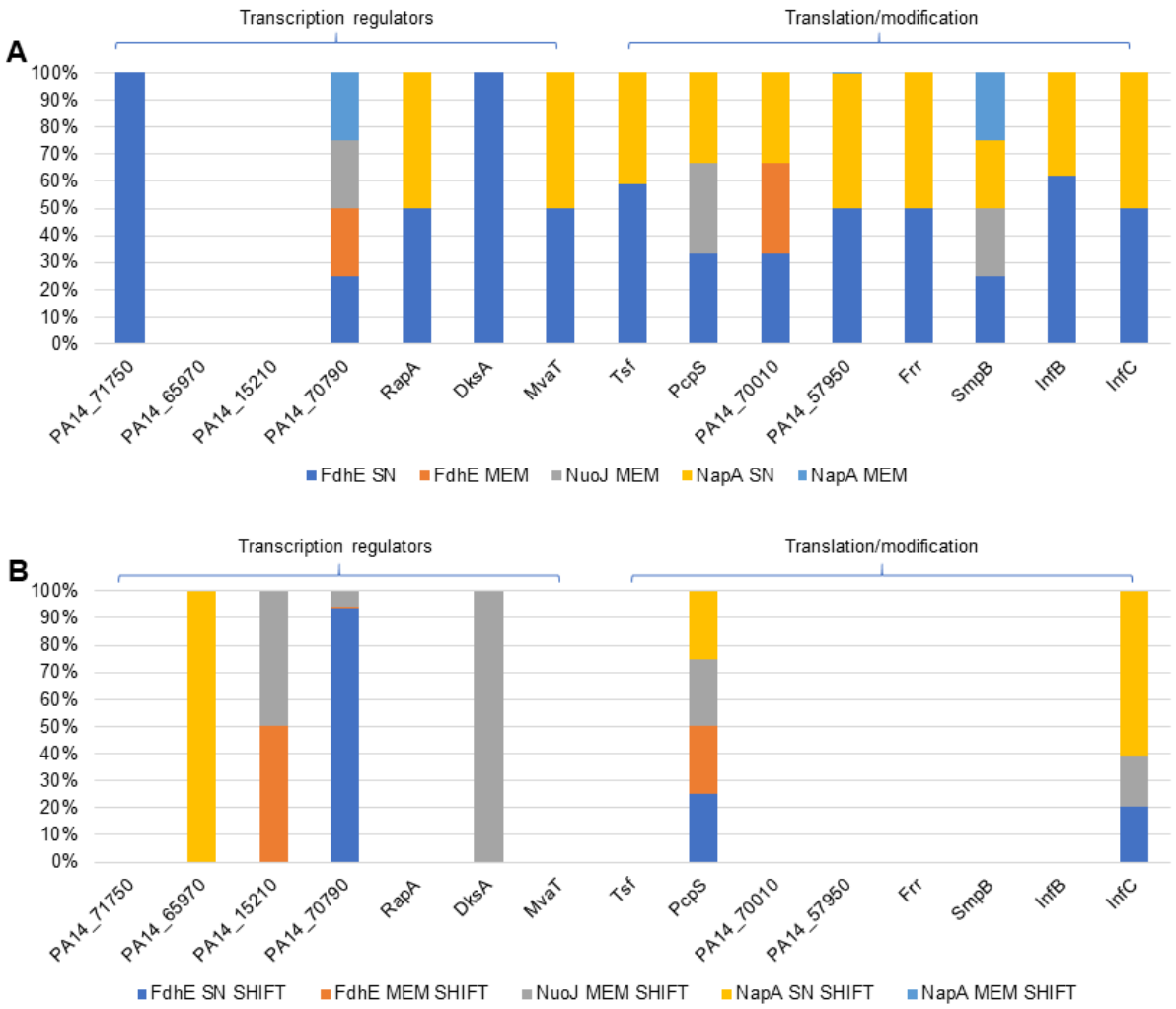

Appendix 7: Identified proteins involved in transcription regulation, translation/modification differentially interacting with the three baits (NuoJ, NapA, FdhE) under aerobic (A) and aerobic to anaerobic shift (B) conditions. A. Identified proteins of transcription regulation and translation/modification interacting under aerobic conditions with FdhE found in the soluble supernatant fraction (blue), interacting partners of FdhE detected in the membrane fraction (orange), interacting partners of NuoJ present in the membrane fraction (grey) under aerobic conditions, interacting partners of NapA found in the supernatant (soluble) fraction (yellow) and interacting partners of NapA present in the membrane fraction (light blue). **B.** Identified proteins of transcription regulation and translation/modification interacting under shift conditions with FdhE found in the soluble supernatant fraction (blue), interacting partners of FdhE detected in the membrane fraction (orange), interacting partners of NuoJ present in the membrane fraction (grey) under shift conditions, interacting partners of NapA found in the soluble supernatant fraction (yellow) and interacting partners of NapA present in membrane fraction (light blue).

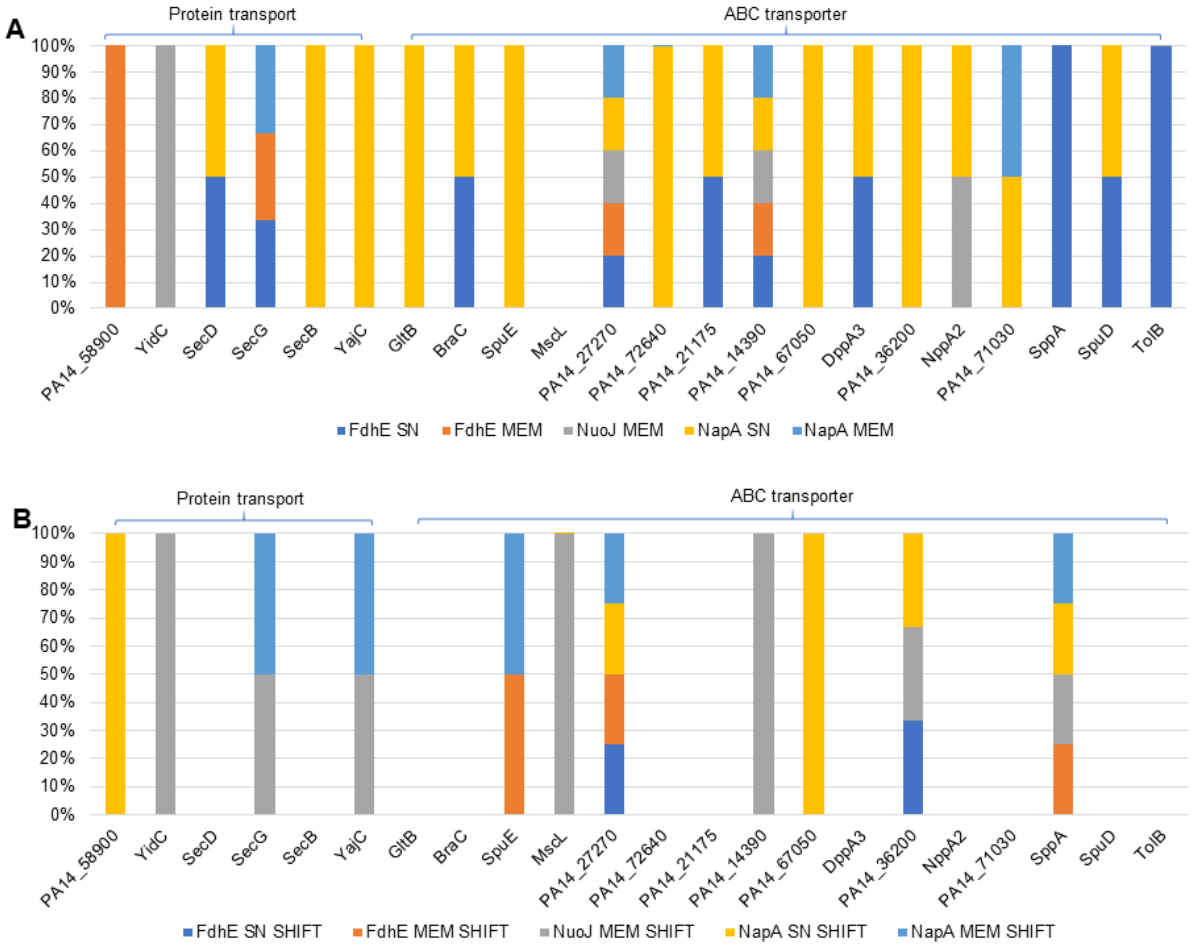

Appendix 8: Identified proteins involved in protein transport und ABC transporter differentially interacting with the three baits (NuoJ, NapA, FdhE) under aerobic (A) and aerobic to anaerobic shift (B) conditions. A. Identified proteins of protein transport and ABC transporter interacting under aerobic conditions with FdhE present in the supernatant (soluble) fraction (blue), interacting partners of FdhE found in the membrane fraction (orange), interacting partners of NuoJ detected in the membrane fraction (grey) under aerobic conditions, interacting partners of NapA found in the soluble supernatant fraction (yellow) and interacting partners of NapA present in the membrane fraction (light blue). **B.** Identified proteins of protein transport and ABC transporter interacting under shift conditions with FdhE detected in the soluble supernatant fraction (blue), interacting partners of FdhE found in the membrane fraction (orange), interacting partners of NuoJ present in the membrane fraction (grey) under shift conditions, interacting partners of NapA found in the supernatant (soluble) fraction (yellow) and interacting partners of NapA present in the membrane fraction (light blue).

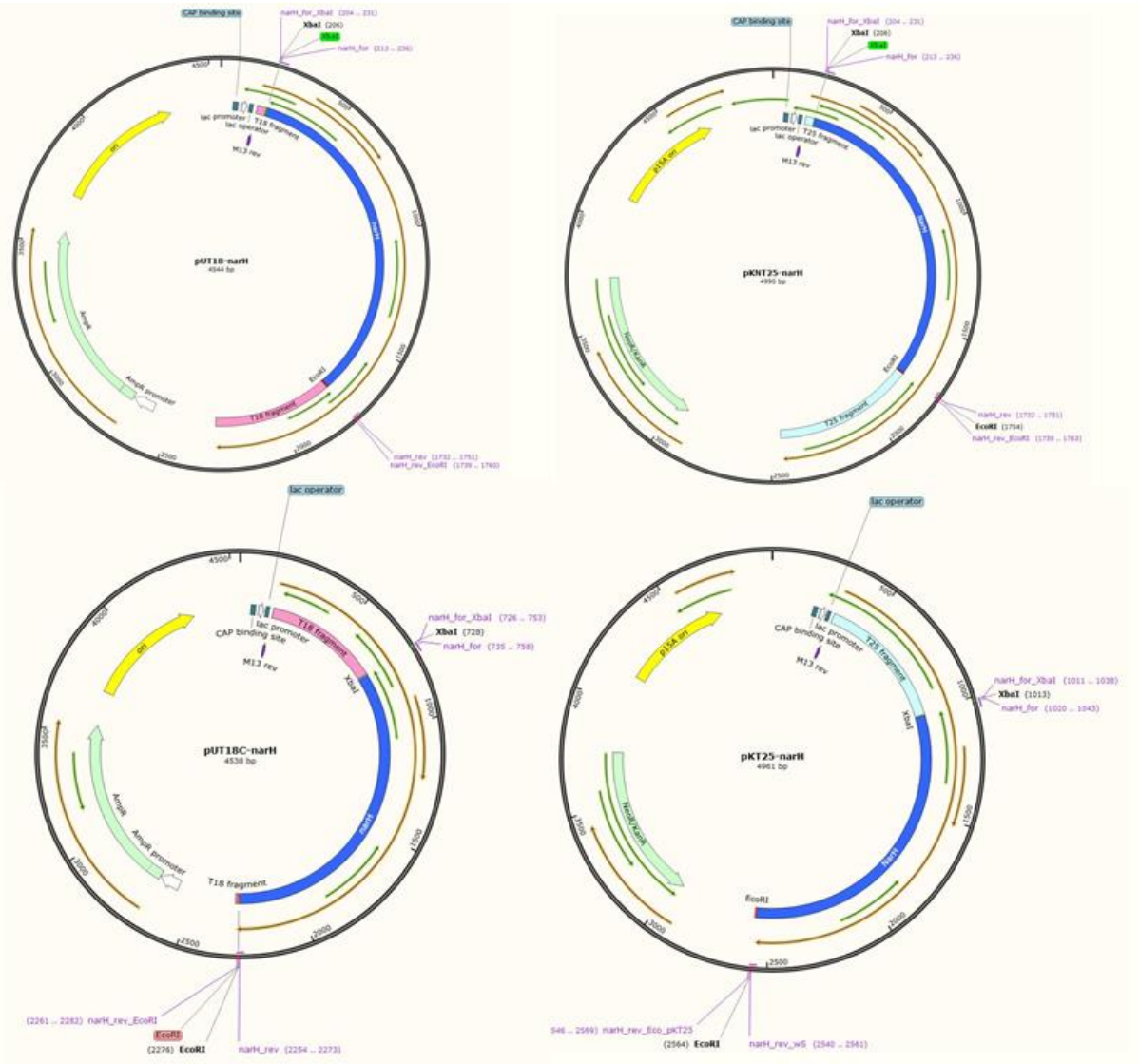

Appendix 9: Plasmid map of BACTH System - Cloning of *narH*

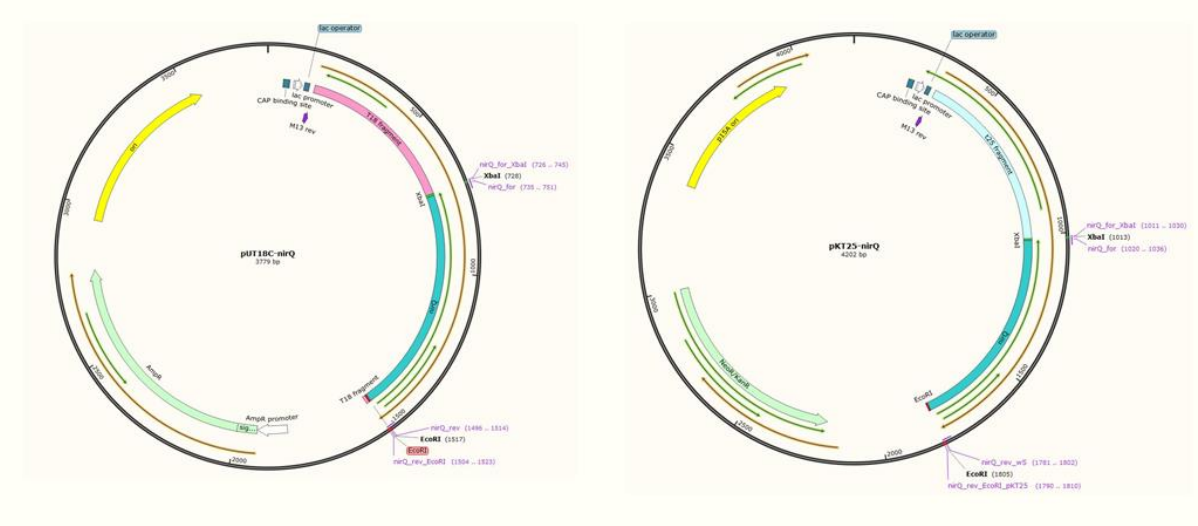

Appendix 10: Plasmid map of BACTH System - Cloning of *nirQ*

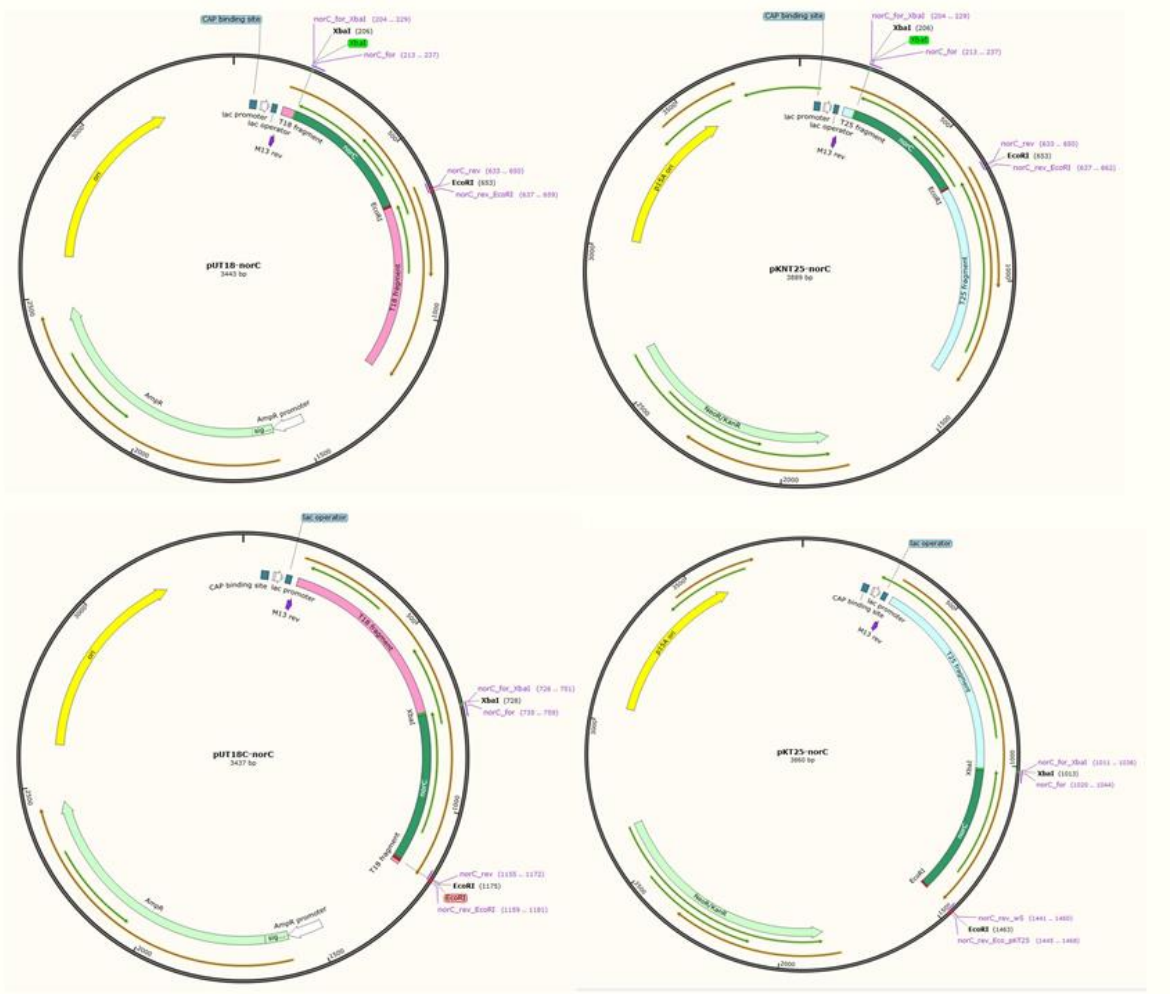

Appendix 11: Plasmid map of BATCH System - Cloning of *norC*

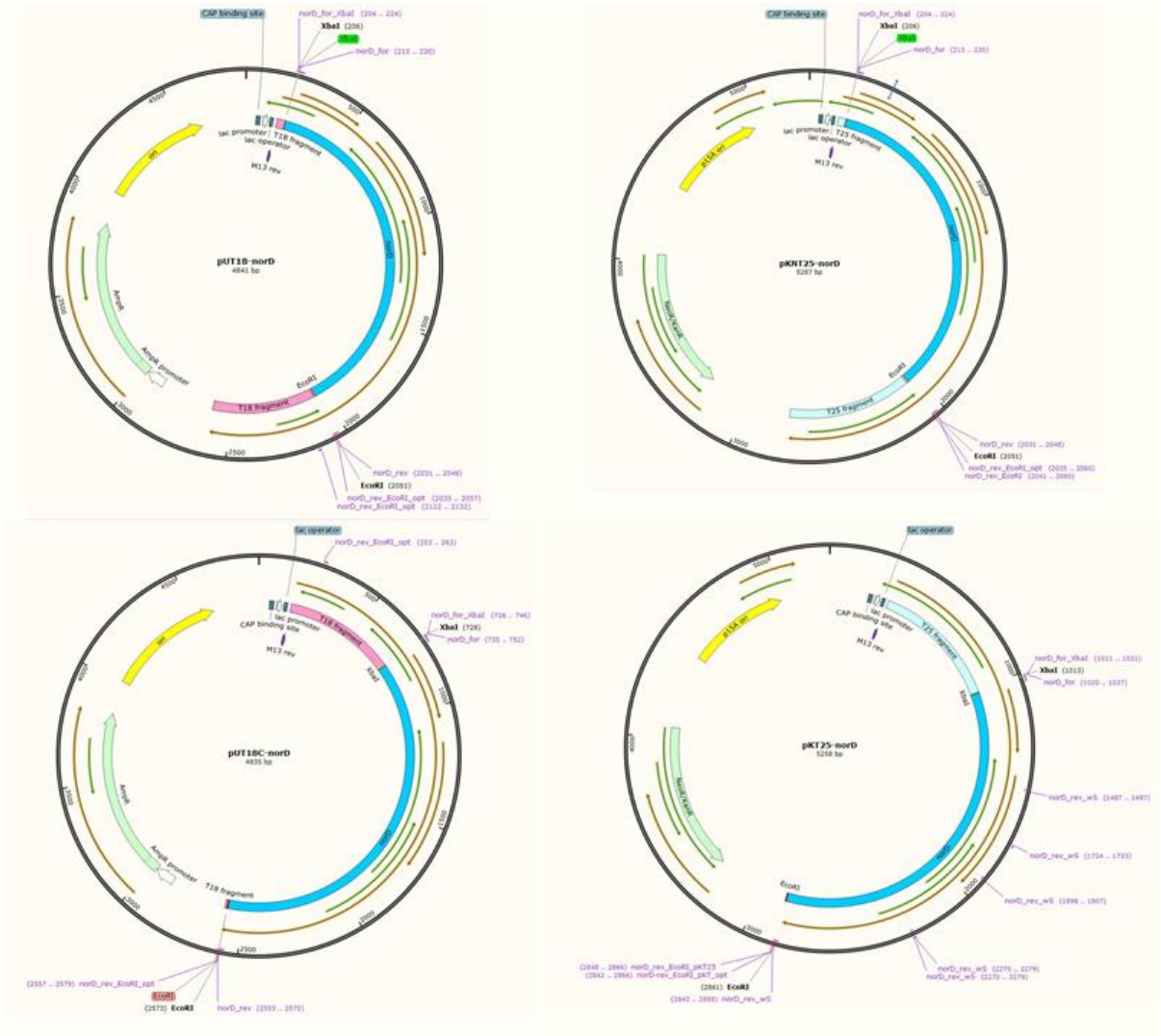

Appendix 12: Plasmid map of BACTH System - Cloning of *norD*

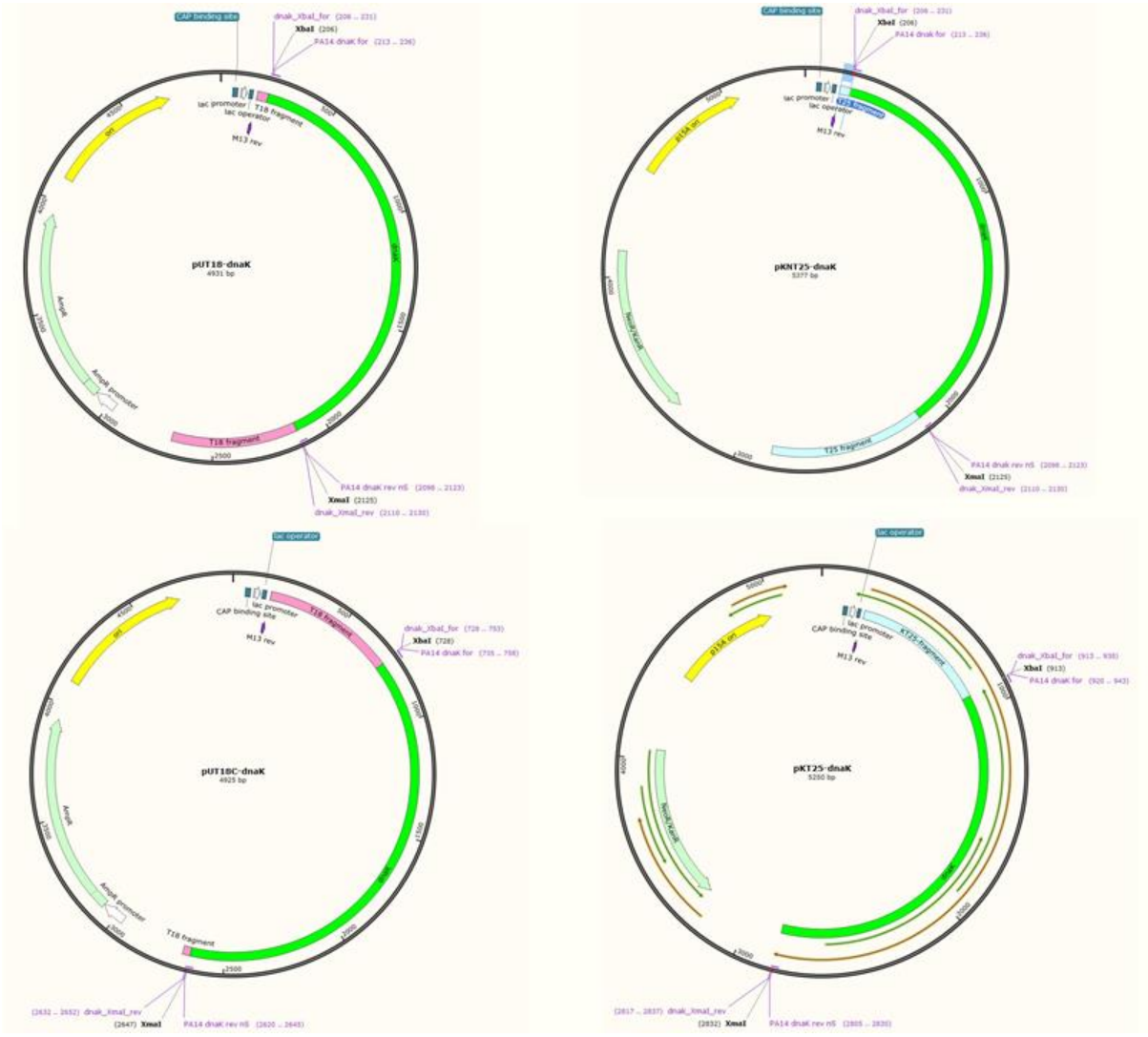

Appendix 13: Plasmid maps of BATCH System - Cloning of *dnaK*

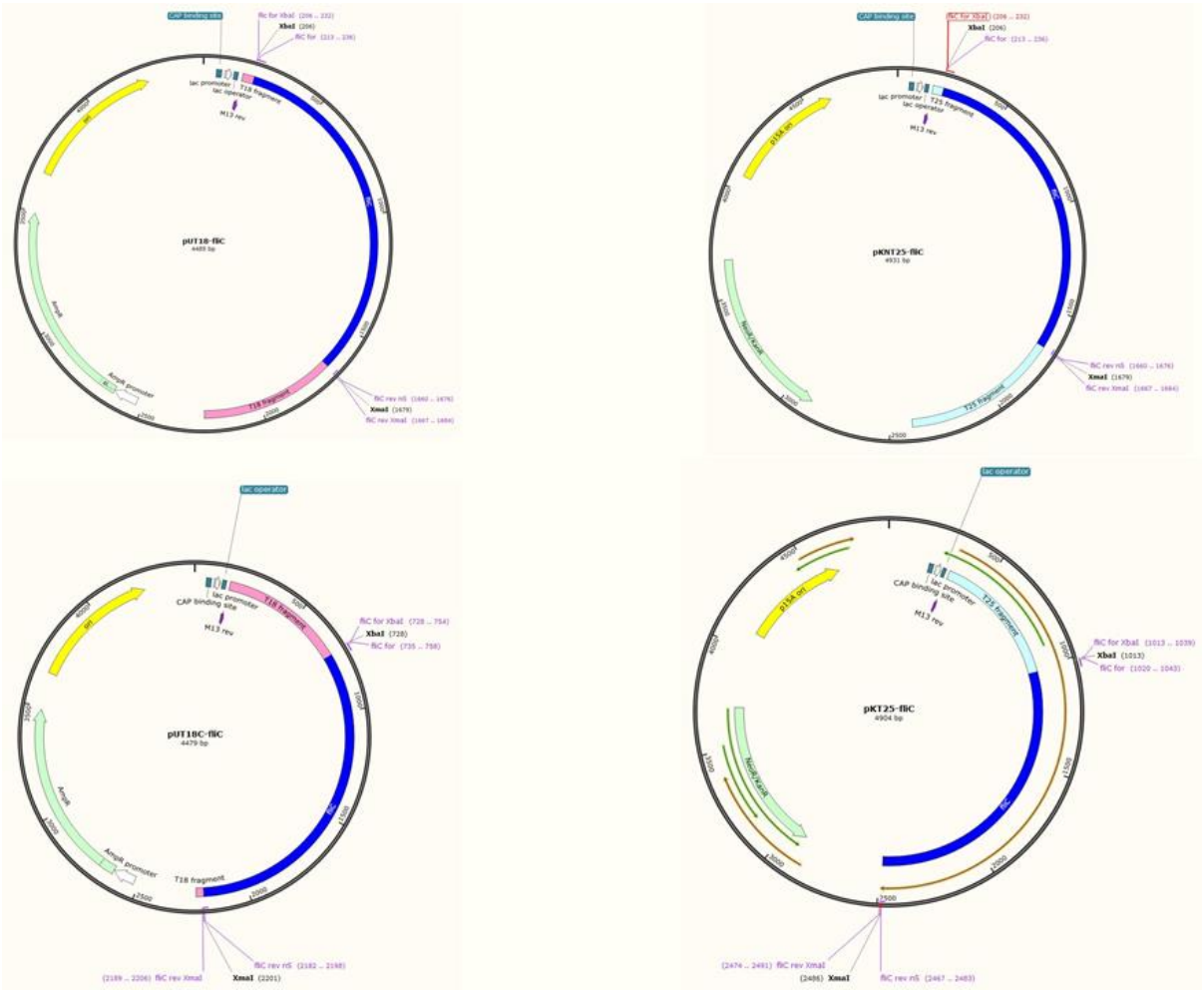

Appendix 14: Plasmid maps of BACTH System - Cloning of *fliC*

pKT25-*zip*/pUT18C-*zip*

Nr	OD_{600}	OD_{420}	OD_{550}	t [sec]	MU
1	0,17	0,181	0,004	105	5848,7395
2	0,179	0,151	0,004	105	4596,96728
3	0,203	0,198	0,006	105	5277,97326
4	0,169	0,183	0,003	105	6010,1437
5	0,187	0,133	0,002	105	3957,21925
6	0,192	0,245	0	105	7291,66667
7	0,223	0,243	0,003	105	6092,24856
8	0,072	0,129	0,001	105	10099,2063

pKT25/pUT18C

Nr	OD_{600}	OD_{420}	OD_{550}	t [sec]	MU
1	0,28	0,174	0,002	600	608,928571
2	0,25	0,157	0,003	600	607
3	0,23	0,048	0,001	600	201,086957
4	0,29	0,235	0,031	600	623,275862
5	0,26	0,131	0,003	600	483,653846
6	0,23	0,161	0,029	600	479,347826

pKNT25-*fliC*/pUT18-*dnaK*

Nr	OD_{600}	OD_{420}	OD_{550}	t [sec]	MU
1	0,128	0,284	0,001	190	6963,40461
2	0,224	0,169	0,006	190	2234,49248
3	0,198	0,065	0	190	1036,68262
4	0,147	0,096	0,001	190	2024,70462
5	0,152	0,111	0,008	190	2015,23546
6	0,124	0,238	0	190	6061,12054
7	0,21	0,082	0,002	190	1180,45113
8	0,122	0,286	0	190	7402,93356

pKNT25-*fliC*/pUT18C-*narH*

Nr	OD_{600}	OD_{420}	OD_{550}	t [sec]	MU
1	0,038	0,055	0,006	450	1561,40351
2	0,07	0,091	0	450	1733,33333
3	0,067	0,056	0,001	450	1079,60199
4	0,081	0,074	0,004	450	1102,88066
5	0,01	0,01	0,003	450	633,333333
6	0,068	0,062	0,007	450	975,490196
7	0,074	0,05	0,008	450	648,648649
8	0,085	0,053	0,004	450	721,568627

pUT18C-*fliC*/pKNT25-*narI*

Nr	OD_{600}	OD_{420}	OD_{550}	t [sec]	MU
1	0,034	0,006	0,003	120	110,294118
2	0,218	0,271	0,012	120	5733,94495
3	0,179	0,204	0	120	5698,32402
4	0,163	0,339	0,054	120	7500
5	0,038	0,065	0,012	120	5789,47368
6	0,095	0,154	0,012	120	7000
7	0,101	0,135	0,015	120	5383,66337
8	0,287	0,385	0,002	120	6646,34146

pKT25-*fliC*/pUT18-*norD*

Nr	OD_{600}	OD_{420}	OD_{550}	t [sec]	MU
1	0,14	0,192	0,021	120	5544,64286
2	0,159	0,288	0,019	120	8011,00629
3	0,193	0,269	0,018	120	6152,84974
4	0,305	0,211	0,015	120	3028,68852
5	0,168	0,304	0,016	120	8214,28571
6	0,134	0,232	0,002	120	8526,1194
7	0,22	0,201	0,009	120	4210,22727
8	0,168	0,307	0,024	120	7886,90476

pKT25-*narH*/pUT18C-*norD*

Nr	OD_{600}	OD_{420}	OD_{550}	t [sec]	MU
1	0,096	0,153	0	150	1006,375
2	0,094	0,147	0	150	1006,25532
3	0,071	0,147	0,005	150	1007,78873
4	0,092	0,158	0,001	150	1006,79348
5	0,075	0,155	0,006	150	1007,70667
6	0,068	0,146	0,001	150	1008,48529
7	0,119	0,297	0	150	1009,98319
8	0,081	0,23	0,001	150	1011,2716

pKNT25-*narI*/pUT18-*dnaK*

Nr	OD_{600}	OD_{420}	OD_{550}	t [sec]	MU
1	0,223	0,044	0,001	210	541,319667
2	0,206	0,161	0,004	210	2135,92233
3	0,255	0,161	0	210	1803,92157
4	0,195	0,144	0,002	210	2058,60806
5	0,202	0,128	0	210	1810,46676
6	0,197	0,197	0,003	210	2781,00073
7	0,183	0,134	0,002	210	2037,47073
8	0,294	0,218	0,002	210	2084,5481

pKNT25-*narI*/pUT18C-*narH*

Nr	OD_{600}	OD_{420}	OD_{550}	t [sec]	MU
1	0,385	0,148	0,001	142	1605,08506
2	0,358	0,097	0	142	1144,85797
3	0,344	0,183	0,003	142	2183,30331
4	0,268	0,168	0,007	142	2455,59176
5	0,277	0,11	0,002	142	1624,54874
6	0,354	0,14	0,002	142	1629,26713
7	0,329	0,146	0,006	142	1740,22861
8	0,387	0,327	0,011	142	3360,08298

pKNT25-*narI*/pUT18C-*norC*

Nr	OD_{600}	OD_{420}	OD_{550}	t [sec]	MU
1	0,389	0,17	0,009	135	1762,35361
2	0,39	0,162	0,008	135	1686,60969
3	0,329	0,088	0,001	135	1165,14691
4	0,225	0,087	0,009	135	1407,40741
5	0,065	0,014	0,008	135	0
6	0,314	0,114	0,011	135	1341,11819
7	0,317	0,115	0,01	135	1366,98212
8	0,403	0,304	0,004	135	3275,43424

pKT25-*narI*/pUT18C-*norD*

Nr	OD_{600}	OD_{420}	OD_{550}	t [sec]	MU
1	0,1	0,195	0,001	130	8919,23077
2	0,121	0,175	0,003	130	6474,88875
3	0,18	0,328	0,009	130	8006,41026
4	0,116	0,195	0,002	130	7619,3634
5	0,101	0,264	0,008	130	11424,2193
6	0,084	0,175	0	130	9615,38462
7	0,109	0,143	0,001	130	5980,94566
8	0,114	0,295	0,011	130	11163,9676

pUT18C-*nirQ*/pKT25-*narI*

Nr	OD_{600}	OD_{420}	OD_{550}	t [sec]	MU
1	0,268	0,182	0,001	115	3509,08501
2	0,261	0,164	0,001	115	3243,37831
3	0,13	0,124	0,005	115	4625,41806
4	0,25	0,148	0	115	3088,69565
5	0,268	0,238	0,001	115	4599,28618
6	0,275	0,188	0,003	115	3467,19368
7	0,282	0,166	0	115	3071,23034
8	0,246	0,44	0,12	115	4878,04878

pKT25-*nirQ*/pUT18C-*norD*

Nr	OD_{600}	OD_{420}	OD_{550}	t [sec]	MU
1	0,155	0,218	0	90	9376,34409
2	0,246	0,052	0,001	90	1361,78862
3	0,284	0,056	0,002	90	1232,39437
4	0,133	0,178	0,002	90	8746,86717
5	0,249	0,147	0,006	90	3654,61847
6	0,132	0,12	0	90	6060,60606
7	0,237	0,037	0,003	90	893,108298
8	0,181	0,179	0,001	90	6528,54512

pUT18-*norD*/pKNT25-*dnaK*

Nr	OD_{600}	OD_{420}	OD_{550}	t [sec]	MU
1	0,127	0,122	0,007	145	3575,88922
2	0,126	0,084	0,001	145	2701,14943
3	0,13	0,09	0,005	145	2586,2069
4	0,061	0,032	0,001	145	2052,00678
5	0,166	0,117	0,005	145	2698,37973
6	0,161	0,219	0,001	145	5583,63675
7	0,195	0,132	0,005	145	2615,38462
8	0,147	0,161	0,001	145	4482,75862

pUT18C-*norD*/pKNT25-*norC*

Nr	OD_{600}	OD_{420}	OD_{550}	t [sec]	MU
1	0,176	0,285	0,001	60	16093,75
2	0,315	0,127	0	60	4031,74603
3	0,266	0,126	0,001	60	4671,05263
4	0,301	0,112	0,001	60	3662,7907
5	0,256	0,12	0,001	60	4619,14063
6	0,281	0,149	0,001	60	5240,21352
7	0,168	0,139	0,007	60	7544,64286
8	0,252	0,16	0,001	60	6279,7619

pKT25-*fliC*/pUT18C-*nirQ*

Nr	OD_{600}	OD_{420}	OD_{550}	t [sec]	MU
1	0,109	0,067	0	315	1170,81695
2	0,244	0,115	0	315	897,736144
3	0,101	0,032	0,002	315	537,48232
4	0,145	0,077	0,001	315	988,505747
5	0,01	0,016	0,004	315	1714,28571
6	0,002	0,01	0,002	315	6190,47619
7	0,105	0,037	0,008	315	417,23356
8	0,003	0,003	0,003	315	-1428,57143

Appendix 15: Tables with measured Miller Units of the β-galactosidase assay of the respective PPI used in the BACTH assay.

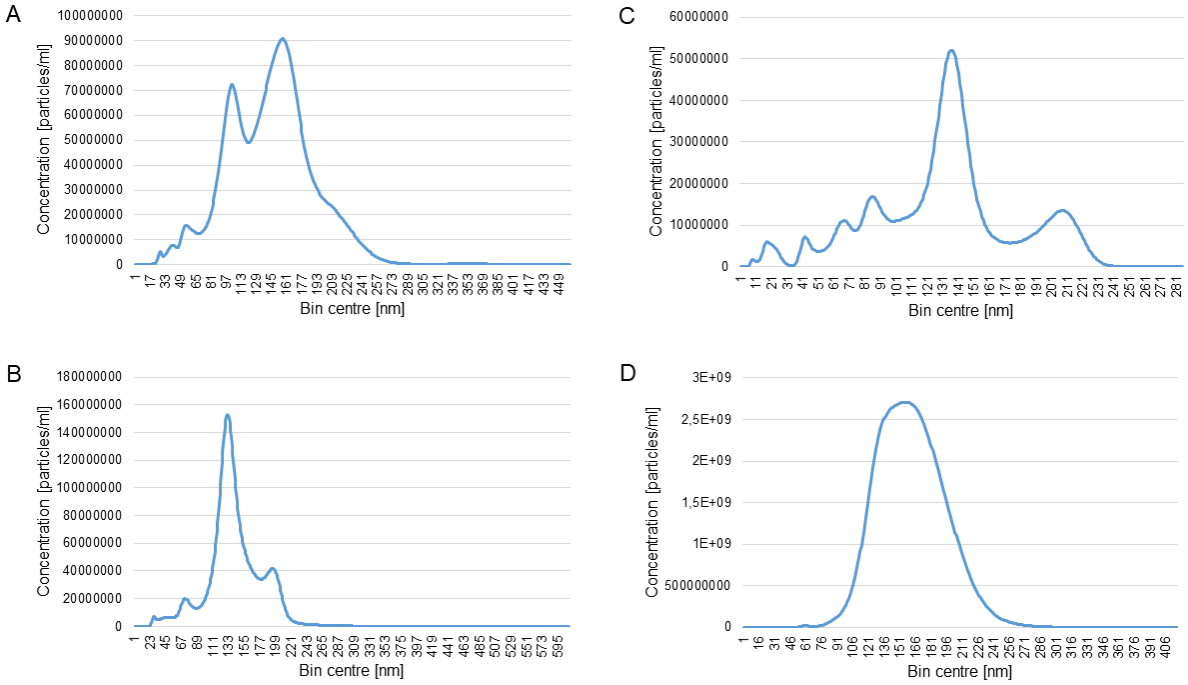

Appendix 16: Measurement of the vesicle diameter *via* Nanosight. A. Measurement of the vesicle diameter of the Δ*lemA1* strain with an average size of 110-160 nm ; **B.** Measurement of the vesicle diameter of the strain Δ*lemA1* + pSEVA634-*lemA1* with an average size of 140 nm, **C.** Measurement of the vesicle diameter of the Δ*lemA2* strain with an average size of 130 nm; **D.** Measurement of the vesicle diameter of the strain Δ*lemA2* + pSEVA634-*lemA2* with an average size of 160 nm.

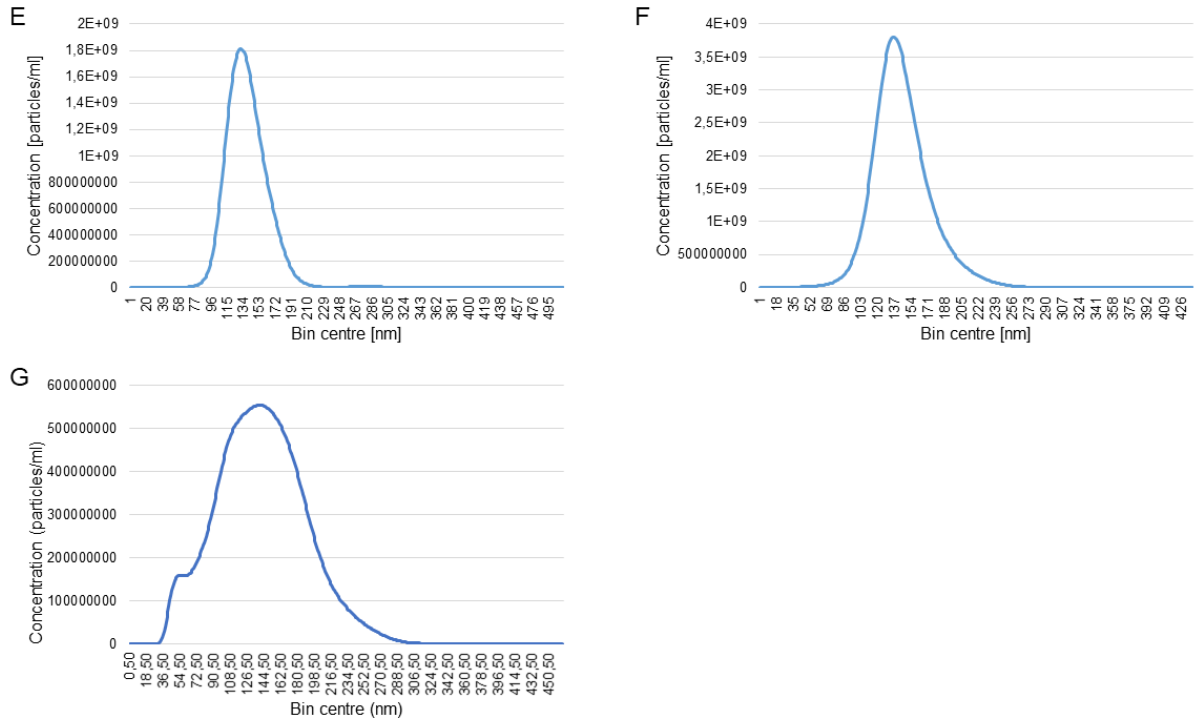

Appendix 17: Measurement of the vesicle diameter *via* Nanosight. E. Measurement oft he vesicle diameter of the Δ*lemA1*Δ*lemA2* strain with an average size of 140 nm; **F.** Measurement of the vesicle diameter of the Δ*lemA1*Δ*lemA2* + pSEVA634-*lemA1-lemA2* with an average size of 150 nm; **G.** Measurement of the vesicle diameter of the PA14 wildtype strain with an average size of 110-160 nm.

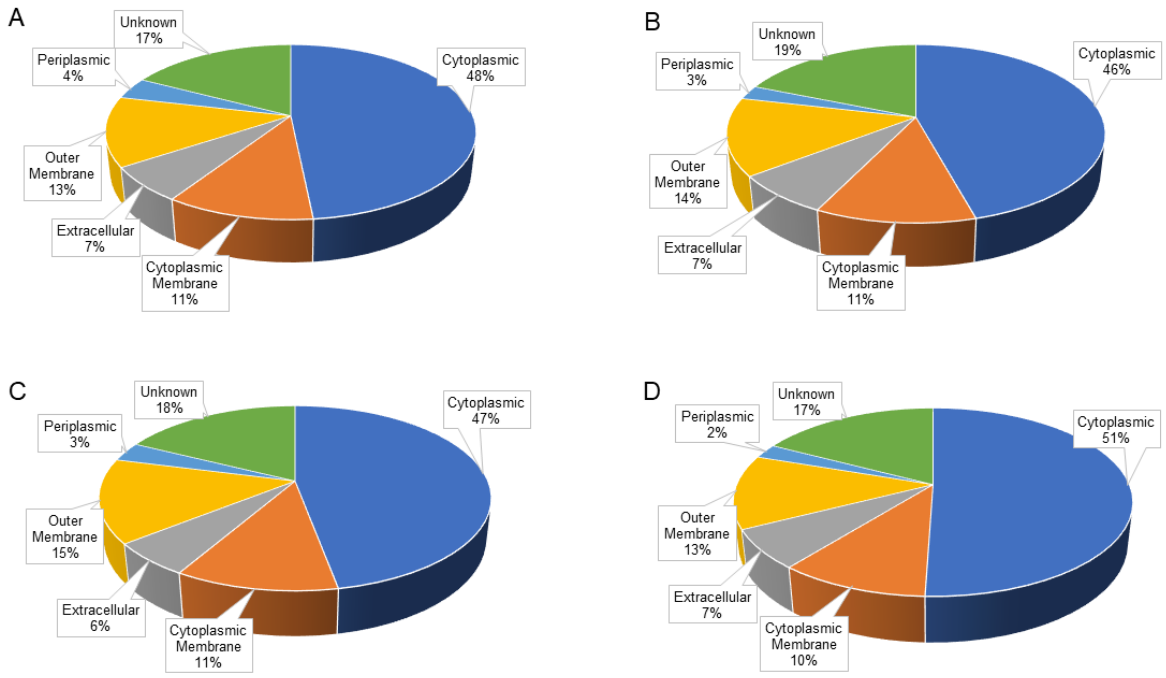

Appendix 18: Cellular localization of proteins detected in vesicles of the different *lemA* deletion and overexpressing strains. A. Δ*lemA1*; **B.** Δ*lemA2*; **C.** Δ*lemA1* + pSEVA634-*lemA1*; **D.** Δ*lemA2* + pSEVA634-*lemA2*

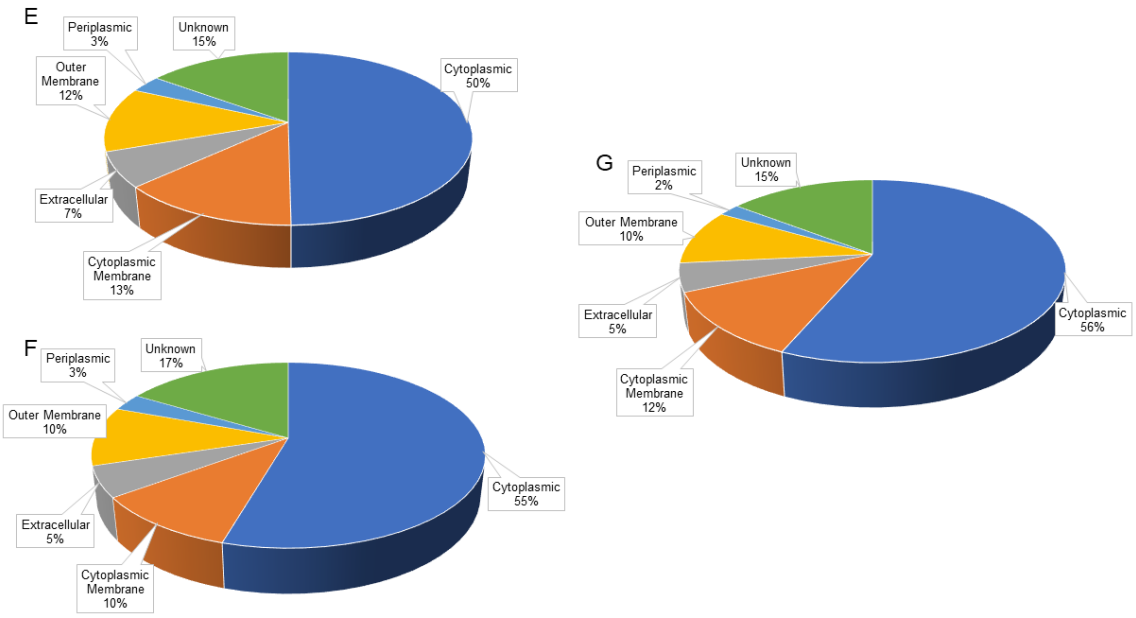

Appendix 19: Cellular localization of proteins detected in vesicles of the different *lemA* deletion and overexpressing strains and the PA14 wildtype strain. E. Δ*lemA1*Δ*lemA2*; **F.** Δ*lemA1*Δ*lemA2* + pSEVA634-*lemA1-lemA2*; **G.** PA14 wildtype

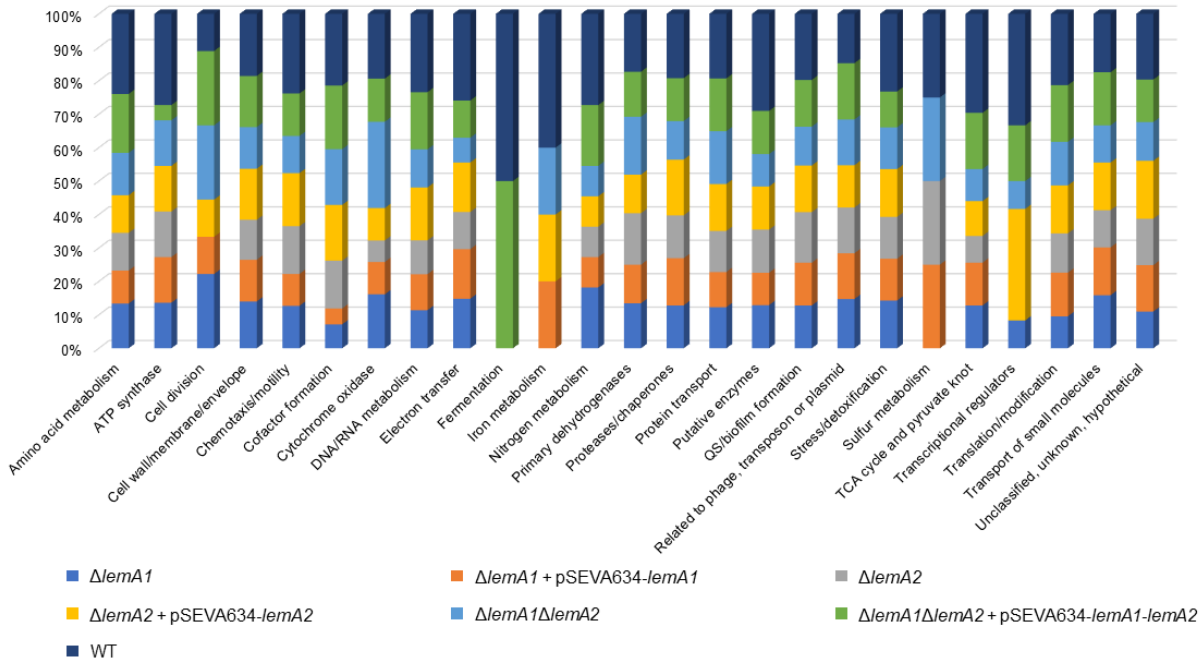

Appendix 20: Functional classification of detected proteins in vesicles of *lemA* deletion and overexpressing strains and the PA14 wildtype strain. The classification of proteins present in vesicles of the PA14 wildtype (dark blue), Δ*lemA1* (blue), Δ*lemA1* + pSEVA634-*lemA1* (orange), Δ*lemA2* (grey), Δ*lemA2* + pSEVA634-*lemA2* (yellow), Δ*lemA1*Δ*lemA2* (light blue) and Δ*lemA1*Δ*lemA2* + pSEVA634-*lemA1-lemA2* (green) strains.

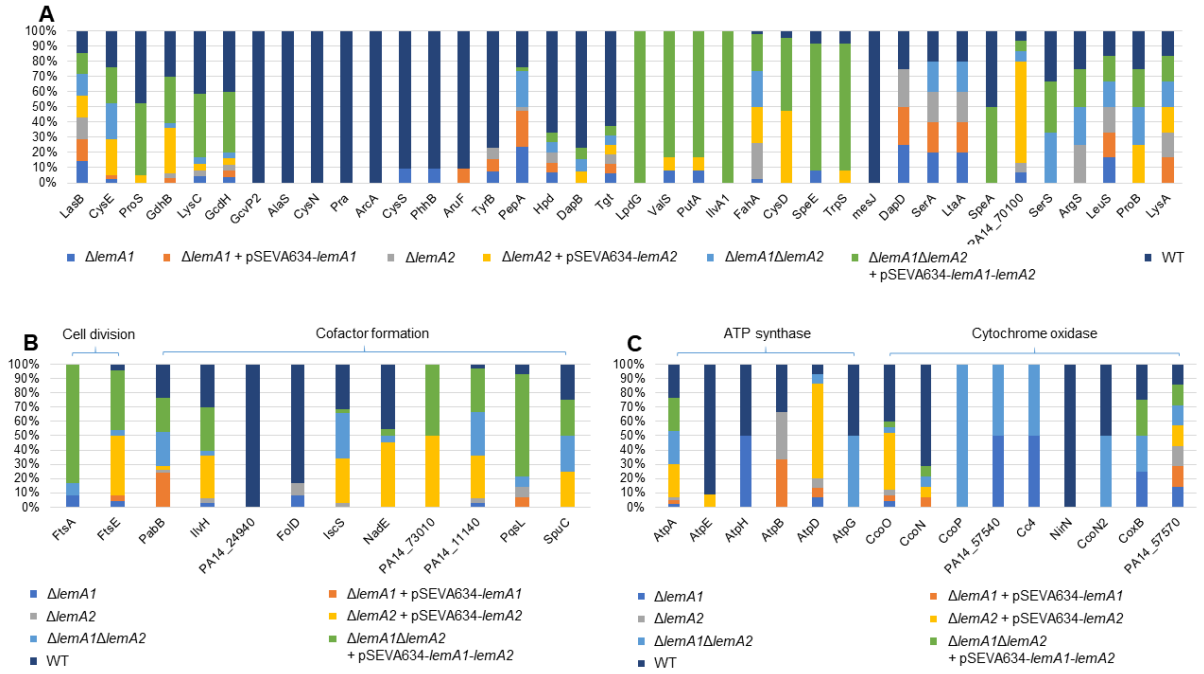

Appendix 21: Changes of the abundance of proteins of amino acid metabolism (A), cell division and cofactor formation (B) and ATP synthase and cytochrome oxidase (C) in dependence of the deletion or overexpression of *lemA* genes compared to the wildtype strain. Abundance of **A.** Amino acid metabolism, **B.** Cell division and cofactor formation, **C.** ATP synthase and cytochrome oxidase in the wildtype (dark blue), Δ*lemA1* (blue), Δ*lemA1* + pSEVA634-*lemA1* (orange), Δ*lemA2* (grey), Δ*lemA2* + pSEVA634-*lemA2* (yellow), Δ*lemA1*Δ*lemA2* (light blue) and Δ*lemA1*Δ*lemA2* + pSEVA634-*lemA1-lemA2* (green) strains.

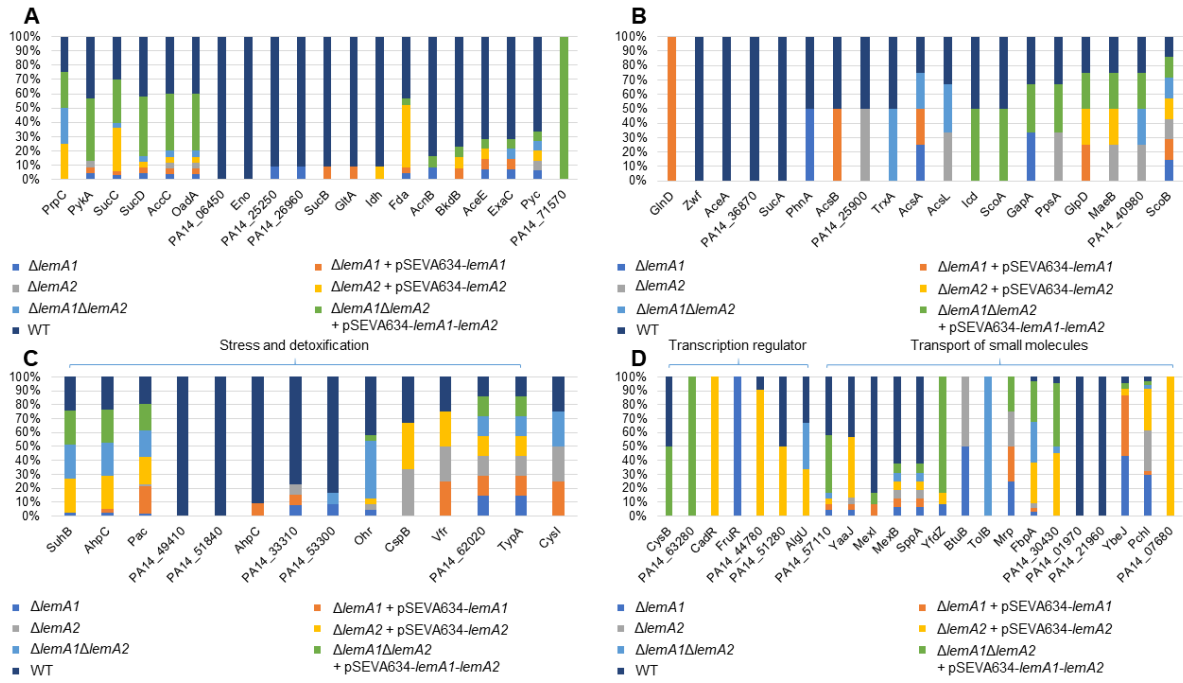

Appendix 22: Changes of the abundance of proteins of the TCA cycle and pyruvate metabolism (A-B), stress/detoxification and sulfur metabolism and transcription regulators and transport of small molecules (D) in dependence of the deletion or overexpression of *lemA* genes compared to the wildtype strain. Abundance of **A-B.** TCA cycle and pyruvate metabolism, **C.** Stress/detoxification and sulfur metabolism, **D.** Transcription regulator and transport of small molecules in the wildtype (dark blue), Δ*lemA1* (blue), Δ*lemA1* + pSEVA634-*lemA1* (orange), Δ*lemA2* (grey), Δ*lemA2* + pSEVA634-*lemA2* (yellow), Δ*lemA1*Δ*lemA2* (light blue) and Δ*lemA1*Δ*lemA2* + pSEVA634-*lemA1-lemA2* (green).

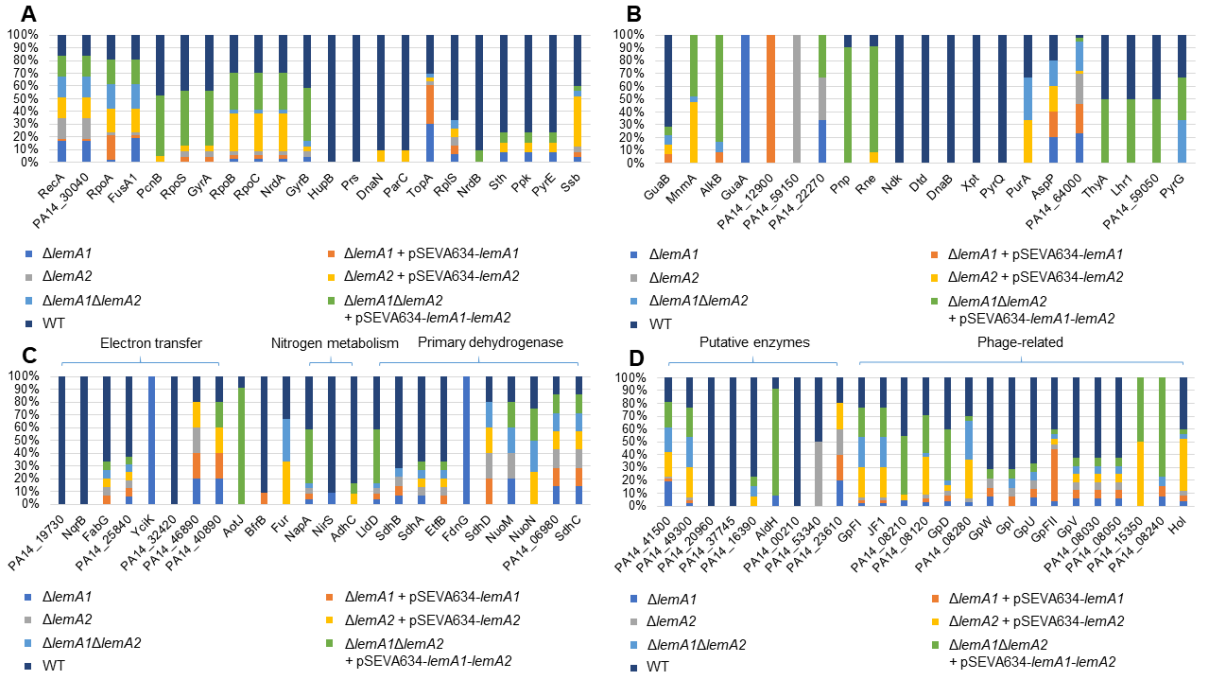

Appendix 23: Changes of the abundance of proteins of the DNA/RNA metabolism (A-B), energy metabolism (C) and putative enzymes and phage-related proteins (D) in dependence of the deletion or overexpression of *lemA* genes compared to the wildtype strain. Abundance of **A-B.** DNA/RNA metabolism, **C.** Energy metabolism, includes electron transfer, fermentation, iron metabolism, nitrogen metabolism and primary dehydrogenases, **D.** Putative enzymes and phage-related proteins in the wildtype (dark blue), Δ*lemA1* (blue), Δ*lemA1* + pSEVA634-*lemA1* (orange), Δ*lemA2* (grey), Δ*lemA2* + pSEVA634-*lemA2* (yellow), Δ*lemA1*Δ*lemA2* (light blue) and Δ*lemA1*Δ*lemA2* + pSEVA634-*lemA1-lemA2* (green) strains.

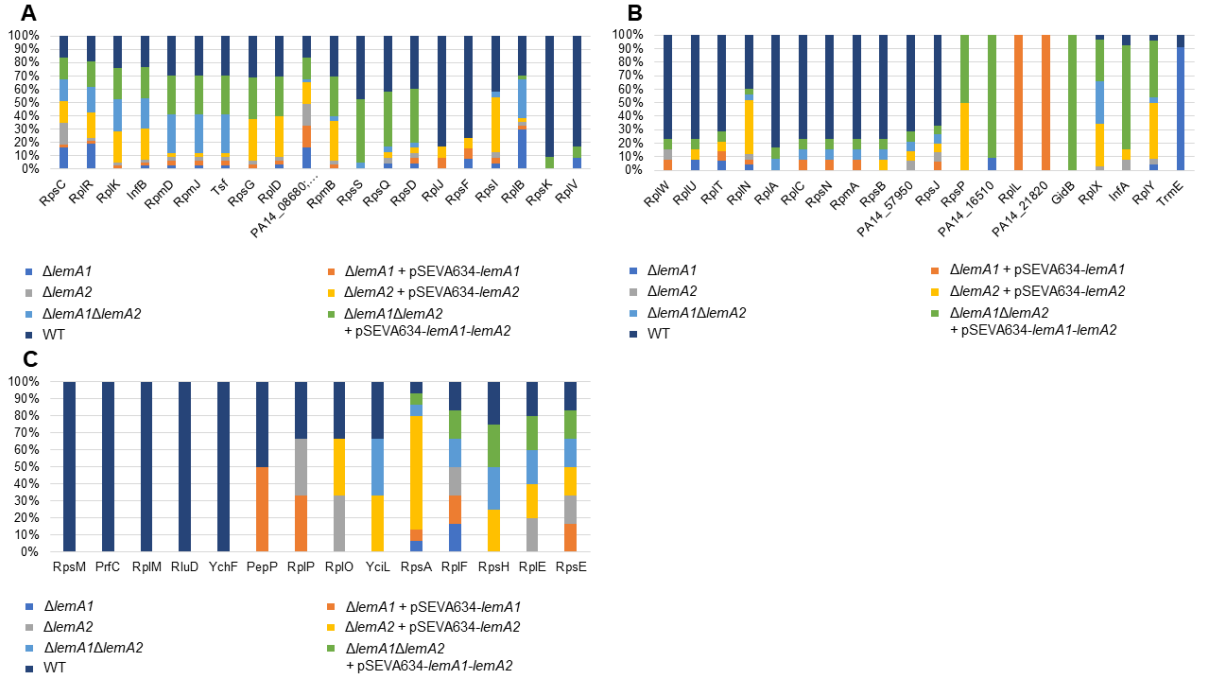

Appendix 24: Changes of the abundance of proteins of the translation and modification in dependence of the deletion or overexpression of *lemA* genes compared to the wildtype strain. Abundance of **A-C.** Translation and modification in the wildtype (dark blue), Δ*lemA1* (blue), Δ*lemA1* + pSEVA634-*lemA1* (orange), Δ*lemA2* (grey), Δ*lemA2* + pSEVA634-*lemA2* (yellow), Δ*lemA1*Δ*lemA2* (light blue) and Δ*lemA1*Δ*lemA2* + pSEVA634-*lemA1-lemA2* (green).

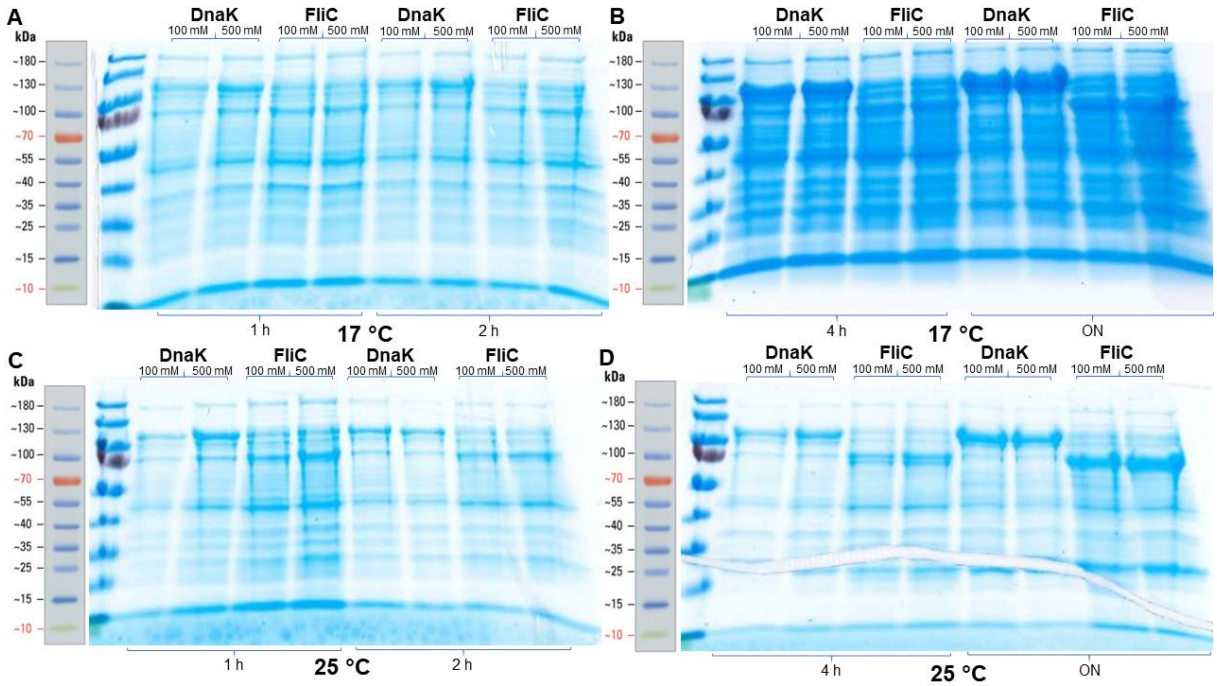

Appendix 25: Pre-testing of the optimal protein production conditions of DnaK and FliC. The protein production of DnaK and FliC were tested under different temperatures and IPTG concentrations (100 mM and 500 mM), samples were taken after one, two and four hours and after over night cultivation. **A-B.** Protein test production of DnaK and FliC at 17 °C **C-D.** Protein test production of DnaK and FliC at 25 °C.

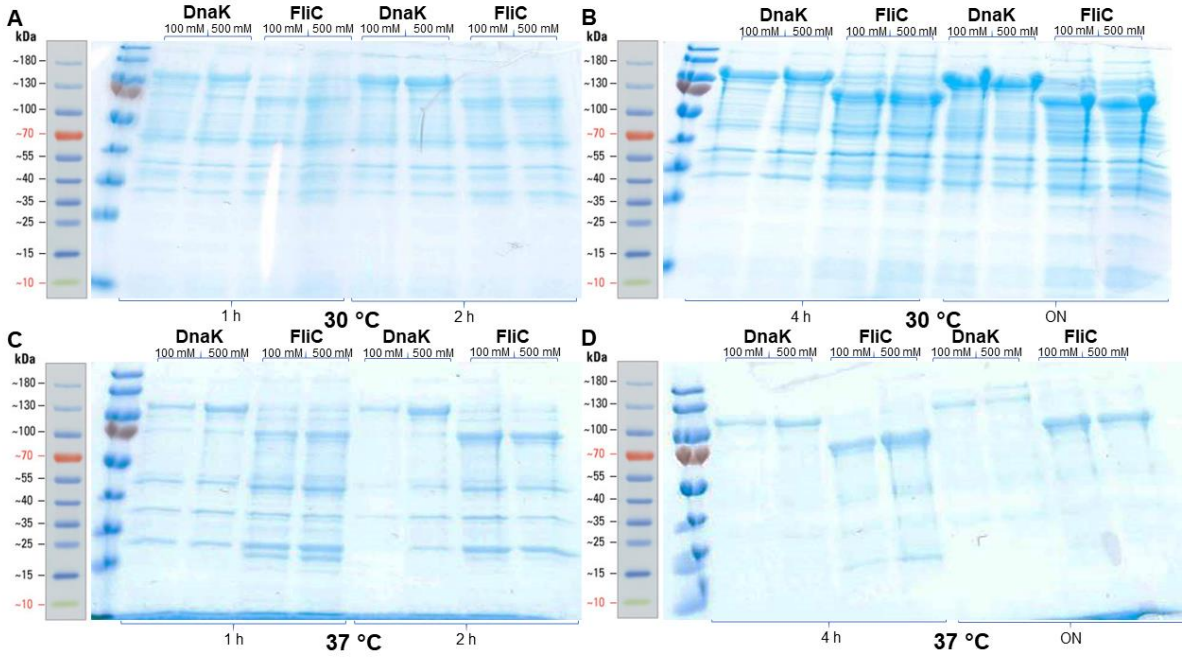

Appendix 26: Pre-testing of the optimal protein production conditions of DnaK and FliC. The protein production of DnaK and FliC were tested under different temperatures and IPTG concentrations (100 mM and 500 mM), samples were taken after one, two and four hours and after over night cultivation. **A-B.** Protein test production of DnaK and FliC at 30 °C **C-D.** Protein test production of DnaK and FliC at 37 °C.

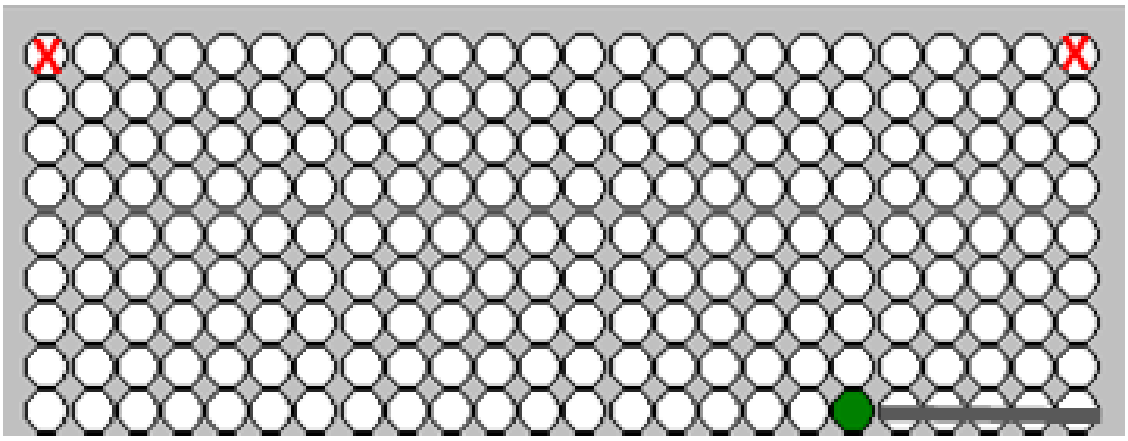

Appendix 27: SPOT membrane application scheme of DnaK. Spotting of DnaK peptides onto the SPOT membrane; excised control peptide (X), last spotted peptide (green dot) and not occupied spotting slots (grey lane).

Appendix 28: List of spotted peptides of DnaK SPOT membrane

(excised control peptide)	A1
MGKIIGIDLGTTNSCZ	A2
IIGIDLGTTNSCVAIZ	A3
IDLGTTNSCVAILENZ	A4
GTTNSCVAILENGNVZ	A5
NSCVAILENGNVKVIZ	A6
VAILENGNVKVIENAZ	A7
LENGNVKVIENAEGAZ	A8
GNVKVIENAEGARTTZ	A9
KVIENAEGARTTPSIZ	A10
ENAEGARTTPSIIAYZ	A11
EGARTTPSIIAYTNDZ	A12
RTTPSIIAYTNDGETZ	A13
PSIIAYTNDGETLVGZ	A14
IAYTNDGETLVGQPAZ	A15
TNDGETLVGQPAKRQZ	A16
GETLVGQPAKRQAVTZ	A17
LVGQPAKRQAVTNPQZ	A18
QPAKRQAVTNPQNTLZ	A19
KRQAVTNPQNTLYAVZ	A20
AVTNPQNTLYAVKRLZ	A21

NPQNTLYAVKRLIGRZ	A22
NTLYAVKRLIGRRFEZ	A23
(excised control peptide)	A24
YAVKRLIGRRFEENVZ	B1
KRLIGRRFEENVVQKZ	B2
IGRRFEENVVQKDIQZ	B3
RFEENVVQKDIQMVPZ	B4
ENVVQKDIQMVPYSIZ	B5
VQKDIQMVPYSIVKAZ	B6
DIQMVPYSIVKADNGZ	B7
MVPYSIVKADNGDAWZ	B8
YSIVKADNGDAWVEVZ	B9
VKADNGDAWVEVKGQZ	B10
DNGDAWVEVKGQKMAZ	B11
DAWVEVKGQKMAPPQZ	B12
VEVKGQKMAPPQISAZ	B13
KGQKMAPPQISAEVLZ	B14
KMAPPQISAEVLKKMZ	B15
PPQISAEVLKKMKKTZ	B16
ISAEVLKKMKKTAEDZ	B17
EVLKKMKKTAEDYLGZ	B18
KKMKKTAEDYLGEPVZ	B19
KKTAEDYLGEPVTEAZ	B20
AEDYLGEPVTEAVITZ	B21
YLGEPVTEAVITVPAZ	B22
EPVTEAVITVPAYFNZ	B23
TEAVITVPAYFNDSQZ	B24
VITVPAYFNDSQRQAZ	C1
VPAYFNDSQRQATKDZ	C2
YFNDSQRQATKDAGRZ	C3
DSQRQATKDAGRIAGZ	C4
RQATKDAGRIAGLDVZ	C5
TKDAGRIAGLDVKRIZ	C6
AGRIAGLDVKRIINEZ	C7
IAGLDVKRIINEPTAZ	C8
LDVKRIINEPTAAALZ	C9
KRIINEPTAAALAYGZ	C10

INEPTAAALAYGLDKZ	C11
PTAAALAYGLDKAKGZ	C12
AALAYGLDKAKGDHTZ	C13
AYGLDKAKGDHTVIVZ	C14
LDKAKGDHTVIVYDLZ	C15
AKGDHTVIVYDLGGGZ	C16
DHTVIVYDLGGGTFDZ	C17
VIVYDLGGGTFDVSVZ	C18
YDLGGGTFDVSVIEIZ	C19
GGGTFDVSVIEIAEVZ	C20
TFDVSVIEIAEVDGEZ	C21
VSVIEIAEVDGEHQFZ	C22
IEIAEVDGEHQFEVLZ	C23
AEVDGEHQFEVLATNZ	C24
DGEHQFEVLATNGDTZ	D1
HQFEVLATNGDTFLGZ	D2
EVLATNGDTFLGGEDZ	D3
ATNGDTFLGGEDFDIZ	D4
GDTFLGGEDFDIRLIZ	D5
FLGGEDFDIRLIDYLZ	D6
GEDFDIRLIDYLVDEZ	D7
FDIRLIDYLVDEFKKZ	D8
RLIDYLVDEFKKESGZ	D9
DYLVDEFKKESGINLZ	D10
VDEFKKESGINLKGDZ	D11
FKKESGINLKGDPLAZ	D12
ESGINLKGDPLAMQRZ	D13
INLKGDPLAMQRLKEZ	D14
KGDPLAMQRLKEAAEZ	D15
PLAMQRLKEAAEKAKZ	D16
MQRLKEAAEKAKIELZ	D17
LKEAAEKAKIELSSTZ	D18
AAEKAKIELSSTQQTZ	D19
KAKIELSSTQQTDVNZ	D20
IELSSTQQTDVNLPYZ	D21
SSTQQTDVNLPYVTAZ	D22
QQTDVNLPYVTADASZ	D23

DVNLPYVTADASGPKZ	D24
LPYVTADASGPKHLNZ	E1
VTADASGPKHLNVKVZ	E2
DASGPKHLNVKVSRAZ	E3
GPKHLNVKVSRAKLEZ	E4
HLNVKVSRAKLESLVZ	E5
VKVSRAKLESLVEDLZ	E6
SRAKLESLVEDLVQRZ	E7
KLESLVEDLVQRTIEZ	E8
SLVEDLVQRTIEPCRZ	E9
EDLVQRTIEPCRTALZ	E10
VQRTIEPCRTALKDAZ	E11
TIEPCRTALKDAGLDZ	E12
PCRTALKDAGLDVSDZ	E13
TALKDAGLDVSDIHEZ	E14
KDAGLDVSDIHEVILZ	E15
GLDVSDIHEVILVGGZ	E16
VSDIHEVILVGGQTRZ	E17
IHEVILVGGQTRMPLZ	E18
VILVGGQTRMPLVQKZ	E19
VGGQTRMPLVQKTVAZ	E20
QTRMPLVQKTVAEFFZ	E21
MPLVQKTVAEFFGKEZ	E22
VQKTVAEFFGKEARKZ	E23
TVAEFFGKEARKDVNZ	E24
EFFGKEARKDVNPDEZ	F1
GKEARKDVNPDEAVAZ	F2
ARKDVNPDEAVAVGAZ	F3
DVNPDEAVAVGAAIQZ	F4
PDEAVAVGAAIQGAVZ	F5
AVAVGAAIQGAVLAGZ	F6
VGAAIQGAVLAGDVKZ	F7
AIQGAVLAGDVKDVLZ	F8
GAVLAGDVKDVLLLDZ	F9
LAGDVKDVLLLDVTPZ	F10
DVKDVLLLDVTPLTLZ	F11
DVLLLDVTPLTLGIEZ	F12

LLDVTPLTLGIETLGZ	F13
VTPLTLGIETLGGVMZ	F14
LTLGIETLGGVMTGLZ	F15
GIETLGGVMTGLIEKZ	F16
TLGGVMTGLIEKNTTZ	F17
GVMTGLIEKNTTIPTZ	F18
TGLIEKNTTIPTKKSZ	F19
IEKNTTIPTKKSQVFZ	F20
NTTIPTKKSQVFSTAZ	F21
IPTKKSQVFSTADDNZ	F22
KKSQVFSTADDNQGAZ	F23
QVFSTADDNQGAVTIZ	F24
STADDNQGAVTIHVLZ	G1
DDNQGAVTIHVLQGEZ	G2
QGAVTIHVLQGERKQZ	G3
VTIHVLQGERKQAAQZ	G4
HVLQGERKQAAQNKSZ	G5
QGERKQAAQNKSLGKZ	G6
RKQAAQNKSLGKFDLZ	G7
AAQNKSLGKFDLADIZ	G8
NKSLGKFDLADIPPAZ	G9
LGKFDLADIPPAPRGZ	G10
FDLADIPPAPRGVPQZ	G11
ADIPPAPRGVPQIEVZ	G12
PPAPRGVPQIEVTFDZ	G13
PRGVPQIEVTFDIDAZ	G14
VPQIEVTFDIDANGIZ	G15
IEVTFDIDANGILHVZ	G16
TFDIDANGILHVSAKZ	G17
IDANGILHVSAKDKAZ	G18
NGILHVSAKDKATGKZ	G19
LHVSAKDKATGKQQSZ	G20
SAKDKATGKQQSIVIZ	G21
DKATGKQQSIVIKASZ	G22
TGKQQSIVIKASSGLZ	G23
QQSIVIKASSGLSEDZ	G24
IVIKASSGLSEDEIQZ	H1

KASSGLSEDEIQQMVZ	H2
SGLSEDEIQQMVRDAZ	H3
SEDEIQQMVRDAEANZ	H4
EIQQMVRDAEANAEEZ	H5
QMVRDAEANAEEDRKZ	H6
RDAEANAEEDRKFEEZ	H7
EANAEEDRKFEELAAZ	H8
AEEDRKFEELAAARNZ	H9
DRKFEELAAARNQGDZ	H10
FEELAAARNQGDALVZ	H11
LAAARNQGDALVHATZ	H12
ARNQGDALVHATRKMZ	H13
QGDALVHATRKMITEZ	H14
ALVHATRKMITEAGDZ	H15
HATRKMITEAGDKATZ	H16
RKMITEAGDKATAEDZ	H17
ITEAGDKATAEDKATZ	H18
AGDKATAEDKATIEKZ	H19
KATAEDKATIEKALGZ	H20
AEDKATIEKALGELEZ	H21
KATIEKALGELEAAVZ	H22
IEKALGELEAAVKGDZ	H23
ALGELEAAVKGDDKAZ	H24
ELEAAVKGDDKAEIEZ	I1
AAVKGDDKAEIEAKMZ	I2
KGDDKAEIEAKMNALZ	I3
DKAEIEAKMNALSQAZ	I4
EIEAKMNALSQASTPZ	I5
AKMNALSQASTPLAQZ	I6
NALSQASTPLAQKMYZ	I7
SQASTPLAQKMYAEQZ	I8
STPLAQKMYAEQAQQZ	I9
LAQKMYAEQAQQGEDZ	I10
KMYAEQAQQGEDAPQZ	I11
AEQAQQGEDAPQGEQZ	I12
AQQGEDAPQGEQAKAZ	I13
GEDAPQGEQAKAADDZ	I14

APQGEQAKAADDVVDZ	I15
GEQAKAADDVVDAEFZ	I16
AKAADDVVDAEFEEVZ	I17
ADDVVDAEFEEVKDNZ	I18
DDVVDAEFEEVKDNKZ	I19
Z	I20
Z	I21
Z	I22
Z	I23
Z	I24

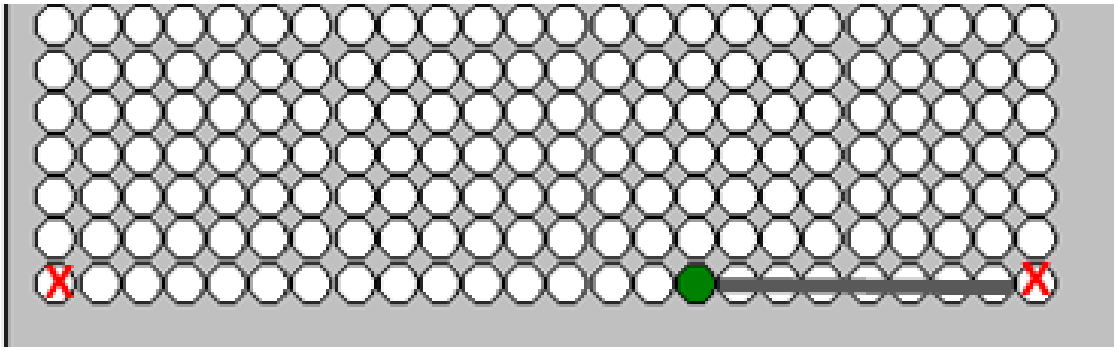

Appendix 29: SPOT membrane application scheme of FliC. Spotting of FliC peptides onto the SPOT membrane; excised control peptide (X), last spotted peptide (green dot) and not occupied spotting slots (grey lane).

Appendix 30: List of spotted peptides of the SPOT membrane of FliC

MALTVNTNIASLNTQZ	A1
TVNTNIASLNTQRNLZ	A2
TNIASLNTQRNLNASZ	A3
ASLNTQRNLNASSNDZ	A4
NTQRNLNASSNDLNTZ	A5
RNLNASSNDLNTSLQZ	A6
NASSNDLNTSLQRLTZ	A7
SNDLNTSLQRLTTGYZ	A8
LNTSLQRLTTGYRINZ	A9
SLQRLTTGYRINSAKZ	A10
RLTTGYRINSAKDDAZ	A11
TGYRINSAKDDAAGLZ	A12
RINSAKDDAAGLQISZ	A13

SAKDDAAGLQISNRLZ	A14
DDAAGLQISNRLSNQZ	A15
AGLQISNRLSNQISGZ	A16
QISNRLSNQISGLNVZ	A17
NRLSNQISGLNVATRZ	A18
SNQISGLNVATRNANZ	A19
ISGLNVATRNANDGIZ	A20
LNVATRNANDGISLAZ	A21
ATRNANDGISLAQTAZ	A22
NANDGISLAQTAEGAZ	A23
DGISLAQTAEGALQQZ	A24
SLAQTAEGALQQSTNZ	B1
QTAEGALQQSTNILQZ	B2
EGALQQSTNILQRIRZ	B3
LQQSTNILQRIRDLAZ	B4
STNILQRIRDLALQSZ	B5
ILQRIRDLALQSANGZ	B6
RIRDLALQSANGSNSZ	B7
DLALQSANGSNSDADZ	B8
LQSANGSNSDADRAAZ	B9
ANGSNSDADRAALQKZ	B10
SNSDADRAALQKEVAZ	B11
DADRAALQKEVAAQQZ	B12
RAALQKEVAAQQAELZ	B13
LQKEVAAQQAELTRIZ	B14
EVAAQQAELTRISDTZ	B15
AQQAELTRISDTTTFZ	B16
AELTRISDTTTFGGRZ	B17
TRISDTTTFGGRKLLZ	B18
SDTTTFGGRKLLDGSZ	B19
TTFGGRKLLDGSFGTZ	B20
GGRKLLDGSFGTTSFZ	B21
KLLDGSFGTTSFQVGZ	B22
DGSFGTTSFQVGSNAZ	B23
FGTTSFQVGSNAYETZ	B24
TSFQVGSNAYETIDIZ	C1
QVGSNAYETIDISLQZ	C2

SNAYETIDISLQNASZ	C3
YETIDISLQNASASAZ	C4
IDISLQNASASAIGSZ	C5
SLQNASASAIGSYQVZ	C6
NASASAIGSYQVGSNZ	C7
ASAIGSYQVGSNGAGZ	C8
IGSYQVGSNGAGTVAZ	C9
YQVGSNGAGTVASVAZ	C10
GSNGAGTVASVAGTAZ	C11
GAGTVASVAGTATASZ	C12
TVASVAGTATASGIAZ	C13
SVAGTATASGIASGTZ	C14
GTATASGIASGTVNLZ	C15
TASGIASGTVNLVGGZ	C16
GIASGTVNLVGGGQVZ	C17
SGTVNLVGGGQVKNIZ	C18
VNLVGGGQVKNIAIAZ	C19
VGGGQVKNIAIAAGDZ	C20
GQVKNIAIAAGDSAKZ	C21
KNIAIAAGDSAKAIAZ	C22
AIAAGDSAKAIAEKMZ	C23
AGDSAKAIAEKMDGAZ	C24
SAKAIAEKMDGAIPNZ	D1
AIAEKMDGAIPNLSAZ	D2
EKMDGAIPNLSARARZ	D3
DGAIPNLSARARTVFZ	D4
IPNLSARARTVFTADZ	D5
LSARARTVFTADVSGZ	D6
RARTVFTADVSGVTGZ	D7
TVFTADVSGVTGGSLZ	D8
TADVSGVTGGSLNFDZ	D9
VSGVTGGSLNFDVTVZ	D10
VTGGSLNFDVTVGSNZ	D11
GSLNFDVTVGSNTVSZ	D12
NFDVTVGSNTVSLAGZ	D13
VTVGSNTVSLAGVTSZ	D14
GSNTVSLAGVTSTQDZ	D15

TVSLAGVTSTQDLADZ	D16
LAGVTSTQDLADQLNZ	D17
VTSTQDLADQLNSNSZ	D18
TQDLADQLNSNSSKLZ	D19
LADQLNSNSSKLGITZ	D20
QLNSNSSKLGITASIZ	D21
SNSSKLGITASINDKZ	D22
SKLGITASINDKGVLZ	D23
GITASINDKGVLTITZ	D24
ASINDKGVLTITSATZ	E1
NDKGVLTITSATGENZ	E2
GVLTITSATGENVKFZ	E3
TITSATGENVKFGAQZ	E4
SATGENVKFGAQTGTZ	E5
GENVKFGAQTGTATAZ	E6
VKFGAQTGTATAGQVZ	E7
GAQTGTATAGQVAVKZ	E8
TGTATAGQVAVKVQGZ	E9
ATAGQVAVKVQGSDGZ	E10
GQVAVKVQGSDGKFEZ	E11
AVKVQGSDGKFEAAAZ	E12
VQGSDGKFEAAAKNVZ	E13
SDGKFEAAAKNVVAAZ	E14
KFEAAAKNVVAAGTAZ	E15
AAAKNVVAAGTAATTZ	E16
KNVVAAGTAATTTVVZ	E17
VAAGTAATTTVVTGYZ	E18
GTAATTTVVTGYVQLZ	E19
ATTTVVTGYVQLNSPZ	E20
TVVTGYVQLNSPTAYZ	E21
TGYVQLNSPTAYSVSZ	E22
VQLNSPTAYSVSGTGZ	E23
NSPTAYSVSGTGTQAZ	E24
TAYSVSGTGTQASQVZ	F1
SVSGTGTQASQVFGNZ	F2
GTGTQASQVFGNASAZ	F3
TQASQVFGNASAAQKZ	F4

SQVFGNASAAQKSSVZ	F5
FGNASAAQKSSVASVZ	F6
ASAAQKSSVASVDISZ	F7
AQKSSVASVDISTADZ	F8
SSVASVDISTADGAQZ	F9
ASVDISTADGAQNAIZ	F10
DISTADGAQNAIAVVZ	F11
TADGAQNAIAVVDNAZ	F12
GAQNAIAVVDNALAAZ	F13
NAIAVVDNALAAIDAZ	F14
AVVDNALAAIDAQRAZ	F15
DNALAAIDAQRADLGZ	F16
LAAIDAQRADLGAVQZ	F17
IDAQRADLGAVQNRFZ	F18
QRADLGAVQNRFKNTZ	F19
DLGAVQNRFKNTIDNZ	F20
AVQNRFKNTIDNLTNZ	F21
NRFKNTIDNLTNISEZ	F22
KNTIDNLTNISENATZ	F23
IDNLTNISENATNARZ	F24
(excised control peptide)	G1
LTNISENATNARSRIZ	G2
ISENATNARSRIKDTZ	G3
NATNARSRIKDTDFAZ	G4
NARSRIKDTDFAAETZ	G5
SRIKDTDFAAETAALZ	G6
KDTDFAAETAALSKNZ	G7
DFAAETAALSKNQVLZ	G8
AETAALSKNQVLQQAZ	G9
AALSKNQVLQQAGTAZ	G10
SKNQVLQQAGTAILAZ	G11
QVLQQAGTAILAQANZ	G12
QQAGTAILAQANQLPZ	G13
GTAILAQANQLPQAVZ	G14
ILAQANQLPQAVLSLZ	G15
AQANQLPQAVLSLLRZ	G16
Z	G17

Z	G18
Z	G19
Z	G20
Z	G21
Z	G22
Z	G23
(excised control peptide)	G24

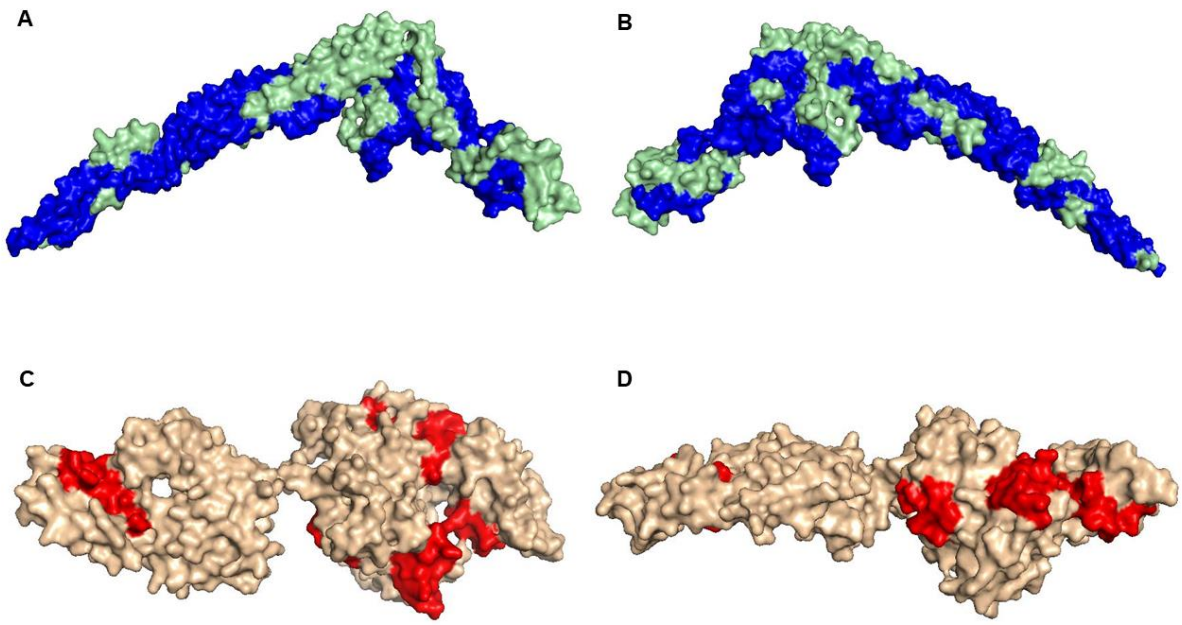

Appendix 31: Model of determined interacting domains of FliC and DnaK. A-**B**. Determined domains (blue) of FliC (light green). **C**-**D**. Determined interacting domains (red) of DnaK (light brown).

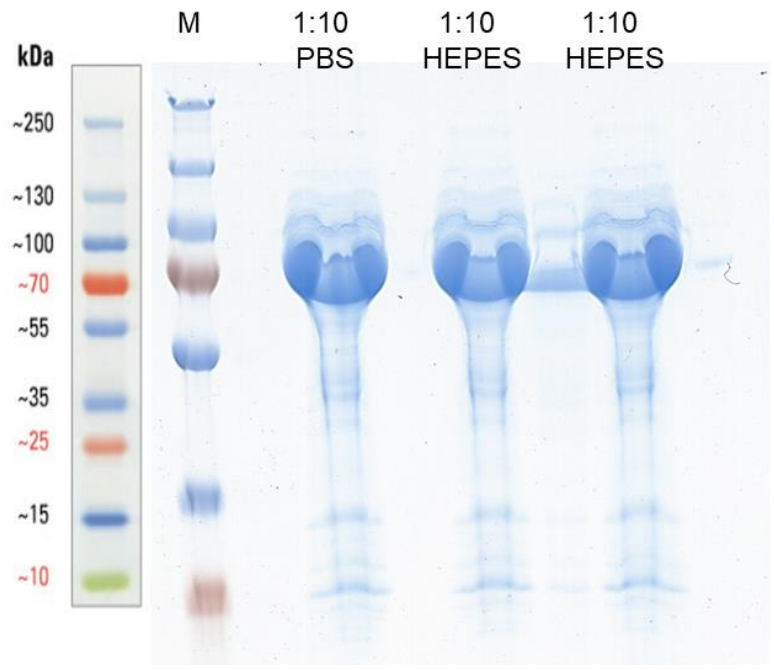

Appendix 32: Production of DnaK testing of different storage solutions. Test of storage conditions for DnaK after affinity purification in PBS and HEPES buffer.

Acknowledgement

I would like to take this opportunity to thank the people who have supported me in one way or another during my PhD. First of all, I would like to thank Prof. Dr. Dieter Jahn, who gave me the opportunity to participate in the graduate school PROCOMPAS (DFG funding GRK2223/1) and to be able to do my PhD thesis in his group of the institute of microbiology. Furthermore, I thank him very much for the scientific input, discussions and support in writing and preparing conference papers, proofreading my work and finally finishing the work with a good ending. I would like to thank Dr. Martina Jahn for her excellent supervision, advice and support during my work. I am also very grateful for the scientific support of Dr. José Borrero-de Acuña, who also became a friend during the time.

Furthermore, I highly appreciate the support of Prof. Dr. Lothar Jänsch, not only for taking the second lecturer position, but also for the scientific input, discussions and support. I would also like to thank Dr. Josef Wissing for his professional support and commitment. Another deep thanks goes to Dr. Gabriella Molinari for her scientific support and technique. I would also like to thank Dr. Werner Tegge for his scientifical support and provision of the SPOT technique. Another deep thanks goes to Sara da-Silva Ribeiro for her scientific support and discussions. I would also like to thank the MIBI for the relaxed atmosphere, especially the working group of Dr. Martina Jahn and deeply thank Toni Mingers, Stefan Barthels and Davina Hiller.

Next, I would like to address my most profound appreciation to my girls, Jännie, Riekä, Lillith, Fränzi, Laura and Carmen, who have always been there and have pulled me back up and brought me to new thoughts. Furthermore, I would like to thank my friends, especially Melli, Jann, Robert, Alina, Andi, Emi, Jassy and Vivi.

A gratefull thank to my parents and Grannys, for their personal support and patience over the entire time.

An especially deep thanks goes to Matze, who has always been there for me, supported me in everything, put up with my special moods and is a rock in the storm.